Development of the SAFT-γ Mie equation of state for predicting the thermodynamic behaviour of strong and weak electrolyte solutions

Georgia Lazarou

A thesis submitted for the Degree of Doctor of Philosophy of the University of London and for the Diploma of Membership of Imperial College London.

Department of Chemical Engineering
Imperial College London
London SW7 2AZ
United Kingdom

September 2017

Declaration of originality

I hereby declare that except where specific reference is made to the work of others, the contents of this dissertation are my own original work. This dissertation has not been submitted in whole or in part for consideration for any other degree or qualification in this, or any other university.

Georgia Lazarou
September 2017

Copyright

Acknowledgements

I thank Amparo Galindo, George Jackson, and Claire S. Adjiman for the supervision of my doctoral thesis, as well as Daniel K. Eriksen, Simon Dufal, and Andrew J. Haslam for useful discussions. I gratefully acknowledge funding from Pfizer, Inc. for the support of my PhD studentship.

Abstract

The thermodynamic modelling of fluid mixtures containing electrolytes using the SAFT-γ Mie equation of state is addressed in detail in this thesis. The SAFT-γ Mie approach allows the implementation of heteronuclear molecules using a group-contribution formalism, and offers a versatile framework for developing models to describe molecules of varying chemical functionality for a broad range of physical properties. In the present work, the SAFT-γ Mie equation of state is extended to electrolyte mixtures with the incorporation of the primitive unrestricted mean spherical approximation (MSA-PM) for describing the Coulombic ion–ion interactions, and the Born solvation free energy to implicitly treat ion–solvent polar interactions. Novel reformulations of the MSA-PM and Born theories within a group-contribution framework are proposed in order to enable ionic species of any size and chemical structure to be modelled, from small inorganic ions to large non-spherical charged molecules. Taking carboxylate anions in linear alkyl chain molecules as an illustrative case study, the proposed theory is shown to effectively account for localised charge effects arising from the structural topology of the charged species. A holistic description of electrolyte solutions is employed in this work; in addition to the short-range dispersion forces and the long-range Coulombic interactions which are pertinent to such mixtures, the models developed here also account for the formation of hydrogen bonds, ion-pairing phenomena, and electrolyte dissociation equilibria. The proposed SAFT-γ Mie equation of state is used to model aqueous solutions of strong electrolytes including alkali halide salts, hydrogen halide acids, and alkali hydroxide bases. Aqueous solutions of sulphuric acid and nitric acid are studied in detail by modelling these as speciating weak electrolytes. Finally, the treatment of ion-pairing phenomena is investigated through a consideration of aqueous alkali nitrate salt solutions. This work presents a new theoretical formulation and SAFT-γ Mie group models for twenty species in total.

Contents

List of Figures

List of Tables

Nomenclature

Roman Symbols

A	Helmholtz free energy
a	Helmholtz free energy of equivalent system
a_i	activity of component i
c	concentration
C	function of the Mie intermolecular potential exponents
D	relative static permittivity (dielectric constant)
e	elementary charge
f_i	fugacity of component i
F_{obj}	objective function
G	Gibbs free energy
ΔG^f	Gibbs free energy of formation
$\Delta_{\mathbf{r}} G$	Gibbs free energy of reaction
$\Delta G^{\mathbf{solv}}$	Gibbs free energy of solvation
I_i	ionisation potential of species i
k_{B}	Boltzmann constant
K_{eq}	thermodynamic equilibrium constant

$K^{\mathrm{HB}}_{ab,ij}$ bonding volume between site a on species i and site b on species j

K_{IP} ion pairing equilibrium constant

K_{sp} thermodynamic solubility product

m_i molality of component i

$\mathbf{m}$ molality composition vector

$\mathbf{N}$ composition vector

MW_j molecular weight of component j

N number of molecules

n_s number of association sites of type s

N_{C} Number of components

N_{g} number of groups

n_{ion} number of ions

N_{phases} number of phases

N_{ST} number of site types

p pressure

P_n MSA parameter

Q MSA effective charge parameter

Q_{C} reaction quotient

q_i charge of species i

R ideal gas constant

S_k shape factor of species k

T temperature

U internal energy

u intermolecular potential

x_i mole fraction of component i

x_k number fraction of species k

Z compressibility factor

z_i charge number of component i

Greek Symbols

$\alpha_{0,i}$ polarisability of species i

Δ MSA packing fraction parameter

ϵ_0 permittivity of vacuum

ε_{ij} dispersion energy between species i and j

$\varepsilon_{ij}^{\mathrm{HB}}$ association energy between species i and j

Γ MSA shielding parameter

γ_i activity coefficient of component i

$\gamma_{i,*}$ rational asymmetric activity coefficient of component i

$\gamma_{\pm,i}$ mean ionic activity coefficient of component i

$\lambda_{\mathrm{a},i}$ attractive exponent of the Mie intermolecular potential

$\lambda_{\mathrm{r},i}$ repulsive exponent of the Mie intermolecular potential

μ_i chemical potential of component i

ν_i stoichiometric coefficient of component i

$\nu_{k,i}$ number of groups k on component i

ν_k^* number of identical segments comprising group k

Ω MSA parameter

ω_o weighting assigned to property o

Φ osmotic coefficient

φ_i fugacity coefficient of component i

ψ integrated intermolecular potential

ρ density

ρ_g density of groups

σ_i diameter of species i

σ_i^{Born} Born cavity diameter of species i

$\tilde{\sigma}_i^{\text{Born}}$ equivalent Born cavity diameter of a non-spherical species i

$\tilde{\sigma}_i$ equivalent spherical diameter of a non-spherical species i

ξ extent of reaction

Superscripts

adj alkyl group adjacent to a carbonyl group in short-chain acids

calc calculated value of quantity

exp experimental value of quantity

HB hydrogen bonding (association) interaction

ideal ideal gas property

ref reference state property

res residual property

sat saturated solution property

short carbonyl group of a short-chain acid

stoich. stoichiometric property

Subscripts

(aq) aqueous phase

(s) solid phase

c concentration scale

m molality scale

x mole fraction scale

Acronyms & Abbreviations

%AAD Percentage Absolute Average Deviation

CPA Cubic Plus Association

EOS Equation of State

LLE Liquid-Liquid Equilibrium

MSA Mean Spherical Approximation

PC-SAFT Perturbed-Chain Statistical Associating Fluid Theory

MSA-PM Mean Spherical Approximation Primitive Model

PR Peng-Robinson

MSA-RPM Mean Spherical Approximation Restricted Primitive Model

SAFT Statistical Associating Fluid Theory

SLE Solid-Liquid Equilibrium

SRK Soave-Redlich-Kwong

TPT1 Thermodynamic Perturbation Theory of the first order

VLE Vapour-Liquid Equilibrium

Chapter 1

Introduction

Thermodynamic models occupy a central role in engineering and physical sciences, with a direct impact on many aspects of the chemical industry. Modelling tools are ever evolving to support the efforts of developing new materials and products, as well as for aiding the optimisation of unit operations and design of novel processes. A fundamental prerequisite for pursuing these endeavours is the availability of thermodynamic models which can be used to reliably describe the physical properties of mixtures under the particular conditions of interest, especially when experimental information is scarce. Two central features dictating the efficacy of thermodynamic models can be identified: firstly, their range of application to mixtures with vastly different chemical properties; and secondly, the ability to do so in an appreciably predictive manner [1].

A class of thermodynamic models which have the potential to fulfil these desired characteristics are molecular-based approaches which allow for a prediction of macroscopic properties of mixtures based on a description of fundamental molecular interactions. One such approach is the Statistical Associating Fluid Theory (SAFT) [2, 3], a formalism for associating chain-like molecules based on statistical thermodynamics. The SAFT approach has undergone numerous adaptations and reformulations, making it applicable to a vast array

of pure fluids and complex mixtures [4, 5]. In pursuit of broader applicability and improved predictive potential, reformulations of the SAFT formalism have been proposed within a group-contribution framework, according to which the macroscopic properties of molecular entities are cumulatively conferred by the functional groups composing the molecules. A particular strain of SAFT-based group-contribution approaches is the SAFT-γ equation of state (EOS) [6, 7]. The most recent variant of this approach is the SAFT-γ Mie EOS [8], which has been extensively applied to a variety of pure fluids and mixtures including linear and branched alkanes and alkenes, alkylbenzenes and alkyl acetates, primary alcohols, and carboxylic acids [9, 10].

The objective of the work presented in this thesis is to further develop the SAFT-γ Mie approach so as to incorporate the capability of modelling systems which contain electrolyte components. Electrolytes are involved in numerous industrial operations, including environmental applications for waste treatment, electrochemical processes, separation processes, extraction of petrochemicals, and hydrometallurgical processes [11]. Electrolytes are also key components in product formulations; for instance, ionic surfactants are used in an array of household products [12]; and active pharmaceutical ingredients are often preferentially formulated as organic salts in order to enhance bioavailability [13, 14]. Although a plethora of studies have been devoted to modelling inorganic salts, those which have dealt with more complex charged multifunctional molecules are still limited. The group-contribution modelling framework is naturally suited to treating charged molecules, as it is possible to specify charged functional groups within the molecular model. By extending the scope of the SAFT-γ Mie group-contribution approach to charged molecules, the aim here is to contribute to the development of a comprehensive platform for modelling fluid mixtures.

1.1 Potential applications of present work

Although the broad applicability of a comprehensive thermodynamic modelling platform across the chemical and related industries is evident, a particular area of application that acts as a strong driving force for its development is that of pharmaceutical product formulation. The physicochemical properties of an active pharmaceutical ingredient have a profound impact on its efficacy: properties such as hydrophilicity and lipophilicity, aqueous solubility and dissolution rate, and the type of solid form, ultimately determine the bioavailability of a drug [15]. With the larger share of active pharmaceutical ingredients being either weakly acidic or weakly basic [13, 14], salts of these molecules are often chosen as the preferred formulated form of the drug, as a means of achieving higher solubility and dissolution rate in the physiological environment, better chemical stability of the dosage form, and desirable mechanical properties during the manufacturing process [15].

The ability to reliably predict physicochemical properties is crucial in the development of new active pharmaceutical ingredients and the formulation of drug products, since these are typically new chemical entities for which very limited experimental data is available. *In silico* molecule optimisation tools are therefore commonly used in the pharmaceutical industry, many of which adopt a group contribution approach [16–18] that gives rise to quantitative structure–activity or structure–property relationships. Such tools are to a large extent empirical in nature and their range of application is highly dependent on the training set of molecules used in the development of the tool [19]. This is a distinct limitation of these tools, since experimental data sets of adequate size, diversity, and quality are not readily available for pharmaceutically relevant compounds [20]. As a result, a growing interest in equation of state modelling approaches for pharmaceutical applications has been demonstrated in recent years: in particular, the PC-SAFT EOS [21, 22] has been widely applied for modelling pharmaceutically-relevant fluid mixtures [23–28]. In recent work by Hutacharoen et al. [10], the SAFT-γ Mie EOS was successfully applied to describe the properties of active pharmaceutical ingredients – including intrinsic aqueous solubilities and

octanol-water partition coefficients – in a completely predictive manner, through a group contribution modelling approach. Having had the pertinence of the SAFT-γ Mie EOS to pharmaceutical applications demonstrated, it is desirable to extend the method's range of applicability to include ionisable active pharmaceutical ingredients. This thesis constitutes the initial step towards this pursuit: by developing the SAFT-γ Mie EOS for predicting the thermodynamic behaviour of aqueous strong and weak electrolytes, this thesis contributes towards a thermodynamic modelling platform that can subsequently be implemented in the context of pharmaceutical product development and formulation, without discounting its applicability in the modelling needs of the wider chemical industry.

1.2 Thesis scope

The fluid mixtures targeted in this thesis correspond to systems of a single solvent and a single electrolyte solute. In particular, aqueous electrolyte solutions of simple salts, acids, and bases are examined. A common assumption made when modelling electrolyte mixtures which is also adopted here is that a clear distinction can be made between strong and weak electrolytes, and the presence or absence of ion pairs. Nevertheless, it is widely recognised that the physical reality of electrolyte solutions is more complex, with no sharp boundaries between strong and weak electrolytes, as in each solution there may be to a lesser or greater extent a distribution of freely solvated ions, ion pairs or clusters, and the undissociated electrolyte [29, 30]. However, in most cases it is possible to make acceptably reasonable simplifications regarding the nature of the solvated species present in a given electrolyte solution, and in this thesis the conventions broadly followed in the scientific literature are adopted. Three types of aqueous electrolyte solutions are addressed in this thesis: firstly, solutions of completely dissociated (i.e. strong) salts, acids, and bases are modelled as mixtures of water + anion + cation; the second type are solutions of partially dissociated (i.e. weak) acids, modelled as mixtures of water + anion + cation + acid; and finally, in a

preliminary investigatory manner, solutions of salts demonstrating an extensive degree of ion pairing are modelled as water + anion + cation + ion pair.

Subsequent to the expansion of the SAFT-γ Mie EOS with the capability to model electrolytes, the above types of electrolyte mixtures are targeted as an avenue to explore suitable workflows for developing models for aqueous electrolytes and thus to establish a core library of models for commonly encountered solvated ionic species. In particular, the present work seeks to develop models that will not only reproduce experimental data for aqueous electrolyte mixtures, but which will also do so with physically meaningful parameters such that the models are intrinsically suited for use in a predictive capacity. Setting the latter as a priority of the present work requires that a minimal level of empiricism is employed in model development; however, this need not set conservative expectations regarding the accuracy of the resultant models. In the body of literature devoted to modelling aqueous electrolyte mixtures with statistical thermodynamic EOS approaches, the accuracy to which experimental data for aqueous electrolyte mixtures are reproduced often varies substantially. Modelling approaches differ most strikingly in their description of the mean ionic activity coefficient (MIAC) of the electrolyte solute – a property which is central to this thesis as it is indicative of whether the EOS can be used to reliably perform chemical reaction equilibrium calculations to predict aqueous solubilities and the solution compositions of weak electrolytes. What constitutes a good description of the MIAC is difficult to quantify, especially since the experimental error associated with data for this property is not typically reported. The absolute average deviation (AAD) of model calculations from experimental data of the MIAC reported for SAFT-type approaches that consider single-solute aqueous solutions ranges from ~0.1% [31] to ~35% [32], with a typical reported accuracy of <10%. Notably, all approaches so far have employed data for the MIAC were for estimating the model parameters. This work intends to demonstrate that, with appropriate model development strategies, a similar level of accuracy as the existing studies can be achieved predictively.

1.3 Thesis overview

An approach for modelling electrolytes using the SAFT-γ Mie group-contribution formalism is presented in this thesis together with models for ionic species developed using the extended functionality of the equation of state. The thermodynamic properties of aqueous strong and weak electrolytes are investigated, including inorganic and organic salts, and inorganic weak acids.

Chapter 2 begins with a description of electrolyte solutions in terms of the chemical equilibria governing their dissociation in solution, and an illustration of how their thermodynamic properties can be obtained using an equation of state. The dominant theories that have been proposed to model electrostatic interactions in solution are outlined, and a review is given of the wide range of thermodynamic modelling tools which have adopted these theories within their framework. Particular attention is devoted to the body of work on modelling electrolytes which has been presented with SAFT approaches. Chapter 3 concerns the premise and evolution of SAFT equations of state leading to the development of the SAFT-γ Mie group-contribution approach. Following this is a proposal of two potential avenues for incorporating electrolyte theories within SAFT-γ Mie for large multifunctional molecules; each option reflects the formulation arrived at when adopting a particular set of assumptions regarding the definition of the species contributing to the electrostatic interactions in a mixture.

The rest of the thesis is devoted to the application of the SAFT-γ Mie EOS to the description of thermodynamic properties of aqueous electrolyte systems. Strong inorganic electrolytes are studied in Chapter 4, specifically alkali halide salts, hydrogen halide acids, and alkali hydroxide bases. A simple geometry is assigned to these models, meaning that the two formulation options presented in Chapter 3 converge. Models for ten monovalent and four divalent ions are presented. In Chapter 5, attention is returned to the electrolyte formulations of the SAFT-γ Mie EOS. The two methodologies are used to develop two sets of models for the functional groups required in the description of sodium carboxylate salts.

Carboxylate anions with alkyl chain lengths ranging from C2 to C6 are considered. The methodologies are compared with respect to the adequacy of the performance of each set of models at describing the thermodynamic properties of aqueous solutions of these salts. Having selected an appropriate electrolyte group-contribution formulation for SAFT-γ Mie, the approach is applied in Chapter 6 to model aqueous solutions of weak acids. In particular, sulphuric acid and nitric acid are studied by developing models for the sulphate, bisulphate, and nitrate anions. The chapter concludes with a study of ion-pairing phenomena in aqueous alkali nitrate salts. Finally, Chapter 7 provides an overview of the outcomes of this thesis, together with the projected outlook for further work based on these findings.

Chapter 2

Theory of electrolyte solutions and their thermodynamic modelling

The dissolution of electrolytes in a polar solvent can substantially alter the thermodynamic properties of the fluid mixture, as the charged ionic components introduce strong electrostatic interactions in the system. In this chapter, the behaviour of electrolyte substances is presented with respect to the relevant chemical equilibria in solution, and the dominant theories for describing electrostatic interactions in electrolyte solutions are discussed. A review of thermodynamic models developed to describe the behaviour of mixtures containing electrolytes is presented, with particular attention devoted to models based on SAFT approaches.

2.1 Classification of electrolytes

2.1.1 Thermodynamic reaction equilibrium

Electrolytes in solution undergo dissociation into their constituent ions, and this speciation process can be treated as a reversible reaction with an associated equilibrium constant:

$$\mathrm{M}_{\nu_+}\mathrm{X}_{\nu_-} \overset{K_{\mathrm{eq}}}{\rightleftharpoons} \nu_+\mathrm{M}^{z_+} + \nu_-\mathrm{X}^{z_-}. \tag{2.1}$$

The salt $\mathrm{M}_{\nu_+}\mathrm{X}_{\nu_-}$ dissociates into the cation M^{z_+} of valency z_+ and the anion X^{z_-} of valency z_- with a stoichiometry $\nu_+ : \nu_-$. The extent to which the electrolyte dissociates is related to the thermodynamic equilibrium constant K_{eq}, which determines the thermodynamic state at which the Gibbs free energy G of the system is minimised at specified conditions of temperature and pressure.

The change in the total Gibbs free energy of a system as a result of a change in the system's composition at constant temperature T and pressure p is obtained as [33]

$$\mathrm{d}G\big|_{T,p} = \sum_{i=1}^{N_{\mathrm{C}}} \mu_i(T,p,\mathbf{N})\mathrm{d}n_i\,, \tag{2.2}$$

where μ_i is the chemical potential (or partial molar Gibbs free energy) of component i and n_i is the number of moles of component i. The total number of components in the system is denoted N_{C} and $\mathbf{N}$ is the mixture's composition vector. The change in amount of a species i can be written as $\mathrm{d}n_i = \nu_i \mathrm{d}\xi$, where ξ is the extent of reaction and ν_i is the stoichiometric coefficient of species i. The reaction Gibbs free energy $\Delta_{\mathrm{r}}G$ is defined as the change in G with respect to the change in the extent of reaction:

$$\Delta_{\mathrm{r}}G(T,p) = \left(\frac{\partial G}{\partial \xi}\right)_{T,p} = \sum_{i=1}^{N_{\mathrm{C}}} \nu_i \mu_i(T,p,\mathbf{N})\,, \tag{2.3}$$

and the condition for chemical equilibrium is that $\partial G/\partial \xi = 0$ such that $\Delta_r G(T,p) = 0$.

The chemical potential of a species i at a specified temperature and pressure is generally written as a deviation from a known reference state:

$$\mu_i(T,p,\mathbf{N}) = \tilde{\mu}_i\left(T,p,\tilde{\mathbf{N}}\right) + RT\ln\left[a_i(T,p,\mathbf{N})\right], \tag{2.4}$$

where $\tilde{\mu}_i$ is the chemical potential of component i at the chosen reference state with composition $\tilde{\mathbf{N}}$, a_i is the activity of i at the system composition, and R is the ideal gas constant. The reaction Gibbs free energy can thus be written by expanding the chemical potential:

$$\Delta_r G(T,p) = \sum_{i=1}^{N_C} \nu_i \tilde{\mu}_i\left(T,p,\tilde{\mathbf{N}}\right) + RT\ln\prod_{i=1}^{N_C}\left(a_i(T,p,\mathbf{N})\right)^{\nu_i} . \tag{2.5}$$

The first term in Equation 2.5 corresponds to the standard reaction Gibbs free energy $\Delta_r G^{\oslash}$, while the product in the second term corresponds to the thermodynamic reaction quotient. When chemical equilibrium is satisfied by $\Delta_r G(T,p) = 0$, the reaction quotient is referred to as the thermodynamic equilibrium constant:

$$K_{eq}(T) = \prod_{i=1}^{N_C}\left(a_i(T,p,\mathbf{N})\right)^{\nu_i} . \tag{2.6}$$

2.1.2 Strong and weak electrolytes

Conventionally, electrolyte compounds are divided into two broad categories, namely 'strong' and 'weak' electrolytes, depending on their degree of dissociation in solution. Strong electrolytes are compounds whose dissociation in a solvent is complete, i.e., the reaction shown in Equation 2.1 is fully shifted towards the dissociated ions such that none of the molecular species is present in the solution mixture at equilibrium. Robinson and Stokes [34] classify such electrolytes in an equivalent manner as 'non-associated' electrolytes, characterised by "the absence of evidence of any lasting union between the ions" in solution.

The thermodynamic equilibrium constant used to characterise solvated strong electrolytes in equilibrium with the pure unsolvated molecular electrolyte is known as the solubility product K_{sp}; for a strong electrolyte $\mathrm{M}_{\nu_+}\mathrm{X}_{\nu_-}$ this is expressed as

$$K_{\mathrm{sp}}(T) = a_{\mathrm{M}^{z+}}(T,p,\mathbf{N})^{\nu_+}\, a_{\mathrm{X}^{z-}}(T,p,\mathbf{N})^{\nu_-} \ . \tag{2.7}$$

Compounds which only partially dissociate in solution are referred to as weak electrolytes. At equilibrium, solution mixtures of weak electrolytes contain the molecular (often covalently bonded) species as well as the solvated ions. Taking the example of a weak electrolyte $\mathrm{M}_{\nu_+}\mathrm{X}_{\nu_-}$, the thermodynamic equilibrium constant is

$$K_{\mathrm{eq}}(T) = \frac{a_{\mathrm{M}^{z+}}(T,p,\mathbf{N})^{\nu_+}\, a_{\mathrm{X}^{z-}}(T,p,\mathbf{N})^{\nu_-}}{a_{\mathrm{M}_{\nu_+}\mathrm{X}_{\nu_-}}(T,p,\mathbf{N})} \ . \tag{2.8}$$

Robinson and Stokes [34] classify weak electrolytes as one of two types of 'associated' electrolytes; the second type of 'associated' electrolytes are those exhibiting ion-pairing behaviour resulting from electrostatic attraction between oppositely charged ions. According to the theory of ion association proposed by Bjerrum [35], ions are considered to be paired when the potential energy resulting from the electrostatic forces between the ions effectively offsets the kinetic energy of random thermal motion [36]. Ion-pairing behaviour can further be subdivided into 'solvent-separated' ion pairs, in which each ion retains a distinct solvation shell; 'solvent-shared' ion pairs, where part of the solvation shells of the two ions overlap; and finally 'contact' ion pairs which consequently constitute a solvated dipolar species [36]; these are illustrated in Figure 2.1. The type of ion pair formed by an electrolyte in solution can be identified by experimental means such as Raman spectroscopy, which hence allows characterisation of the ion association equilibrium constant. Ion pairing can be exhibited by both weak and strong electrolytes at sufficiently high solute concentrations and high temperatures. This means that ion-pairing phenomena are of limited concern in the present work since the focus lies primarily on modelling electrolyte solutions at dilute and moderate concentrations. Nevertheless, the profound effect of ion pairing on the properties

of electrolytes solutions is assessed within the analysis of carboxylate salts in Chapter 5, and the modelling of weak acids and oxoanions in Chapter 6.

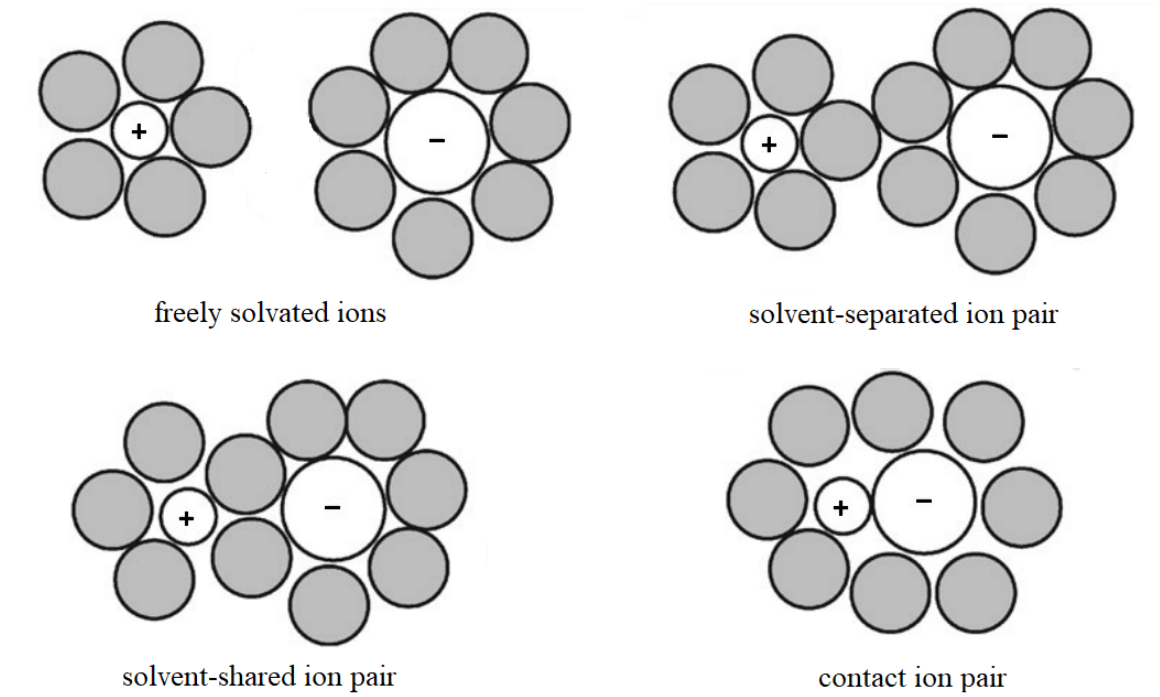

Figure 2.1 Schematic illustration of solvated electrolytes; solvent molecules are shown in grey and ions are shown in white. Ions in solution may be freely solvated or form ion pairs, including solvent-separated, solvent-shared, and contact ion pairs. The image has been adapted from Ref. [37].

2.2 Chemical potential and activity coefficients in electrolyte solutions

The activity of component i in a mixture is related to the concentration c_i (expressed in the units of choice) through the activity coefficient $\gamma_{i,c}$:

$$a_{i,c} = \frac{c_i}{c^\circ}\,\gamma_{i,c}\,, \tag{2.9}$$

where the subscript 'c' denotes that the magnitude of $\gamma_{i,c}$ is commensurate with the concentration scale chosen for c_i, and the standard concentration c° ensures that both the activity and activity coefficient are dimensionless quantities. The activity coefficient of component i is therefore defined relative to the chemical potential μ_i at given conditions of temperature, pressure, and mixture composition, by invoking Equation 2.4:

$$\mu_i\left(T,p,\mathbf{N}\right) = \tilde{\mu}_i\left(T,p,\tilde{\mathbf{N}}\right) + RT\ln\left[c_i\gamma_{i,c}\left(T,p,\mathbf{N}\right)\right] \ . \tag{2.10}$$

Depending on the nature of the system in question, it can be convenient to express the activity coefficient in one of a variety of ways as concerns both the reference state and the concentration scale. The standard *symmetrical* activity coefficient of component i is typically expressed in terms of the mole fraction, x_i, and the reference chemical potential is taken as that corresponding to the pure component i at the system temperature and pressure, i.e. $\tilde{\mu}_i\left(T,p,x_i=1\right) = \mu_i^0\left(T,p\right)$, where the superscript '0' denotes a pure component. The symmetrical activity coefficient can therefore be obtained from [38, 39]

$$\begin{aligned}\mu_i\left(T,p,\mathbf{N}\right) &= \mu_i^0\left(T,p\right) + RT\ln\left[x_i\gamma_{i,x}\left(T,p,\mathbf{N}\right)\right] \\ &= \mu_i^0\left(T,p\right) + RT\ln\left[a_{i,x}\left(T,p,\mathbf{N}\right)\right] \ ,\end{aligned} \tag{2.11}$$

and it is commonly used for components whose pure reference state is well-defined.

As a result of the constraint of electroneutrality, a pure ion cannot exist in isolation and therefore ionic species cannot be related meaningfully to the pure system. The chemical potential of ions is therefore expressed by employing an *asymmetric* convention [39, 40], whereby the activity coefficient of the ion at the specified system conditions is normalised relative to its activity coefficient at infinite dilution:

$$\gamma_{i,*}(T,p,\mathbf{N}) = \frac{\gamma_{i,x}(T,p,\mathbf{N})}{\gamma_{i,x}(T,p,\mathbf{N}^*)} \ . \tag{2.12}$$

The composition vector $\mathbf{N}^*$ corresponds to ion i infinitely diluted in solvent j, i.e., a mixture where $x_i \to 0$ and $x_j \to 1$. According to this normalisation, known as the *rational asymmetric* scale [41], the activity coefficient of an ion has a value of one in the limit of infinite dilution of the ion ($x_i \to 0 \Rightarrow \gamma_{i,*} \to 1$), thereby providing a practical reference state for the ionic species. The asymmetric reference chemical potential for ions is taken as that corresponding to the infinitely dilute solution of ion i [38]:

$$\tilde{\mu}_i(T,p,\mathbf{N}^*) \equiv \mu_i^0(T,p) + RT\ln\gamma_{i,x}(T,p,\mathbf{N}^*)\,. \tag{2.13}$$

The chemical potential of ionic species is therefore expressed as:

$$\begin{aligned}\mu_i(T,p,\mathbf{N}) &= \tilde{\mu}_i(T,p,\mathbf{N}^*) + RT\ln\left[x_i\gamma_{i,*}(T,p,\mathbf{N})\right] \\ &= \tilde{\mu}_i(T,p,\mathbf{N}^*) + RT\ln a_{i,*}(T,p,\mathbf{N})\,,\end{aligned} \tag{2.14}$$

where $a_{i,*}$ is the rational asymmetric activity of the ion.

Properties of ions are conventionally reported with reference to the molality concentration of the electrolyte solution. The *molal-based* scale (denoted by the subscript m) for reporting the activity coefficients of ions, $\gamma_{i,m}$, employs the convention of a hypothetical ideal solution at unit molality such that $m_i \to 1 \Rightarrow \gamma_{i,m} \to 1$. Assuming a solution involving a single solvent j, conversion between the mole fraction scale and the molality scale concentrations is achieved through [41]:

$$x_i = m_i x_j MW_j\,, \tag{2.15}$$

where MW_j is the molecular weight of solvent j. Equation 2.14 can hence be rewritten as:

$$\mu_i(T,p,\mathbf{N}) = \tilde{\mu}_i(T,p,\mathbf{N}^*) + RT\ln\left[MW_j m^\circ\right] + RT\ln\left[\frac{m_i x_j \gamma_{i,*}(T,p,\mathbf{N})}{m^\circ}\right], \tag{2.16}$$

where the unit molality $m^\circ = 1$ mol kg^{-1} (corresponding to the mixture composition vector $\mathbf{m}^\circ$) has been introduced to maintain the activity dimensionless when separating the residual

term. The reference state chemical potential at unit molality can thus be expressed as:

$$\begin{aligned}\mu_i^{\circ}(T,p,\mathbf{m}^{\circ}) &= \tilde{\mu}_i(T,p,\mathbf{N}^*) + RT\ln\left[MW_j m^{\circ}\right] \\ &= \mu_i^0(T,p) + RT\ln\left[MW_j m^{\circ}\gamma_{i,*}(T,p,\mathbf{N}^*)\right] \ . \end{aligned} \tag{2.17}$$

Bearing in mind that the magnitude of the chemical potential is unaffected by the concentration scale adopted (i.e., $\mu_i(T,p,\mathbf{m}) \equiv \mu_i(T,p,\mathbf{N})$ provided that the vectors **m** and **N** correspond to the same mixture composition), the chemical potential of an ion written on the molal-based scale is

$$\mu_i(T,p,\mathbf{m}) = \mu_i^{\circ}(T,p,\mathbf{m}^{\circ}) + RT\ln\left[\frac{m_i\gamma_{i,m}(T,p,\mathbf{N})}{m^{\circ}}\right] \ . \tag{2.18}$$

The conversion between the rational asymmetric mole fraction-based scale and the molal-based scale follows as [41]

$$\gamma_{i,m} = x_j\gamma_{i,*} \ . \tag{2.19}$$

2.2.1 The chemical potential of a salt

The chemical potential of a dissociated salt in solution may be expressed as a sum of the chemical potentials of its constituent ions. In the case of a salt $M_{\nu_+}X_{\nu_-}$ dissociating according to Equation 2.1 to form ions M^{z+} and X^{z-}, its chemical potential is obtained by

$$\mu_{M_{\nu_+}X_{\nu_-}}(T,p,\mathbf{N}) = \nu_+\mu_+(T,p,\mathbf{N}) + \nu_-\mu_-(T,p,\mathbf{N}) \ . \tag{2.20}$$

By expressing the chemical potential on the molal-based scale and simplifying Equation 2.18 by omitting m°, the salt's chemical potential can be written as

$$\begin{aligned}\mu_{\mathrm{M}_{\nu_+}\mathrm{X}_{\nu_-}} =& \mu_+^\circ(T,p,\mathbf{m}^\circ) + \mu_-^\circ(T,p,\mathbf{m}^\circ) + RT\ln\left(m_+^{\nu_+} m_-^{\nu_-}\right) \\ &+ RT\ln\left[\left(\gamma_{+,m}(T,p,\mathbf{N})\right)^{\nu_+}\left(\gamma_{-,m}(T,p,\mathbf{N})\right)^{\nu_-}\right] .\end{aligned} \tag{2.21}$$

Accordingly, the molal-scale mean ionic activity coefficient (MIAC) of the salt, $\gamma_{\pm,m}$, is defined as

$$\gamma_{\pm,m} \equiv \left[\left(\gamma_{+,m}(T,p,\mathbf{N})\right)^{\nu_+}\left(\gamma_{-,m}(T,p,\mathbf{N})\right)^{\nu_-}\right]^{(1/\nu)} , \tag{2.22}$$

where $\nu = \nu_+ + \nu_-$ is the sum of the ions' stoichiometric coefficients. The MIAC conveniently collates the properties of the salt's constituent ions into a single quantity which can be obtained experimentally, e.g., via electromotive force measurements, thus overcoming the limitation of not being able to measure the activities of individual ions.

The mean ionic activity coefficient accentuates the deviation from ideal behaviour of the electrolyte solute by augmenting the variation of the activity coefficients of the ions through knowledge of the solution's ionic composition. In a solution of a strong electrolyte with molal composition m_{salt}, the concentration of an ion i will be $m_i = \nu_i m_{\mathrm{salt}}$; however, the ionic composition in a solution of a weak electrolyte is not determined in straightforward fashion. Experimental data of the MIAC for solutions of weak electrolytes are conventionally reported as *stoichiometric* quantities, $\gamma_{\pm,m}^{\mathrm{stoich.}}$, as a means of circumventing the complexity of experimentally determining the actual solution composition, which would be required in order to determine the 'real' values of these properties in accordance with Equation 2.21. The stoichiometric definition adopts the assumption that the concentration of the constituent ions in solution is equal to what it would be if the electrolyte were completely dissociated. The stoichiometric and real MIAC are related through the relationship:

$$m_+^{\nu_+} m_-^{\nu_-}\left(\gamma_{\pm,m}\right)^{\nu} = (\nu_+ m_{\mathrm{salt}})^{\nu_+}(\nu_- m_{\mathrm{salt}})^{\nu_-}\left(\gamma_{\pm,m}^{\mathrm{stoich.}}\right)^{\nu} . \tag{2.23}$$

It follows that the real and stoichiometric MIAC are equivalent for solutions of strong electrolytes.

2.2.2 The osmotic coefficient

The chemical potential of a neutral solvent species in a mixture is given by Equation 2.11 with the activity coefficient expressed on the symmetric scale. The activity of the solvent is usually rescaled as the osmotic coefficient, Φ, in order to accentuate its variation in the region of low solute concentrations, where the solution deviates more from ideal-fluid behaviour. In a single-solvent solution, the osmotic coefficient is related to the activity of solvent j through

$$\Phi\left(T,p,\mathbf{N}\right) = -\frac{1}{\sum_{i=1}^{n_{\text{ion}}}(m_i)MW_j}\ln a_j\left(T,p,\mathbf{N}\right)\,, \tag{2.24}$$

where n_{ion} is the number of types of ions in the solution and MW_j is the molecular weight of solvent j.

Relating the activity of the solvent to the osmotic coefficient of the solution requires knowledge of the mixture composition, leading to a similar practical limitation for weak electrolytes as has been discussed above for the MIAC. Therefore, for solutions of weak electrolytes, the osmotic coefficient is reported as a stoichiometric quantity assuming that the composition of each ion in the solution mixture is equal to the stoichiometric composition which would arise from complete dissociation. As with the MIAC, the real and stoichiometric osmotic coefficients are equivalent for strong electrolytes. The stoichiometric osmotic coefficient of a single-salt solution is obtained as follows:

$$\Phi^{\text{stoich.}}\left(T,p,\mathbf{N}\right) = -\frac{1}{\left(\nu_+ + \nu_-\right)m_{\text{salt}}MW_j}\ln a_j\left(T,p,\mathbf{N}\right)\,. \tag{2.25}$$

In a given solution mixture, the properties of the solvents and solutes are not independent and must fulfil the Gibbs-Dühem relation, which relates the changes in chemical potential to the change in temperature and pressure. The osmotic coefficient and MIAC are related

through the following relationship [39]:

$$\ln \gamma_{\pm,m} = \Phi - 1 + \int_0^{m_{\text{salt}}} \frac{(\Phi - 1)}{m_{\text{salt}}} \mathrm{d}m_{\text{salt}} \,. \tag{2.26}$$

2.2.3 Obtaining activity coefficients from an equation of state

The expressions for the chemical potentials of both neutral and ionic species, given respectively in Equations 2.11 and 2.14, are expressed in terms of pressure as the independent variable, in line with the manner in which thermodynamic properties tend to be measured and reported. Equations of state such as the variants of the SAFT EOS are typically expressed with volume as the independent variable, thereby requiring a conversion between the two ensembles in order to compute the activity coefficients at specified conditions of temperature, pressure, and composition.

The symmetric activity coefficient $\gamma_{i,x}$ of a component i in a mixture of defined composition is related to its fugacity coefficient φ_i in the mixture and its fugacity coefficient φ_i^0 in the pure state, at the same temperature and pressure [42]:

$$\gamma_{i,x}(T, p, \mathbf{N}) = \frac{\varphi_i(T, p, \mathbf{N})}{\varphi_i^0(T, p)} \,. \tag{2.27}$$

The fugacity coefficient is related to the fugacity f_i of the species in the mixture [33],

$$f_i(T, p, \mathbf{N}) = p x_i \varphi_i(T, p, \mathbf{N}) \,, \tag{2.28}$$

which in turn is obtained as a function of the chemical potential of component i [39]:

$$f_i(T, p, \mathbf{N}) = p x_i \exp\left[\frac{\mu_i(T, p, \mathbf{N}) - \mu_i^{\text{ideal}}(T, p, \mathbf{N})}{RT}\right] \,. \tag{2.29}$$

The residual chemical potential is obtained when the chemical potential of component i at specified temperature, pressure, and composition is defined with reference to that of the ideal gas mixture at the same conditions:

$$\mu_i^{\mathrm{res}}(T,p,\mathbf{N}) = \mu_i(T,p,\mathbf{N}) - \mu_i^{\mathrm{ideal}}(T,p,\mathbf{N}) \tag{2.30}$$

It thereby follows that the fugacity coefficient can be written as

$$\ln\varphi_i(T,p,\mathbf{N}) = \frac{\mu_i^{\mathrm{res}}(T,p,\mathbf{N})}{RT}\,. \tag{2.31}$$

In order to obtain $\varphi_i(T,p,\mathbf{N})$ using an equation of state written as a function of T, V, and $\mathbf{N}$, one may invoke the following relation [38]:

$$\mu_i^{\mathrm{res}}(T,p,\mathbf{N}) = \mu_i^{\mathrm{res}}(T,V_p,\mathbf{N}) - RT\ln Z\,, \tag{2.32}$$

where V_p is the volume corresponding to the specified pressure p, and Z is the compressibility factor:

$$Z = \frac{pV_p}{nRT}\,. \tag{2.33}$$

The fugacity coefficient at specified $(T,p,\mathbf{N})$ is therefore related to the residual chemical potential at the corresponding $(T,V_p,\mathbf{N})$ through

$$\varphi_i(T,p,\mathbf{N}) = \frac{1}{Z}\exp\left(\frac{\mu_i^{\mathrm{res}}(T,V_p,\mathbf{N})}{RT}\right)\,. \tag{2.34}$$

The residual chemical potential of component i is defined as the derivative of the residual Helmholtz free energy A^{res} (given by an equation of state) with respect to the total number of particles of type i, N_i:

$$\mu_i^{\mathrm{res}}(T,V_p,\mathbf{N}) = \left.\frac{\partial A^{\mathrm{res}}(T,V_p,\mathbf{N})}{\partial N_i}\right|_{T,V,N_{j\neq i}}\,. \tag{2.35}$$

Applying Equations 2.34 and 2.35 to the case of a system composed of pure component i returns $\varphi_i^0(T,p)$, and therefore the activity coefficient of a neutral component may be determined through Equation 2.27. For ionic species present in a fluid mixture, the rational asymmetric activity coefficient is related to the ion's fugacity coefficient at infinite dilution [41]:

$$\gamma_{i,*}(T,p,\mathbf{N}) = \frac{\varphi_i(T,p,\mathbf{N})}{\varphi_i(T,p,\mathbf{N}^*)}, \tag{2.36}$$

in which case $\varphi_i(T,p,\mathbf{N}^*)$ can again be obtained by applying Equation 2.34.

2.3 Particle interactions in electrolyte systems

Particles in an electrolyte solution will experience both electrostatic and non-electrostatic interactions, which will both contribute to the overall intermolecular potential, u^{total}. Electrostatic contributions to u^{total} result from long-range Coulombic interactions between ionic species; these electrostatic interactions are screened by the solvent molecules surrounding the individual ions. The non-electrostatic contributions arise from short-range dispersive and, depending on the nature of the electrolyte and solvent, directional physical interactions such as hydrogen bonding. The formation of a hydrogen bond arises from the approach of a partial positive charge on an H atom and the partial negative charge on an atom that possesses a lone pair of electrons; the latter is usually an N, O, or F atom, but in principle an anionic species (such as Cl^-) may also participate in hydrogen bonding [43]. The complexity of hydrogen bonding is reduced in this work by considering only such interactions of type O–H$\cdots$O, i.e. hydrogen bonding is only applied between water molecules and between oxoanions and water. Hydrogen bonding is directional and necessitates the spatial proximity of the participating species, as electrostatic interactions arising from partial charges act over a short range. For this reason, hydrogen bonding is treated distinctly from the comparatively

long-range and non-directional Coulombic interactions. When polar solvents are involved, one must also consider the polar interactions between the solvent molecules and the electrostatic ion–solvent interactions arising as a consequence of the solvent molecules' permanent or ion-induced dipole. Such ion–dipole interactions together with any ion–solvent hydrogen bonding will determine the solvation of the electrolyte solute [44]. Due to their long range, Coulombic interactions are particularly important in dilute solutions where their effect will dominate, causing the behaviour of electrolyte solutions to be markedly non-ideal even at low ion concentrations [41]. Short-range dispersion forces and association interactions among ions and solvent molecules become increasingly significant at higher ion concentrations, again resulting in non-ideal mixtures as the three types of interactions are simultaneously manifested to a large extent.

Thermodynamic models for fluids containing electrolytes typically treat the long-range electrostatic interactions distinctly from short-range directional interactions, by coupling a theory for electrostatic interactions with a separate framework for the neutral species. This distinction is practical, as the most prevalent theories for ionic interactions are so-called 'primitive' theories which eliminate the explicit representation of the solvent and introduce in its place a uniform dielectric medium. 'Non-primitive' electrolyte theories, by contrast, treat the solvent molecules explicitly by including a description of the interactions between ions and dipolar molecules in addition to the ion–ion electrostatic interactions. This type of approach is less commonly used in thermodynamic modelling of electrolytes due to the additional effort required to describe the dipole moment of individual molecules as compared to imposing a dielectric continuum. The two dominant theories for modelling electrolytes are in fact primitive models, namely the earlier Debye-Hückel theory [45] and the more recent Mean Spherical Approximation (MSA) [46–48], both of which are further discussed in the next section.

2.4 Theories for electrostatic interactions in the fluid phase

The Debye-Hückel and MSA theories describe the electrostatic interactions between charged species in a dielectric medium by means of the Coulombic pair potential between two point charges, $q_i = z_i e$ and $q_j = z_j e$, given by:

$$u_{ij}^{\text{Coulomb}}(r) = \frac{z_i z_j e^2}{4\pi\epsilon_0 D r_{ij}}, \tag{2.37}$$

where r_{ij} is the separation distance, z is the valency of the ion, ϵ_0 is the permittivity of vacuum, and D is the dielectric constant (relative static permittivity) of the medium. The theories differ in two main respects: firstly, in their description of the ionic species' geometry, and consequently in terms of their approach to obtaining the radial distribution function for the fluid.

The Debye-Hückel theory represents ions as point charges q_i with a defined distance of closest approach d_i characterising the radius of a spherical volume. As d_i is an ion-specific parameter, the ions can take distinct 'sizes'. Debye and Hückel approximated the radial distribution function of the ions as a Boltzmann distribution and, by solving the linearized Poisson–Boltzmann equation, arrived at an expression for the excess Helmholtz energy arising from the electrostatic forces between point charges. The resultant closed analytical theory is exact in the limit of infinite dilution, however it is only valid at low concentrations.

The MSA approach for electrolytes differs from the Debye-Hückel approach in that the ions are modelled as hard spheres with a diameter σ_i and a central charge q_i. The fact that ion sizes are explicitly taken into account gives a better description of the fluid which thus renders it applicable to higher ion concentrations. The MSA model for charged spheres was first presented by Waisman and Lebowitz [46] as a restricted primitive model (MSA-RPM) where ions are considered to be of the same size. Blum and Hoye [47, 48] subsequently

generalised the theory by allowing asymmetric ion diameters (MSA-PM). This unrestricted version of the MSA finds more practical application in thermodynamic modelling, as it allows electrolytes to be modelled with ion-specific parameters. The MSA theory has also been presented within a non-primitive framework by Blum and Wei [49, 50], in which the interactions between the ions and the dipolar fluid are taken into account in order to emulate the effects of solvation.

As has already been noted, the Debye-Hückel and MSA theories must be used in combination with other theories for short-range interactions in order to obtain a complete description of the fluid, hence sparking a debate as to which theory should be used for this purpose. It is generally expected [51, 52] that the MSA will provide a better performance over a wider range of electrolyte concentrations up to high ion concentrations, owing to the hard-sphere contribution of the MSA which is absent in the Debye-Hückel theory [53]. A comprehensive analysis by Maribo-Mogensen et al. [54] in which the MSA-PM and the Debye-Hückel theories are compared with respect to the temperature, volume, and compositional derivatives of the Helmholtz energy, has demonstrated that both theories perform similarly in reproducing the properties of strong electrolyte solutions for concentrations up to 5 molal. The authors argue that neither theory can be considered superior provided that the model parameters are treated as adjustable. However, Gil-Villegas and co-workers [55, 56] have shown that if the sizes of the ions are set to specific values, the MSA-PM approach tends to give a better description for the solution properties compared to the Debye-Hückel theory, even at low electrolyte concentrations.

A theory commonly used alongside the Debye-Hückel or MSA in thermodynamic models for electrolytes is the Born solvation model [57], the proposal of which in fact precedes these electrostatic theories. The Born theory is a primitive model which describes the change in Helmholtz free energy due to transferring an ion from vacuum to a spherical cavity inside a dielectric medium. The free energy computed by the Born theory is commonly referred to as the ‘solvation energy’, however it must be noted it only covers one aspect of ion solvation and does not consider changes to the structure of the fluid due to any short- or long-range

intermolecular interactions. Although the necessity of including the Born solvation energy in thermodynamic modelling of electrolytes has been disputed in the past [58, 59], more recent modelling efforts have found the contribution significant in improving the thermodynamic consistency of modelling approaches [60–62].

2.5 Thermodynamic modelling of electrolyte solutions

A broad range of thermodynamic models have been extended with either the Debye-Hückel or MSA theories in order to make them applicable to electrolyte solution mixtures. Some prominent implementations will be discussed here; these may be broadly categorised as either models based on activity coefficient approaches or models based on equation-of-state approaches. Beyond the fundamental divisions arising from the chosen theory for electrostatic interactions and the base model applied for the non-electrostatic interactions, these approaches also differ in the type of modelling strategies. Two types of strategies have been applied for characterising model parameters for electrolytes: models defined with respect to the dissociated solvated ions are referred to as 'ion-specific', whereas models defined with respect to the molecular electrolyte are said to be 'salt-specific'. Thermodynamic models for electrolytes employing a salt-specific approach tend to produce results that are more accurate since parameters are optimised directly from experimental data of the corresponding salt [63]. On the other hand, ion-specific models offer the possibility of transferring the optimised ion parameters to any salt of which they are a constituent, thus minimising the parameter optimisation effort and providing the prospect of greater predictive power. This constitutes a significant advantage, as this approach allows one to make predictions for electrolytes for which no data are available.

2.5.1 Activity coefficient models

Activity coefficient models are semi-empirical models which express the activity coefficients of the species in a mixture as a function of temperature and composition at a fixed pressure. Being independent of pressure, these models are intrinsically limited to describing the liquid phase, which means that an alternative treatment of the vapour phase needs to be applied alongside the activity coefficient model. In such approaches, ionic species are excluded from the vapour phase so that it may be modelled using an equation of state. Despite this apparent limitation, activity coefficient models are widely used in engineering applications with considerable success [64]. Owing to the large number of parameters involved in activity coefficient modelling approaches, the properties of electrolyte solutions can be reproduced with high accuracy over a wide range of temperatures and solution compositions; however, these models lack any predictive capability.

The activity coefficient model of Pitzer [65] is one of the most widely used activity coefficient models for describing the thermodynamic properties of electrolytes. The Pitzer model is a modification of the Debye-Hückel theory that includes short-range hard-sphere contributions to the free energy of the mixture, thus allowing the theory to be applied beyond the limit of dilute solutions to which the Debye-Hückel model is best suited [66]. The model has been applied to systems of single and mixed strong electrolytes [67, 68], as well as weak electrolytes by including a description of the dissociation equilibria [69–72]. Among the abundant work employing the Pitzer model, its capability is perhaps best exemplified by the work of Kim and Frederick Jr [73, 74], in which model parameters for a total of 353 aqueous electrolyte solutions are presented.

Models for electrolytes have also been developed by combining the Debye-Hückel theory with local-composition activity coefficient models. These have included the non-random two-liquid (NRTL) model of Renon and Prausnitz [75] and the UNIQUAC (universal quasi-chemical) model of Abrams and Prausnitz [76], both of which are based on the quasi-

chemical theory proposed by Guggenheim [77, 78], as well as the UNIFAC (UNIQUAC functional-group activity coefficient) group-contribution model developed by Frendenslund et al. [79].

The electrolyte-NRTL (e-NRTL) model was developed by Chen et al. [80]; these authors incorporated the Debye-Hückel term and modified the local-composition conditions for the ionic species in order to account for local electroneutrality. First applied to single-salt, single-solvent solutions of strong electrolytes [80] using salt-specific parameters, the e-NRTL model was later extended for mixed-electrolyte and mixed-solvent systems [81–83] by including the solvent–solvent and solvent–ion interactions. In order to apply the e-NRTL model to multicomponent systems, binary interaction parameters for each pair of salt components must be obtained using experimental data of systems containing the specific combination of salts. Weak electrolytes have also been described using e-NRTL, for example in the work of Austgen et al. [84], while Posey and Rochelle [85] have used e-NRTL to obtain fair predictions of the pH of electrolyte mixtures.

Christensen et al. [86] presented an electrolyte-UNIQUAC model for strong electrolytes in pure and mixed solvents by combining the UNIQUAC equation with a Debye-Hückel term and employing an ion-specific modelling scheme. Sander et al. [87] modified the electrolyte-UNIQUAC model of Christensen et al. [86] to include concentration-dependent parameters, and used the model to represent salt effects on the vapour-liquid equilibria of ternary alcohol-water-salt mixtures. Nicolaisen et al. [88] have presented a simplified version of the model of Sander et al. [87] which requires only binary interaction parameters with no concentration dependence. Nicolaisen et al.'s simplified model was extended by Thomsen et al. [89] to also account for the thermal properties of mixtures, thereby adding the capability to describe solid-liquid equilibria and heat capacities of aqueous solutions of strong electrolytes. Thomsen and Rasmussen [90] used this model to describe the liquid phase while using the Soave-Redlich-Kwong (SRK) EOS [91] for the vapour phase, and applied the resultant approach to ternary mixtures containing mixed weak electrolytes to obtain fair agreement with experiment for vapour-liquid and solid-liquid equilibria, as well as thermal

properties. Retaining the form of the extended UNIQUAC, Thomsen [92] later proposed an improved method for obtaining the model parameters, with which a good representation of vapour-liquid, liquid-liquid, and solid-liquid equilibria, and thermal properties for a range of strong and weak electrolyte solutions were obtained.

Despite the high-quality performance of the various electrolyte-UNIQUAC models, the problem of requiring extensive experimental data persists. For example, for a five-component electrolyte system investigated by Kaewsichan et al. [93], estimation of the binary interaction parameters required binary, ternary, and quaternary system VLE data. Such an effort in the parameter estimation can be reduced using a group-contribution approach, such as UNIFAC, which allows for an increased predictive capability through the use of transferable parameters. A UNIFAC model for electrolytes (e-UNIFAC) was developed by Kikic and Fermeglia [94] by adopting the approach of Sander et al. [87]; the resulting e-UNIFAC model has concentration-independent group interaction parameters, and the ions are represented as individual groups. The original e-UNIFAC model has seen a number of modifications which have effected an enhanced performance with respect to the phase behaviour of mixed-solvent solutions of strong electrolytes. In the work of Achard et al. [95], for example, solvation equations were included to account for the hydration of ions. Yan et al. [96] introduced an additional term to represent the ion-dipole interactions, while also simplifying the UNIFAC contribution by neglecting the ion-solvent and ion-ion short-rnage interactions, such that these are only accounted for in the Debye-Hückel term.

2.5.2 Equation of state models

Equations of state provide unified thermodynamic models that can be used to treat all phases and species in a system. Unlike activity coefficient models, they are less constrained in their range of application and they can be used to obtain thermodynamic properties beyond those accessible from activity coefficients. Furthermore, model parameters associated with equation-of-state approaches are fewer than those required by activity coefficient models,

while they also tend to be associated with clearer physical meanings, hence their value can be assessed for correctness and their influence can be tested independently. For these reasons, equations of state provide a more attractive framework for developing predictive models for electrolytes.

Electrolyte models have been proposed within the framework of classical cubic equations of state and Cubic-Plus-Association (CPA) approaches, as well as equations of state based on statistical mechanics, such as the Perturbed Anisotropic Chain Theory (PACT) and variants of the SAFT approach. In each approach, the number and type of parameters vary, as does the choice of theory for the ionic interactions, therefore a direct comparison of the approaches would be unfair. It is not surprising, however, that due to the explicit treatment of the solvent's intermolecular association interactions, approaches based on CPA or SAFT have been among the most popular.

One of the earliest electrolyte models based on a cubic equation of state was proposed by Furst and Renon [97]; this model coupled the MSA-PM approach with a version of the SRK EOS given by Schwartzentruber et al. [98], to which an additional short-range term for non-electrostatic ion–ion interactions (called the SR2 term) was added so as to account for solvation effects. The model was found to be successful in describing excess properties of multi-component strong electrolyte solutions using adjustable ion-specific parameters [99, 100]. Myers et al. [51] also extended the Peng-Robinson (PR) EOS [101] with the MSA-PM and also the Born theory for including the effects of solvation. The resultant model involved salt-specific parameters and gave good descriptions of the properties of the 138 aqueous salt solutions considered.

A turning point in the use of cubic equations of state came with the advent of the Cubic-Plus-Association (CPA) approach proposed by Kontogeorgis et al. [102], according to which a cubic EOS is combined with a Wertheim association term. The particular CPA approach proposed by Kontogeorgis et al. [102] is based on the SRK EOS, and it has been extended to electrolyte systems by other authors through the implementation of either the MSA

and Debye-Hückel theories for representing the Coulombic contributions. Lin et al. [103] examined the possible variations of an electrolyte CPA model by assessing the use of the MSA-PM and Debye-Hückel theories and the optional inclusion of a Born term, implemented within a framework utilising ion-specific parameters. Shortly afterwards Inchekel et al. [60] supplemented this investigation by considering the Born energy contribution alongside the SR2 solvation term, finally proposing an electrolyte CPA EOS employing the MSA-PM and the Born term free-energy contributions. This implementation of the electrolyte CPA proposed by Inchekel et al. [60] was successfully applied by Courtial et al. [104] to model the phase behaviour of aqueous sodium chloride solutions containing carbon dioxide and methane at conditions of very high temperature and pressure. The most recent implementation of the electrolyte CPA EOS has been presented by Maribo-Mogensen et al. [105], who instead advocated the use of the Debye-Hückel theory together with the Born term. In this work, the authors implemented a highly accurate composition-dependent model [106, 107] for establishing the permittivity of the solvent medium, which significantly improved the description of the solvent medium and thus permitted the use of the simpler Debye-Hückel theory for the electrostatic interactions even at high ionic concentrations. This electrolyte CPA EOS has been extensively applied by Maribo-Mogensen et al. [105] and later Schlaikjer et al. [62] to describe an incredible range of multi-solvent, multi-component mixtures comprising strong electrolytes and non-electrolyte solutes, and has successfully described an array of phase-equilibrium properties.

Among statistical mechanical equations of state, the Perturbed Anisotropic Chain Theory (PACT) of Vimalchand and Donohue [108] was first applied to electrolyte systems in a series of publications by Jin and Donohue [109–111]. The PACT approach takes into account the solvent's multipolar interactions, to which Jin and Donohue [109] added ion–dipole and ion–induced dipole interactions, thus explicitly incorporating solvation effects. Electrostatic interactions among ions were incorporated using an MSA-PM approach, and a salt-specific modelling scheme with the ionic size treated as the only adjustable parameter was adopted for characterising the models. The comprehensive PACT EOS for electrolytes

was initially applied to model liquid phase properties for 50 aqueous solutions of strong electrolytes [109], followed by phase equilibrium properties for solutions of single volatile weak electrolytes [110]. Shifting to an ion-specific modelling scheme, Jin and Donohue [111] presented models for a range of monovalent and divalent ions and applied the PACT EOS to predict the solubilities of strong electrolytes in multi-salt aqueous solutions to a high degree of accuracy. The Associated Perturbed Anisotropic Chain Theory (APACT) [112, 113] – an extension of the PACT EOS for associating fluids – was subsequently used by Economou et al. [114] to model electrolytes solutions at conditions of elevated temperature and pressure, at which salts exist in solution predominantly as ion pairs rather than free solvated ions. At these thermodynamic conditions, Economou et al. [114] proposed that the ion pairs may be modelled as molecular species which posses a strong dipole moment and interact with solvent molecules through dipole–dipole and association interactions. Using this treatment, the properties of aqueous alkali metal halide solutions were predicted effectively in the range of 423–773 K, including vapour-liquid and solid-liquid-vapour equilibria.

The SAFT approach has been more commonly used as a basis for developing electrolyte models than other equation of state approaches. A contributor to its popularity is the existence of numerous variants of SAFT-based equations of state, which provide equally many avenues for proposing electrolytes models. Some dominant strains of work pertaining to electrolyte-SAFT models are discussed in the next section.

2.6 Extensions of SAFT for electrolyte mixtures

A substantial body of work on thermodynamic modelling of electrolytes with equations of state has been performed with variants of the Statistical Associating Fluid Theory. As will be discussed in Chapter 3, SAFT approaches provide a sound physical basis for modelling molecular interactions in fluid mixtures. Solvent components in particular are typically modelled well by SAFT approaches due to the ability to explicitly take into account polar

interactions and hydrogen bonding. An accurate representation of the solvent medium therefore provides a good foundation for modelling electrolyte solution mixtures.

Besides the various versions of SAFT which have been used as the base EOS, the various studies differ in the implementation of free energy perturbations relevant to electrolytes, i.e. the theories accounting for Coulombic forces, dipole-induced electrostatic interactions, and ion solvation effects. Firstly, the Helmholtz free energy contribution arising from Coulombic interactions between ionic species has been incorporated using either the Debye-Hückel theory or the MSA, in either the primitive or non-primitive model. Of these, Debye-Hückel theory has been a more common choice, although a critical assessment of the two theories by Maribo-Mogensen et al. [54] has suggested that no significant advantage of one over the other can be identified in practice. The same conclusion was reached by Gil-Villegas et al. [56], who compared the MSA and Debye-Hückel theory within a SAFT implementation.

Choices as to the treatment of ion solvation have further divided electrolyte-SAFT approaches. In primitive models, the Born contribution to the Helmholtz free energy is sometimes included to account for solvation effects. In solvent-explicit approaches, however, free energy changes due to solvation can be effected through polar ion–solvent interactions. A noteworthy simplification adopted in many SAFT modelling approaches for electrolytes is the omission of dispersion interactions between ions, aiming to reflect the prevalence of Coulombic forces affecting the ion–ion interactions. Furthermore, each approach using a primitive modelling framework tends to implement a distinct way of determining the dielectric constant of the solvent medium, leading to variation in the validity of the implicit model.

Some of the key implementations of SAFT-based equations of state for electrolytes are discussed below, focusing first on primitive and then on non-primitive implementations. The breadth of model variations is compounded by the choices made with regard to parameter estimation, such as whether to apply a salt-specific or ion-specific strategy, and which types of experimental data to employ. Common choices of experimental data used for parameterising

models are the solution density, vapour pressure, osmotic coefficient, and mean ionic activity coefficient. The MIAC in particular gives the closest indication of the thermodynamic behaviour of the solvated ionic species (cf. Equation 2.22). Of the EOS approaches described below, those which quantifiably report the model performance with respect to the MIAC are summarised in Table 2.1. The percentage average absolute deviation (%AAD) for this property can vary substantially, even among electrolyte solutions considered within a single study. Table 2.1 reports the average %AAD value for the particular solutions included in a given study, hence giving an indication of the performance achievable with these approaches.

Table 2.1 Reported performance of some SAFT-based EOS models with respect to the description of the MIAC for single-salt aqueous strong electrolyte solutions. All models included here have used data for the MIAC to optimise model parameters. The %AAD values correspond to the average value for the particular solutions studied in each work.

EOS	Ref.	Number of solutions	MIAC %AAD
SAFT	[31]	15	0.44
SAFT2	[115]	24	0.78
ePC-SAFT	[32]	106	9.17
PC-SAFT	[116]	16	1.28
PPC-SAFT	[117]	19	2.85
SAFT-VRE SW	[61]	15	4.07
SAFT2	[118]	8	2.14

2.6.1 Primitive electrolyte-SAFT models

The SAFT-VR family of equations has had several extensions to electrolyte systems, primarily through application of the MSA theory. Galindo et al. [55] presented the SAFT-VRE EOS, by coupling the MSA-RPM with the SAFT-VR EOS of Gil-Villegas and co-workers [119, 120], which assumes a square-well (SW) potential form to represent dispersive interactions.

Dispersion forces between only ion–solvent and solvent–solvent pairs were accounted for, while those between ions were neglected. Using ion-specific models, SAFT-VRE SW was used to study bulk phase properties of single-salt solutions of strong electrolytes, including liquid phase densities and vapour pressures, although more sensitive properties such as the MIAC were not assessed. Gil-Villegas et al. [56] later used the SAFT-VRE SW EOS to evaluate the application of associative interactions between ions and the solvent as a possible route to incorporate ion solvation effects, and also studied ion-pairing by means of association interactions. Finally, Patel et al. [121] applied the SAFT-VRE SW EOS to describe the salting out of *n*-alkanes in aqueous solutions of strong electrolytes up to high temperature and pressures, achieving reasonable predictions.

A later version of SAFT-VRE SW presented by Schreckenberg et al. [61] used the MSA-PM and considered the dispersion interactions between ions explicitly alongside the ion–solvent and solvent–solvent interactions. This SAFT-VRE SW implementation also included a Born energy contribution to the Helmholtz free energy, thus describing – albeit implicitly – the ion solvation effects which are otherwise not considered in the primitive MSA. In parallel to this, Schreckenberg et al. proposed a temperature- and density-dependent model for the relative static permittivity of the solvent. Following these developments, Dufal [122] proposed the SAFT-VRE Mie EOS by extending the SAFT-VR Mie EOS with the incorporation of the MSA-PM and Born energy contributions while also implementing the aforementioned static permittivity model. Both Schreckenberg et al. [61] and Dufal [122] applied, respectively, the SAFT-VRE SW and SAFT-VRE Mie EOS to strong electrolytes, modelling multi-salt and multi-solvent (water + alcohol) brines up to high temperatures and concentrations.

Behzadi et al. [123, 124] paired the unrestricted MSA-PM with a SAFT-VR EOS employing the Yukawa intermolecular potential. Single- and multi-salt solutions of strong electrolytes in aqueous and alcohol solvents were examined using three separate modelling strategies: ion-specific, cation-specific, and salt-specific. Of these strategies, the salt-specific approach was found to yield models which perform better at higher salt concentrations.

This is a reasonable outcome considering that the parameterisation of salt-specific models intrinsically incorporates the effects on macroscopic properties brought about by increased occurrence of ion-pairing at higher concentrations.

In a separate line of work, Tan et al. [125, 126] presented the SAFT1-RPM and SAFT2 equations of state for electrolytes, based on the square-well SAFT1 EOS of Adidharma and Radosz [127]. Both SAFT1-RPM and SAFT2 apply the restricted primitive MSA and incorporate a temperature-dependent model for the relative static permittivity. These approaches model ions as hard spheres, neglecting ion–ion dispersion interactions. A salt-specific ionic size parameter was included as part of implementing the RPM, and the ion model parameters were assigned a temperature dependence; both these factors contributed to very good model performance within the temperature range studied. Though Tan and co-workers [125, 126] considered single-salt solutions, SAFT1-RPM and SAFT2 were later applied to aqueous multi-salt brines by Ji et al. [115, 128]. Due to the salt-specific modelling strategy, an additional adjustable parameter was required to characterise pairs of salts. In subsequent applications of SAFT2 by Ji and Adidharma [129, 130, 131], an ion-specific modelling strategy was adopted, and it was found that the inclusion of ion–ion dispersion interactions were needed in order to extend the application of the EOS to high temperatures and pressures. This may be perceived as an indication that ion pairing is significant at such conditions. More recently, Jiang et al. [118] paired the SAFT2 EOS with the KMSA theory [132], which includes a density-dependent correction factor to the MSA-PM. Furthermore, the size of the anions was modelled as temperature-dependent in this work, which contributes to an improved description of the fluid density across a wider range of thermodynamic conditions. As a result, a fair reproduction of the thermodynamic properties of mixed strong electrolytes was achieved in the temperatures range of 298–473 K.

Extensive work on electrolyte modelling based on the PC-SAFT EOS has also been presented, typically coupled with the Debye-Hückel theory for incorporating ion–ion Coulombic interactions. Cameretti et al. [133] first proposed the ePC-SAFT EOS by extending PC-SAFT with the electrostatic contribution to the free energy obtained through the Debye-Hückel

theory. The temperature and pressure dependence of the dielectric constant of the solvent was neglected in this work, as were the dispersion forces between ions. A salt-specific parameterisation strategy was used, achieving a good description of bulk phase properties at moderate conditions of temperature and concentration. However, Held et al. [32] later showed that the approach led to unsatisfactory predictions for the MIAC, prompting the development of new models for the ePC-SAFT EOS using an ion-specific strategy [134]. This approach, together with the introduction of a temperature dependence to the size parameter of the solvent species, resulted in a better description of the MIAC. The models of Cameretti et al. [133] were also applied to mixed-solvent (water + alcohol) salt solutions by Held et al. [135], with the inclusion of a temperature- and composition-dependent model for the dielectric constant.

Unlike the ePC-SAFT approaches mentioned so far, other work for electrolytes within the PC-SAFT framework have included a consideration of ion solvation effects to some extent. Lee and Kim [116] modelled aqueous strong electrolytes with the PC-SAFT EOS by incorporating the MSA-PM and the Born energy contribution to the free energy, as well as including association interactions between all ions and the solvent. Rozmus et al. [117] followed the same approach for extending the PPC-SAFT EOS of Nguyen-Huynh et al. [136], and further included a free-energy contribution due to polar interactions. Although dispersion between ions was omitted in the ePPC-SAFT EOS, a good representation of multi-salt solutions was achieved in both of these approaches.

A number of studies have modelled aqueous solutions of weak electrolytes by taking into consideration partial dissociation equilibria and formation of ion pairs. Using the ePC-SAFT EOS [32], Held and Sadowski [137] considered incompletely dissociated salts by treating the ion pairs in solution as distinct species with a net charge, and the undissociated salts as neutral species. The equilibrium constants K_{ip} governing the ion pairing reactions were estimated by regression to experimental data of the mean ionic activity coefficients; vastly varying degrees of agreement with the experimental values of K_{ip} were attained for each ion pair species. In subsequent work with ePC-SAFT, Reschke et al. [138] adopted an alternative

methodology whereby experimentally-determined dissociation equilibrium constants were used to model aqueous sulphuric and phosphoric acids. By using the anion models obtained in this manner as constituents of alkali phosphate or alkali sulphate salts – for which the cation models were taken from previous work [32] – an improved description of the salt's properties was attained compared to using the anion models of Held and Sadowski [137].

Thermodynamic modelling of non-spherical ionic species appears only sparingly in the literature, and the few studies relevant to such systems have been presented in recent years within primitive modelling frameworks. One such study follows from the line of work discussed above for weak electrolyte modelling using the ePC-SAFT EOS; it involves the modelling of aqueous solubilities of partially ionisable pharmaceutical compounds. Cassens et al. [28] modelled pharmaceutical bases as homonuclear chain molecules, using the same model parameters for the ionised molecule as for the neutral molecule, with the exception that a single segment on the ionised molecule was assigned a charge. Electrostatic interactions were assumed to apply to the individual charged segments of the ionised molecules. The remaining two studies that have considered non-spherical ions have done so within the context of aqueous ionic liquids: Shahriari et al. [139] employed a homosegmented PC-SAFT EOS coupled with the MSA-PM, while Jiang and Adidharma [140] used a heterosegmented (group contribution) SAFT approach in combination with the MSA-RPM theory. In both of these approaches, the charge of any non-spherical ion was assigned to a specified segment, and the electrostatic interactions were assumed to occur among charged segments.

2.6.2 Non-primitive electrolyte-SAFT models

In the SAFT-based models for electrolytes discussed so far, the effect of the dipolar nature of the solvent is represented implicitly via the dielectric constant of the medium, meaning that any charge–dipole interactions are neglected. A more formal approach is to treat these dipolar interactions explicitly, thus giving a more realistic physical representation of the system. This can be achieved with a solvent-explicit (i.e. non-primitive) theory for electrostatic

interactions, commonly pursued with an equation of state including an explicit treatment of polar forces.

Liu et al. [31] first combined SAFT with the non-primitive semi-restricted MSA, with a parameter scheme including both salt-specific and ion-specific parameters. The resultant EOS considers contributions to the free energy arising from ion–ion, dipole–dipole, and dipole–ion interactions, in addition to ion–solvent association, thereby achieving a comprehensive description of electrolyte systems. A non-primitive electrolyte-SAFT model was also presented by Zhao et al. [141] based on the previously developed SAFT-VR+D EOS for dipolar fluids [142]. In the electrolyte extension of this theory (SAFT-VR+DE), electrostatic interactions are incorporated by the non-primitive unrestricted MSA and as a result the fluid is described by Coulombic ion–ion interactions, dipole–ion interactions, and dipole–dipole interactions. A highly accurate representation of electrolyte mixture thermodynamics was achieved by the SAFT-VR+DE EOS, as was verified by comparison to molecular simulation studies of systems assigned equivalent ionic parameters. The SAFT-VR+DE EOS was later applied by Das et al. [143] to model concentrated solutions of strong electrolytes up to 20 mol kg^{-1}; in order to achieve a reasonable description of the thermodynamic properties at high molality, the models included ion–solvent association interactions to facilitate ion solvation, and ion–ion association to represent ion pairing.

Within the PC-SAFT framework, a non-primitive modelling approach for electrolytes has been proposed by Herzog et al. [144] by pairing the PC-SAFT EOS with the semi-restricted non-primitive MSA. Dispersion between ions was neglected (as is typical for ePC-SAFT models) and a salt-specific modelling scheme was adopted, including cation–water association modelled on a salt-specific basis. Using this approach, close agreement with experimental data was achieved for properties of strong inorganic electrolytes at moderate temperatures up to the solubility limit of each salt.

2.7 Summary

The review conducted here covering the thermodynamic modelling tools for mixtures containing electrolytes has aimed to illustrate the great volume of work performed in this area. Over the years, much effort has been exerted in choosing between the Debye-Hückel and MSA theories; primitive and non-primitive modelling approaches; whether or not to explicitly include a distinct treatment for ion solvation; and whether to adopt a parameterisation scheme that is ion- or salt-specific. In spite of these many considerations, the major difference between the approaches has been the choice of accompanying model for describing the non-electrostatic aspects of the fluid thermodynamics; this choice has followed the evolution of thermodynamic modelling tools, and in recent years it has gravitated towards increasingly sophisticated equations of state such as the SAFT approach.

A prominent aspect of electrolyte thermodynamic modelling has been the almost exclusive focus on studying inorganic electrolytes. This is unsurprising considering that both the Debye-Hückel and MSA theories adopt a spherical geometry for the ionic species – an assumption which is most closely matched by a real system when ions are monatomic or oligoatomic. The emergence of SAFT-based approaches has provided an attractive avenue for modelling larger organic ions and this has been pursued in a small number of publications. However, none of these have provided insights regarding the methodology and mathematical formulation for doing so. This particular knowledge gap is addressed in the following chapter, by reformulating the MSA and Born theories such that they may be used compatibly with the SAFT-γ Mie EOS.

Chapter 3

Modelling electrolytes with the SAFT equation of state

3.1 The Statistical Associating Fluid Theory

The Statistical Associating Fluid Theory (SAFT) has its origins in the work of Wertheim [145–150], who presented a thermodynamic perturbation theory (TPT) based on statistical mechanics for calculating the free energy of associating fluids, given a hard-sphere reference fluid with known thermodynamic properties. Employing first-order TPT (TPT1), Jackson et al. [151] proposed a theory for modelling phase equilibria for hard-core spherical molecules with multiple bonding sites. The theory was extended to chain molecules by Chapman et al. [152], leading to the development of the SAFT equation of state for associating fluids [2, 3].

In the SAFT approach, molecules are modelled as chains of bonded spherical monomers, interacting through a defined intermolecular potential $u(r)$ describing the dispersion interactions. Strong directional interactions, such as hydrogen bonding, are mediated via association sites on the interacting chains. The SAFT approach expresses the total Helmholtz free energy

A of a system at specified temperature, volume, and composition $(T, V, \mathbf{N})$ as a sum of the ideal and residual free energy contributions:

$$\begin{aligned} A(T,V,\mathbf{N}) &= A^{\text{ideal}}(T,V,\mathbf{N}) + A^{\text{res}}(T,V,\mathbf{N}) \\ &= A^{\text{ideal}}(T,V,\mathbf{N}) + A^{\text{monomer}}(T,V,\mathbf{N}) + A^{\text{chain}}(T,V,\mathbf{N}) + A^{\text{assoc}}(T,V,\mathbf{N}) \,. \end{aligned} \tag{3.1}$$

A^{ideal} is the contribution to the Helmholtz free energy arising from the ideal-gas system; A^{monomer} is the free energy arising due to the interactions between the spherical monomer segments; A^{chain} accounts for the free energy contributed by the formation of chains through bonding of the monomer segments; and finally A^{assoc} is the free energy change due to the formation of complexes via short-range association interactions. Knowledge of the Helmholtz free energy of a mixture at specified T, V, and $\mathbf{N}$ allows computation of the thermodynamic properties of the system through standard thermodynamic relations.

The perturbation approach intrinsic to the SAFT equation of state allows a detailed yet versatile representation of physical systems, making it possible to adapt the theoretical formulation to specific applications by adapting the contributing terms in Equation 3.1. Certain Helmholtz free energy terms may be neglected in systems where they do not apply and additional terms may be included to account for certain interactions explicitly, such as in the case of mixtures containing electrolytes. As a result of this versatility, as well as the ability to treat each term independently, there have been numerous adaptations of the SAFT approach presented in the literature. The most fundamental variation has been the choice of reference fluid, leading to two dominant strains of the EOS: the original SAFT formulation [2, 3] employs a hard-sphere reference fluid, whereas a subsequent PC-SAFT formulation by Gross and Sadowski [21, 22] employs a hard-chain reference fluid with dispersion forces acting between the chains rather than the monomer segments. A second prominent difference between versions of the SAFT approach is the form of intermolecular potential representing the intermolecular dispersion forces. Intermolecular potentials implemented in SAFT-type models have included, for example, the square-well, Sutherland [153], Yukawa [154], Lennard-Jones [155], and Mie [156] potentials. The from

of intermolecular potential has a profound effect on the performance of the EOS, as it not only influences the monomer term but also the chain and association terms which must be computed in accordance with the reference fluid.

Numerous variations of SAFT-type equations of state have been presented to accommodate the breadth of physical systems through appropriate reformulation of the EOS and suitably corresponding model development. Some prominent families include SAFT-HR [157], soft-SAFT [158], SAFT1 [127], SAFT-VR [119, 120], and PC-SAFT [22], many of which have seen progressive adaptations to contributing Helmholtz free energy terms of the EOS. The particular family of SAFT equations of state relevant to the present work is that based on the SAFT-VR approach, as it has acted as the predecessor for the SAFT-γ Mie approach employed here.

In the SAFT-VR EOS presented by by Gil-Villegas and co-workers [119, 120], molecules are modelled as chains of tangentially bonded hard-core segments interacting through an attractive potential of variable range (VR). More specifically, square-well (SW), Sutherland, and Yukawa potentials of variable range were implemented [119]. Lafitte et al. [159] adapted the SAFT-VR EOS to allow soft-sphere monomer segments by applying a Mie intermolecular potential, which allows both attractive and repulsive variable-range interactions. The resultant SAFT-VR Mie EOS was shown to improve predictions of second-derivative thermophysical properties of fluids and the description in the near-critical region when compared to its SAFT-VR predecessor. The SAFT-VR Mie EOS has been shown to be widely applicable to molecular fluids characterized by a broad range of interactions, from soft potentials to very repulsive and short-ranged potentials, providing global representation of the thermodynamic properties and fluid-phase equilibria of pure fluids and mixtures [160].

A subset of SAFT-type approaches have been reformulated within a group-contribution framework; one of these is SAFT-VR Mie, thereby giving rise to the SAFT-γ Mie EOS. Before proceeding to a more extensive description of the SAFT-γ Mie EOS in Section 3.2, an overview will be given of SAFT-based group-contribution efforts.

3.1.1 Group-contribution methodologies within the SAFT framework

The representation of molecules as bonded monomer segments makes the SAFT approach inherently compatible with group-contribution (GC) formulations. Group-contribution methods are a class of thermodynamic methodologies in which the properties of compounds are approximated by considering contributions from the chemically distinct functional groups that compose the compounds. The parameters which characterise each functional group are considered to be transferable between different molecules, hence making it possible to describe the physical properties of a substance in a purely predictive manner from knowledge of its constituent functional groups. The formulation of SAFT with respect to monomer segments means that implementing a group-contribution framework within SAFT arises by regarding the monomers as distinct functional groups.

Group-contribution implementations of the SAFT approach have been proposed employing both a homonuclear model, in which all functional-group monomers are approximated as having the same size, and a heteronuclear model, in which the size is distinct for each type of functional group monomer. The greater versatility of heteronuclear approaches is especially desirable as it permits a more detailed representation of the system and consequently affords greater predictive capability to the thermodynamic model. Homonuclear group-contribution SAFT models have been developed by Tamouza et al. [161, 162] within the framework of the SAFT-VR EOS, while Vijande et al. [163] and Tihic et al. [164] developed homonuclear group-contribution implementations of the PC-SAFT EOS. Heteronuclear models have been proposed with numerous versions of SAFT as the base EOS, including SAFT-HR [165], SAFT1 [127], soft-SAFT [158], PC-SAFT [166, 167], and SAFT-VR [168, 169].

As for non-GC SAFT models, the aforementioned heteronuclear and homonuclear group-contribution models represent molecules as chains of tangentially bonded monomer segments. A significant step in GC SAFT models came with the novel approach proposed by Lymperiadis and co-workers [6, 7], whereby chain molecules are composed of fused segments.

This constitutes the foundation of the SAFT-γ equation of state, which was developed as a heteronuclear group contribution formulation of the SAFT-VR SW EOS. Since the SAFT-γ approach considers the degree of overlap between a molecule's functional groups, the resultant fused heteronuclear models represent the structural topology of molecules more accurately. Initially, Lymperiadis et al. implemented a square-well intermolecular potential to the SAFT-γ EOS, which has been extensively applied to model numerous fluid systems [170–173].

Following the successful application of the SAFT-γ SW EOS, Papaioannou et al. [8] reformulated the SAFT-VR Mie EOS of Lafitte et al. [174] in a similar group-contribution framework, thereby introducing the SAFT-γ Mie EOS. Within SAFT-γ Mie, monomer segments are represented as soft heteronuclear spheres interacting through a Mie potential of variable repulsive and attractive range, and molecules are modelled as chains of overlapping monomer segments. As a result, the SAFT-γ Mie EOS combines favourably the variability of the Mie potential with the predictive characteristics of the group-contribution approach to give higher accuracy and confidence in property predictions. A number of publications have demonstrated the extensive applicability of the SAFT-γ Mie EOS, for both pure fluids and multicomponent mixtures [9, 10, 175, 176].

3.2 SAFT-γ Mie

In the SAFT-γ Mie group-contribution equation of state, molecules are represented as heteronuclear chains of fused spherical segments. A united-atom approach is adopted, whereby a certain chemical functional group k is modelled as a spherical segment or an aggregation of ν_k^* identical fused segments, where each segment comprising group k is represented as a soft sphere of diameter σ_k. The shape factor S_k of a segment characterises the degree of overlap between fused segments ($0 < S_k \leq 1$), and therefore determines the extent to which a segment contributes to the properties of the fluid. More precisely, S_k

describes the proportion to which a segment contributes to the free energy the fluid, hence making the united-atom method compatible with Wertheim's first-order thermodynamic perturbation theory for chains of tangentially bonded segments.

Two segments k and l interact through a Mie potential [156] of variable attractive and repulsive range:

$$u_{kl}^{\mathrm{Mie}} = C_{kl}\varepsilon_{kl}^{\mathrm{Mie}}\left[\left(\frac{\sigma_{kl}}{r_{kl}}\right)^{\lambda_{\mathrm{r},kl}} - \left(\frac{\sigma_{kl}}{r_{kl}}\right)^{\lambda_{\mathrm{a},kl}}\right], \tag{3.2}$$

where r_{kl} is the distance between the centres of the two segments; σ_{kl} is defined as the separation at which $u_{kl}^{\mathrm{Mie}} = 0$; ε_{kl} is the depth of the potential well; and $\lambda_{\mathrm{a},kl}$ and $\lambda_{\mathrm{r},kl}$ are the attractive and repulsive exponents of the inter-segment interaction. When considering the potential between two similar segments, the σ_{kl} parameter corresponds to the diameter of the segment. The prefactor C_{kl} is a function of the Mie potential exponents:

$$C_{kl} = \frac{\lambda_{\mathrm{r},kl}}{\lambda_{\mathrm{r},kl} - \lambda_{\mathrm{a},kl}}\left(\frac{\lambda_{\mathrm{r},kl}}{\lambda_{\mathrm{a},kl}}\right)^{\frac{\lambda_{\mathrm{a},kl}}{\lambda_{\mathrm{r},kl}-\lambda_{\mathrm{a},kl}}} \tag{3.3}$$

Short-range directional attractive forces (such as hydrogen bonding) between certain types of functional groups are treated within SAFT-γ Mie by assigning association sites on the appropriate segments. Associating groups are characterised by the number of different site types $N_{\mathrm{ST},k}$ they possess, and the number of sites of each type, $n_{k,a}, n_{k,b}, ..., n_{k,N_{\mathrm{ST},k}}$. The association interaction between a site of type a on segment k and a site of type b on segment l is modelled via a square-well potential:

$$u_{ab,kl}^{\mathrm{HB}} = \begin{cases} -\varepsilon_{ab,kl}^{\mathrm{HB}} & \text{if } \; r_{ab,kl} \leq r_{ab,kl}^{\mathrm{c}} \\ 0 & \text{if } \; r_{ab,kl} > r_{ab,kl}^{\mathrm{c}} \end{cases} \tag{3.4}$$

where $r_{ab,kl}$ is the distance between the centres of sites a and b, $r_{ab,kl}^{\mathrm{c}}$ is the cutoff range of the interaction, and $-\varepsilon_{ab,kl}^{\mathrm{HB}}$ is the association energy. The cutoff distance $r_{ab,kl}^{\mathrm{c}}$ is equivalently

represented in terms of a bonding volume $K^{\mathrm{HB}}_{ab,kl}$. Association sites are positioned at a distance $r^{\mathrm{d}}_{aa,kk}$ from the centre of the segment; both $r^{\mathrm{d}}_{aa,kk}$ and $r^{\mathrm{c}}_{aa,kk}$ are fixed to $0.4\sigma_{kk}$ [177].

The form of the SAFT-γ Mie equation of state follows that given by Equation 3.1. The expressions corresponding to each term of the EOS representing a certain contribution to the Helmholtz free energy are briefly summarised below. The ideal, monomer, and chain contribution terms are obtained the work of Papaioannou et al. [8], which is based on the preceding work of Lafitte et al. [174]. The association contribution term is implemented according to Dufal et al. [177]. The Helmholtz free energy $A(T, V, N)$ is written for a fluid mixture of N molecules that comprises a total number of components N_{C}, i.e. $N = \sum_i^{N_{\mathrm{C}}} N_i$. A total number of functional groups N_{G} form the molecules in the fluid, and a total of number of association site types N_{ST} are possessed by these groups. In the expressions that follow, the state variables (T, V, N) are omitted for conciseness.

3.2.1 Ideal gas term

The Helmholtz free energy A^{ideal} corresponding to an ideal gas mixture of N non-interacting molecules represented as point particles is given by [178]

$$\frac{A^{\mathrm{ideal}}}{N k_{\mathrm{B}} T} = \left(\sum_{i=1}^{N_{\mathrm{C}}} x_i \ln \left(\rho_i \Lambda_i^3 \right) \right) - 1 \,, \tag{3.5}$$

where $x_i = N_i/N$ is the mole fraction of molecules of type i, $\rho_i = N_i/V$ is the number density of component i, and N_i is the number of molecules of component i in the mixture. The thermal de Broglie wavelength Λ_i implicitly incorporates the effects of translational, rotational, and vibrational contributions to the kinetic energy of the ideal gas mixture.

3.2.2 Monomer term

The monomer term describes the contribution to the free energy of the mixture arising from dispersion forces between spherical monomers characterised by a Mie interaction potential. It is obtained via a Barker-Henderson [179–181] high-temperature perturbation expansion up to third order, following Lafitte et al. [174]:

$$\frac{A^{\text{monomer}}}{Nk_{\text{B}}T} = \frac{A^{\text{HS}}}{Nk_{\text{B}}T} + \frac{A_1}{Nk_{\text{B}}T} + \frac{A_2}{Nk_{\text{B}}T} + \frac{A_3}{Nk_{\text{B}}T} \,. \tag{3.6}$$

The repulsive term A^{HS} represents the free energy of a hard-sphere reference system, obtained as:

$$\frac{A^{\text{HS}}}{Nk_{\text{B}}T} = \left(\sum_{i=1}^{N_{\text{C}}} x_i \sum_{k=1}^{N_{\text{G}}} \nu_{k,i} \nu_k^* S_k \right) a^{\text{HS}} \,, \tag{3.7}$$

where $\nu_{k,i}$ is the number of groups of type k in a molecule of type i, and a^{HS} is the dimensionless hard-sphere free energy per segment, obtained using the expression of Boublík [182] and Mansoori [183]:

$$a^{\text{HS}} = \frac{6}{\pi\rho_s} \left[\left(\frac{\zeta_2^3}{\zeta_3^2} - \zeta_0 \right) \ln(1-\zeta_3) + \frac{3\zeta_1\zeta_2}{(1-\zeta_3)} + \frac{\zeta_2^3}{\zeta_3 (1-\zeta_3)^2} \right] \,. \tag{3.8}$$

Here, $\rho_s = N_s/V$ is the segment number density, which is related to the molecular number density $\rho = N/V$ through

$$\rho_s = \rho \left(\sum_{i=1}^{N_{\text{C}}} x_i \sum_{k=1}^{N_{\text{G}}} \nu_{k,i} \nu_k^* S_k \right) \,; \tag{3.9}$$

and ζ_m are the moments of the number density of monomeric segments:

$$\zeta_m = \frac{\pi\rho_s}{6} \sum_{k=1}^{N_{\text{G}}} x_{s,k} d_{kk}^m \qquad\qquad m = 0, 1, 2, 3 \,. \tag{3.10}$$

which depend on the Barker-Henderson hard-sphere effective diameter d_{kk}:

$$d_{kk} = \int_0^{\sigma_{kk}} \left[1 - \exp\left(-\frac{u_{kk}^{\text{Mie}}(r_{kk})}{k_{\text{B}}T} \right) \right] \mathrm{d}r \,, \tag{3.11}$$

and the fraction $x_{s,k}$ of segments of type k in the mixture:

$$x_{s,k} = \frac{\sum_{i=1}^{N_{\text{C}}} x_i \nu_{k,i} \nu_k^* S_k}{\sum_{i=1}^{N_{\text{C}}} x_i \sum_{l=1}^{N_{\text{G}}} \nu_{l,j} \nu_l^* S_l} \,. \tag{3.12}$$

The remaining terms of the Barker-Henderson expansion for A^{monomer} are similarly obtained by summing over the free-energy contributions per segment, with a corresponding power of inverse temperature:

$$\frac{A_q}{N k_{\text{B}} T} = \left(\frac{1}{k_{\text{B}} T} \right)^q \left(\sum_{i=1}^{N_{\text{C}}} x_i \sum_{k=1}^{N_{\text{G}}} \nu_{k,i} \nu_k^* S_k \right) a_q \qquad q = 1, 2, 3 \,. \tag{3.13}$$

The free-energy contribution per segment a_q for each term of order q is obtained by summing the pairwise interactions $a_{q,kl}$ between groups k and l over all pairs of functional groups present in the system:

$$a_q = \sum_{k=1}^{N_{\text{G}}} \sum_{l=1}^{N_{\text{G}}} x_{s,k} x_{s,l} a_{q,kl} \qquad q = 1, 2, 3 \,. \tag{3.14}$$

The precise expressions for $a_{q,kl}$ are fairly involved and are therefore omitted for the sake of brevity; these are detailed in the original publication of Papaioannou et al. [8] for the SAFT-γ Mie EOS.

3.2.3 Chain term

The A^{chain} term contributes the change in Helmhotz free energy due to the formation of chain molecules through bonding of the spherical group segments. The theory for chain formation corresponds to association between segments in the limit of infinite association

strength at contact [149, 152], leading to tangentially bonded segments. In order to align the chain theory's description of tangential bonding at regular intervals with the fused group-contribution formulation of the SAFT-γ Mie EOS, average molecular parameters are defined for the segments of each molecular component i. These are evaluated according to the fraction $z_{k,i}$ of each group k in a given molecule i:

$$z_{k,i} = \frac{\nu_{k,i}\nu_k^* S_k}{\sum_{l=1}^{N_G} \nu_{l,i}\nu_l^* S_l} \,. \tag{3.15}$$

The average molecular segment diameter $\bar{\sigma}_{ii}$ and the reference hard-sphere effective diameter $\bar{d}_{ii}$ are defined as follows:

$$\bar{\sigma}_{ii}^3 = \sum_{k=1}^{N_G}\sum_{l=1}^{N_G} z_{k,i} z_{l,i} \sigma_{kl}^3 \,; \tag{3.16}$$

$$\bar{d}_{ii}^3 = \sum_{k=1}^{N_G}\sum_{l=1}^{N_G} z_{k,i} z_{l,i} d_{kl}^3 \,. \tag{3.17}$$

Similarly, the average dispersion energy $\bar{\varepsilon}_{ii}$ and the average attractive and repulsive exponents of the Mie potential $\bar{\lambda}_{y,ii}$ are obtained through:

$$\bar{\varepsilon}_{ii} = \sum_{k=1}^{N_G}\sum_{l=1}^{N_G} z_{k,i} z_{l,i} \varepsilon_{kl} \,; \tag{3.18}$$

$$\bar{\lambda}_{y,ii} = \sum_{k=1}^{N_G}\sum_{l=1}^{N_G} z_{k,i} z_{l,i} \lambda_{y,kl} \qquad y = a, r \,. \tag{3.19}$$

The contribution to the free energy of the system due to chain formation is therefore given by

$$\frac{A^{\text{chain}}}{N k_B T} = -\sum_{i=1}^{N_C} x_i \left(\sum_{k=1}^{N_G} \nu_{k,i}\nu_k^* S_k - 1 \right) \ln g_{ii}^{\text{Mie}}(\bar{\sigma}_{ii}; \zeta_x) \,, \tag{3.20}$$

where the radial distribution function $g_{ii}^{\mathrm{Mie}}(\bar{\sigma}_{ii};\zeta_x)$ corresponding to the monomeric Mie system is evaluated at a distance $\bar{\sigma}_{ii}$ in a hypothetical fluid with a packing fraction of:

$$\zeta_x = \frac{\pi\rho_s}{6}\sum_{k=1}^{N_\mathrm{G}}\sum_{l=1}^{N_\mathrm{G}} x_{s,k}x_{s,l}d_{k,l}^3 \,. \tag{3.21}$$

The detailed expressions related to evaluating the radial distribution function of the Mie fluid are given the original SAFT-γ Mie publication by Papaioannou et al. [8]; again, for reasons of conciseness, these are omitted from this summary.

3.2.4 Association term

The contribution to the system's Helmholtz free energy arising due to association interactions between molecules is obtained following the TPT1 theory in the following manner:

$$\frac{A^{\mathrm{assoc}}}{Nk_\mathrm{B}T} = \sum_{i=1}^{N_\mathrm{C}} x_i \sum_{k=1}^{N_\mathrm{G}} \nu_{k,i} \sum_{a=1}^{N_\mathrm{ST}} n_{k,a}\left(\ln X_{i,k,a} + \frac{1-X_{i,k,a}}{2}\right), \tag{3.22}$$

where $X_{i,k,a}$ is the fraction of molecules i comprising an associating group k which is not bonded at site type a. This is given by

$$X_{i,k,a} = \left[1 + \rho\sum_{j=1}^{N_\mathrm{C}} x_j \sum_{l=1}^{N_\mathrm{G}} \nu_{l,j} \sum_{b=1}^{N_\mathrm{ST},l} n_{l,b}X_{j,l,b}\Delta_{ij,kl,ab}\,.\right]^{-1} \tag{3.23}$$

$\Delta_{ij,kl,ab}$ is the integrated association strength between site a positioned on functional group k within molecule i, and site b on functional group l in molecule j. It is expressed as:

$$\Delta_{ij,kl,ab} = F_{kl,ab}K_{kl,ab}I_{ij,kl,ab} \tag{3.24}$$

where $F_{kl,ab}$ is the Mayer function:

$$F_{kl,ab} = \exp\left(\frac{\varepsilon^{\mathrm{HB}}_{kl,ab}}{k_{\mathrm{B}}T}\right) - 1 \; ; \tag{3.25}$$

$K_{kl,ab}$ is an empirical bonding-volume parameter; and $I_{ij,kl,ab}$ is the association integral expressed as a temperature–density polynomial correlation for a Lennard-Jones monomer:

$$I_{ij,kl,ab} = \sum_{p=0}^{10} \sum_{q=0}^{10-p} c_{pq} \left(\rho\sigma_x^3\right)^p \left(\frac{k_{\mathrm{B}}T}{\bar{\varepsilon}_{ij}}\right)^q \; . \tag{3.26}$$

for which the set of coefficients c_{pq} (each corresponding to a pair of indexes p and q) are given in the work Dufal et al. [177]. The remaining averaged segment and molecular parameters of the polynomial are defined as follows:

$$\sigma_x^3 = \sum_{k=1}^{N_{\mathrm{G}}} \sum_{l=1}^{N_{\mathrm{G}}} x_{s,k} x_{s,l} \sigma_{k,l}^3 \; ; \tag{3.27}$$

$$\bar{\varepsilon}_{ij} = \frac{\sqrt{\bar{\sigma}_{ii}^3 \bar{\sigma}_{jj}^3}}{\bar{\sigma}_{ij}^3} \sqrt{\bar{\varepsilon}_{ii}\bar{\varepsilon}_{jj}} \; ; \tag{3.28}$$

$$\bar{\sigma}_{ij} = \frac{\bar{\sigma}_{ii}\bar{\sigma}_{jj}}{2} \; . \tag{3.29}$$

3.2.5 Combining rules for mixtures

The model parameters for a given functional group are typically determined through regression to bulk-phase experimental data of substances belonging to a particular chemical family in which the functional group appears. Model parameters characterising the interaction

between two unlike functional groups k and l can also be obtained in the same manner using relevant mixture data; however, this is not always possible and it is sometimes necessary to estimate the magnitude of these cross-interaction parameters by applying appropriate combining rules. Of course, the interactions between a given pair of unlike groups can only be obtained through combining rules provided that the parameters of the individual groups are already known.

In the SAFT-γ Mie EOS, the unlike segment diameter is obtained as a simple arithmetic (Lorentz) mean [170]:

$$\sigma_{kl} = \frac{\sigma_{kk} + \sigma_{ll}}{2}; \tag{3.30}$$

likewise, the unlike reference hard-sphere diameter is set as

$$d_{kl} = \frac{d_{kk} + d_{ll}}{2}; \tag{3.31}$$

The unlike dispersion energy is obtained using an augmented geometric (Berthelot-like) mean which accounts for the size asymmetry of the groups [170]:

$$\varepsilon_{kl} = \frac{\sqrt{\sigma_{kk}^3 \sigma_{ll}^3}}{\sigma_{kl}^3} \sqrt{\varepsilon_{kk} \varepsilon_{ll}}. \tag{3.32}$$

The unlike attractive and repulsive exponents of the Mie potential are estimated as follows [8, 174]:

$$\lambda_{y,kl} = 3 + \sqrt{(\lambda_{y,kk} - 3)(\lambda_{y,ll} - 3)}, \qquad y = \mathrm{a}, \mathrm{r}\,. \tag{3.33}$$

Combining rules may also be used to determine the parameters of the association interaction between an unlike pair of groups associating via site a on group k and site b on group l. A

simple geometric combining rule is used for the unlike association energy [9, 177]:

$$\varepsilon^{\mathrm{HB}}_{kl,ab} = \sqrt{\varepsilon^{\mathrm{HB}}_{kk,aa}\varepsilon^{\mathrm{HB}}_{ll,bb}}, \tag{3.34}$$

and the unlike bonding volume is obtained by an arithmetic mean rule averaging the volumes of the like-interaction parameters [9, 177]:

$$K^{\mathrm{HB}}_{kl,ab} = \left(\frac{\sqrt[3]{K^{\mathrm{HB}}_{kk,aa}} + \sqrt[3]{K^{\mathrm{HB}}_{ll,bb}}}{2} \right)^3 . \tag{3.35}$$

The application of these combining rules is especially useful when it is not practical or possible to optimise the unlike interaction parameters due to a paucity of mixture data. The unlike segment diameter is almost invariably taken as the value given by Equation 3.30, even when data are abundant. By contrast, Equation 3.32 is often used to obtain an initial estimate of the unlike dispersion energy in order to guide optimisation of this parameter. For non-associating groups, it is usually possible to match the thermodynamic behaviour of the fluid by optimising only ε_{kl}; however, when groups k and l comprise distinctly different chemical compositions it is often found that the Mie potential exponents also require optimisation. For associating groups, the estimates given by Equations 3.34 and 3.35 also often require further optimisation; in these cases, an understanding of the type of physical interaction mediated by a given unlike association interaction often acts as guidance for narrowing the optimisation landscape.

3.3 Helmholtz free energy terms for electrostatic interactions

The implementation of electrostatic contributions to the SAFT-γ Mie EOS is performed by incorporating additional contributions to the Helmholtz free energy of the system, given by

the MSA and Born theories. Before proceeding to the proposed adaptations of these theories to comply with a group-contribution formulation in Section 3.6, the regular forms of the MSA theory and Born theories are presented below.

3.3.1 Mean spherical approximation theory

The MSA approach for an implicit-solvent (i.e. primitive) model for electrolyte solutions gives the Coulombic contribution to the Helmholtz free energy of the fluid. In the MSA theory, an ion i is represented as a hard sphere of diameter σ_i, with a central point charge $q_i = z_i e$. Coulomb's law gives the pair potential between two point charges q_i and q_j:

$$u_{ij}^{\text{Coulomb}}(r) = \frac{z_i z_j e^2}{4\pi\epsilon_0 D r_{ij}}, \tag{3.36}$$

where r_{ij} is the separation distance, z is the valency of the ion, ϵ_0 is the permittivity of vacuum, and D is the dielectric constant (relative static permittivity) of the medium.

The primitive mean spherical model for asymmetric ions was presented by Blum [47] and Blum and Hoye [48] by solving the Ornstein-Zernike [184] equation with the mean spherical approximation closure, giving an analytical solution for the radial distribution function for a fluid of charged hard spheres interacting through a Coulombic potential in a dielectric continuum. The Ornstein-Zernike equation is written for a mixture as [185]

$$g_{ij}(r) - 1 = c_{ij}(r) + \sum_y \rho_y \int (g_{jy}(|\mathbf{r} - \mathbf{r}'|)\, c_{iy}(r') d\mathbf{r}', \tag{3.37}$$

where $c_{ij}(r)$ is the direct correlation function, the summation is over all species y, and the integral is over all positions $\mathbf{r}'$. The mean spherical approximation closure of the Ornstein-

Zernike equation for the charged-hard-sphere system is

$$\begin{cases} g_{ij}(r) = 0 & \text{if } \; r_{ij} \leq \sigma_{ij} \\ c_{ij}(r) = -\dfrac{1}{k_{\mathrm{B}}T}\dfrac{z_i z_j e^2}{4\pi\epsilon_0 D r_{ij}} & \text{if } \; r_{ij} > \sigma_{ij} \end{cases} \tag{3.38}$$

The internal energy of the fluid given by the unrestricted MSA-PM model is expressed as [47, 48]

$$\begin{aligned} U^{\mathrm{MSA}} &= -\frac{e^2 V}{(4\pi\epsilon_0)D}\left[\frac{\Gamma}{V}\sum_{\text{ions},i=1}^{n_{\text{ion}}}\left(\frac{N_i z_i^2}{1+\Gamma\sigma_i}\right) + \frac{\pi}{2\Delta}\Omega P_n^2\right] \\ &= -\frac{e^2 V}{(4\pi\epsilon_0)D}\left[\Gamma\rho\sum_{\text{ions},i=1}^{n_{\text{ion}}}\left(\frac{x_i z_i^2}{1+\Gamma\sigma_i}\right) + \frac{\pi}{2\Delta}\Omega P_n^2\right], \end{aligned} \tag{3.39}$$

and the corresponding Helmholtz free energy of the system is given by

$$A^{\mathrm{MSA}} = U^{\mathrm{MSA}} + \frac{\Gamma^3 k_{\mathrm{B}} T V}{3\pi} \, . \tag{3.40}$$

The shielding parameter Γ characterises the screening length of the electrostatic forces, i.e. the range over which these forces act:

$$\Gamma^2 = \frac{\pi e^2}{(4\pi\epsilon_0)D k_{\mathrm{B}} T V}\sum_{\text{ions},i=1}^{n_{\text{ion}}} N_i Q_i^2 \, . \tag{3.41}$$

Q_i represents an effective charge of ion i and it is given by

$$Q_i = \frac{z_i - \sigma_i^2 P_n(\pi/(2\Delta))}{1+\Gamma\sigma_i} \, . \tag{3.42}$$

Two coupling parameters P_n and Ω relate the charge and size of an ion and its packing fraction Δ as follows:

$$P_n = \frac{1}{\Omega V}\sum_{\text{ions},i=1}^{n_{\text{ion}}}\frac{N_i\sigma_i z_i}{1+\Gamma\sigma_i} \, , \tag{3.43}$$

$$\Omega = 1 + \frac{\pi}{2\Delta V} \sum_{\text{ions},i=1}^{n_{\text{ion}}} \frac{N_i \sigma_i^3}{1 + \Gamma \sigma_i} \,. \tag{3.44}$$

The packing fraction Δ is obtained from the number density of the ions in the fluid:

$$\Delta = 1 - \frac{\pi}{6V} \sum_{\text{ions},i=1}^{n_{\text{ion}}} N_i \sigma_i^3 \,. \tag{3.45}$$

From Equations 3.41 and 3.42 it can be seen that the MSA theory gives an implicit formulation of the shielding parameter Γ, which therefore needs to be obtained iteratively. This is easily achieved through successive substitution starting from an initial guess Γ_0 estimated from the Debye-Hückel screening length κ:

$$\Gamma_0 = \frac{\kappa}{2} = 0.5 \sqrt{\frac{e^2}{4\epsilon_0 D k_{\text{B}} T V} \sum_{\text{ions},i=1}^{n_{\text{ion}}} N_i z_i^2} \,. \tag{3.46}$$

Using the Helmholtz free energy electrostatic contribution given by Equation 3.40, the corresponding contribution to the chemical potential of a species i is derived by partial differentiation. If the dielectric constant of the medium is assumed not to vary with the concentration of the ions, one obtains:

$$\begin{aligned} \mu_i^{\text{MSA}} &= \left(\frac{\partial A^{\text{MSA}}}{\partial N_i} \right)_{N_{j\neq i}, D} \\ &= \left(\frac{\partial A^{\text{MSA}}}{\partial N_i} \right)_{\Gamma,\Delta,\Omega,P_n,N_{j\neq i},D} + \left(\frac{\partial A^{\text{MSA}}}{\partial \Delta} \right)_{N,D} \frac{\partial \Delta}{\partial N_i} + \left(\frac{\partial A^{\text{MSA}}}{\partial \Omega} \right)_{N,D} \frac{\partial \Omega}{\partial N_i} \\ &\quad + \left(\frac{\partial A^{\text{MSA}}}{\partial P_n} \right)_{N,D} \frac{\partial P_n}{\partial N_i} + \left(\frac{\partial A^{\text{MSA}}}{\partial \Gamma} \right)_{N,D} \frac{\partial \Gamma}{\partial N_i} \,, \end{aligned} \tag{3.47}$$

and the ionic contribution to an ionic component's chemical potential is given by expanding the derivatives in Equation 3.47:

$$\mu_i^{\mathrm{MSA}} = -\frac{e^2}{4\pi\epsilon_0 D}\left\{\frac{\Gamma z_i^2}{1+\Gamma\sigma_i} + \frac{\Omega\sigma_i^3}{12}\left(\frac{\pi P_n}{\Delta}\right)^2 - \frac{\pi^2 P_n^2\sigma_i^3}{4\Delta^2}\left(\frac{1}{1+\Gamma\sigma_i} - \frac{1-\Omega}{3}\right) + \frac{\pi P_n\sigma_i z_i}{\Delta(1+\Gamma\sigma_i)}\right\}. \tag{3.48}$$

The dielectric constant does not, however, remain constant with concentration, and it is common to implement an auxiliary (often empirical) model for predicting the variation of the dielectric constant with respect to the density or composition of the fluid. This is accounted for in the derivation of the chemical potential expression via:

$$\begin{aligned}\mu_i^{\mathrm{MSA}} &= \left(\frac{\partial A^{\mathrm{MSA}}}{\partial N_i}\right)_{N_{j\neq i},D} + \left(\frac{\partial A^{\mathrm{MSA}}}{\partial D}\right)_N \left(\frac{\partial D}{\partial N_i}\right)_{N_{j\neq i}} \\ &= \left(\frac{\partial A^{\mathrm{MSA}}}{\partial N_i}\right)_{N_{j\neq i},D} - \frac{U^{\mathrm{MSA}}}{D}\left(\frac{\partial D}{\partial N_i}\right)_{N_{j\neq i}},\end{aligned} \tag{3.49}$$

and the complete expression for μ_i^{MSA} therefore becomes:

$$\mu_i^{\mathrm{MSA}} = -\frac{e^2}{4\pi\epsilon_0 D}\left\{\frac{\Gamma z_i^2}{1+\Gamma\sigma_i} + \frac{\Omega\sigma_i^3}{12}\left(\frac{\pi P_n}{\Delta}\right)^2 - \frac{\pi^2 P_n^2\sigma_i^3}{4\Delta^2}\left(\frac{1}{1+\Gamma\sigma_i} - \frac{1-\Omega}{3}\right) + \frac{\pi P_n\sigma_i z_i}{\Delta(1+\Gamma\sigma_i)}\right\} - \frac{U^{\mathrm{MSA}}}{D}\left(\frac{\partial D}{\partial N_i}\right)_{N_{j\neq i}}. \tag{3.50}$$

The MSA's electrostatic contribution to the free energy of the fluid also contributes to the pressure of the system. If D is considered to be independent of the ionic composition, this contribution is given by

$$P^{\mathrm{MSA}} = \left(\frac{\partial A^{\mathrm{MSA}}}{\partial V}\right)_N = -\frac{\Gamma^3 k_{\mathrm{B}} T}{3\pi} - \frac{e^2}{8D\epsilon_0}\left(\frac{P_n}{\Delta}\right)^2; \tag{3.51}$$

and when the compositional dependence of D is taken into account the pressure contribution becomes

$$\begin{aligned} P^{\mathrm{MSA}} &= \left(\frac{\partial A^{\mathrm{MSA}}}{\partial V}\right)_N + \left(\frac{\partial A^{\mathrm{MSA}}}{\partial D}\right)_N \left(\frac{\partial D}{\partial V}\right)_N \\ &= -\frac{\Gamma^3 k_{\mathrm{B}} T}{3\pi} - \frac{e^2}{8 D \epsilon_0}\left(\frac{P_n}{\Delta}\right)^2 - \frac{U^{\mathrm{MSA}}}{D}\left(\frac{\partial D}{\partial V}\right)_N . \end{aligned} \tag{3.52}$$

3.3.2 Born solvation free energy

The change of free energy corresponding to the solvation of ions in a solvent may be taken into account using the primitive model proposed by Born [57]. Specifically, the Born model expresses the Helmholtz free energy associated with transferring a charged particle from vacuum into a spherical cavity in a dielectric medium. This may be conceptualised as an equivalent thermodynamic cycle incorporating the work of discharging the ions in a solvent, and recharging them in a uniform dielectric medium which implicitly represents the solvent, while neglecting the work of transferring the uncharged particles into the solvent medium. The Born solvation free energy is expressed as

$$A^{\mathrm{Born}} = -\frac{e^2}{4\pi\epsilon_0}\left(1 - \frac{1}{D}\right) \sum_{\mathrm{ions},i=1}^{n_{\mathrm{ion}}} \frac{N_i z_i^2}{\sigma_i^{\mathrm{Born}}} , \tag{3.53}$$

where σ_i^{Born} is the effective diameter of ion i in the solvent, representing the size of the cavity created in the solvent to accept the insertion of the ion.

The Born contribution to the chemical potential of the ion is equivalent to the free energy of solvation of an ion at infinite dilution. If the concentration dependence of the dielectric constant is neglected, the chemical potential is obtained as

$$\mu_i^{\mathrm{Born}} = \left(\frac{\partial A^{\mathrm{Born}}}{\partial N_i}\right)_{N_{j\neq i}, D} = -\frac{e^2}{4\pi\epsilon_0}\left(1 - \frac{1}{D}\right)\frac{z_i^2}{\sigma_i^{\mathrm{Born}}} ; \tag{3.54}$$

whereas by accounting for the change in dielectric constant with ion composition, the chemical potential becomes

$$\begin{aligned}\mu_i^{\text{Born}} &= \left(\frac{\partial A^{\text{Born}}}{\partial N_i}\right)_{N_{j\neq i},D} + \left(\frac{\partial A^{\text{Born}}}{\partial D}\right)_N \left(\frac{\partial D}{\partial N_i}\right)_{N_{j\neq i}} \\ &= -\frac{e^2}{4\pi\epsilon_0}\left[\left(1-\frac{1}{D}\right)\frac{z_i^2}{\sigma_i^{\text{Born}}} + \frac{1}{D^2}\left(\frac{\partial D}{\partial N_i}\right)_{V,T,N_{j\neq i}} \sum_{\text{ions},i=1}^{n_{\text{ion}}} \frac{N_i z_i^2}{\sigma_i^{\text{Born}}}\right].\end{aligned} \tag{3.55}$$

The Born solvation energy contributes to the pressure of the system only if a composition-dependent dielectric constant is considered, in which case the following pressure contribution is obtained:

$$\begin{aligned}P^{\text{Born}} &= -\left(\frac{\partial A^{\text{Born}}}{\partial V}\right)_{N,T} + \left(\frac{\partial A^{\text{Born}}}{\partial D}\right)_{N,T}\left(\frac{\partial D}{\partial V}\right)_{N,T} \\ &= \frac{e^2}{4\pi\epsilon_0}\frac{1}{D^2}\left(\frac{\partial D}{\partial V}\right)_{N,T} \sum_{\text{ions},i=1}^{n_{\text{ion}}} \frac{N_i z_i^2}{\sigma_i^{\text{Born}}}.\end{aligned} \tag{3.56}$$

3.4 Group-contribution modelling of molecular ionic species within SAFT-γ Mie

The SAFT-γ Mie equation of state enables thermodynamic modelling of complex molecules through the versatility of a group-contribution approach, a capability which is hereby extended to include charged species of all sizes and complexity, ranging from atomic and small molecular ions to large complex molecules with one or multiple charged sites. To achieve this, established theories for electrostatic interactions – which are derived for spherical ions – are carefully rewritten to allow incorporation into the group-contribution framework of SAFT-γ. This leads to two additional Helmholtz free energy terms, A^{Ion} and A^{Born}.

Within SAFT-γ Mie, charged species may be composed of one or multiple functional groups such that the overall charge is contributed by the particular groups which are charged.

The charge of a group k is a *group-specific* parameter regardless of the number of segments ν^* comprising the group. Two possible formulations integrating the MSA and Born theories with the group contribution framework of SAFT-γ are proposed in the current work; these are presented here together with their respective reasoning, approximations, and limitations.

In the first formulation presented in Section 3.4.1, charged chain molecules are approximated as equivalent charged spheres; whereas in the second formulation presented in Section 3.4.2, it is assumed that the electrostatic interactions occur between the individual charged groups. Both formulations offer a way to effect a spherical geometry to which the MSA and Born theories can be applied. Since the Born energy is closely associated with the implementation of the MSA, the same choice of formulation is used in both for the A^{MSA} and A^{Born} terms.

3.4.1 Free-energy perturbation for spherically-approximated charged species

A charged chain molecule i may be approximated as a sphere with a volume equal to the total combined volume of the segments comprising the chain. The diameter $\tilde{\sigma}_{ii}$ of this equivalent sphere is obtained by

$$\tilde{\sigma}_{ii}^3 = \sum_{k=1}^{\text{NG}} (\nu_{k,i} \nu_k^* S_k \sigma_{kk}^3)\,, \tag{3.57}$$

where $\nu_{k,i}$ is the number of groups of type k in molecule i, S_k is the shape factor of group k, and σ_{kk} is the diameter of group k. The approximated sphere is assigned a central point charge equal to the net charge q_i of the chain molecule:

$$q_i = \sum_{k=1}^{\text{NG}} (z_k e). \tag{3.58}$$

The conversion from chain geometry to equivalent-volume spherical geometry is assumed to occur at no cost of free energy, i.e., $A^{\text{chain}\rightarrow\text{sphere}} = 0$, and its purpose is to effect a spherical ion geometry whilst conserving the overall charge density of the ion. Such a conversion can be considered appropriate for relatively short-length chain molecules for which the charge is highly delocalised across the molecule. The conversion of the approximated spheres back to the original chain molecules is also assumed to have no free energy contribution, $A^{\text{sphere}\rightarrow\text{chain}} = 0$. The set of thermodynamic perturbations involved in the SAFT-γ Mie EOS when this electrolyte formulation is adopted is illustrated in Figure 3.1, including the aforementioned nil-contribution perturbations. Since the primitive model of the MSA is adopted, all neutral molecules in the mixture, including the solvent and any neutral solute molecules, are treated implicitly in the MSA and Born terms. The mixture of neutral molecules is represented as a dielectric medium with dielectric constant D.

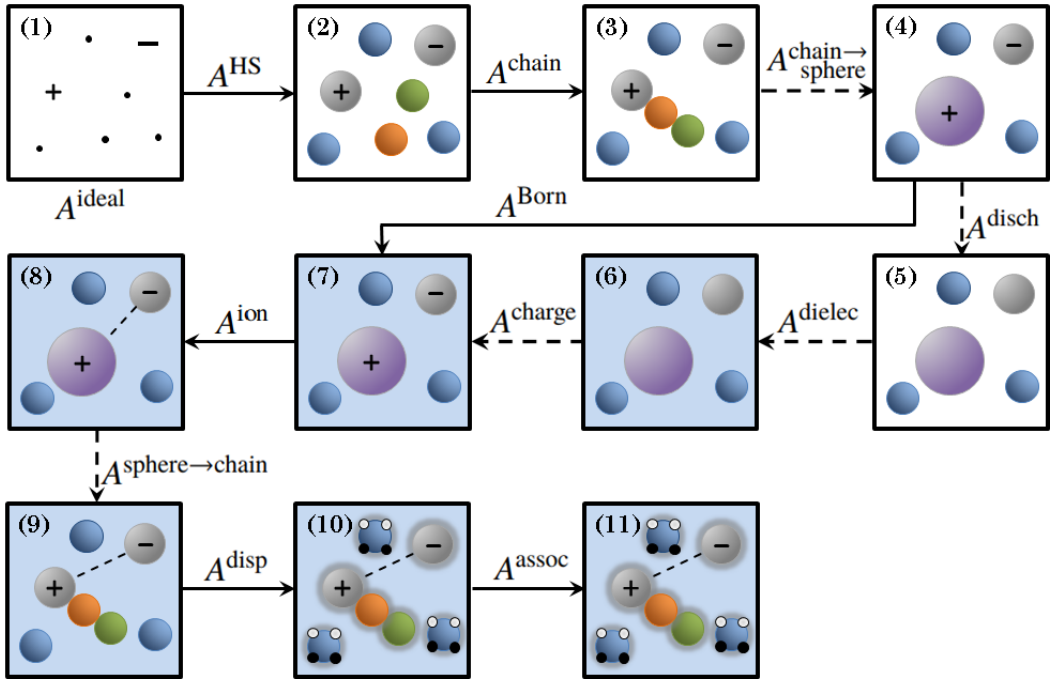

Figure 3.1 Schematic representation of the SAFT-γ Mie formulation for charged species represented as equivalent charged spheres. Groups are illustrated for the case where $\nu^* = 1$ and $S_k = 1$. The ideal gas mixture of non-interacting point particles and point charges (A^{ideal}) is shown in Frame (1). The hard-sphere fluid where ions possess embedded point charges (A^{HS}) is shown in Frame (2). Frame (3) shows the formation of molecular chains from groups (A^{chain}). In Frame (4), the charged molecular chains are converted to spheres of equivalent volume and net charge ($A^{\text{chain}\rightarrow\text{sphere}} = 0$). Frames (5) to (7) represent the equivalent thermodynamic cycle conceptualising the Born solvation free energy: ions are discharged, leading to a mixture of hard spheres in vacuum (A^{disch}); a uniform dielectric medium is introduced (schematically shown as the shaded background) to the hard-sphere fluid (A^{dielec}); and the ions are charged in the presence of the dielectric medium (A^{charge}). The Born free energy term corresponding to the mathematical model is shown in the transition from Frame (4) to Frame (7). Coulombic interactions between ions are represented as dashed lines (A^{ion}) in Frame (8). In Frame (9), the spherically-approximated ions are converted back to charged molecular chains ($A^{\text{sphere}\rightarrow\text{chain}} = 0$). Dispersion interactions between segments are schematised as shaded halos (A^{disp}) in Frame (10). Association sites for mediating association interactions (A^{assoc}) are depicted in Frame (11).

3.4.1.1 MSA term

When the MSA-PM is applied to the mixture in which the charged molecules are approximated as spheres, the electrostatic Helmholtz free energy contribution is obtained as

$$\frac{A^{\mathrm{MSA}}}{Nk_{\mathrm{B}}T} = \frac{U^{\mathrm{MSA}}}{Nk_{\mathrm{B}}T} + \frac{\Gamma^3}{3\pi\rho} \,. \tag{3.59}$$

Here, the free energy is expressed in reduced units, i.e., per molecule, in accordance with the convention used for the terms of the SAFT-γ Mie EOS. Accordingly, the internal energy is given by

$$\begin{aligned} \frac{U^{\mathrm{MSA}}}{Nk_{\mathrm{B}}T} &= -\frac{e^2 V}{(4\pi\epsilon_0)DNk_{\mathrm{B}}T}\left[\Gamma\rho \sum_{\mathrm{ions},i=1}^{n_{\mathrm{ion}}}\left(\frac{x_i z_i^2}{1+\Gamma\tilde{\sigma}_{ii}}\right) + \frac{\pi}{2\Delta}\Omega P_n^2\right] \\ &= -\frac{e^2}{(4\pi\epsilon_0)Dk_{\mathrm{B}}T}\left[\Gamma \sum_{\mathrm{ions},i=1}^{n_{\mathrm{ion}}}\left(\frac{x_i z_i^2}{1+\Gamma\tilde{\sigma}_{ii}}\right) + \frac{\pi}{2\Delta}\Omega P_n^2\right] . \end{aligned} \tag{3.60}$$

The parameters of the MSA expressions are given within this framework as follows:

$$\Gamma^2 = \frac{\pi e^2 \rho}{(4\pi\epsilon_0)Dk_{\mathrm{B}}T} \sum_{\mathrm{ions},i=1}^{n_{\mathrm{ion}}} x_i Q_i^2 \,; \tag{3.61}$$

$$Q_i = \frac{z_i - \tilde{\sigma}_{ii}^2 P_n(\pi/(2\Delta))}{1+\Gamma\tilde{\sigma}_{ii}} \,; \tag{3.62}$$

$$P_n = \frac{\rho}{\Omega} \sum_{\mathrm{ions},i=1}^{n_{\mathrm{ion}}} \frac{x_i \tilde{\sigma}_{ii} z_i}{1+\Gamma\tilde{\sigma}_{ii}} \,; \tag{3.63}$$

$$\Omega = 1 + \frac{\pi\rho}{2\Delta} \sum_{\mathrm{ions},i=1}^{n_{\mathrm{ion}}} \frac{x_i \tilde{\sigma}_{ii}^3}{1+\Gamma\tilde{\sigma}_{ii}} \,; \tag{3.64}$$

$$\Delta = 1 - \frac{\pi\rho}{6} \sum_{\text{ions},i=1}^{n_{\text{ion}}} x_i \tilde{\sigma}_{ii}^3 \,. \tag{3.65}$$

The electrostatic contribution to the chemical potential of such spherically-approximated charged molecules is derived from Equation 3.59 following the derivatives given by Equations 3.47 and 3.49:

$$\begin{aligned} \mu_i^{\text{MSA}} = &- \frac{e^2}{4\pi\epsilon_0 D}\left\{\frac{\Gamma z_i^2}{1+\Gamma\tilde{\sigma}_{ii}} + \frac{\Omega\tilde{\sigma}_{ii}^3}{12}\left(\frac{\pi P_n}{\Delta}\right)^2\right. \\ &\left. - \frac{\pi^2 P_n^2 \tilde{\sigma}_{ii}^3}{4\Delta^2}\left(\frac{1}{1+\Gamma\tilde{\sigma}_{ii}} - \frac{1-\Omega}{3}\right) + \frac{\pi P_n \tilde{\sigma}_{ii} z_i}{\Delta(1+\Gamma\tilde{\sigma}_{ii})}\right\} - \frac{U^{\text{MSA}}}{D}\left(\frac{\partial D}{\partial N_i}\right)_{N_{j\neq i}} . \end{aligned} \tag{3.66}$$

Similarly, by taking the derivative given by Equation 3.52, the electrostatic contribution to the mixture's total pressure is obtained:

$$P^{\text{MSA}} = -\frac{\Gamma^3 k_{\text{B}} T}{3\pi} - \frac{e^2}{8D\epsilon_0}\left(\frac{P_n}{\Delta}\right)^2 - \frac{U^{\text{MSA}}}{D}\left(\frac{\partial D}{\partial V}\right)_N . \tag{3.67}$$

3.4.1.2 Born term

The Born solvation energy accompanying the above MSA formulation also adopts an approximated spherical geometry for the charged molecules. The cavity size associated with the insertion of a spherically-approximated charged molecule (cf. Equation 3.57) reflects a spherical volume equivalent to the combined cavity volume of the individual groups comprising the molecule. The Born cavity diameter $\tilde{\sigma}_{ii}^{\text{Born}}$ of a spherically-approximated charged species i is obtained as follows:

$$(\tilde{\sigma}_{ii}^{\text{Born}})^3 = \sum_{k=1}^{\text{NG}} \left(\nu_{k,i}\nu_k^* S_k (\sigma_{kk}^{\text{Born}})^3\right) . \tag{3.68}$$

where $\sigma_{kk}^{\text{Born}}$ is a group specific parameter characterising the Born cavity diameter of an individual group k. The Born solvation energy for the primitive system comprising the spherically-approximated charged molecules is expressed as

$$\frac{A^{\text{Born}}}{Nk_{\text{B}}T} = -\frac{e^2}{(4\pi\epsilon_0)k_{\text{B}}T}\left(1-\frac{1}{D}\right)\sum_{\text{ions},i=1}^{n_{\text{ion}}}\frac{x_i z_i^2}{\tilde{\sigma}_{ii}^{\text{Born}}}, \tag{3.69}$$

The contribution to the chemical potential of component i is obtained by taking the derivative shown in Equation 3.55:

$$\mu_i^{\text{Born}} = -\frac{e^2}{(4\pi\epsilon_0)}\left[\left(1-\frac{1}{D}\right)\frac{z_i^2}{\tilde{\sigma}_{ii}^{\text{Born}}} + \frac{1}{D^2}\left(\frac{\partial D}{\partial N_i}\right)_{V,T,N_{j\neq i}}\rho V\sum_{\text{ions},i=1}^{n_{\text{ion}}}\frac{x_i z_i^2}{\tilde{\sigma}_{ii}^{\text{Born}}}\right]; \tag{3.70}$$

and finally, through application of the derivative shown in Equation 3.56, the Born contribution to the total system pressure is given by

$$P^{\text{Born}} = \frac{e^2}{(4\pi\epsilon_0)}\frac{1}{D^2}\left(\frac{\partial D}{\partial V}\right)_{N,T}\sum_{\text{ions},i=1}^{n_{\text{ion}}}\frac{N_i z_i^2}{\tilde{\sigma}_{ii}^{\text{Born}}}. \tag{3.71}$$

3.4.2 Free-energy perturbations for charged functional groups

For certain types of charged molecules the spherically approximated geometry adopted in the above formulation may become inappropriate for a number of reasons. Firstly, the molecule may possess a charged functional group where the charge is highly localised relative to the size of the molecule, for example when considering long-chain linear molecules. Furthermore, molecules may possess more than one charged functional group, such as in the case of zwitterions or polyelectrolytes. In the former case, considering the net charge falsely leads to a neutral species, while in the latter case a net charge density would oversimplify the electrostatic forces. The following formulation intends to accommodate such ionic species.

The MSA-PM is applied here to account for the Coulombic interactions between individual charged groups (CG) in the presence of a dielectric medium representing the remaining

neutral groups in the system. The A^{MSA} term is calculated for the mixture of *unbound* groups, as illustrated in Figure 3.2 which includes the complete set of thermodynamic perturbations involved in the SAFT-γ Mie EOS when this electrolyte formulation is adopted.

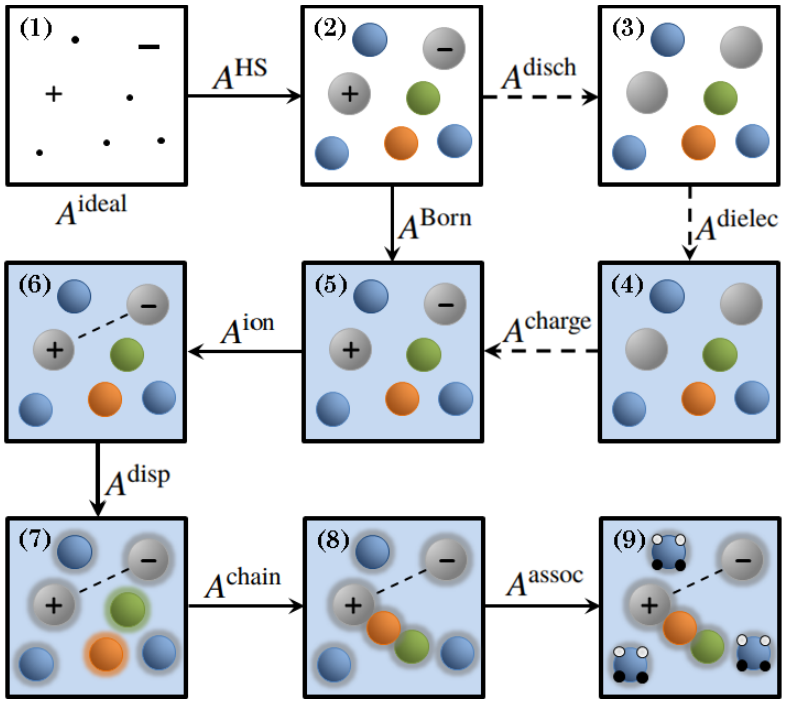

Figure 3.2 Schematic representation of the SAFT-γ Mie formulation for charged groups. Groups are illustrated for the case where $\nu^* = 1$ and $S_k = 1$. The ideal gas mixture of non-interacting point particles and point charges (A^{ideal}) is shown in Frame (1). The hard-sphere fluid where ions possess embedded point charges (A^{HS}) is shown in Frame (2). Frames (3) to (5) represent the equivalent thermodynamic cycle conceptualising the Born solvation free energy: ions are discharged, leading to a mixture of hard spheres in vacuum (A^{disch}); a uniform dielectric medium is introduced (schematically shown as the shaded background) to the hard-sphere fluid (A^{dielec}); and the ions are charged in the presence of the dielectric medium (A^{charge}). The Born free energy term corresponding to the mathematical model is shown in the transition from Frame (2) to Frame (5). Coulombic interactions between ions are represented as dashed lines (A^{ion}) in Frame (6). Dispersion interactions between segments are schematised as shaded halos (A^{disp}) in Frame (7). Frame (8) shows the formation of molecular chains from groups (A^{chain}). Association sites for mediating association interactions (A^{assoc}) are depicted in Frame (9).

For charged groups comprising more than one segment, the group is approximated as a sphere of equivalent volume to the combined volume of the segments comprising the group. The diameter $\tilde{\sigma}_{kk}^3$ of this equivalent spherical group is obtained as

$$\tilde{\sigma}_{kk}^3 = \nu_k^* S_k \sigma_{kk}^3 \,. \tag{3.72}$$

The fraction x_k of a group of type k in the system of unbound groups is given by

$$x_k = \frac{N_k}{N_\mathrm{g}} = \frac{N \sum_{i=1}^{\mathrm{NC}} x_i \nu_{k,i} S_k}{N_\mathrm{g}} \,, \tag{3.73}$$

where N_k is the number of groups of type k, and N_g is the total number of groups:

$$N_\mathrm{g} = N \sum_{i=1}^{\mathrm{NC}} \sum_{k=1}^{\mathrm{NG}} (x_i \nu_{k,i}) \,. \tag{3.74}$$

Accordingly, the total number density of groups ρ_g is related to the total number density of molecules through

$$\rho_\mathrm{g} = \frac{N_\mathrm{g}}{V} = \rho \left(\sum_{i=1}^{\mathrm{NC}} x_i \sum_{k=1}^{\mathrm{NG}} (\nu_{k,i}) \right) \,. \tag{3.75}$$

The 'solvent' applicable to this formulation of the MSA-PM consists of the mixture of unbound neutral groups, so the dielectric constant D must reflect permittivity of this medium. Since in SAFT-γ Mie charge is a group-specific parameter, the neutral groups comprising the dielectric medium may belong to both neutral and charged molecules. Determining the dielectric constant of such a mixture is not straightforward, since there is no analogous real physical system. An appropriate group contribution model for the relative static permittivity would be needed in order to carry out this formulation. This issue may be overcome by adopting the assumption that the fraction of unbound neutral groups arising from the ionic species in the mixture exert a negligible effect on the magnitude of the dielectric constant. This may be considered a reasonable simplification provided that moderate concentrations of electrolyte are considered, such that the fraction of neutral groups belonging to the ionic

species remains small. The remaining mixture of unbound groups – i.e., those belonging to neutral molecules – can be expected to have the same dielectric properties as the mixture of neutral molecules. As a result, it is possible to use a molecular dielectric constant model to estimate the dielectric constant of this mixture of groups.

3.4.2.1 MSA term

The internal energy U^{MSA} arising from electrostatic interactions in the system of unbound groups is obtained as follows:

$$\begin{aligned} U^{\text{MSA}} &= -\frac{e^2}{(4\pi\epsilon_0)D}\left[\Gamma \sum_{\text{CG},k=1}^{n_{\text{CG}}}\left(\frac{N_k z_k^2}{1+\Gamma\tilde{\sigma}_{kk}}\right)+\frac{\pi}{2\Delta}\Omega P_n^2\right] \\ &= -\frac{e^2 V}{(4\pi\epsilon_0)D}\left[\Gamma\rho_{\text{g}} \sum_{\text{CG},k=1}^{n_{\text{CG}}}\left(\frac{x_k z_k^2}{1+\Gamma\tilde{\sigma}_{kk}}\right)+\frac{\pi}{2\Delta}\Omega P_n^2\right] \\ &= -\frac{e^2 V}{(4\pi\epsilon_0)D}\left[\Gamma\rho \sum_{\text{ions},i=1}^{n_{\text{ion}}}\sum_{\text{CG},k=1}^{n_{\text{CG}}}\left(\frac{x_i \nu_{k,i} z_k^2}{1+\Gamma\tilde{\sigma}_{kk}}\right)+\frac{\pi}{2\Delta}\Omega P_n^2\right]. \end{aligned} \tag{3.76}$$

In reduced units, the internal energy per group u^{MSA} is written as

$$\begin{aligned} u^{\text{MSA}} &= \frac{U^{\text{MSA}}}{N_{\text{g}} k_{\text{B}} T} \\ &= -\frac{e^2}{k_{\text{B}} T(4\pi\epsilon_0)D\rho_{\text{g}}}\left[\Gamma\rho \sum_{\text{ions},i=1}^{n_{\text{ion}}}\sum_{\text{CG},k=1}^{n_{\text{CG}}}\left(\frac{x_i \nu_{k,i} z_k^2}{1+\Gamma\tilde{\sigma}_{kk}}\right)+\frac{\pi}{2\Delta}\Omega P_n^2\right], \end{aligned} \tag{3.77}$$

and the dimensionless Helmholtz free energy per group a^{MSA} is therefore evaluated from

$$a^{\text{MSA}} = \frac{A^{\text{MSA}}}{N_g k_{\text{B}} T} = u^{\text{MSA}} + \frac{\Gamma^3}{3\pi\rho}. \tag{3.78}$$

The MSA parameters are obtained as follows:

$$\Gamma^2 = \frac{\pi e^2}{(4\pi\epsilon_0)Dk_\mathrm{B}T}\rho_\mathrm{g}\sum_{\mathrm{CG},k=1}^{n_\mathrm{CG}}(x_k Q_k^2) = \frac{\pi e^2}{(4\pi\epsilon_0)Dk_\mathrm{B}T}\rho\sum_{\mathrm{ions},i=1}^{n_\mathrm{ion}}\sum_{\mathrm{CG},k=1}^{n_\mathrm{CG}}(x_i\nu_{k,i}Q_k^2)\,, \tag{3.79}$$

$$Q_k = \frac{z_k - \tilde{\sigma}_{kk}^2 P_n(\pi/(2\Delta))}{1+\Gamma\tilde{\sigma}_{kk}}\,, \tag{3.80}$$

$$P_n = \frac{\rho_\mathrm{g}}{\Omega}\sum_{\mathrm{CG},k=1}^{n_\mathrm{CG}}\frac{x_k\tilde{\sigma}_{kk}z_k}{1+\Gamma\tilde{\sigma}_{kk}} = \frac{\rho}{\Omega}\sum_{\mathrm{ions},i=1}^{n_\mathrm{ion}}\sum_{\mathrm{CG},k=1}^{n_\mathrm{CG}}\frac{x_i\nu_{k,i}\tilde{\sigma}_{kk}z_k}{1+\Gamma\tilde{\sigma}_{kk}}\,, \tag{3.81}$$

$$\Omega = 1+\frac{\pi\rho_\mathrm{g}}{2\Delta}\sum_{\mathrm{CG},k=1}^{n_\mathrm{CG}}\frac{x_k\tilde{\sigma}_{kk}^3}{1+\Gamma\tilde{\sigma}_{kk}} = 1+\frac{\pi\rho}{2\Delta}\sum_{\mathrm{ions},i=1}^{n_\mathrm{ion}}\sum_{\mathrm{CG},k=1}^{n_\mathrm{CG}}\frac{x_i\nu_{k,i}\tilde{\sigma}_{kk}^3}{1+\Gamma\tilde{\sigma}_{kk}}\,, \tag{3.82}$$

$$\Delta = 1-\frac{\pi\rho_\mathrm{g}}{6}\sum_{\mathrm{CG},k=1}^{n_\mathrm{CG}}(x_k\tilde{\sigma}_{kk}^3) = 1-\frac{\pi\rho}{6}\sum_{\mathrm{ions},i=1}^{n_\mathrm{ion}}\sum_{\mathrm{CG},k=1}^{n_\mathrm{CG}}(x_i\nu_{k,i}\tilde{\sigma}_{kk}^3)\,. \tag{3.83}$$

In order to be incorporated meaningfully alongside the free energy perturbations of the SAFT-γ Mie EOS, the electrostatic contribution to the free energy should relate to the mixture of chain molecules. The Helmholtz free energy per molecule (A^MSA) can be obtained from the Helmholtz free energy per group (a^MSA) using the relationship between N_g and N given by Equation 3.74:

$$\frac{A^\mathrm{MSA}}{Nk_\mathrm{B}T} = a^\mathrm{MSA}\frac{N_\mathrm{g}}{N} = a^\mathrm{MSA}\sum_{i=1}^{n_\mathrm{NC}}\sum_{k=1}^{n_\mathrm{NG}}(x_i\nu_{k,i})\,. \tag{3.84}$$

Using 3.84, one may obtain the electrostatic contribution to the chemical potential of a molecule i by applying the chain derivative shown in Equations 3.47 and 3.49:

$$\begin{aligned}\mu_i^{\mathrm{MSA}} = &-\frac{e^2}{4\pi\epsilon_0 D}\Bigg\{\Gamma \sum_{\text{ions},i=1}^{n_{\text{ion}}}\sum_{\text{CG},k=1}^{n_{\text{CG}}}\left(\frac{\nu_{k,i}z_k^2}{1+\Gamma\tilde{\sigma}_{kk}}\right) \\ &+\frac{\Omega}{12}\left(\frac{\pi P_n}{\Delta}\right)^2\sum_{\text{ions},i=1}^{n_{\text{ion}}}\sum_{\text{CG},k=1}^{n_{\text{CG}}}(\nu_{k,i}\tilde{\sigma}_{kk}^3) - \frac{\pi^2 P_n^2}{4\Delta^2}\sum_{\text{ions},i=1}^{n_{\text{ion}}}\sum_{\text{CG},k=1}^{n_{\text{CG}}}(\nu_{k,i}\tilde{\sigma}_{kk}^3) \\ &\times\left[\sum_{\text{CG},k=1}^{n_{\text{CG}}}\left(\frac{1}{1+\Gamma\tilde{\sigma}_{kk}}\right) - \frac{1-\Omega}{3}\right] + \frac{\pi P_n}{\Delta}\sum_{\text{ions},i=1}^{n_{\text{ion}}}\sum_{\text{CG},k=1}^{n_{\text{CG}}}\left(\frac{\nu_{k,i}\tilde{\sigma}_{kk}z_k}{1+\Gamma\tilde{\sigma}_{kk}}\right)\Bigg\} \\ &-\frac{U^{\mathrm{MSA}}}{D}\left(\frac{\partial D}{\partial N_i}\right)_{N_{j\neq i}}.\end{aligned} \tag{3.85}$$

Finally, the electrostatic contribution to the total pressure of the system is derived according to Equation 3.52, which gives:

$$P^{\mathrm{MSA}} = -\frac{\Gamma^3 k_{\mathrm{B}}T}{3\pi} - \frac{e^2}{8D\epsilon_0}\left(\frac{P_n}{\Delta}\right)^2 - \frac{U^{\mathrm{MSA}}}{D}\left(\frac{\partial D}{\partial V}\right)_N. \tag{3.86}$$

3.4.2.2 Born term

The Born energy corresponding to the mixture of unbound groups may be computed by defining the cavity diameter $\tilde{\sigma}_{kk}^{\mathrm{Born}}$ applicable to the spherically-approximated group k (cf. Equation 3.72). The volume of this cavity is equal to the combined cavity volume of the segments comprising the group; it is obtained as follows:

$$(\tilde{\sigma}_{kk}^{\mathrm{Born}})^3 = \nu_k^* S_k (\sigma_{kk}^{\mathrm{Born}})^3 . \tag{3.87}$$

The Born energy of the system of unbound groups (a^{Born}) can be related to the Born contribution to the Helmholtz free energy for the mixture of molecules (A^{Born}) in a similar manner as a^{MSA} is related to A^{MSA} through Equation 3.84. First, the dimensionless Born energy per

group is obtained as

$$\begin{aligned} a^{\text{Born}} &= \frac{A^{\text{Born}}}{N_{\text{g}} k_{\text{B}} T} \\ &= -\frac{e^2}{(4\pi\epsilon_0) N_{\text{g}} k_{\text{B}} T}\left(1-\frac{1}{D}\right)\sum_{\text{CG},k=1}^{n_{\text{CG}}}\frac{N_k z_k^2}{\tilde{\sigma}_{kk}^{\text{Born}}} \\ &= -\frac{e^2 \rho}{(4\pi\epsilon_0)\rho_{\text{g}} k_{\text{B}} T}\left(1-\frac{1}{D}\right)\sum_{\text{ions},i=1}^{n_{\text{ion}}}\sum_{\text{CG},k=1}^{n_{\text{CG}}}\frac{x_i \nu_{k,i} z_k^2}{\tilde{\sigma}_{kk}^{\text{Born}}}\,. \end{aligned} \tag{3.88}$$

The dimensionless Born energy per molecule may be obtained from a^{Born} by invoking equation 3.74:

$$\begin{aligned} \frac{A^{\text{Born}}}{N k_{\text{B}} T} &= a^{\text{Born}}\frac{N_s}{N} \\ &= a^{\text{Born}}\sum_{i=1}^{n_{\text{NC}}}\sum_{k=1}^{n_{\text{NG}}}(x_i \nu_{k,i}) \\ &= -\frac{e^2}{(4\pi\epsilon_0) k_{\text{B}} T}\left(1-\frac{1}{D}\right)\sum_{\text{ions},i=1}^{n_{\text{ion}}}\sum_{\text{CG},k=1}^{n_{\text{CG}}}\left(\frac{x_i \nu_{k,i} z_k^2}{\tilde{\sigma}_{kk}^{\text{Born}}}\right). \end{aligned} \tag{3.89}$$

The Born contribution to the chemical potential of a component i is then derived following Equation 3.55:

$$\begin{aligned} \mu_i^{\text{Born}} = -\frac{e^2}{(4\pi\epsilon_0)}\Bigg[&\left(1-\frac{1}{D}\right)\sum_{\text{CG},k=1}^{n_{\text{CG}}}\frac{\nu_{i,k} z_k^2}{\tilde{\sigma}_{kk}^{\text{Born}}} \\ &+\frac{1}{D^2}\left(\frac{\partial D}{\partial N_i}\right)_{V,T,N_{j\neq i}}\rho V\sum_{\text{ions},i=1}^{n_{\text{ion}}}\sum_{\text{CG},k=1}^{n_{\text{CG}}}\frac{x_i \nu_{i,k} z_k^2}{\tilde{\sigma}_{kk}^{\text{Born}}}\Bigg], \end{aligned} \tag{3.90}$$

and finally, following Equation 3.56, the Born pressure contribution for the mixture of molecules is

$$P^{\text{Born}} = \frac{e^2 N}{(4\pi\epsilon_0)}\frac{1}{D^2}\sum_{\text{ions},i=1}^{n_{\text{ion}}}\sum_{\text{CG},k=1}^{n_{\text{CG}}}\left(\frac{x_i \nu_{k,i} z_k^2}{\tilde{\sigma}_{kk}^{\text{Born}}}\right)\left(\frac{\partial D}{\partial V}\right)_{N,T}. \tag{3.91}$$

3.5 Ion-ion dispersion interactions

The dispersion energy ε_{kl} between any two charged groups k and l may be determined by analogy to the work of Hudson and McCoubrey [186] and later Haslam et al. [187] in relation to the prediction of binary intermolecular potential parameters, following Eriksen [188]. In this approach, the dispersion energy between two ions is obtained by relating the London dispersion interaction potential [189] with the Mie potential model given by Equation 3.2. Following Haslam et al. [187], the London interaction potential is expressed as a function of the ionization potentials I_k and electronic polarisabilities $\alpha_{0,k}$ of the interacting species:

$$u_{kl}^{\text{London}} = -\frac{3}{2}\frac{\alpha_{0,k}\alpha_{0,l}}{r_{kl}^6(4\pi\epsilon_0)^2}\frac{I_k I_l}{I_k + I_l}\,, \tag{3.92}$$

where r_{kl} is the centre–centre distance between the charged groups.

In order to obtain a physical relation for the dispersive interaction energy, the London and Mie potentials must be related. For reasons of practicality, it is easier to operate with the van der Waals integrated form of each potential. The spherically symmetric potentials are integrated over the azimuthal (ϕ) and polar (θ) angles. Since the potentials tend towards infinity for short separations, a lower cut-off range of σ_{kl} is imposed for the distance of centre–centre separation distance, in order to suppress the sensitivity of this methodology to the steepness of the potential at close range. The integrated form ψ_{kl} of a centro-symmetric potential is

$$\psi_{kl} = \int_{\theta=0}^{\pi}\int_{\phi=0}^{2\pi}\int_{r_{kl}=\sigma_{kl}}^{\infty} u_{kl} r_{kl}^2 \mathrm{d}r_{kl}\sin\theta\mathrm{d}\theta\mathrm{d}\phi\,. \tag{3.93}$$

For the London interaction, this leads to the expression:

$$\frac{\psi_{kl}^{\text{London}}}{4\pi} = -\frac{\alpha_{0,k}\alpha_{0,l}}{2\sigma_{kl}^3(4\pi\epsilon_0)^2}\frac{I_k I_l}{I_k + I_l}\,; \tag{3.94}$$

and following the same procedure for the Mie potential, one obtains:

$$\frac{\psi_{kl}^{\mathrm{Mie}}}{4\pi} = -\frac{C\varepsilon_{kl}(\lambda_{\mathrm{r},kl} - \lambda_{\mathrm{a},kl})\sigma_{kl}^3}{(\lambda_{\mathrm{r},kl} - 3)(\lambda_{\mathrm{a},kl} - 3)} \,. \tag{3.95}$$

Equating and rearranging the expressions for the integrated potentials leads to a relation for the dispersive interaction energy parameter:

$$\varepsilon_{kl} = \frac{(\lambda_{\mathrm{r},kl} - 3)(\lambda_{\mathrm{a},kl} - 3)}{2C(\lambda_{\mathrm{r},kl} - \lambda_{\mathrm{a},kl})} \frac{\alpha_{0,k}\alpha_{0,l}}{(4\pi\epsilon_0)^2\sigma_{kl}^6} \frac{I_k I_l}{I_k + I_l} \,. \tag{3.96}$$

This approach may be used to estimate the value of the ε_{kl} parameter for any pair of charged groups, provided that the polarisabilities and ionisation potentials are known. These quantities are usually well documented in the literature for the a wide range of ionic species and charged functional groups.

3.6 Relative static permittivity model

Thermodynamic modelling of electrostatic interactions employing a primitive approach requires a means of determining the dielectric constant of the implicitly represented solvent medium. The electric properties of the solvent change according to the system temperature and composition, which means that the change in the dielectric constant with electrolyte solute concentration should be taken into account when implementing the A^{ion} and A^{Born} terms.

The empirical model presented by Schreckenberg et al. [61] is applied in the present work. This model expresses the dielectric constant of a solvent as a function of temperature and the density of the solvent; for single-solvent solutions, it takes the following form:

$$D = 1 + \rho_{\mathrm{solv}} d_i \,, \tag{3.97}$$

where $\rho_{\text{solv}} = N_{\text{solv}}/V$ is the number density of the solvent species and d_i is a temperature-dependent parameter for solvent component i. In turn, d_i is obtained as a function of two component-specific parameters:

$$d_i = d_{V,i}\left(\frac{d_{T,i}}{T} - 1\right), \tag{3.98}$$

where $d_{V,i}$ and $d_{T,i}$ are expressed in units of $\text{dm}^3\ \text{mol}^{-1}$ and K, respectively.

An important aspect of this particular model is that the ionic composition of the solution is only taken into account implicitly, through the change in the solvent density ρ_{solv} effected by a change in electrolyte solute composition. The model is nevertheless chosen firstly due to its relative simplicity, and secondly due to its proven performance in describing the dielectric properties of a wide range of solvents and solvent mixtures. Although only single-solvent mixtures are considered in the current work, this allows the prospect of applying the ionic models to mixed aqueous + organic solvents. Despite not explicitly taking into account the ionic composition of the mixture, the model has been used effectively alongside the SAFT-VRE EOS [61] for modelling strong electrolyte solutions up to 10 mol kg^{-1}, so it can be considered suitable for use alongside the SAFT-γ Mie approach for electrolytes.

3.7 Summary

The SAFT-γ Mie equation of state expresses the Helmholtz free energy of fluid mixtures at equilibrium, knowledge of which allows computation of the system's thermodynamic properties. In particular, the free energy is calculated as perturbative free energy contributions to the hard sphere reference system, therefore the SAFT-γ Mie approach provides an adaptable thermodynamic framework in which specific molecular interactions may be described explicitly. The present work extends the applicability of the SAFT-γ Mie EOS by introducing the two additional free energy terms arising form the presence of charged species. Firstly, the MSA-PM theory is employed to account for electrostatic forces between

charged species interacting through a Coulomb potential. Secondly, the Born theory is used to account for the electrostatic component of the solvent–ion interaction contributing to ion solvation.

In this chapter, these two theories have been formulated so as to be compatible with the group-contribution framework of SAFT-γ Mie, in which molecules are composed of fused functional-group segments, some of which may carry a charge. An appropriate formulation for such molecules should adopt suitable assumptions as to the spherical charged species to which the theories are applicable; two options have been proposed for achieving this. The first formulation described in Section 3.4.1 assumes that a charged heteronuclear molecule may be approximated as a spherical species with a equivalent volume and thus equivalent charge density, which is speculated to be better suited to smaller molecules with delocalised charge. The second formulation presented in Section 3.4.2 applies the MSA and Born theories to the individual charged functional groups, and it is speculated to be better suited to larger and more linear molecules, and molecules possessing multiple charged functional groups.

The expressions for these two group-contribution electrolyte formulations converge to the general MSA and Born expressions (cf. Section 3.3). In other words, the formulations can be used interchangeably when modelling mixtures in which all ionic components are spherical. This scenario is encountered in Chapter 4 when modelling inorganic electrolyte solutes. Non-spherical organic ions are encountered in Chapter 5, in which the performance of the two proposed avenues for modelling electrolytes using SAFT-γ Mie will be evaluated.

Chapter 4

Strong inorganic electrolytes: salts, acids, and bases

This chapter considers the thermodynamic properties of solutions of strong electrolytes, including salts, acids, and bases, at conditions of equilibrium. Specifically, aqueous solutions of alkali halide salts, hydrogen halides, and alkali hydroxides are modelled. The types of charged components involved in these systems are small, mostly atomic, inorganic ions, which are generally accepted as having a spherical geometry [190, 191]. This assumption is also made for the oligoatomic inorganic ions in this chapter, which means that the two SAFT-γ Mie avenues for electrolytes described in Chapter 3 may be used interchangeably, because they simplify to the general expressions for the MSA and Born equations when describing spherical ionic components. Given that all ionic components modelled in this Chapter are spherical, the SAFT-γ Mie formalism simplifies to the SAFT-VRE Mie model which was first presented in the work of Dufal [122]. The thermodynamic model adopted throughout this chapter is therefore referred to as SAFT-VRE Mie. Nevertheless, the models presented here are consistent with the group-contribution framework of SAFT-γ Mie.

A range of thermodynamic properties are investigated for the aqueous electrolyte solutions studied in this chapter. Besides the common properties of equilibrium fluids, such as saturated vapour pressures and densities, the mean ionic activity coefficients of the salt solutes and the osmotic coefficient of the solution are key properties commonly reported for electrolyte solutions. These two properties are directly linked to the activities of the electrolyte solute and the solvent, thereby manifesting the behaviour of each component in the solution mixture. Two further important properties for electrolyte solutions are the Gibbs free energy of solvation of the ions, which relates to the properties of the ions at the infinite dilution reference state, and the solubility limit of the salt, which gives an indication of the predictive capability of the proposed ionic models.

4.1 Thermodynamic properties

Strong electrolytes are considered to be completely dissociated in solution, with the equilibrium defined by Equation 2.1 lying fully to the right such that no neutral salt molecule exists in the solution mixture and the dissociated ions exist as free solvated ions. The concentration of an electrolyte $M_{\nu_+}X_{\nu_-}$ is quantified here in terms of the molality m_{MX}, defined as the molar amount (mol) of salt per kilogram of solvent j. In the case of fully dissociated electrolytes, the mole fraction of a given ion i can be calculated from the molality as:

$$x_i = \frac{\nu_i m_{MX}}{\nu m_{MX} + 1/MW_j}, \tag{4.1}$$

where ν_i is the stoichiometric coefficient of ion i, $\nu = \nu_+ + \nu_-$, and MW_j denotes the molecular weight of the solvent in units of kg mol^{-1}.

The electrolytic properties of the solution of a fully dissociated electrolyte are typically collated in the mean ionic activity coefficient (MIAC), $\gamma_\pm$, calculated as an average of cationic

and anionic contributions (cf. Section 2.2.1):

$$\gamma_{\pm,m}(T,p,\mathbf{N}) = \left(\left(\gamma_{+,m}(T,p,\mathbf{N})\right)^{\nu_+}\left(\gamma_{-,m}(T,p,\mathbf{N})\right)^{\nu_-}\right)^{1/(\nu_+ + \nu_-)}. \tag{4.2}$$

The contribution of the solvent j to the thermodynamics of the system can be characterised through the osmotic coefficient, Φ (cf. Section 2.2.2):

$$\Phi(T,p,\mathbf{N}) = -\frac{1}{(\nu_+ + \nu_-)\, m_{\mathrm{MX}} MW_j} \ln a_{\mathrm{j}}(T,p,\mathbf{N}). \tag{4.3}$$

According to Equation 2.26, the MIAC and the osmotic coefficient are directly related such that the thermodynamic properties of the solvents and solutes in a mixture are not independent. It is required, therefore, that a correct thermodynamic model for electrolytes should predict both of these properties to a similar degree of agreement with experimental data. Achieving this is a core target of this chapter.

4.1.1 Ion solvation

The Gibbs free energy of solvation $\Delta G_{\mathrm{solv},i}$ of an ion i corresponds to the residual chemical potential of the ion at infinite dilution, according to the definition of Myers et al. [51], which relates the solvation energy to the fugacity φ_i^* of the ion at infinite dilution:

$$\Delta G_{\mathrm{solv},i} = -N k_{\mathrm{B}} T \ln\left(\varphi_i^*(T,p,\mathbf{N}^*)\frac{pMW_j m^\circ}{p_{\mathrm{ref}}}\right), \tag{4.4}$$

Here, p_{ref} is the pressure of the reference state (1 bar) for the change in the Gibbs free energy, and m° is the standard state molality of 1 mol kg^{-1}; these arise, respectively, from taking into account the difference in pressure between the state of interest and the reference pressure, and from converting between the mole-fraction and molality scales.

4.2 Phase equilibria

The conditions which enforce phase equilibrium of electrolyte solutions are similar to those of non-electrolyte systems, with additional constraints related to the charge balances and the necessary charge neutrality of a given phase. For a number of phases N_{phases}, with individual phases denoted by superscript Greek letters, the thermal and mechanical phase equilibrium conditions must be satisfied, i.e.

$$T^{\alpha} = T^{\beta} = \cdots = T^{N_{\text{phases}}}, \tag{4.5}$$

$$p^{\alpha} = p^{\beta} = \cdots = p^{N_{\text{phases}}}. \tag{4.6}$$

In addition, a relationship in each equilibrium phase is required for the chemical potentials of each species in the mixture. As a consequence of treating strong electrolyte solutes as fully ionised in solution, the additional constraints required to characterise phase equilibrium will depend on the nature of the phases considered.

4.2.1 Vapour-liquid equilibrium

In the consideration of equilibrium between two (or more) fluid phases, equality of chemical potentials is required for each neutral species. For the single-solvent solutions of fully dissociated electrolytes considered here, the solvent j is the only neutral species present such that:

$$\mu_j^{\alpha} = \mu_j^{\beta} = \cdots = \mu_j^{N_{\text{phases}}}. \tag{4.7}$$

For any pair of charged species i and i', a constant relative difference of chemical potentials across electroneutral phases must be satisfied, according to Grossmann and Maurer [192]:

$$\begin{aligned}
\left(\mu_i^{\alpha} - \mu_i^{\beta}\right)/z_i &= \left(\mu_{i'}^{\alpha} - \mu_{i'}^{\beta}\right)/z_{i'}, \\
&\vdots \\
\left(\mu_i^{\alpha} - \mu_i^{N_{\text{phases}}}\right)/z_i &= \left(\mu_{i'}^{\alpha} - \mu_{i'}^{N_{\text{phases}}}\right)/z_{i'} \qquad \forall i, i' \in (z_i, z_{i'} \neq 0).
\end{aligned} \tag{4.8}$$

The solution of the equilibrium conditions is obtained with a Levenberg-Marquardt [193, 194] algorithm, allowing for the presence of ions in all fluid phases; including the gas phase. The volume dependence of the relative static permittivity model and the inclusion of the Born free energy term in the underlying theory deliver a model where the ions naturally partition predominantly into the denser liquid phase, with only trace amounts (of the order of $x_{\text{salt}} = 10^{-70}$) in the gaseous phase, in agreement with experimental observation.

4.2.2 Solid-liquid equilibrium

The description of phase equilibrium between solid and liquid phases containing electrolytes is linked to the chemical equilibrium governing the dissociation of the solvated electrolyte leading to the formation of charged species in solution. The solid phase consists of the pure unsolvated crystalline salt $\mathrm{M}_{\nu_+}\mathrm{X}_{\nu_-}$ in equilibrium with a liquid phase saturated in salt. Assuming complete dissociation of the dissolved salt, the phase and chemical equilibria require that the chemical potential $\mu_{\mathrm{MX}_{(s)}}$ of the crystalline salt in the solid phase is equal to the sum of the chemical potentials of the solvated ions $\mu_{i_{(\mathrm{aq})}}$, with i =M, X:

$$\mu_{\mathrm{MX}_{(\mathrm{s})}}(T, p) = \nu_+ \mu_{\mathrm{M}_{(\mathrm{aq})}}(T, p, \mathbf{m}^{\mathrm{sat}}) + \nu_- \mu_{\mathrm{X}_{(\mathrm{aq})}}(T, p, \mathbf{m}^{\mathrm{sat}}), \tag{4.9}$$

where M represents the cation and X the anion. The molal composition vector of the saturated aqueous phase is represented by $\mathbf{m}^{\mathrm{sat}}$, and the molality of solvated ion i is related to the salt

molality through

$$m_i^{\text{sat}} = \nu_i m_{\text{MX}}^{\text{sat}} \,, \tag{4.10}$$

where $m_{\text{MX}}^{\text{sat}}$ is the solubility limit of salt $\text{M}_{\nu_+}\text{X}_{\nu_-}$.

The solid phase is taken to be the unhydrous crystalline salt, for which the chemical potential is obtained from

$$\begin{aligned} \mu_{\text{MX}}(T,p) &= \mu_{\text{MX}}^0(T,p) + RT\ln(a_{\text{MX}}(T,p)) \\ &= \Delta G_{\text{MX}_{(\text{s})}}^f(T,p) \,. \end{aligned} \tag{4.11}$$

The chemical potential of the pure solid salt, μ_{MX}^0, is equivalent to the molar Gibbs free energy of formation $\Delta G_{\text{MX}_{(\text{s})}}^f$ of the solid from its constituent elements in their standard states; a_{MX} is the activity of the pure salt, which takes the value of 1 according to the rational symmetric standard state.

The chemical potential of solvated ion i in the saturated liquid phase is expressed on a molality basis as

$$\begin{aligned} \mu_i(T,p,\mathbf{m}^{\text{sat}}) &= \mu_i^\circ(T,p,\mathbf{m}^\circ) + RT\ln\left(\frac{m_i\gamma_{i,m}(T,p,\mathbf{m}^{\text{sat}})}{m_\circ}\right) \\ &= \Delta G_{i_{(\text{aq})}}^f(T,p) + RT\ln\left(\frac{m_i\gamma_{i,m}(T,p,\mathbf{m}^{\text{sat}})}{m^\circ}\right), \end{aligned} \tag{4.12}$$

where the reference chemical potential $\mu_i^\circ(T,p,\mathbf{m}^\circ)$ of ion i (defined by Equation 2.17) refers to a hypothetical ideal solution of unit molality ($m^\circ = 1$ mol kg^{-1}) and is equivalent to the molar Gibbs free energy of formation $\Delta G_{i_{(\text{aq})}}^f$ of a 1 mol kg^{-1} solution of the solvated ion from its constituent elements in their standard states.

Employing the expressions for the chemical potential of the solid salt and solvated ions given by Equations 4.11 and 4.12 and relating the ion molality to the salt molality through

Equation 4.10, the solid-liquid equilibrium condition for fully dissociated salts given by Equation (4.9) can be rewritten to obtain a working solubility equation for the salt:

$$m_{\mathrm{MX}}^{\mathrm{sat}\ (\nu_+ + \nu_-)} = \frac{K_{\mathrm{sp,MX}}(T,p)}{\left(\frac{\nu_+ \gamma_{+,m}(T,p,\mathbf{m}^{\mathrm{sat}})}{m^\circ}\right)^{\nu_+} \left(\frac{\nu_- \gamma_{-,m}(T,p,\mathbf{m}^{\mathrm{sat}})}{m^\circ}\right)^{\nu_-}}, \tag{4.13}$$

where, $K_{\mathrm{sp}}(T,p)$ is the solubility product of the salt, expressed as:

$$K_{\mathrm{sp,MX}} = \exp\left(-\frac{\nu_+ \Delta G^f_{\mathrm{M}_{(\mathrm{aq})}}(T,p) + \nu_- \Delta G^f_{\mathrm{X}_{(\mathrm{aq})}}(T,p) - \Delta G^f_{\mathrm{MX}_{(\mathrm{s})}}(T,p)}{RT}\right). \tag{4.14}$$

The working solubility equation used in the present work inherently includes a temperature dependence through the variation of the solubility product with temperature, although it is not dealt with explicitly.

4.3 Model development

Aqueous solutions of strong electrolytes are considered in this work, focusing particularly on the halide salts of alkali metals and alkaline earth metals as well as aqueous strong acids and bases. These solutions are modelled as ternary mixtures composed of water, anions, and cations, under the assumption of a fully dissociated solute. The electrolyte solutes are therefore modelled by means of the constituent monovalent and divalent atomic ions in the case of salts, while molecular ions are also considered for the acid and base solutions.

In order to model these aqueous solutions, the solvent is treated using the model for water presented by Dufal et al. [177]. In this model, the water molecule comprises a single segment possessing four off-centre association sites, two of which are of type 'H' ($n_{\mathrm{H}} = 2$) and two of type 'e' ($n_{\mathrm{e}} = 2$), which mediate hydrogen bonding interactions. The molecular potential

parameters for this model of water are presented in Table 4.1, together with the parameters required for the correlation of the dielectric constant.

In this work the ions are modelled as spherical, consisting of a single segment ($m_{\mathrm{seg},i} = 1$), and carrying a single point charge $q_i = z_i e$. All ions experience dispersion interactions, represented with Mie potentials of variable range, both with the solvent and with other ions. A full description of the intermolecular potential necessitates the like-interaction energetic parameters as well as the cross-interaction parameters. The like-interaction parameters of an ion i include the segment diameter σ_{ii}, the interaction energy ε_{ii}, and the repulsive and attractive exponents of the Mie potential, $\lambda_{\mathrm{r},ii}$ and $\lambda_{\mathrm{a},ii}$ respectively. Similarly, the cross-interaction parameters between ions i and j include the unlike diameter σ_{ij}, the unlike interaction energy ε_{ij}, and the unlike repulsive and attractive Mie exponents, $\lambda_{\mathrm{r},ij}$ and $\lambda_{\mathrm{a},ij}$.

Molecular ions which interact with the solvent via hydrogen bonding are further characterised by additional association parameters: the number of sites of a certain type a on ion i ($n_{a,i}$), the unlike bonding energy $\varepsilon^{\mathrm{HB}}_{ab,ij}$, and the corresponding bonding volume $K_{ab,ij}$ between site a on ion i and site b on solvent j. For the development of molecular ions, the model of such ions should be physically consistent with the model of the smallest neutral parent molecule giving rise to the ion. In this work, the SAFT-VR Mie model of the neutral parent molecule is used as a reference for developing the model for the molecular ion. Consequently, the parameters of the two species – including the association parameters – will be related.

The parametrization of the intermolecular potentials for the solvent and solute species naturally dictate the fidelity of the proposed model. However, the complexity of the SAFT model demands a significant number of parameters to be determined, both for pure species and for binary interactions. This results in a large, complex parameter space with high degeneracy, yielding significant variability in the description of individual species. Model development for charged species with equations of state is further complicated by the underlying premise that ionic species can only be assessed in solution. In order to simplify the parameter estimation problem, the number of free parameters is limited here by assigning reasonable estimates

to those parameters for which it is possible to use physical relationships to determine their value in the model. Depending on the type of the two interacting species i and j, the cross-interaction parameters are obtained either via combining rules or by optimisation, while pure-component parameters are assigned values *a priori* whenever reasonably possible.

4.3.1 The ion segment diameter and Born diameter

Addressing first the physical geometry of the ions, the size parameters required to treat the ions in the SAFT model are the segment diameter σ_{ii} and Born cavity diameter $\sigma_{ii}^{\text{Born}}$. The segment diameters of the ion models in previous work with SAFT-VRE were determined either by assigning the values of experimentally determined sizes of bare ions [55, 56, 121], or by fitting to experimental data of salt solution properties [61]. In the latter case, the optimised segment parameters were found to take similar values to the experimentally determined ion diameters reported by Shannon [191] and Pauling [190]. Out of consideration for the number adjustable model parameters, the values for σ_{ii} are assigned in this work based on experimental results for the ionic sizes, where these are available. The segment diameters chosen for the atomic ions are the experimentally derived ionic diameters presented by Shannon [191] corresponding to the ions with a coordination number of 6 in a crystal lattice. Shannon has reported a number of values of the crystal ionic diameters for a range of coordination numbers; of these, a coordination number of 6 was reported for all of the ions of interest in the present work, therefore the ionic size corresponding to this structure was selected for consistency. Furthermore, the work of Shannon includes data for a comprehensive collection of ionic species, thus providing an internally consistent source for the sizes of ions.

The diameters of the hydrated ions are also reported, and certain electrolyte solution simulation studies [195, 196] have suggested that the hydration coordination numbers of the ions are important for modelling their behaviour accurately. This is a factor that needs to be accounted for by models in which the ion's segment size is not distinguished from its cavity size, and when the model is intended to be used only in single-solvent aqueous environments.

The present implementation of the SAFT-VRE Mie approach does account for the difference between the structural size of the ion and the effective size it occupies. The choice of σ_{ii} is freed from any considerations relating to the solvent environment as a direct consequence of introducing a distinct Born cavity diameter, which implicitly accounts for the structure of solvent molecules around the ions. As a result, the size for the ions is assigned to be equal to the experimentally derived crystal ionic diameter, rather than the effective ionic diameter of the solvated ion in water, as the former is expected to better represent the real size of the ions in the absence of any influence from the solvent.

In the case of the molecular ion H_3O^+, the SAFT-VR model of water being the closest neutral parent molecule is taken as a reference in order to characterise its size. Taking the assumption that the protonation of water does not effect a significant change in the size of the molecule, the diameter of the H_3O^+ ion can be assigned to be equal to that of H_2O. This is considered to be a reasonable approximation, given that H_3O^+ occurs only in aqueous solution as a solvated ion. By contrast, OH^- also exists in crystalline form so, for consistency with the diameters of other ions, the ionic diameter assigned for OH^- is that reported in the work of Shannon [191]. This choice nevertheless leads to a OH^- segment diameter value which is in proportion to the diameter of water in the SAFT-VR Mie model.

The Born cavity diameter has commonly been treated in other work to be equal to the structural ionic diameter [31, 51, 61, 116]. Rashin and Honig [197] have defined the value of the Born cavity diameter $\sigma_{ii}^{\text{Born}}$ such that the ion cavity experiences a minimum contribution of electrons from the surrounding dielectric medium. By analysis of electron-density maps of crystals of alkali fluoride salts, combined with a 7% correction increase in the cavity diameter attributed to non-sphericity of the actual ion cavity, Rashin and Honig have proposed an approach for deriving internally consistent Born diameters. The ion cavity diameters for the atomic ion models developed in this work are taken directly from the original work of these authors [197]. An equation of state for electrolytes presented by Harvey and Prausnitz [58] also draws upon the analysis of Rashin and Honig to define the cavity diameter of ions as an

independent parameter from the structural ionic diameter, though it omits the non-sphericity correction factor recommended by the latter.

The parent neutral molecule is again used as a reference for the molecular ions H_3O^+ and OH^- by considering that the Born diameter of both these ions must be well represented by the magnitude of the segment diameter of the H_2O model, which has been determined by comparison to bulk fluid properties [177]. Rashin and Honig do not report an optimal Born diameter for H_3O^+, but the value they report for OH^- ($\sigma_{OH^-}^{Born}$ = 2.9960 Å) is very similar to that of the H_2O model diameter (σ_{H_2O} = 3.0063 Å), which corroborates the chosen approach for characterising this parameter. Helgeson and Kirkham [198] have shown that a linear correlation exists between the enthalpy of solvation of ions and the inverse of the effective ionic radius, while Marcus [199] has also demonstrated a correlation between the Gibbs free energy of solvation and the ionic radius. In Figure 4.1 these observations are applied as a means of evaluating the choice of Born cavity diameters for the ions, which are indeed found to correlate linearly with their Gibbs free energy of solvation. This lends confidence to the values of σ_{ii}^{Born} chosen for the ions, especially to the approximation for that of the H_3O^+ ion. The linear correlation of σ_{ii}^{Born} with $\Delta G_{solv,i}$ can therefore be used for estimating the cavity diameter of ions as an alternative to the approach of Rashin and Honig, and in the absence of other means of determination such as molecular simulation studies.

4.3.2 Ion–ion dispersion interactions

The like and unlike ion–ion dispersion energies are calculated using Equation (3.96) with the polarisabilities $\alpha_{0,i}$ and ionisation potentials I_i presented in Tables 4.2 and 4.3. The ionisation potential of anions is taken to be the negative of the electron affinity of the parent species, and that of the atomic cations is taken as the higher-order ionisation potential of the parent species. The values of these properties are obtained from Ref. [202] for the atomic ions, and from Ref. [203–206] for the molecular ions.

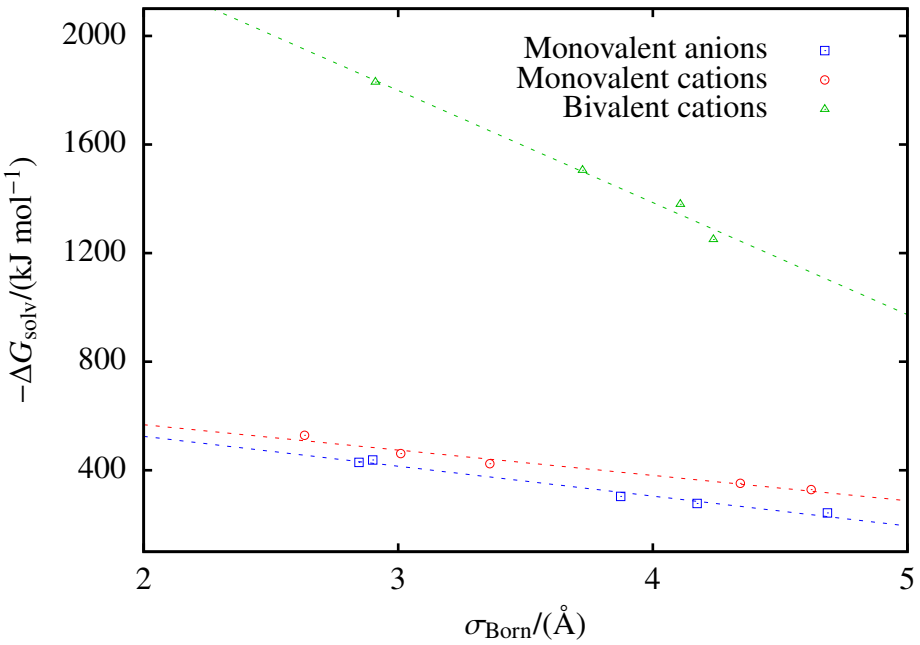

Figure 4.1 The values of the Born cavity diameter, denoted by symbols, are shown to correlate linearly with the experimentally measured Gibbs free energy of solvation reported in Refs. [199–201] for 298 K and 1 bar. This provides a means of validating the values assigned to the $\sigma_{ii}^{\mathrm{Born}}$ parameter in the SAFT-VR Mie models of the ions. (The dashed lines are provided as guides for the eye.)

Equation (3.33) for determining the unlike Mie potential exponents λ_{r} and λ_{a} for pairs of species requires knowledge of the species' like-interaction Mie exponents. In the case of ions, the Mie exponents are set *a priori* depending on the nature of the ion: for atomic ions, the Lennard-Jones potential [155] (which is a special case of the Mie potential with $\lambda_{\mathrm{r}} = 12$ and $\lambda_{\mathrm{a}} = 6$) is applied, following the work of Dufal [122]; while the molecular ions adopt the form of the potential of their reference parent molecule.

The resulting values for ε_{ii} and ε_{ij}, shown in Tables 4.4 and 4.5 respectively, follow physically reasonable trends relative to the size and charge of the ions. For atomic ions of a given charge, ε_{ii} becomes larger with increasing ionic size. Furthermore, within a given period, the ε_{ii} of the divalent cation is stronger than that of the monovalent cation but weaker than that of the monovalent anion. The ion–ion dispersion energy is strongly dependent not only on the size of the ions but also on the form of the intermolecular potential. As well as

following the correct trends, the ion–ion dispersion interactions are of a reasonable order of magnitude. This substantiates both the choice of using the Lennard-Jones potential for the atomic ions and the application of the Mie potential of the water model to represent the H_3O^+ and OH^- molecular ions.

Table 4.1 Parameters for the molecular model of water used in this work, taken from Ref. [177], and for the dielectric constant correlation, taken from Ref. [61]. (The original SAFT-VR Mie model for water sets $m_{\text{seg}} = 1$ (where m_{seg} is the number of segments). In SAFT-γ Mie, the following parameters are defined: $\nu^* = 1$, $S = 1$.)

	σ/Å	λ_{r}	λ_{a}	$(\varepsilon/k_{\text{B}})$/K	n_{H}	n_{e}	$(\varepsilon_{ab}^{\text{HB}}/k_{\text{B}})$/K	$\text{K}_{ab}^{\text{HB}}$ /Å^3	d_V/(dm^3 mol^{-1})	d_T/K
H_2O	3.0063	17.020	6.0000	266.68	2	2	1985.4	101.69	0.3777	1403.0

Table 4.2 Values for the polarisabilities and ionisation potentials of the cations, taken from Refs [202, 205, 206].

i	Li^+	Na^+	K^+	Rb^+	H_3O^+	Mg^{2+}	Ca^{2+}	Sr^{2+}	Ba^{2+}
$\alpha_{0,i}$ / (10^{-24}cm^3)	0.0290	0.1790	0.8300	1.4000	0.9330	0.0940	0.4700	0.8600	1.5500
I_i / eV	75.6400	47.2864	31.6300	27.2895	14.2300	80.1483	50.9131	42.8900	35.8400

Table 4.3 Values for the polarisabilities and ionisation potentials of the anions, taken from Ref. [202–204].

i	F^-	Cl^-	Br^-	I^-	OH^-
$\alpha_{0,i}$ / (10^{-24}cm^3)	1.0400	3.6600	4.7700	7.1000	2.2520
I_i / eV	3.4012	3.6127	3.3636	3.0590	1.8300

4.3.3 Ion–solvent interactions: dispersion and hydrogen bonding

Two types of interactions between the ionic and solvent species are relevant to systems of electrolytes: firstly, the dispersive ion–solvent interaction which is applicable to all ions; and secondly the hydrogen-bonding interaction between the solvent and the molecular ions possessing association sites.

For both molecular ions considered in the context of strong electrolytes, H_3O^+ and OH^-, the smallest neutral parent molecule is water. Consistency between these three interrelated species is achieved in part by relating their association parameters. Specifically, the ion–water association parameters are determined by scaling the cross-association energy and bonding volume to those of the water–water association interaction. To achieve this, the ion–water bonding volume $K^{\mathrm{HB}}_{ab,\mathrm{H_2O}-i}$ is scaled by the corresponding unlike ion–water diameter $\sigma_{\mathrm{H_2O}\text{-}i}$ (obtained from equation (3.30)):

$$\frac{K^{\mathrm{HB}}_{ab,\mathrm{H_2O}-i}}{(\sigma_{\mathrm{H_2O}\text{-}i})^3} = \frac{K^{\mathrm{HB}}_{ab,\mathrm{H_2O}-\mathrm{H_2O}}}{(\sigma_{\mathrm{H_2O}-\mathrm{H_2O}})^3} \,. \tag{4.15}$$

Subsequently, the ion–water association energy $\varepsilon^{\mathrm{HB}}_{ab,\mathrm{H_2O}-i}$ is scaled to the resulting bonding volume:

$$\frac{\varepsilon^{\mathrm{HB}}_{ab,\mathrm{H_2O}-i}}{K^{\mathrm{HB}}_{ab,\mathrm{H_2O}-i}} = \frac{\varepsilon^{\mathrm{HB}}_{ab,\mathrm{H_2O}-\mathrm{H_2O}}}{K^{\mathrm{HB}}_{ab,\mathrm{H_2O}-\mathrm{H_2O}}} \,. \tag{4.16}$$

4.3.4 Parameter estimation methodology

Having established ways of determining the ion size parameters, the ion–ion dispersion interaction parameters, and the ion–solvent association parameters, the ion–solvent dispersion interaction parameters now remain to be determined. The exponents of the cross-interaction Mie potential are obtained using the combining rule of equation (3.33), while the interaction

energy ε_{H_2O-i} is treated as an adjustable parameter optimised by comparison to appropriate thermodynamic experimental data. As a result, the model development procedure requires only one adjustable parameter per ion in the case of single-solvent solutions.

The optimisation approach for determining the $\varepsilon_{H_2O\text{-}i}$ parameters makes use of experimental data for aqueous single-solute solutions, which are modelled as ternary mixtures consisting of water and the solvated ions arising from complete dissociation of the electrolyte solute. The assumption of complete dissociation is commonly adopted in the modelling of strong electrolytes using an EOS, nevertheless the physical reality of the system under consideration is known to deviate to varying degrees from this approximation [207], especially at higher salt concentrations. Furthermore, as the concentration of ions in solution increases, the treatment of the solvent as a continuous dielectric medium becomes less appropriate. In previous work with SAFT-VRE, Schreckenberg et al. [61] adopted an upper salinity limit for the approximation of a dielectric continuum as 10 molal: in solutions of 1:1 electrolytes, this translates to less than six solvent molecules per pair of ions. Assuming a coordination number of six for all ions, this would allow on average only the first solvation shell to form around each ion.

In order to maintain the integrity of these assumptions in the theory (complete dissociation and a uniform dielectric continuum), experimental data only at moderate concentrations are used in this work for optimising the ion–water interaction energy parameters. By limiting the range of experimental data to solute molalities up to 3 molal, one can avoid biasing the ion models towards either extreme of salinity, whilst simultaneously providing a good description of the non-ideal solution behaviour at low concentrations. Aside from the careful selection of the data set's molality range, the temperature range considered is also restricted to a range between 278 and 473 K, so as to avoid the density anomaly of water close to its freezing temperature as well as the region close to the critical temperature of water.

The properties considered in the optimisation procedure are limited to the saturated vapour pressure (p), the liquid and saturated liquid densities (ρ), and the osmotic coefficient

(Φ) of aqueous single-salt solution mixtures. Osmotic coefficient data, being a magnifying re-scaling of the activity of the solvent, are crucial to determining the strength of the ion–water dispersion energy, as this property gives a direct indication of how well the model reproduces the behaviour of the solvent under the influence of the electrolyte solute. Saturated vapour pressure data are also useful for characterising $\varepsilon_{\mathrm{H_2O}\text{-}i}$, as the strength of this interaction directly influences the partition of the water between the liquid and vapour phases. Finally, density data not only provides insight as to the strength of the attraction between the ions and the solvent, but also regarding the structural parameters of the species in the mixture, thus allowing an evaluation of the size parameters assigned to the ions.

The use of these properties leads to robust, physically sound models for the ionic species in solution, thus allowing other thermodynamic properties, such as the MIACs of the salts to be determined in a fully predictive manner with the resulting models. In previous work with SAFT-VRE, Schreckenberg et al. [61] included the MIAC of the salts in the optimisation of the ion models instead of the osmotic coefficient. The experimental data chosen for this work reflect the fact that the osmotic coefficient has been studied experimentally much more extensively than the MIAC, with the latter often determined indirectly via measurements of the former using the relationship given by Equation (2.26).

The $\varepsilon_{\mathrm{H_2O}-i}$ model parameters are optimised by minimising an objective function consisting of the relative difference between the experimental and calculated values of the selected properties. A least-squares objective function is used following the Levenberg-Marquardt method [193, 194]:

$$\min F_{\mathrm{obj}} = \sum_{o} \left(\frac{\omega_o}{n_{\mathrm{p},o}} \sum_{j}^{n_{\mathrm{p},o}} \left[\frac{X_{o,j}^{\mathrm{exp}} - X_{o,j}^{\mathrm{calc}}}{X_{o,j}^{\mathrm{exp}}} \right]^2 \right), \tag{4.17}$$

where $n_{\mathrm{p},o}$ is the number of data points j for property of type o; ω_o is the weight given to property o ($\omega_o = 1$ was used for all properties of the strong electrolyte systems considered); and $X_{o,j}^{\mathrm{exp}}$ and $X_{o,j}^{\mathrm{calc}}$ are the experimental and calculated values of the property, respectively.

The ranges of the experimental data considered are summarised in Table 4.6, and the sources are listed in Table 4.8. The optimisation was carried out in stages, starting first by considering all the monovalent atomic cations and anions simultaneously, using experimental aqueous solution data for 15 1:1 salts. This was followed by simultaneous estimation for all divalent atomic cations, with experimental data for 12 1:2 salts. The molecular ions were parametrised individually, using data for $KOH_{(aq)}$ and $HBr_{(aq)}$ to optimise the OH^--water and H_3O^+-water dispersion energies, respectively.

4.4 SAFT-VRE Mie electrolyte models

The ion models developed in this work include five monovalent cations: Li^+, Na^+, K^+, Rb^+, H_3O^+; five monovalent anions: F^-, Cl^-, Br^-, I^-, OH^-; and four bivalent cations: Ba^{2+}, Ca^{2+}, Mg^{2+}, Sr^{2+}. Each of these ions can be used as constituent components to describe multiple electrolytes in solution mixtures.

The optimal unlike ε_{i-H_2O} parameters are shown in Table 4.4 and are seen to follow physically meaningful trends relative to the size and charge of the ions. The dispersion interactions between the atomic cations and water molecules increase in strength as the cations become smaller, due to the higher charge density and therefore greater polarising effect on the water molecules. The ion–water interaction of each divalent cation is also larger than that of a monovalent cation in the same period, correctly reflecting stronger polarising effect of the smaller, higher-charge-density, divalent ions on the water molecules. For the interactions of atomic anions with water, a stronger dispersion energy is obtained with increasing ionic size, as the ion becomes more polarisable.

The ε_{i-H_2O} parameters of the molecular ions also adopt physically reasonable values, although a direct evaluation relative to the atomic ions is not possible as they both differ in the range of the Mie potential, having been assigned the Mie potential parameters of the water model rather than those of the Lennard-Jones potential. More importantly, OH^- and

H_3O^+ are modelled as associating ions. The hydronium ion is assigned three 'H'-type sites to mediate hydrogen bonding with water. Experimental evidence for this hydrogen bonding interaction scheme has been reviewed by Eigen [208], and it has also been substantiated by means of molecular dynamics simulations of the hydration shell of H_3O^+ in water by Markovith and Agmon [209]. The hydroxide ion is modelled with three 'e'-type association sites, in line with the spectroscopic evaluation of the OH^- hydration shells presented by Robertson et al. [210]. In the aqueous solutions of strong acids and bases under consideration here, OH^- and H_3O^+ form hydrogen bonds with water molecules only. The association parameters of these ion–water interactions are determined by scaling the hydrogen-bonding energy and bonding volume to those of pure water, using Equations 4.15 and 4.16, based on the sizes of the segment cores. The H_3O^+-water association parameters obtained with this approach are therefore the same as for pure water since the ion diameter is equal to that of water in this case.

Table 4.4 SAFT-VR Mie molecular potential parameters for the models of the solvated ions. The ion diameters σ_{ii} and Born cavity diameters $\sigma_{ii}^{\text{Born}}$ are obtained from the literature [191, 197]; the like ion dispersion attraction energies ε_{ii} are calculated using Equation 3.96; and the ion-water unlike dispersion attraction energies $\varepsilon_{i\text{-}H_2O}$ are optimised using the experimental solution data summarised in Table 4.6. For associating ions, the number of each site type, $n_{H,i}$ and $n_{e,i}$, the bonding energy with water $\varepsilon_{ab,i\text{-}H_2O}$ and corresponding bonding volume $K^{HB}_{ab,i\text{-}H_2O}$ are determined by considering the parent molecule following Section 4.3.3.

Ion, i	σ_{ii}/Å	$\sigma_{ii}^{\text{Born}}$/Å	$\lambda_{r,i}$	$\lambda_{a,i}$	(ε_{ii}/k_B)/K	$(\varepsilon_{i\text{-}H_2O}/k_B)$/K	$n_{H,i}$	$n_{e,i}$	$(\varepsilon^{HB}_{ab,i\text{-}H_2O}/k_B)$/K	$K^{HB}_{ab,i\text{-}H_2O}$/Å^3
Li^+	1.8000	2.6320	12.000	6.0000	6.1039	1023.1	-	-	-	-
Na^+	2.3200	3.3600	12.000	6.0000	31.711	539.68	-	-	-	-
H_3O^+	3.0063	3.0063	17.020	6.0000	68.190	391.04	3	-	1985.4	101.69
K^+	3.0400	4.3440	12.000	6.0000	90.097	376.25	-	-	-	-
Rb^+	3.3200	4.6220	12.000	6.0000	130.35	354.23	-	-	-	-
Mg^{2+}	1.7200	2.9100	12.000	6.0000	16.745	2430.9	-	-	-	-
Ca^{2+}	2.2800	3.7240	12.000	6.0000	60.925	1546.8	-	-	-	-
Sr^{2+}	2.6400	4.1080	12.000	6.0000	78.641	1080.5	-	-	-	-
Ba^{2+}	2.9800	4.2380	12.000	6.0000	112.00	830.79	-	-	-	-
F^-	2.3800	2.8460	12.000	6.0000	66.059	30.571	-	-	-	-
OH^-	2.4600	3.0063	17.020	6.0000	170.24	134.41	-	3	1492.0	76.411
Cl^-	3.3400	3.8740	12.000	6.0000	113.77	95.406	-	-	-	-
Br^-	3.6400	4.1740	12.000	6.0000	107.38	112.01	-	-	-	-
I^-	4.1200	4.6860	12.000	6.0000	102.90	142.66	-	-	-	-

Table 4.5 Dispersion energies ε_{ij} between unlike ions, calculated using Equation 3.96.

	(ε_{ij}/k_B)/K				
	F^-	Cl^-	Br^-	I^-	OH^-
Li^+	7.6879	8.2904	7.1802	5.8749	9.1482
Na^+	22.891	27.938	24.990	21.383	27.898
K^+	43.681	61.010	56.592	50.963	54.733
Rb^+	53.634	78.254	73.489	67.344	67.944
H_3O^+	51.100	70.552	65.806	59.657	66.439
Mg^{2+}	23.847	24.942	21.711	17.864	33.269
Ca^{2+}	52.716	63.171	57.024	49.340	77.245
Sr^{2+}	60.690	78.247	72.007	64.012	80.711
Ba^{2+}	72.079	98.707	92.369	84.073	97.975

4.5 Description of thermodynamic properties

The adequacy of the models presented in Table 4.4 is assessed by comparing the SAFT-VRE Mie predictions with experimental data for the vapour pressure, liquid density, osmotic coefficient, and mean ionic activity coefficient of 32 aqueous electrolyte solutions, as well as with experimental data for the Gibbs energy of solvation of the ions and the solubility limit of the salts. The quality of the SAFT-VRE Mie description for these thermodynamic properties is quantified by the percentage average absolute deviation (%AAD) of each property with respect to the experimental data for that property:

$$\%\text{AAD} = \frac{100}{n_{\text{p},o}} \sum_{j}^{n_{\text{p},o}} \left| \frac{X_{o,j}^{\text{exp}} - X_{o,j}^{\text{calc}}}{X_{o,j}^{\text{exp}}} \right|. \tag{4.18}$$

The SAFT-VRE Mie electrolyte methodology provides a good description of the thermodynamic properties used in the development of the ion models within the range of thermodynamic conditions of the experimental data points used for parameter optimisation. The %AAD values corresponding to the experimental dataset of Table 4.6 are shown in Table 4.9. On average, across all solutions considered, the optimisation dataset is described with %AAD of 1.85% for the saturated vapour pressure, 1.64% for the liquid density, and 2.49% for the osmotic coefficient. For comparison, Table 4.10 gives the %AAD values of the properties of the aqueous electrolyte solutions calculated with SAFT-VRE Mie from experimental data across a wide range of conditions, well beyond those considered in the model development. This expanded dataset, summarised in Table 4.7, includes higher salt concentrations up to 10 mol kg^{-1}, as well as data for acid and base solutions not included in the parameter optimisation procedure. The expanded dataset is described – on average across all solutions considered – with %AAD of 3.87% for the saturated vapour pressure, 2.96% for the liquid density, 4.90% for the osmotic coefficient, and 10.8% for the mean ionic activity coefficient. The sources of all aforementioned data are listed in Table 4.8.

As a means of assessing the influence of variation in the parameters on the performance of the model, the parameters relevant to an aqueous NaCl solution are taken as case study, with each ionic group interaction and cross-interaction parameter varied by ±10%, and the effect on the calculated properties' %AAD checked with reference to the expanded dataset. Variation in the ε_{ii} and $\sigma_{ii}^{\mathrm{Born}}$ parameters (for both the anion and cation species), as well as the ε_{ij} parameter for unlike ion–ion interaction, were found to have a limited effect on all properties, with absolute changes in %AAD varying from a minimum of +3.74E-4% to a maximum of +0.84%. An increase in σ_{anion} changes the %AAD of the solution density by +1.73% and a decrease changes it by -1.28%. Changes in σ_{cation} have a large effect on the descriptions of the MIAC and osmotic coefficient: increasing σ_{cation} changes the %AAD by +9.81% for the MIAC and +1.88% for Φ, while decreasing σ_{cation} changes the %AAD by +4.16% for the MIAC and +2.56% for Φ. The sensitivity of the models to the segment size assigned to the species is attributed firstly to the change in charge density of the ions, and also

to the packing of the segments in the fluid mixture. Changes in the $\varepsilon_{\text{ion-water}}$ parameter also have a large effect on the MIAC: an increase in $\varepsilon_{\text{anion-water}}$ changes the %AAD by +1.27%, and an increase in $\varepsilon_{\text{cation-water}}$ changes the %AAD by +5.30%. A decrease in $\varepsilon_{\text{cation-water}}$ changes the %AAD by +1.45% for the MIAC and by +1.77% for Φ. The sensitivity of the model to the ion–water dispersion interaction can be attributed to the resultant effect on the hydration of the solvated ions, which is treated implicitly by this parameter. The effect of the σ_{ion} and $\varepsilon_{\text{ion-water}}$ parameters is small on all other properties in the extended dataset not noted above, with changes in %AAD smaller than ±0.85%.

The performance of the SAFT-VRE Mie models is exemplified in the following sections by calculating the osmotic coefficients, MIACs, Gibbs energies of solvation, and solubility limits at ambient conditions (298 K and 1.01 bar), and the densities and vapour pressures at a range of temperatures. The results obtained for these key thermodynamic properties validate the implementation of the SAFT-VRE Mie approach for electrolytes, together with the ion models developed in this work. A good description of the electrolyte solution properties is achieved across a breadth of conditions and compositions, with predictive capability beyond the molality range considered in the optimisation.

Table 4.6 Overview of the experimental solution data used in the optimisation procedure for the intermolecular parameters. The ranges of temperatures, maximum molality, pressure, and the number of data points per property per salt are summarised.

Salt	p			ρ				Φ		
	T (K)	$m_{\max}$ (mol kg^{-1})	n_p	T (K)	p (bar)	$m_{\max}$ (mol kg^{-1})	n_p	T (K)	$m_{\max}$ (mol kg^{-1})	n_p
LiCl	293–423	3.0	31	278–343	1.01	2.7	200	298	3.0	43
LiBr	313–368	2.9	12	278–343	1.01	2.9	114	298	3.0	23
LiI	291–343	2.5	13	298–373	1.01	3.0	74	298	3.0	23
NaF	373–448	0.01	24	298–323	1.01	0.9	161	298	1.0	17
NaCl	283–383	3.0	100	283–353	1.01	3.0	48	298	3.0	52
NaBr	303–368	3.0	20	283–343	1.01	2.9	76	298	2.9	28
NaI	298–368	2.7	28	293–303	1.01	1.7	34	298	3.0	23
KF	291	2.8	4	298	1.01	3.0	138	298	3.0	23
KCl	298–368	3.0	74	278–353	1.01	3.0	48	298	3.0	36
KBr	298–368	2.8	30	283–348	1.01	3.0	188	298	3.0	23
KI	303–343	3.0	24	278–368	1.01	1.0	283	298	3.0	23
KOH	293–473	3.0	8	298–348	1.01	3.0	73	298	3.0	23
RbF	291	2.6	5	298	1.01	0.5	7	298	3.0	23
RbCl	263–368	3.0	32	298	1.01	3.0	23	298	3.0	23
RbBr	291	2.4	16	298–323	1.01	3.0	23	298	3.0	23
RbI	291	2.7	9	298–310	1.01	0.4	15	298	3.0	23
HBr	298–327	2.6	6	298–348	1.01	3.0	78	298	3.0	42
$MgBr_2$	373	3.0	4	298	-	2.9	12	298–323	3.0	46
$MgCl_2$	295–394	3.0	140	288–372	-	2.9	118	298–343	3.0	65
MgI_2	-	-	-	-	-	-	-	298	3.0	36
$CaBr_2$	298–373	3.0	33	298	-	2.7	26	298–473	3.0	84
$CaCl_2$	291–391	3.0	356	288–298	-	3.0	42	288–473	3.0	282
CaI_2	298–343	2.9	29	-	-	-	-	-	-	-
$SrBr_2$	303–373	3.0	39	298	-	2.4	13	298	2.1	40
$SrCl_2$	303–343	2.9	30	-	-	-	-	298	3.0	36
SrI_2	303–43	2.9	30	-	-	-	-	298	2.0	38
$BaBr_2$	303–373	3.0	39	298	-	1.6	12	298–343	2.5	92
$BaCl_2$	298–343	1.7	51	288–298	-	1.5	49	298–372	2.5	45
BaI_2	-	-	-	-	-	-	-	298	2.0	38

Table 4.7 Overview of the experimental solution data used for evaluating the SAFT-VRE Mie ion models. The ranges of temperatures, maximum molality, pressure, and the number of data points per property per salt are summarised.

Salt	p			ρ				Φ			$\gamma_{\pm,m}$		
	T (K)	$m_{\max}$ (mol kg^{-1})	n_p	T (K)	p (bar)	$m_{\max}$ (mol kg^{-1})	n_p	T (K)	$m_{\max}$ (mol kg^{-1})	n_p	T (K)	$m_{\max}$ (mol kg^{-1})	n_p
LiCl	298–423	9.1	106	278–343	1.01	10.0	236	298–473	10.0	75	298	10.0	48
LiBr	291–373	9.8	94	278–343	1.01	10.0	249	298–498	10.0	33	298	9.0	34
LiI	291–343	9.8	35	298–373	1–1.01	4.9	84	298	3.0	23	298	3.0	33
NaF	373–448	0.0	24	297–498	1.01	1.0	161	298	1.0	17	298	1.0	6
NaCl	273–383	6.8	203	298–473	1.01	5.0	64	298–373	6.1	94	298	6.1	30
NaBr	283–368	9.9	71	283–343	1.01	8.3	162	298–473	9.5	100	298	8.2	47
NaI	298–368	9.3	88	298	1.01	1.7	34	298	10.0	33	298	3.5	14
NaOH	293–298	10.0	20	298–348	1.01	3.0	86	298	10.0	33	298	10.0	34
KF	291	9.2	9	297–372	1.01	8.9	167	298	10.0	23	298	4.0	15
KCl	298–373	6.9	125	298–353	1.01	4.0	64	273–473	6.0	49	298	4.0	80
KBr	283–368	6.2	79	283–348	1.01	5.8	265	298–498	7.4	28	298	5.5	36
KI	303–343	5.6	40	278–373	1.01	1.0	283	298–343	5.6	26	298	4.0	35
KOH	293–473	10.0	30	298–348	1.01	3.0	73	298	10.0	33	298	10.0	34
RbF	291	9.8	7	298	1.01	0.5	7	298	3.5	24	298	3.5	14
RbCl	291	7.1	89	298	1.01	5.0	27	298	7.8	32	298	5.0	17
RbBr	263–368	4.8	32	298–323	1.01	6.8	27	298	5.0	27	298	5.0	32
RbI	291	5.6	10	298–310	1.01	0.4	15	298	5.0	27	298	5.0	34
HCl	298–373	10.0	154	298–348	1.01	9.9	117	298	10.0	64	298	10.0	34
HBr	298–338	7.9	26	298–348	1.01	3.0	78	298	10.0	60	298	10.0	34
HI	298	8.8	5	298–348	1.01	2.5	79	298	10.0	33	298	10.0	34
$MgBr_2$	373	4.0	5	298	-	3.7	13	298–323	5.0	54	298	3.0	15
$MgCl_2$	295–398	5.0	210	288–372	-	4.8	153	298–343	5.0	95	298	5.9	53
MgI_2	-	-	-	-	-	-	-	298	5.0	44	298	1.6	13
$CaBr_2$	298–373	5.7	53	298	-	3.4	27	298–473	5.0	100	298	3.0	15
$CaCl_2$	291–403	5.0	541	288–328	-	4.0	49	288–498	5.4	362	298	3.0	67
CaI_2	298–343	2.9	29	-	-	-	-	-	-	-	298	1.8	14
$SrBr_2$	303–373	4.0	45	298	-	2.4	13	298	2.1	40	298	2.0	30
$SrCl_2$	303–343	4.2	40	-	-	-	-	298	4.0	42	298	4.0	78
SrI_2	303–343	4.2	40	-	-	-	-	298	2.0	38	298	2.0	30
$BaBr_2$	303–373	3.4	44	298	-	1.6	12	298–343	3.4	97	278–318	2.3	49
$BaCl_2$	298–343	1.7	51	288–328	-	1.5	49	298–372	2.5	45	298	1.4	14
BaI_2	-	-	-	-	-	-	-	298	2.0	38	298	2.0	30

Table 4.8 Sources of the experimental solution data summarised in Tables 4.6 and 4.7.

Salt	p	ρ	Φ	$\gamma_{\pm,m}$
KBr	[211–214]	[215–218]	[219]	[219]
KCl	[212–214, 220–223]	[216, 218]	[219, 224–226]	[219]
KF	[227]	[228–230]	[219]	[219]
KI	[212]	[228, 229, 231–233]	[212, 219]	[219]
LiBr	[213, 234–237]	[216, 217, 238]	[219, 239]	[219]
LiCl	[213, 240–242]	[216, 243, 244]	[219, 245]	[219]
LiI	[227, 235]	[246–248]	[219]	[219]
NaBr	[211–213]	[216, 217, 249]	[219, 239, 250]	[219]
NaCl	[223, 251, 252]	[216, 218]	[219, 224, 250, 252–254]	[219]
NaF	[255]	[228–230, 256]	[219]	[219]
NaI	[212, 213, 257]	[228, 229, 258, 259]	[219]	[219]
RbBr	[227, 260]	[228, 261, 262]	[219]	[219]
RbCl	[212, 213, 227, 260]	[229, 258, 263]	[219]	[219]
RbF	[227]	[228]	[219]	[219]
RbI	[227]	[228, 264]	[219]	[219]
HCl	[265–267]	[268, 269]	[219, 266]	[266]
HBr	[270, 271]	[268]	[219, 272]	[219]
HI	[273]	[268]	[219]	[219]
NaOH	[242]	[274, 275]	[219]	[219]
KOH	[242, 276]	[274, 277]	[219]	[219]
$MgBr_2$	[278]	[279]	[280]	[281]
$MgCl_2$	[212, 278, 282–284]	[285, 286]	[212, 287]	[287, 288]
MgI_2	-	-	[280]	[289, 290]
$CaBr_2$	[212, 273, 278]	[279, 291]	[292]	[281, 292]
$CaCl_2$	[212, 278, 283, 284, 293–302]	[303]	[212, 292, 304–309]	[281, 292, 310–312]
CaI_2	[212, 273]	-	-	[290]
$SrBr_2$	[212, 278]	[279]	[280]	[290, 313]
$SrCl_2$	[212]	-	[280]	[314–316]
SrI_2	[212]	-	[280]	[290, 313]
$BaBr_2$	[212, 278]	[279]	[212, 280, 290]	[281, 317]
$BaCl_2$	[212, 294]	[303]	[280, 318]	[281]
BaI_2	-	-	[280]	[290, 313]

Table 4.9 %AAD of the vapour pressure (p), liquid density (ρ), and osmotic coefficient (Φ) of the aqueous salt solutions calculated with SAFT-VRE Mie, from the experimental solution data used in the parameter optimisation (cf. Table 4.6). (Dashes indicate that experimental data for the comparison are unavailable.)

Salt	p	ρ	Φ
LiCl	1.32	0.75	2.41
LiBr	1.82	0.85	2.53
LiI	1.56	1.25	1.81
NaF	1.16	0.41	0.80
NaCl	1.23	3.09	1.69
NaBr	1.48	2.18	4.99
NaI	2.17	0.57	5.42
KF	5.78	2.13	1.64
KCl	1.65	3.70	2.94
KBr	0.92	3.16	0.48
KI	0.70	0.82	1.25
KOH	1.69	2.87	0.41
RbF	2.19	0.23	1.20
RbCl	1.26	1.74	2.25
RbBr	2.11	2.12	0.48
RbI	2.20	0.22	0.89
HBr	1.04	1.05	0.88
$MgBr_2$	1.23	0.61	3.82
$MgCl_2$	1.29	1.42	5.09
MgI_2	–	–	5.12
$CaBr_2$	1.13	1.83	5.11
$CaCl_2$	3.79	2.01	4.31
CaI_2	4.25	–	–
$SrBr_2$	1.42	1.51	2.11
$SrCl_2$	3.54	–	2.04
SrI_2	1.10	–	2.41
$BaBr_2$	0.81	2.92	2.83
$BaCl_2$	1.24	2.02	2.81
BaI_2	–	–	2.11

Table 4.10 %AAD of the vapour pressure (p), liquid density (ρ), osmotic coefficient (Φ), and MIAC ($\gamma_{\pm,m}$) of the aqueous salt solutions calculated with SAFT-VRE Mie, from experimental data across a wide range of temperature and pressure conditions, subject to the availability of data (cf. Table 4.7). (Dashes indicate that experimental data for the comparison are unavailable.)

Salt	p	ρ	Φ	$\gamma_{\pm,m}$
LiCl	2.22	1.85	2.47	16.79
LiBr	4.45	1.09	1.49	14.22
LiI	6.20	2.18	2.02	10.98
NaF	1.40	1.02	2.21	8.40
NaCl	1.71	5.07	3.04	20.43
NaBr	1.98	4.36	4.24	7.92
NaI	4.91	10.10	10.71	5.01
NaOH	3.96	2.44	3.51	17.34
KF	4.56	1.69	1.59	8.02
KCl	3.29	7.03	1.40	11.60
KBr	1.65	2.91	8.42	1.73
KI	3.71	3.02	17.34	11.73
KOH	7.48	3.28	4.61	5.33
RbF	4.84	7.11	1.99	4.74
RbCl	2.23	0.76	4.18	1.03
RbBr	3.20	4.56	5.72	7.68
RbI	3.60	3.07	14.36	26.51
HCl	15.29	2.12	5.96	21.89
HBr	3.94	1.05	4.75	8.53
HI	–	1.21	4.88	8.12
$MgBr_2$	1.87	0.74	5.33	8.52
$MgCl_2$	2.95	2.50	7.44	16.49
MgI_2	–	–	6.07	18.21
$CaBr_2$	3.67	1.98	7.27	11.43
$CaCl_2$	4.24	2.59	5.10	8.31
CaI_2	4.25	–	–	21.34
$SrBr_2$	2.20	1.51	2.11	7.95
$SrCl_2$	7.02	–	3.42	5.87
SrI_2	3.15	–	2.41	6.57
$BaBr_2$	1.03	2.92	3.03	5.60
$BaCl_2$	1.24	2.02	2.81	10.61
BaI_2	–	–	2.11	7.62

4.5.1 Solution densities and saturated vapour pressures

Liquid-phase densities at 298 K and 323 K at 1.01 bar are shown in Figure 4.2 for a selection of salt solutions. The SAFT-VR Mie representation of the density allows an assessment of the methodology for the choice of diameters used to describe the ions, since this property is heavily dependent on the sizes of the species in the mixture. The lithium salts are of particular interest in this respect, because Li^+ is the smallest ion considered in this work and the assumptions made regarding the ion sizes are expected to have a greater impact on the smaller ions. Given the fair agreement between the calculated densities and experimental data, the selected crystal ionic diameters are considered to provide a reasonable estimate of the ion size. The depression of the vapour pressure with increasing salt concentration is of

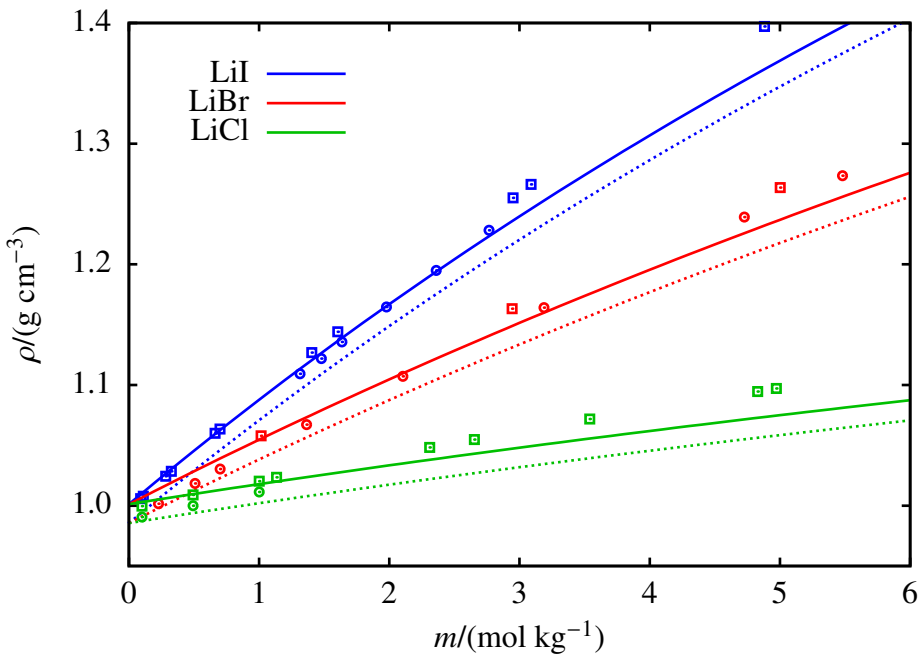

Figure 4.2 The concentration dependence of the liquid-phase density ρ for aqueous solutions of lithium salts LiI, LiBr, and LiCl. The continuous curves and squares represent the SAFT-VRE Mie calculations and experimental data, respectively, at 298 K and 1.01 bar. The dashed curves and circles represent the SAFT-VRE Mie calculations and experimental data at 323 K and 1.01 bar. The experimental data were obtained from the sources listed in Table 4.8.

central importance for evaluating the proposed models, considering the vast difference in composition between the vapour and liquid phases. Exemplified by the calculated vapour pressures of aqueous NaCl solutions for a range of temperatures depicted in Figure 4.3, the capability of the proposed model to reproduce the temperature dependence of the vapour pressure to a high level of accuracy is demonstrated.

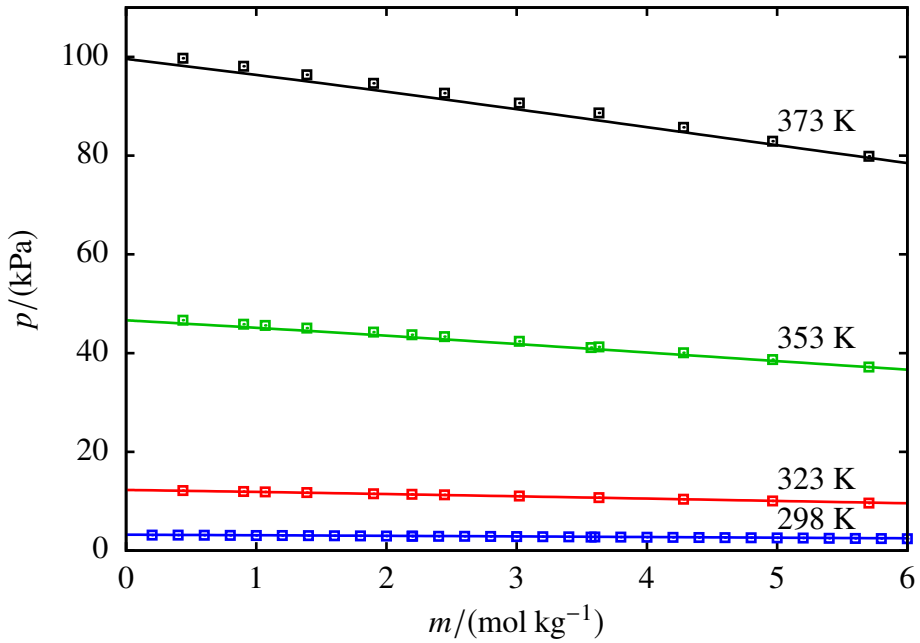

Figure 4.3 The concentration dependence of the saturated vapour pressures p of aqueous solutions of NaCl for temperatures ranging from 298 to 373 K. The continuous curves represent the SAFT-VR Mie calculations and the squares represent the experimental data obtained from the sources listed in Table 4.8.

4.5.2 Osmotic coefficient and mean ionic activity coefficient

The description of osmotic coefficients of a range of 1:1 and 1:2 salts solutions is illustrated in Figures 4.4 and 4.5, while the osmotic coefficients of acid and base solutions are shown in Figure 4.6. The SAFT-VR Mie calculations are seen to follow the trends of the experimental data, with particularly good quantitative agreement in the highly non-ideal low-molality region. One may perceive that greater deviations between the model predictions and the experimental data are observed for 1:2 salts in Figure 4.5 and acids and bases in Figure 4.6, as compared to the 1:1 salts in Figure 4.4. This is to be expected, as the monovalent ion models were optimised first, meaning that the subsequent model optimisation for the bivalent cations, hydroxide ion, and hydronium ion was restricted by the fixed parameters of the counterion in the solution mixture. Nevertheless, from these results for the osmotic coefficient of a wide range of electrolyte solutions it is deduced that the models provide a good representation of the change in the behaviour of the dipolar water solvent as a result of its interaction with the charged ions.

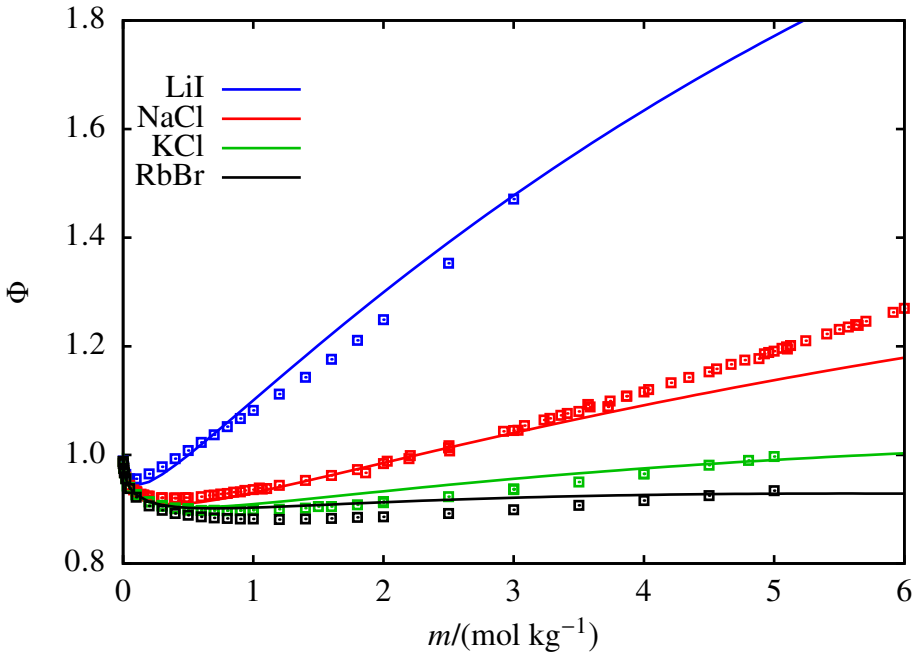

Figure 4.4 The concentration dependence of the osmotic coefficients Φ for a selection of aqueous solutions of 1:1 salts at 298 K and 1.01 bar. The continuous curves represent the SAFT-VRE Mie calculations and the squares represent the experimental data obtained from the sources listed in Table 4.8.

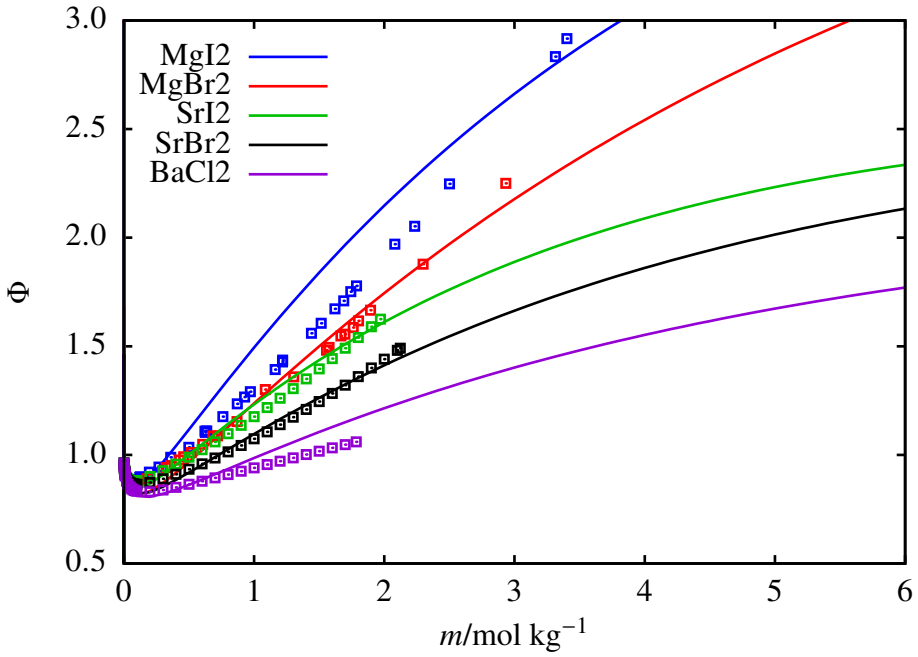

Figure 4.5 The concentration dependence of the osmotic coefficients Φ for a selection of aqueous solutions of 1:2 salts at 298 K and 1.01 bar. The continuous curves represent the SAFT-VRE Mie calculations and the squares represent the experimental data obtained from the sources listed in Table 4.8.

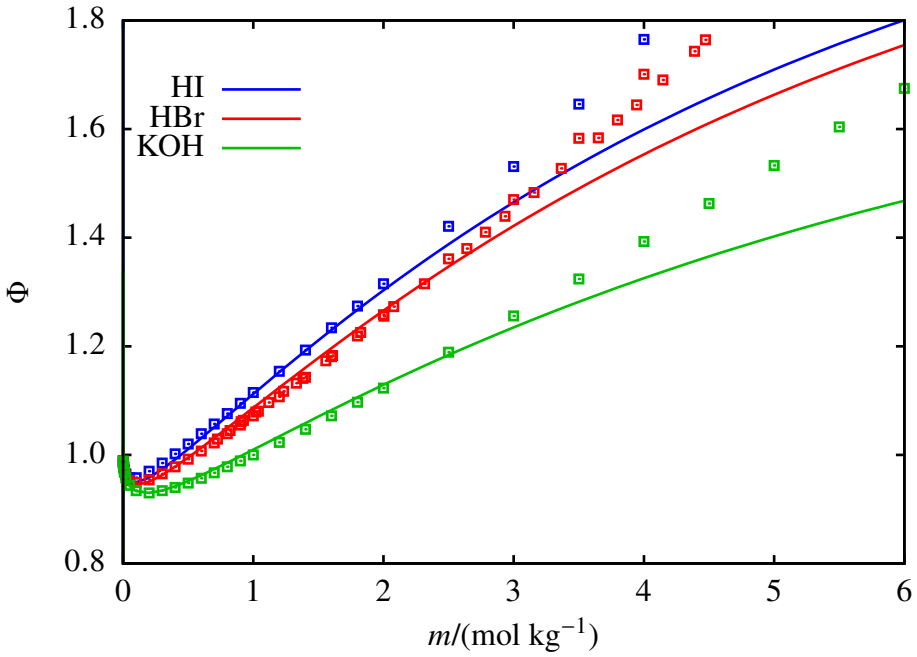

Figure 4.6 The concentration dependence of the osmotic coefficients Φ for a selection of aqueous solutions of acids and bases at 298 K and 1.01 bar. The continuous curves represent the SAFT-VRE Mie calculations and the squares represent the experimental data obtained from the sources listed in Table 4.8.

A direct way of assessing the reliability of the ion models and the predictive capability of the SAFT-VRE approach is via the MIAC of the aqueous salts, which is directly related to the chemical potential of the solvated ions and consequently provides a measure of how well the thermodynamic properties of the ions are represented in solution. In the present work, the MIAC has not been used for the development of the ion models, and the prediction of this property can hence serve as a benchmark for ensuring that the model parameters are physically sound. The MIAC of a selection of salts, acids, and bases in aqueous solution are shown in Figures 4.7, 4.8, and 4.9; the %AAD of the predicted values from the corresponding experimental data for all of the salts considered are reported in Table 4.10. The SAFT-VRE Mie predictions for the MIAC are in very good agreement with the experimental data despite not having been used in the model development. By limiting the molality range of the dataset used in the parameter optimisation procedure, the non-ideality of the solution at low salinity is well accounted for by the resultant models, as has been already illustrated through the description of the osmotic coefficient. As a result, this leads to very good predictions for the MIAC.

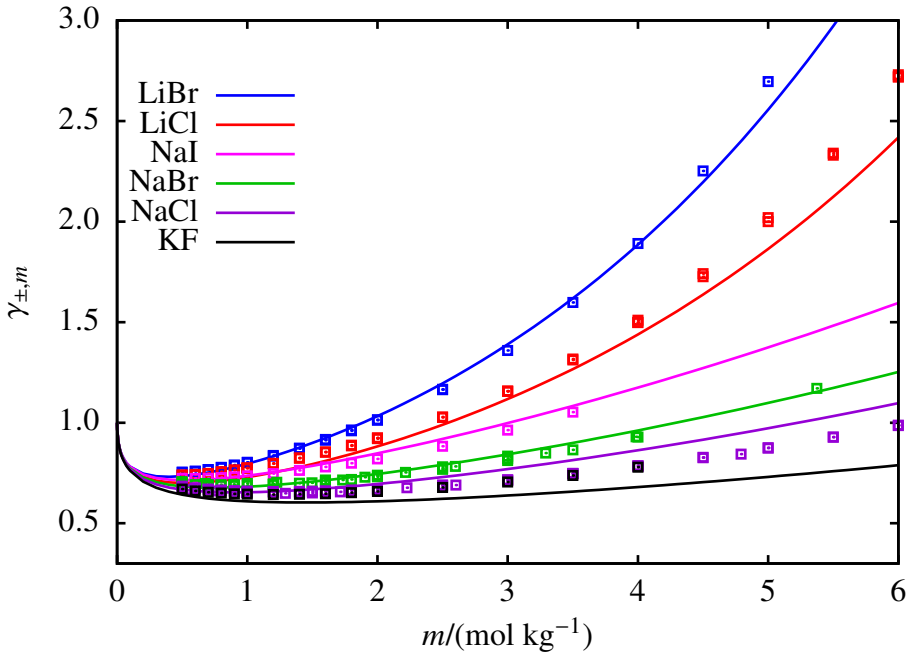

Figure 4.7 The concentration dependence of the mean ionic activity coefficients $\gamma_{\pm,m}$ conditions at of vapour-liquid equilibrium for a selection of aqueous solutions of 1:1 salts at 298 K. The continuous curves represent the SAFT-VR Mie calculations and the squares represent the experimental data obtained from the sources listed in Table 4.8.

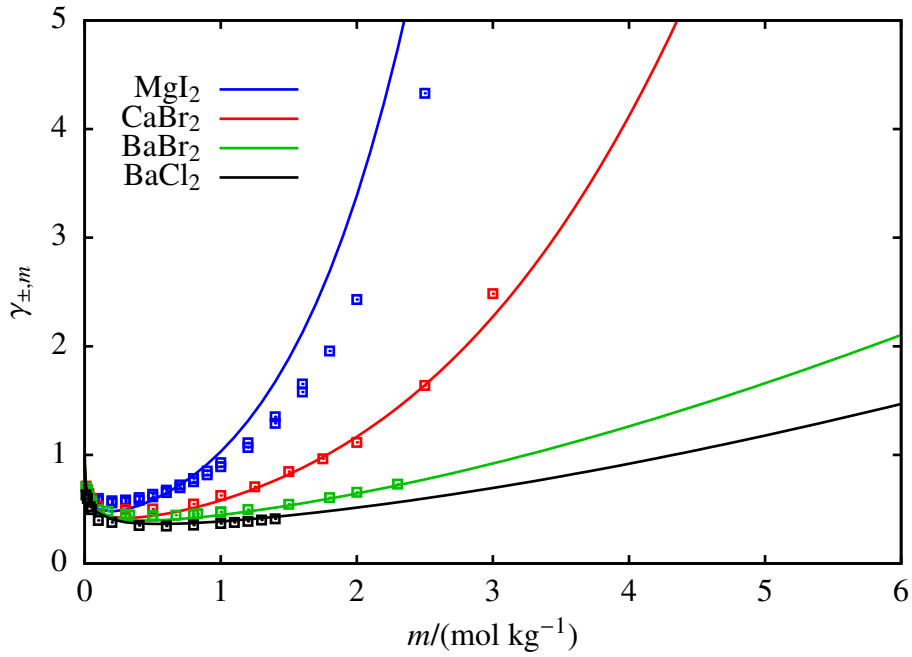

Figure 4.8 The concentration dependence of the mean ionic activity coefficients $\gamma_{\pm,m}$ at conditions of vapour-liquid equilibrium for a selection of aqueous solutions of 1:2 salts at 298 K. The continuous curves represent the SAFT-VR Mie calculations and the squares represent the experimental data obtained from the sources listed in Table 4.8.

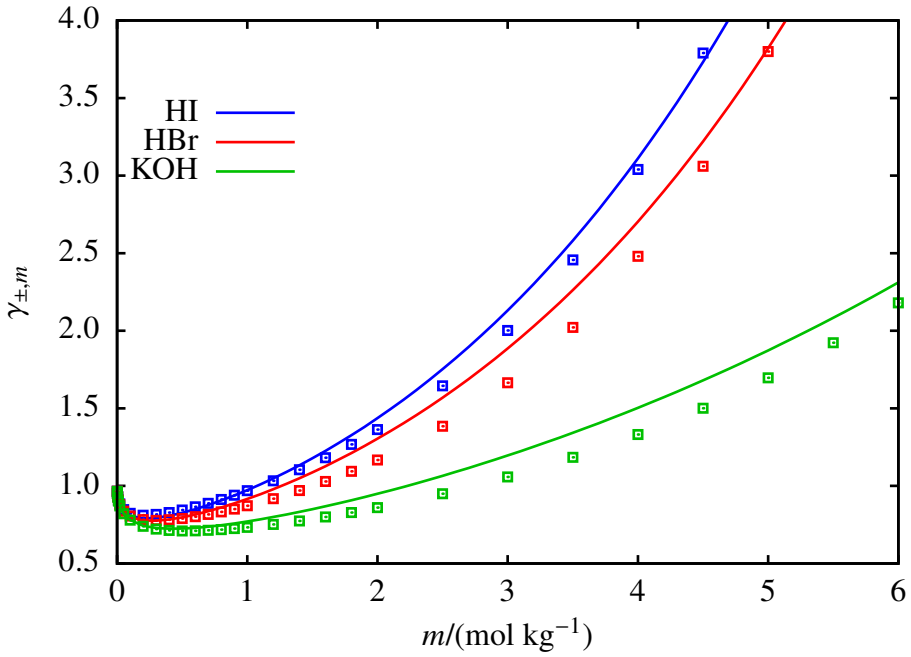

Figure 4.9 The concentration dependence of the mean ionic activity coefficients $\gamma_{\pm,m}$ at conditions of vapour-liquid equilibrium for a selection of aqueous solutions of acids and bases at 298 K. The continuous curves represent the SAFT-VR Mie calculations and the squares represent the experimental data obtained from the sources listed in Table 4.8.

Four isotherms of the MIAC of aqueous NaCl solutions are shown in Figure 4.10 for temperatures in the range of 288–333 K. Correctly representing the experimental trend at low concentrations, the SAFT-VRE Mie model is able to predict the decrease of the MIAC with increasing temperature for aqueous solutions of NaCl, thereby illustrating the predictive capability of the approach with regard to property's dependence on temperature. At higher salt concentrations the SAFT-VRE Mie predictions continue to follow the order demonstrated by the data in the low-salinity region. The predictions at higher salinities appear to be at odds with the experimental trend which shows the MIAC at 333 K becoming larger than that at 288 K; the deviations of the theoretical predictions from the experimental data are ~20% at the highest concentrations considered. It should be noted, however, that the trend depicted by the experimental data for the MIAC is inconsistent with that presented by the data for the osmotic coefficient in Figure 4.11. As the MIAC and osmotic coefficient are directly related through Equation 2.26, one would expect a similar trend with temperature; the apparent absence of this connection between the two types of data casts some doubt on the quality of the experimental data for the MIAC at higher temperatures and concentrations. On the other hand, keeping in mind that the approximate description of the polarity of the solvent with a dielectric continuum within the SAFT-VRE approach is expected to be less adequate at very high salt concentrations, the approach is intrinsically hindered from highly accurate predictions of sensitive properties such as the MIAC at high salinities. Regardless of these uncertainties, it should be noted that the temperature dependence predicted with the presently proposed SAFT-VRE method and accompanying models is in agreement with that predicted with other methods; for example, the SAFT2-KMSA EOS of Jiang et al. [118], the ePPC-SAFT EOS of Rozmus et al. [117], and the semi-empirical model of Pitzer et al. [319] have also predicted that the MIAC of aqueous strong electrolytes decrease with increasing temperature.

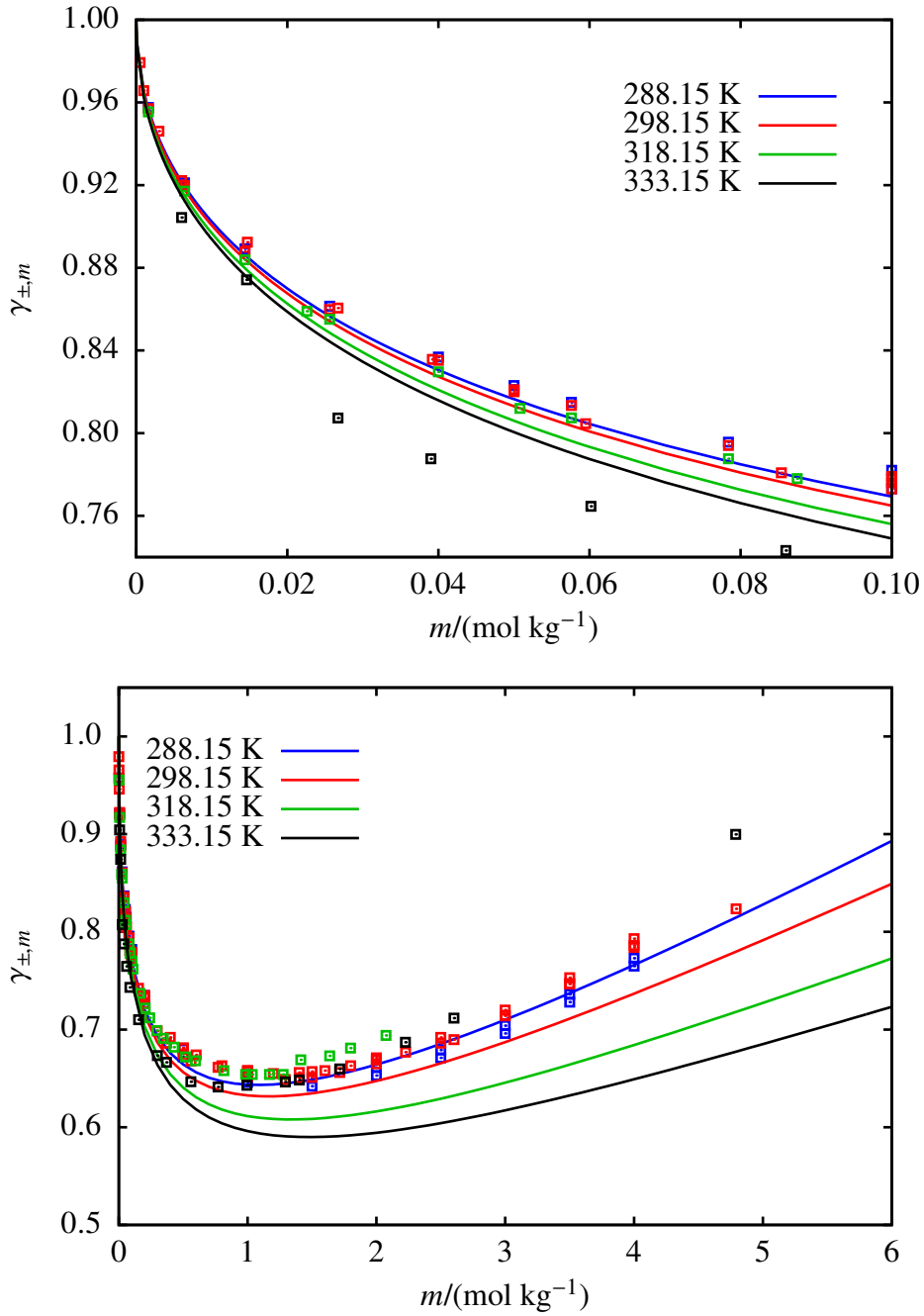

Figure 4.10 The concentration dependence of the mean ionic activity coefficient $\gamma_{\pm,m}$ for aqueous solutions of NaCl at 1.01 bar for temperatures ranging from 288 to 333 K, shown both at low (top) and high (bottom) salinity. The continuous curves represent the SAFT-VR Mie predictions, and the squares represent the experimental data [320–326].

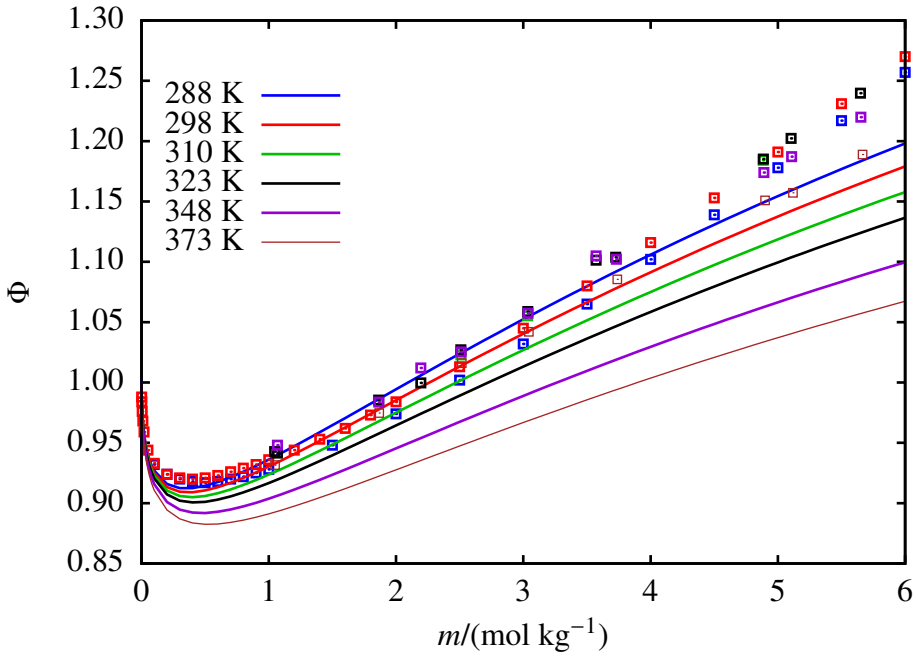

Figure 4.11 The concentration dependence of the osmotic coefficient Φ for aqueous solutions of NaCl at 1.01 bar for temperatures ranging from 288 to 373 K. The continuous curves represent the SAFT-VR Mie predictions, and the squares represent the experimental data obtained from the sources listed in Table 4.8.

4.5.3 Gibbs free energy of solvation

The approach proposed for the implementation of the Born contribution in the SAFT-VRE Mie EOS is evaluated by assessing the description of the Gibbs free energy of solvation $\Delta G_{\text{solv},i}$ of the individual ions in aqueous solution. The predictions of $\Delta G_{\text{solv},i}$ are presented in Table 4.11, alongside the experimentally determined values [199–201]. These predictions are a significant improvement over those achieved in previous implementations of SAFT-VRE [61], where the Born diameter was not differentiated from the segment diameter of the ion. By adhering to the appropriate definition of the Born diameter as the cavity formed by the ion in the solvent, it has been possible to obtain not only qualitative agreement with the trend of the solvation energies, but also good quantitative agreement with the experimental values. The level of the description of solvation effects achieved with the current implementation of SAFT-VRE Mie is similar to that of SAFT approaches in which the ion–solvent polar interactions are treated explicitly [31, 141, 144].

4.5.4 Aqueous solubility of salts

In addition to the ions' Gibbs free energy of solvation, it is also interesting to consider the limit of solubility of the salts, which can be calculated with a classical thermodynamic approach using equation 4.13. This requires the activity coefficients of the salt's constituent ions, which are calculated using the SAFT-VRE Mie methodology, as well as the solubility product $K_{\text{sp,MX}}$ of the salt. One way of estimating the $K_{\text{sp,MX}}$ is via tabulated data of the Gibbs formation free energies ΔG^f of the species using equation 4.14. The ΔG^f of the salts and ions considered here are taken from the literature [327] and summarised in Table 4.12. It is important to note that these values should be used with caution as they are not direct measurements, but rather deduced from a wide array of reported experimental data so as to provide 'best estimates' rather than absolute quantities. Alternatively, the experimental solubility product $K^{\text{exp.}}_{\text{sp,MX}}$ can be calculated directly from experimental data for the mean

Table 4.11 Free energy of solvation energy, ΔG_{solv} of ions in aqueous solution: SAFT-VRE Mie predictions are compared to the experimentally derived values reported in Refs. [199–201].

	$-\Delta G_{\text{solv},i}/(\text{kJ mol}^{-1})$	
Ion, i	SAFT-VR Mie	Experiment
Li^+	535.72	529.00
Na^+	403.85	424.00
H_3O^+	461.92	461.39
K^+	304.00	352.00
Rb^+	283.55	329.00
F^-	444.60	429.00
OH^-	432.58	437.94
Cl^-	313.04	304.00
Br^-	286.54	278.00
I^-	249.59	243.00
Ba^{2+}	1331.45	1250.00
Ca^{2+}	1524.81	1505.00
Mg^{2+}	1946.03	1830.00
Sr^{2+}	1378.75	1380.00

ionic activity coefficient of the salt in saturated aqueous solution $\gamma^{\text{exp}}_{\pm,m}$, by rearrangement of 4.13:

$$K^{\text{exp.}}_{\text{sp,MX}} = m^{\text{sat,exp.}\,(\nu_+ + \nu_-)}_{\text{MX}}\, \gamma^{\text{exp}\,(\nu_+ + \nu_-)}_{\pm,m} \frac{\nu_+^{\nu_+}\nu_-^{\nu_-}}{m^{\circ(\nu_+ + \nu_-)}}. \tag{4.19}$$

The solubility product of a salt obtained from equation 4.19 can be used with greater confidence since the data used for its calculation is specific to the salt in question. By contrast, the ΔG^f_i reported for ion i is a value which has been computed from experimental data of an array of salts in which this ion i is a constituent [327]. The experimental $\gamma^{\text{exp}}_{\pm,m}$ values at salt saturation were obtained from Refs. [219, 223, 290, 304, 312, 328–332], and the values of K_{sp} calculated from Equation 4.19 or taken from Ref. [128] are presented in Table 4.13.

The solubility limits for a number of salts, predicted using Equation 4.13 and the SAFT-VRE Mie EOS, at conditions of 298 K and 1.01 bar are presented in Table 4.14 alongside the experimental solubility data. Predictions using both the solubility product obtained from Equation 4.14 and that obtained from Equation 4.19 are shown. It is immediately evident that the predicted solubilities for the most commonly studied salts are in better agreement with the reported experimental solubilities; it is plausible that the tabulated reference data of the formation Gibbs free energy and the solubility product for these more common salts are more reliable. This is supported by the fact that for such salts the two routes for the calculation of the solubility lead to similar predicted values. It should be noted that many of the salts considered here have a solubility limit which is well above the salt concentration for which SAFT-VRE Mie is applicable. The range of application for the SAFT-VRE Mie approach can be estimated to be at a maximum salt molality of 10 mol kg^{-1} [61], assuming a 1:1 salt and a solvation shell for the ions with six coordinated water molecules. Beyond this salt concentration the dielectric constant of the mixture can no longer be expected to be the same as that of the pure solvent, as is inherently assumed by the current SAFT-VRE Mie approach. As a consequence, it is not surprising that better predictions are achieved for the solubility limits of the salts whose solubility falls within the limits of applicability of the theory. By contrast, for salts which have a solubility limit well beyond the capability of SAFT-VRE Mie, such as lithium salts, the solubility is highly over-predicted.

The prediction of aqueous solubilities of inorganic salts has also been extensively pursued in the literature through molecular simulation studies of electrolyte solutions, therefore it is interesting to compare the predictions obtained in such studies with those obtained with the present approach. The predicted salt solubilities reported in three molecular simulation studies [333–335] have also been included in Table 4.14. Although most such studies focus on solutions of NaCl, the work of Moucka et al. [335] has included multiple salts and has obtained aqueous salt solubilities using three different sets of models. When the solubility of a given salt falls within the concentration range of applicability of the SAFT-VRE Mie EOS, the predictions obtained in this work are typically in better agreement with experimental data

as compared to the molecular simulation predictions, which typically underpredict the salt solubilities. However, for salts whose solubilities are beyond the applicable concentration range of SAFT-VRE Mie, the molecular simulation approaches provide a much better prediction of this property, owing to their explicit representation of the solvent's polarity rather than implementing a uniform dielectric medium as in the present model.

Table 4.12 Values used in equation 4.14 for the Gibbs free energies of solvation, ΔG^f, of the solid salts and solvated ions, obtained from Ref. [327]. The ΔG^f of the salts correspond to the crystalline anhydrous salt at 298 K and 1 bar; and the ΔG^f of the ions correspond to the ion in aqueous solution at unit molality at 298 K and 1 bar.

Salt	$-\Delta G^f_{\mathrm{salt}_{(s)}}/(\mathrm{kJ\ mol^{-1}})$	Ion	$-\Delta G^f_{\mathrm{ion}_{(aq)}}/(\mathrm{kJ\ mol^{-1}})$
LiCl	384.37	Li^+	293.31
LiBr	342.00	Na^+	261.91
LiI	270.29	K^+	283.27
NaF	543.49	Rb^+	283.98
NaCl	384.14	F^-	278.79
NaBr	348.98	Cl^-	131.23
NaI	286.06	Br^-	103.96
KCl	409.14	I^-	51.570
KBr	380.66	Ca^{2+}	533.58
KI	324.89	Sr^{2+}	559.48
RbCl	407.80		
RbBr	381.79		
$CaCl_2$	748.10		
$CaBr_2$	663.60		
$SrCl_2$	781.10		

Table 4.13 Values for the experimental solubility product $K_{sp}^{exp.}$ at 298 K and 1.01 bar used for the calculation of the solubilities of the salts in aqueous solution.

Salt	$K_{sp}^{exp.}$	Salt	$K_{sp}^{exp.}$
LiCl	1.388×10^{6} [a]	$CaCl_2$	1.309×10^{7} [a]
LiBr	1.021×10^{8} [a]	$CaBr_2$	1.011×10^{11} [a]
LiI	2.180×10^{6} [a]	$SrCl_2$	459.3 [a]
NaF	3.397×10^{-1} [a]		
NaCl	38.05 [b]		
NaBr	114.7 [b]		
KCl	8.003 [b]		
KBr	13.53 [b]		
KI	48.82 [a]		
RbCl	20.24 [a]		

[a] Values calculated using Equation 4.19.

[b] Values taken from Ref. [128].

Table 4.14 Solubility limits, m^{sat}, for salts at conditions of 298 K and 1.01 bar: SAFT-VRE Mie predictions are compared to the experimentally obtained values reported in Refs. [202, 220, 336, 337]. Dashes denote that the $K_{\text{sp}}^{\text{exp.}}$ for the salt was unavailable due to lack of data for the MIAC of the salt in saturated aqueous solution $\gamma_{\pm,m}^{\text{exp}}$.

Salt	$m^{\text{sat}}/(\text{mol kg}^{-1})$					
	SAFT-VRE Mie		Experiment	Molecular simulation		
	using ΔG^f cf. Eqn. 4.14	using $K_{\text{sp}}^{\text{exp.}}$ cf. Eqn. 4.19		Ref. [333]	Ref. [334]	Ref. [335]
LiCl	49.11	34.16	19.94	–	–	–
LiBr	138.0	64.93	20.83	–	–	22.80
LiI	468.51	24.71	12.35	–	–	–
NaF	1.010	1.039	0.980	–	–	1.030–1.850
NaCl	6.830	6.900	6.150	5.400	4.800	4.740–5.410
NaBr	17.33	12.50	9.190	–	–	7.000–8.180
NaI	54.87	–	12.28	–	–	11.06–16.30
KCl	4.870	4.683	4.770	–	–	3.600–4.800
KBr	5.963	5.761	5.700	–	–	3.740–4.110
KI	10.73	10.07	8.920	–	–	5.790–8.220
RbCl	8.518	8.61	7.717	–	–	5.680–8.350
RbBr	7.072	–	6.916	–	–	4.550–4.700
RbI	6.855	–	7.630	–	–	4.240–4.490
$CaCl_2$	10.65	8.571	7.320	–	–	–
$CaBr_2$	44.47	13.29	7.820	–	–	–
$SrCl_2$	11.56	3.825	3.350	–	–	–

4.6 Summary

In this chapter, the SAFT-VRE Mie EOS has been taken as the limiting case to which the SAFT-γ Mie EOS converges to when applied to spherical ionic components. The contents of this chapter have been published in a co-authored article which presents the SAFT-VRE Mie EOS [338] and the accompanying models for the ionic species presented here.

Models have been developed for five monovalent cations, five monovalent anions, and four bivalent cations. The parameterisation of models was performed with a methodology that combines literature values of ionic properties with an established theory relating to molecular interactions. Each ionic species requires only one unlike interaction parameter, namely the ion–solvent dispersion energy, to be adjusted using experimental mixture data. This is the case even for the hydronium and hydroxide ions which interact with the solvent via association, as the unlike association parameters of these ion–solvent pairs have been determined by relation to the hydrogen-bonding parameters of the water model.

A distinguishing feature of the methodology employed in this work is the choice to limit the range of concentration considered for the determination of this parameter to less than 3 mol kg^{-1} in order to adhere to the inherent assumptions of the MSA primitive model, i.e., the representation of the solvent as a uniform dielectric medium, and the assumption of complete dissociation of ionic species. In doing so, the ion models developed here can also be employed in other work in which more complex phenomena such as ion pairing are accounted for, since the models have not been skewed by high-concentration data to implicitly encompass these interactions.

The models developed for the ionic species were applied to describe the properties of 32 single-salt aqueous solutions. The performance of the models is accurate up to high salt concentrations for thermodynamic properties including the liquid-phase solution densities, vapour pressure, and osmotic coefficients. A high level of agreement with experimental data

is also seen in the predictions of the mean ionic activity coefficients of a range of salts, and the predictions of the Gibbs free energy of solvation of the ions. Finally, for salts whose solubility limit falls within the range to which this modelling approach is applicable, i.e. ≤ 10 mol kg^{-1}, the aqueous solubility at ambient conditions was reproduced very well.

Chapter 5

Complex organic electrolytes

The application of SAFT-γ Mie to mixtures comprising non-spherical molecular ions first requires characterisation of the ions' charged functional groups and their unlike interactions with other neutral and charged groups in the mixture. In this chapter, sodium carboxylate salts of varying alkyl chain length are modelled. This requires model parameters to be developed for the carboxylate functional group, COO^-, while the model for the Na^+ ion is obtained from Chapter 4. A convenient feature of SAFT-based models is that chemical species adopt model parameters whose magnitude can be assessed for correctness relative to other closely similar species. This arises due to the sound physical meaning of the model parameters, and it has been exemplified in Chapter 4 by the similarity between the model for water and the models for the hydronium and hydroxide ions. In order to leverage this characteristic in the development of the COO^- group, the SAFT-γ Mie model for the carboxyl group (COOH) is examined first, by studying alkyl carboxylic acids. The COO^- group is then parameterised using both SAFT-γ Mie electrolyte formulations proposed in Chapter 3, and the efficacy of each approach is assessed with respect to the reproduction of bulk-phase properties of the solutions.

5.1 Insights from carboxylic acid modelling

The SAFT-γ Mie group parameters required for modelling alkyl carboxylic acids include CH_2, CH_3, and COOH, models for which have been developed in previous work [8, 175] and are collected in Tables 5.1 and 5.2. A model for the COOH group has been presented by Sadeqzadeh et al. [175], where COOH is represented as a single segment possessing four 'e'-type sites and one 'H'-type site. The dimerisation of carboxylic acids is taken into account via self-association interactions mediated by the 'H'-type site on each of the COOH groups. The 'e'-type sites represent the lone-pair orbitals on the oxygen atoms, and are labelled as two 'e_1' and two 'e_2' sites to distinguish between the different behaviour of each oxygen. Sadeqzadeh et al. focused on modelling alkyl carboxylic acids of moderate length, specifically butanoic acid through to decanoic acid molecules, while the smaller molecules of this homologous series – ethanoic and propanoic acids – were excluded from the scope of model development due to the strong polarity of the COOH group. In these molecules, the CH_2 and CH_3 functional groups adjacent to the COOH group are highly polarised and are expected to behave differently than in longer-chain acid molecules where the polarisation effect is more diffuse. Due to polarisation being much more pronounced in the shorter homologues, Sadeqzadeh et al. have recommended the application of so-called "second-order" [1] group parameters for describing the unlike interactions between COOH and alkyl groups in short-length acids.

[1] Second-order parameters address the limitation of the group-contribution approach with regard to the challenge of modelling vastly differing mixtures with a unique set of group parameters. For a mixture of components where the generic group parameter set is inadequate in reproducing the behaviour of the fluid, certain group-group interactions relevant to that mixture can be adjusted in order to improve the performance of the model. These adjusted parameters are referred to as "second-order" and are applied only in the particular type of mixture for which they have been developed, in place of the equivalent value for the parameter corresponding to the generic parameter set. However, in order to maintain the integrity of the group-contribution methodology, this approach is only resorted to for group interactions within a molecular component for which appropriate reasoning can be identified from the topological environment of the groups comprising the molecule.

Table 5.1 SAFT-γ Mie group model parameters relevant to alkyl carboxylic acids. The carboxyl group applicable to short-chains is denoted $^{\text{short}}$COOH but shares the same like-interaction parameters as the COOH group developed for longer-chain acids by Sadeqzadeh et al. [175]. Similarly, the alkyl groups adjacent to carboxyl group in short-chain acids are denoted $^{\text{adj}}CH_2$ and $^{\text{adj}}CH_3$, but share the same like-interaction parameters as the standard SAFT-γ Mie groups presented by Papaioannou et al. [8].

Group, k	v_k^*	S_k	σ_{kk}/Å	$\lambda_{r,k}$	$\lambda_{a,k}$	(ε_{kk}/k_B)/K	$n_{H,k}$	$n_{e_1,k}$	$n_{e_2,k}$	Source
CH_2 / $^{\text{adj}}CH_2$	1	0.22932	4.8801	19.871	6.0000	473.39	–	–	–	[8]
CH_3 / $^{\text{adj}}CH_3$	1	0.57255	4.0773	15.050	6.0000	256.77	–	–	–	[8]
COOH / $^{\text{short}}$COOH	1	0.55593	4.3331	8.0000	6.0000	405.78	1	2	2	[175]

Table 5.2 SAFT-γ Mie group cross-interaction parameters for modelling medium- and long-length alkyl carboxylic acids and mixtures of these with water, taken from the work of Papaioannou et al. [8], Sadeqzadeh et al. [175], and Hutacharoen et al. [10]. CR indicates that the unlike repulsive exponent $\lambda_{r,kl}$ of the Mie potential is obtained using the combining rule given by Equation 3.33. The unlike attractive exponent of the Mie potential is assigned to $\lambda_{a,kl} = 6.0000$ for all groups. The unlike segment diameter σ_{kl} is obtained from the arithmetic combining rule given by Equation 3.30.

Group		Site		$(\varepsilon^{HB}_{ab,kl}/k_B)$/K	$K^{HB}_{ab,kl}$ /Å^3	$\lambda_{r,kl}$	(ε_{kl}/k_B)/K	Source
k	l	k,a	l,b					
CH_2	CH_3	–	–	–	–	CR	350.77	[8]
CH_2	COOH	–	–	–	–	CR	413.74	[175]
CH_3	COOH	–	–	–	–	CR	255.99	[175]
CH_2	H_2O	–	–	–	–	100.00	423.63	[10]
CH_3	H_2O	–	–	–	–	100.00	358.18	[10]
COOH	COOH	H	H	6427.9	0.8062	8.0000	405.78	[175]
COOH	H_2O	e_1	H	1451.8	280.89	CR	289.76	[10]
COOH	H_2O	e_2	H	1252.6	150.98	CR	289.76	[10]
COOH	H_2O	H	e	2567.7	270.09	CR	289.76	[10]

In order to model mixtures of carboxylic acids and water, the COOH group's cross interaction parameters with the H_2O group are required. These are obtained from the work of Hutacharoen et al. [10] and are also shown in Table 5.2. Hydrogen bonding between the alkyl carboxylic acids and water is mediated through the 'e1' and 'e2' association sites on the COOH group (where the distinction between 'e'-type sites reflects the difference between the lone pairs on each oxygen atom in the group), interacting with the 'H'-type sites on the H_2O group. These hydrogen bonds consequently compete with the acid self-association interactions. An important aspect of the established SAFT-γ Mie modelling approach for water–carboxylic acid mixtures is that the partial dissociation of carboxylic acids is not taken into account [339], as their degree of ionisation can be treated as negligible (c.f. Table 5.3 for a comparison of the pK_a values of carboxylic acids with that of other strong and weak acids modelled in this work). Furthermore, the COOH–H_2O cross interactions satisfy only the phase behaviour of carboxylic acid mixtures containing acids of moderate length (butanoic to decanoic acids) and are ineffective in reproducing the behaviour of mixtures comprising ethanoic and propanoic acids.

Table 5.3 pK_a values (taken from Refs. [340–342]) for some strong and weak acids in water, and the modelling approach taken for each acid in this work.

Acid	pK_a	Dissociation modelling approach
HI	-9.500	complete
HBr	-8.800	complete
HCl	-5.900	complete
H_2SO_4	-3.000	partial
HNO_3	-1.400	partial
CH_3COOH	4.756	undissociated
C_3H_7COOH	4.822	undissociated
$C_5H_{11}COOH$	4.879	undissociated

Modelling of short-chain carboxylic acids with SAFT-γ Mie is pursued in this work by developing second-order group interaction parameters for ethanoic and propanoic acids. The pure acids are examined first, followed by mixtures of these with water, ultimately leading to the proposal of three new second-order group interactions arising from the strong polarising nature of the COOH group. The insights gained into developing second-order groups to account for the effect of polarisation on group-contribution models are then taken forward to inform the development of models for alkyl carboxylate salts.

5.1.0.1 Short-length carboxylic acids

The predictions obtained for pure ethanoic and propanoic acids using the standard SAFT-γ Mie group model parameters are illustrated by the dashed lines in Figures 5.1 and 5.2. As mentioned above, the deviation observed from the experimental data for these systems is attributed to the strong polarising effect of the COOH group on the neighbouring alkyl group in these molecules. In order to model such molecules with the SAFT-γ group-contribution approach, these polarisation effects can be taken into account by introducing second-order group interactions applicable to the specific molecules.

In this work, the unlike interactions between the alkyl and carboxyl groups in short-chain carboxylic acid molecules are described by second-order parameters optimised specifically to satisfy the thermodynamic behaviour of ethanoic acid and propanoic acid, using experimental data for vapour-liquid equilibrium properties of the pure acids. Specifically, data for the vapour pressure and liquid density of pure ethanoic acid at 290–500 K [343–348] are used to optimise the cross interaction between the short-acid COOH group (denoted $^{\text{short}}$COOH) and the adjacent CH_3 group (denoted $^{\text{adj}}CH_3$). The same types of VLE data for pure propanoic acid at 250–500 K [346, 349–357] are used to optimise the cross interaction between the $^{\text{short}}$COOH group and the adjacent CH_2 group (denoted $^{\text{adj}}CH_2$).

The new SAFT-γ Mie second-order cross interaction parameters applicable to the ethanoic acid and propanoic acid molecules are shown in Table 5.4. Both the $^{adj}CH_3$–$^{short}COOH$ and $^{adj}CH_2$–$^{short}COOH$ cross interactions are found to be characterised by a stronger attractive dispersion energy ε_{ij} than the corresponding cross interaction applicable to the longer carboxylic acid homologues (cf. Table 5.2). This reflects the strong polarising effect of the COOH group on the neighbouring functional groups, which is more pronounced in these smaller molecules. The description of the thermodynamic behaviour of the short-chain acids achieved with the introduction of second-order cross interactions is illustrated by the continuous curves in Figure 5.1 for ethanoic acid and in Figure 5.2 for propanoic acid. A significant improvement is seen in the case of ethanoic acid: the stronger interaction between $^{adj}CH_3$ and $^{short}COOH$ lowers the predicted vapour pressure and increases the liquid phase density at VLE, compared to the parameter set developed for the longer acids. This improvement corresponds in a decrease of the %AAD from 83.9% to 3.66% for the vapour pressure, and from 5.91% to 2.78% for the density of ethanoic acid. The quality of the predictions achieved for propanoic acid are improved in a similar way by the stronger interaction between $^{adj}CH_2$ and $^{short}COOH$, although the effect is less pronounced as the original deviation from experimental values was smaller to begin with. This improvement for propanoic acid corresponds in a decrease of the %AAD from 17.6% to 3.14% for the vapour pressure, and from 2.79% to 1.99% for the density. The importance of maintaining the $^{adj}CH_2$–$^{short}COOH$ cross interaction becomes even more evident in the prediction of mixture behaviour as discussed in Section 5.1.0.2.

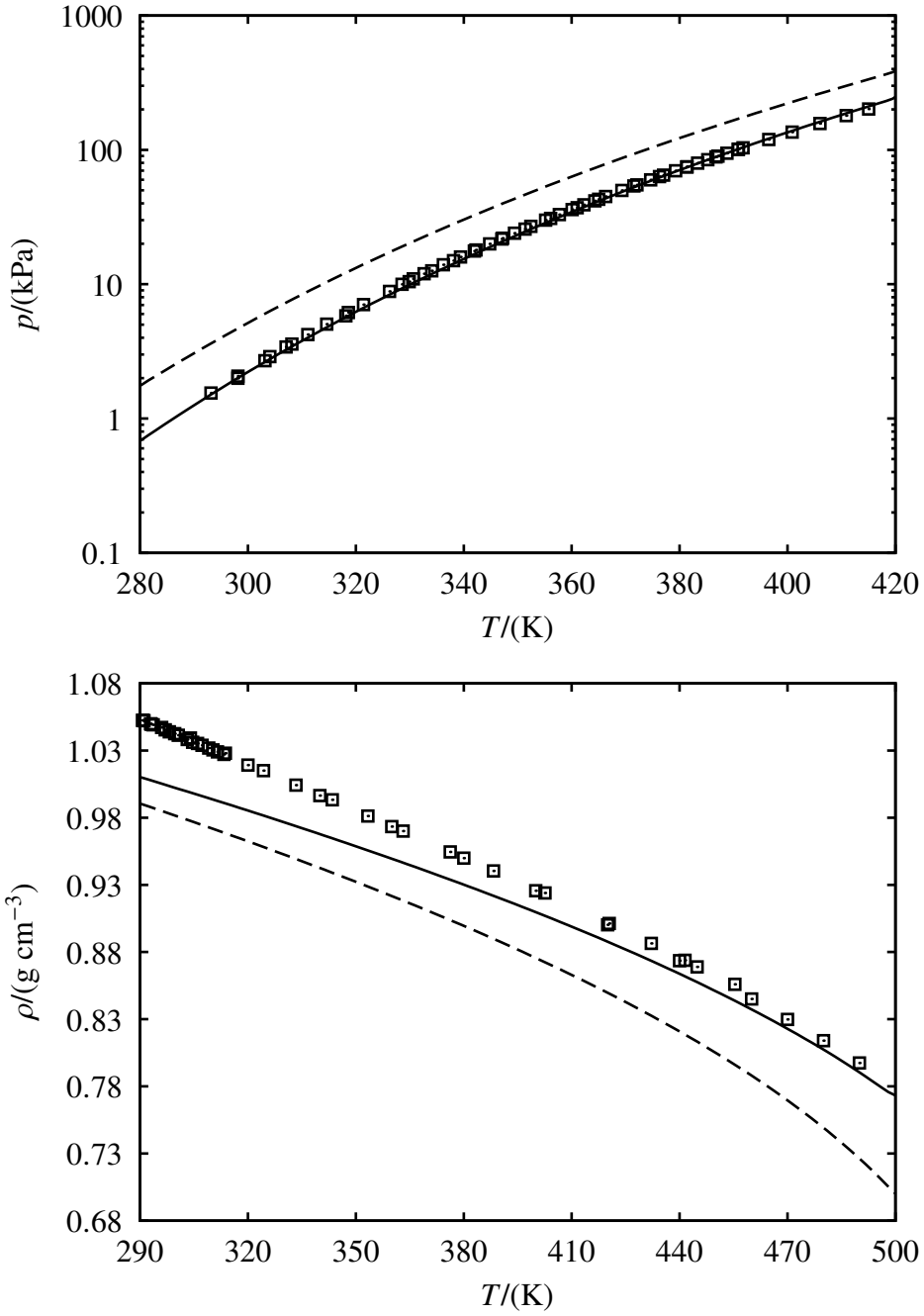

Figure 5.1 Vapour–liquid phase coexistence properties of pure ethanoic acid: the vapour pressure p for temperatures between 280–420 K (top), and the liquid phase density ρ for temperatures between 290–500 K (bottom). The continuous curves represent the results obtained using the second-order group-interaction model parameters for short chain acids shown in Table 5.4. The dashed curves represent the result given by the generic set of cross interaction parameters shown in Table 5.2. The symbols correspond to experimental data for p [343–345] and ρ [346–348].

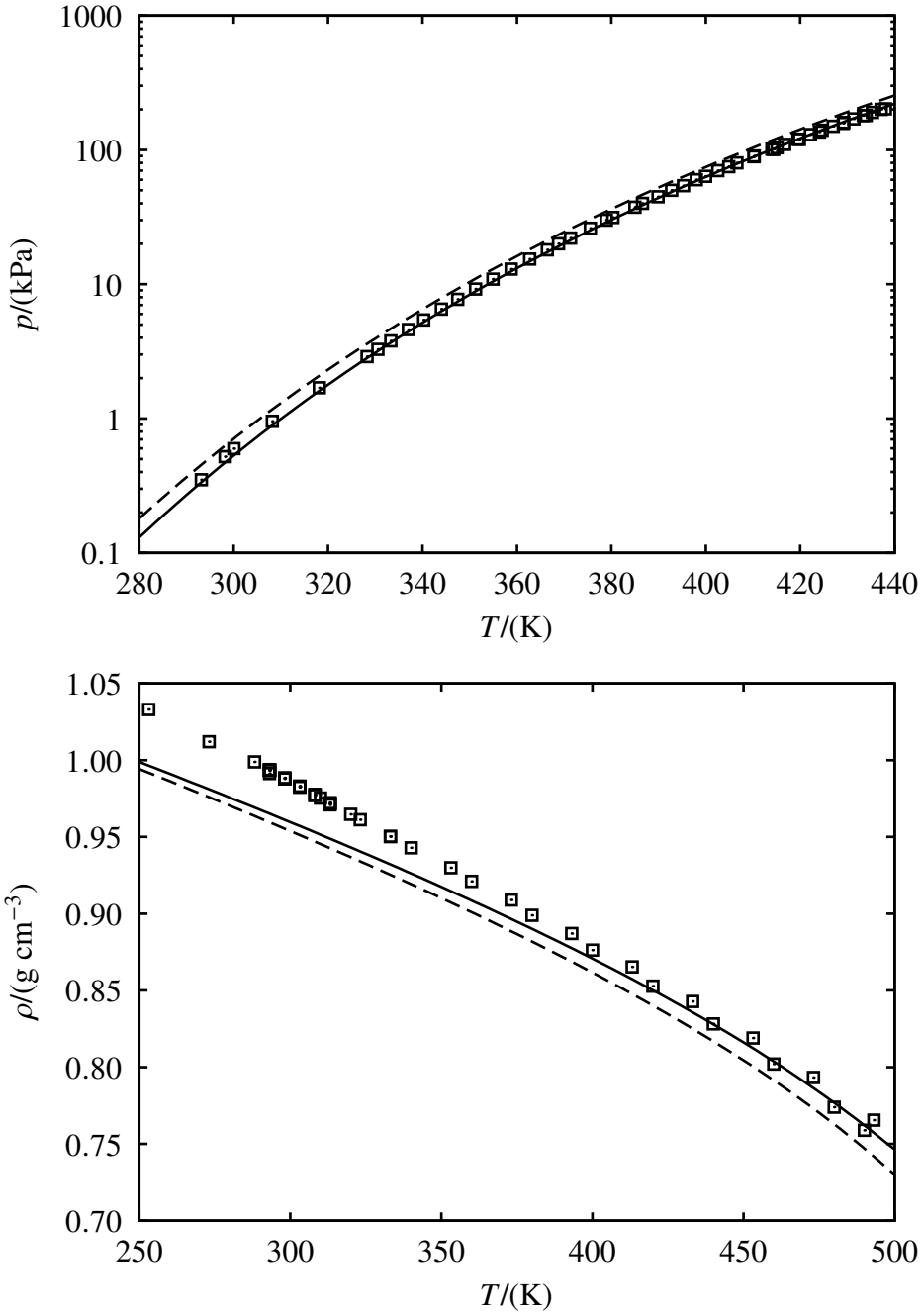

Figure 5.2 Vapour–liquid phase coexistence properties of pure propanoic acid: the vapour pressure p for temperatures between 280–440 K (top), and the liquid phase density ρ for temperatures between 250–500 K (bottom). The continuous curves represent the results obtained using the second-order group-interaction model parameters for short chain acids shown in Table 5.4. The dashed curves represent the result given by the generic set of cross interaction parameters shown in Table 5.2. The symbols correspond to experimental data for p [349–352] and ρ [346, 353–357].

Table 5.4 SAFT-γ Mie group cross interaction parameters for modelling mixtures comprising short-length alkyl carboxylic acid homologues: ethanoic acid and propanoic acid. The interactions of the carboxyl group $^{\text{short}}$COOH with the adjacent alkyl groups $^{\text{adj}}$CH$_2$ and $^{\text{adj}}$CH$_3$ reflect the strong polarisation of these groups. The $^{\text{short}}$COOH–H$_2$O interaction reflects the different type of dimers formed by shorter acids compared to their longer homologues (see text). The strength of the CH$_2$–CH$_3$, CH$_2$–H$_2$O, and CH$_3$–H$_2$O interactions are independent of whether the alkyl groups is adjacent to COOH; these cross interactions are obtained from Ref. [8]. For each pair of groups, the unlike segment diameter σ_{kl} is obtained from Equation 3.30. 'CR' indicates that the unlike Mie potential exponent $\lambda_{\text{r},kl}$ is obtained using Equation 3.33 (this is always applied for $\lambda_{\text{a},kl}$).

Group		Site		$(\varepsilon^{\text{HB}}_{ab,kl}/k_{\text{B}})$/K	$\text{K}^{\text{HB}}_{ab,kl}$ /Å^3	$\lambda_{\text{r},kl}$	$(\varepsilon_{kl}/k_{\text{B}})$/K
k	l	k,a	l,b				
$^{\text{adj}}$CH$_2$/CH$_2$	$^{\text{adj}}$CH$_3$/CH$_3$	–	–	–	–	CR	350.77
$^{\text{adj}}$CH$_2$	$^{\text{short}}$COOH	–	–	–	–	CR	454.46
CH$_2$	$^{\text{short}}$COOH	–	–	–	–	CR	413.74
$^{\text{adj}}$CH$_3$	$^{\text{short}}$COOH	–	–	–	–	CR	301.20
CH$_3$	$^{\text{short}}$COOH	–	–	–	–	CR	255.99
CH$_3$/$^{\text{adj}}$CH$_3$	H$_2$O	–	–	–	–	100.00	358.18
CH$_2$/$^{\text{adj}}$CH$_2$	H$_2$O	–	–	–	–	100.00	423.63
$^{\text{short}}$COOH	H$_2$O	e$_1$	H	1451.8	280.89	CR	289.76
$^{\text{short}}$COOH	H$_2$O	e$_2$	H	1252.6	150.98	CR	289.76
$^{\text{short}}$COOH	H$_2$O	H	e	2172.6	228.00	CR	289.76

5.1.0.2 Mixtures of short-length carboxylic acids and water

An important aspect to modelling mixtures of carboxylic acids and water is the hydrogen bonding between these species and the resultant impact on the acid dimerisation. The approach taken for representing the carboxylic acid dimerisation in SAFT-γ Mie is not mediated by 'true' hydrogen bonding between an 'e'-type site and a 'H'-type site, but rather through the 'H'-type sites on each COOH group [175]. However, it has been demonstrated both by experimental observation [358] and through theoretical calculations [359] that the nature of the dimers in aqueous solution varies as a function of the acid chain length. In particular, long-length carboxylic acids tend to form extended dimers with only one C=O$\cdots$HO hydrogen bond forming between the carboxyl groups, whereas short-length acids predominantly form cyclic dimers with two C=O$\cdots$HO hydrogen bonds forming between the carboxyl groups; the two forms of dimerization are illustrated in Figure 5.3. In the extended dimers, a single hydrogen bond is more favourable as it allows the two carboxylic acid molecules to experience maximum interaction between their alkyl chains, hence minimising hydrophobic interactions with water. The association sites (three lone pair orbitals and one hydrogen on one COOH group, and four lone pair orbitals on the second COOH group) which are not involved in this dimer-forming bond are consequently available to form four more hydrogen bonds with water per group. In cyclical dimers, the C=O and OH on both molecules are engaged in dimer-forming hydrogen bonds, thus leaving only three lone-pair orbitals per group available for hydrogen bonding with water. A lesser degree of association therefore occurs between water and the short-length carboxylic acid molecules, as opposed to longer-length homologues, as a consequence of cyclical acid dimers occupying more of the available association sites.

The fact that the pure short acids are not accurately represented with the standard SAFT-γ Mie models results also in errors in the prediction of mixture phase behaviour, as shown by the dotted curves in Figures 5.4–5.6 for mixtures composed of water and ethanoic or propoanoic acids. Replacing the group cross interactions for the alkyl–carboxyl pair with

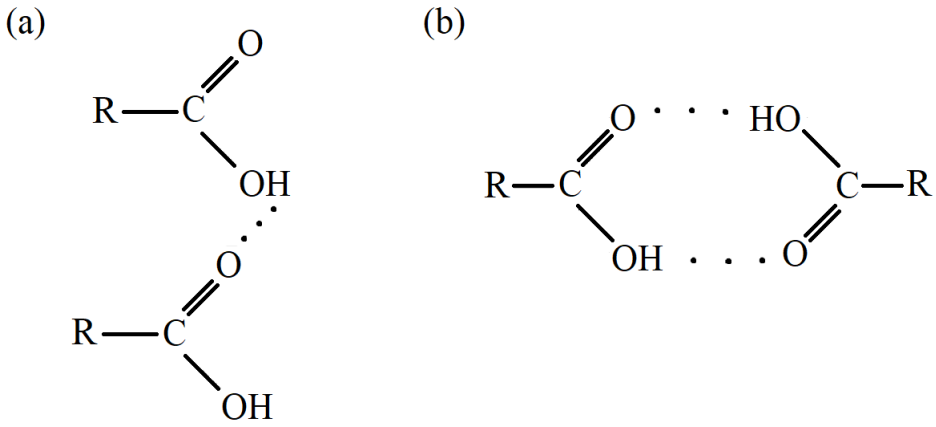

Figure 5.3 Dimerization of carboxylic acids: (a) extended dimers; (b) cyclic dimers.

the newly optimised second-order parameters for short-chain acids ($^{adj}CH_3$–$^{short}COOH$ and $^{adj}CH_2$–$^{short}COOH$) improves the prediction of the mixture's phase behaviour, especially in the case of the water–ethanoic acid mixture, as shown by the dashed lines in Figures 5.4 and 5.6. This improvement is attained without readjustment of any of the groups' cross-interaction parameters with water. The remaining deviation from the correct mixture behaviour may be attributed to the different type of acid dimerisation and resultant difference in the associative interaction between water and the carboxylic acid molecules. In order to address this behaviour, second-order group cross interactions are developed for describing the association between the $^{short}COOH$ group and the H_2O group. Experimental data for the vapour-liquid phase equilibrium properties of water–ethanoic acid mixtures, namely isobaric phase composition data [360], were employed in this procedure, by minimising an objective function of the form given by Equation 4.17.

The new second-order association parameters relevant to the $^{short}COOH$–H_2O cross interaction in mixtures containing ethanoic acid or propanoic acid are shown in Table 5.4. The association energy between 'e'-type sites on H_2O and 'H'-type sites on $^{short}COOH$ is found to be weaker than the equivalent interaction of H_2O with COOH (cf. 5.2). This mimics the fact that when cyclic dimers are favoured over extended dimers, fewer free OH donor sites are available on the carboxyl groups for associating with water lone pair orbitals. Equivalently, the carboxyl groups engaged in cyclic dimers will also have fewer free C=O

lone pair orbitals available to bond with donor sites on water molecules, yet modifying the parameters for this type of associative interaction doe not exert a particularly large influence on the acid–water mixture behaviour. This happens because the SAFT-γ Mie model mediates acid dimerisation only through the 'H'-type sites on the carboxyl groups, therefore the acid–water association parameters related to the 'H' site of the COOH group are found to exert much more influence over the thermodynamic behaviour of the mixture. For the same reason, modifying the cross-interaction dispersion energies for the $^{\text{short}}$COOH–H_2O or $^{\text{adj}}CH_3$–H_2O pairs also has a relatively small impact the mixture behaviour. This firstly emphasises that the difference in the thermodynamic behaviour between mixtures of long and short carboxylic acids is in fact a result of the shorter acids hydrogen bonding differently to water; and secondly, it demonstrates that the SAFT-γ Mie equation of state can be a useful tool for elucidating the nature of molecular interactions.

The thermodynamic properties calculated with the SAFT-γ Mie EOS for the water–ethanoic acid mixture using the new set of parameters are shown by the continuous curves in Figures 5.4 and 5.5, which demonstrate the improved description of the isobaric temperature–composition (T–x) phase diagram and the predicted saturated liquid density, respectively. Having established the benefit of using second-order $^{\text{short}}$COOH–H_2O associative parameters, these are also applied to the water–propanoic acid mixture, data for which were excluded from the optimisation procedure. The resultant predictions for this mixture's VLE properties, which are represented by the continuous curve in Figure 5.6 depicting the T–x phase diagram, are in much better agreement with the experimental data compared to the modelling approach employing the generic cross-interaction parameters. Figure 5.7 depicts the saturated liquid density of the the water–propanoic acid mixture; a comparison with the results using the generic parameter set is omitted as the improvement in the predictions is small for this property.

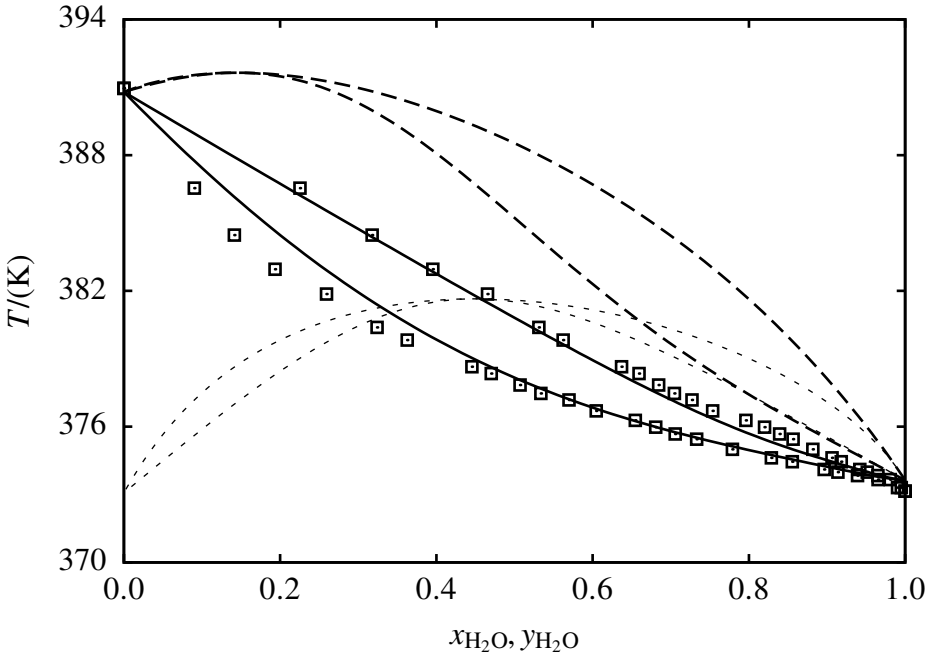

Figure 5.4 Isobaric temperature–mole fraction (T–x) phase diagram for the vapour-liquid equilibrium of ethanoic acid + water mixtures at 1.01 bar. The continuous curve represents the result obtained using the second-order group-interaction model parameters shown in Table 5.4 for the $^{adj}CH_3$–$^{short}COOH$ and $^{short}COOH$–H_2O pairs. The dashed curve represents the result obtained using the second-order $^{adj}CH_3$–$^{short}COOH$ interaction parameters shown in Table 5.4 and the generic $^{short}COOH$–H_2O interaction parameters shown in Table 5.2. The dotted curve represents the result obtained using the generic group-interaction model parameters shown in Table 5.2. The symbols correspond to experimental data [360].

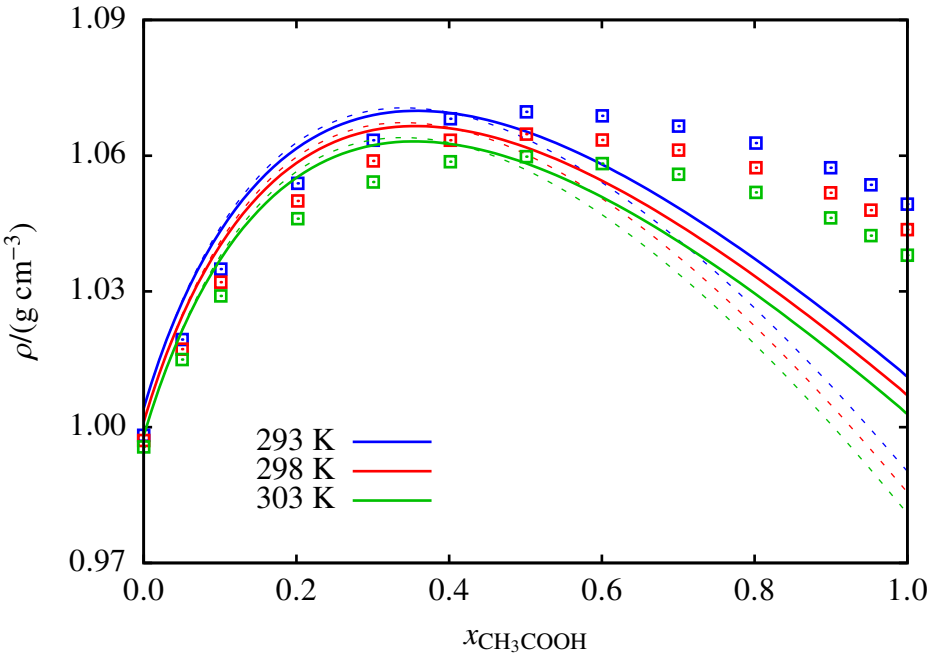

Figure 5.5 The concentration dependence of the density of ethanoic acid + water mixtures at 1.01 bar for temperatures between 293–303 K. The continuous curves represent the result obtained using the second-order group-interaction model parameters shown in Table 5.4 for the $^{\mathrm{adj}}\mathrm{CH_3}$–$^{\mathrm{short}}\mathrm{COOH}$ and $^{\mathrm{short}}\mathrm{COOH}$–$\mathrm{H_2O}$ pairs. The dotted curves represent the result obtained using the generic group-interaction model parameters shown in Table 5.2. The symbols correspond to experimental data [361].

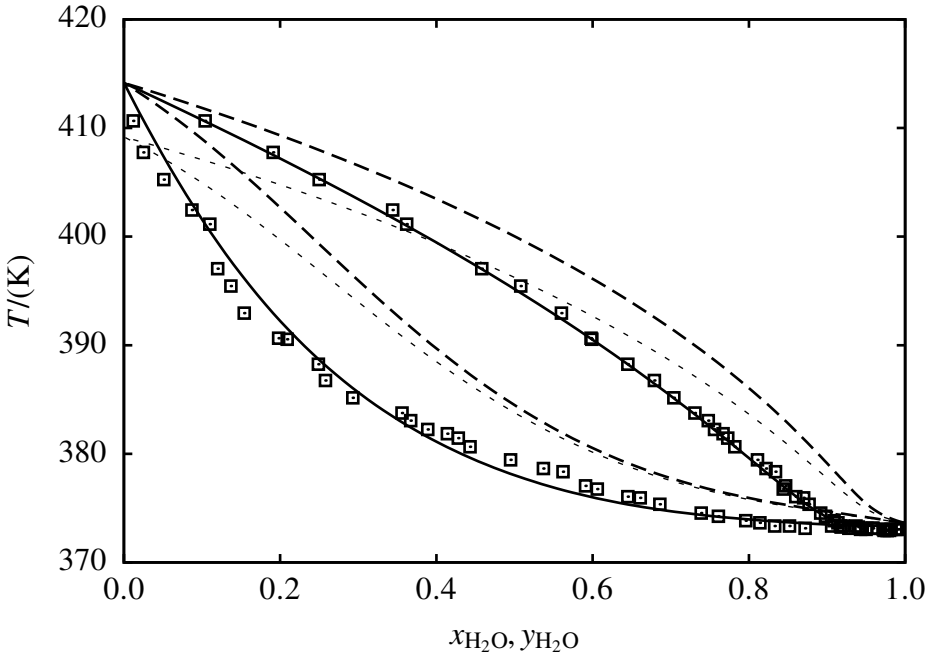

Figure 5.6 Isobaric temperature–mole fraction (T–x) phase diagram for the vapour-liquid equilibrium of propanoic acid + water mixtures at 1.01 bar. The continuous curve represents the result obtained using the second-order group-interaction model parameters shown in Table 5.4 for the $^{adj}CH_2$–$^{short}COOH$ and $^{short}COOH$–H_2O pairs. The dashed curve represents the result obtained using the second-order $^{adj}CH_2$–$^{short}COOH$ interaction parameters shown in Table 5.4 and the generic $^{short}COOH$–H_2O interaction parameters shown in Table 5.2. The dotted curve represents the result obtained using the generic group-interaction model parameters shown in Table 5.2. The symbols correspond to experimental data [362].

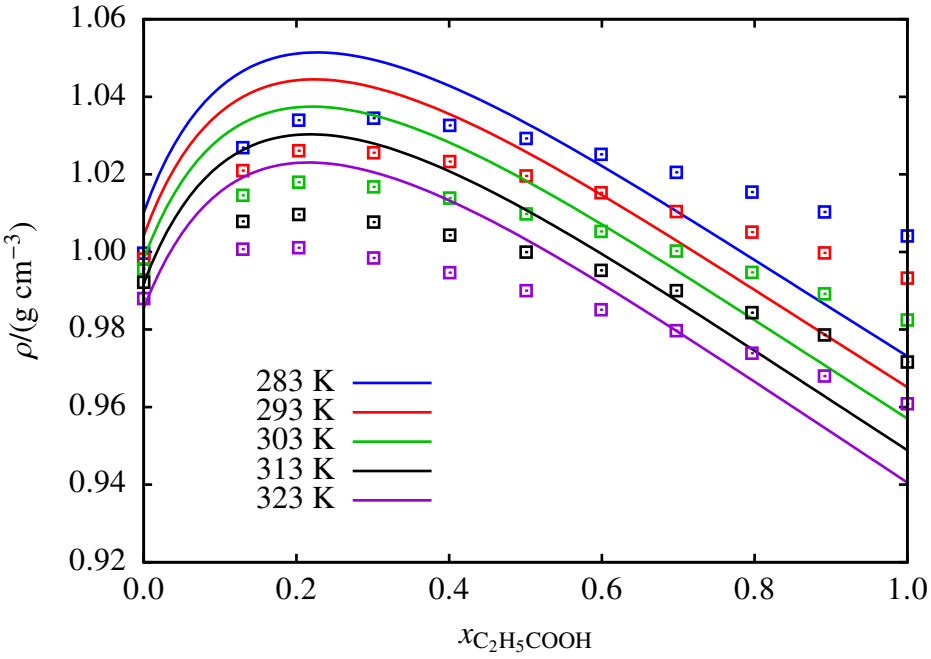

Figure 5.7 The concentration dependence of the density of propanoic acid + water mixtures at 1.01 bar for temperatures between 283–323 K. The continuous curves represent the result obtained using the second-order group-interaction model parameters shown in Table 5.4 for the $^{adj}CH_3$–$^{short}COOH$ and $^{short}COOH$–H_2O pairs. The symbols correspond to experimental data [354].

5.2 Modelling alkyl carboxylate salts with SAFT-γ Mie

The approaches proposed in Chapter 3 for modelling charged molecules within the SAFT–γ Mie EOS are applied to aqueous solutions of sodium carboxylate salts, R–COONa, of various alkyl chain lengths (R). Sodium carboxylate salts are treated here as strong electrolytes, dissociating in aqueous solution according to:

$$\text{R–COONa(aq)} \longrightarrow \text{R–COO}^-\text{(aq)} + \text{Na}^+\text{(aq)} \,. \tag{5.1}$$

Certain behaviours of carboxylate salts in aqueous solution are neglected in this work as a means of simplifying the model and allowing an easier comparison of the SAFT-γ Mie modelling approaches for charged molecules. The first neglected behaviour is the formation of ion pairs between the carboxylate anions and the alkali metal counter ions in solution. This is commonly reported for the shorter homologues of the alkyl carboxylate anions (the formate and acetate ions) [363–367], which are better solvated and have higher charge density. Still, the extent of ion pairing is very small, with association constants reported similar to those of NaCl or HCl. The second behaviour which is neglected here is the formation of micelles at high concentrations in aqueous solution [368–371]. This phenomenon is most pronounced for the longer homologues of alkyl carboxylate anions, with the critical micelle concentration decreasing as the alkyl chain length increases [372]. Sodium acetate and sodium propanoate demonstrate typical 1:1 electrolyte behaviour, whereas homologues longer than sodium butanoate demonstrate increasingly atypical behaviour due to anion aggregation.

Reducing the complexity of the electrolyte mixture by approximating the sodium carboxylate salts as simple 1:1 strong electrolytes constrains the applicability of the modelling approach to low concentrations where the extents of ion pairing and anion aggregation are small enough to neglect. Dilute and moderately concentrated salt solutions up to $m_{\text{salt}} \leq 4$ mol kg^{-1} are considered in this work. Furthermore, the size of the carboxylate anions is limited, with

the largest homologue included in the study being the hexanoate anion while the smallest is acetate.

5.2.1 Parameter estimation methodology

The methodology adopted for characterising the COO^- group follows the approach proposed in Chapter 4 regarding the development of models for molecular charged groups by estimating its parameters with reference to the optimised model of the smallest neutral parent group. The SAFT-γ Mie model parameters for the COO^- group are based on those optimised for the COOH group, assuming that the loss of a proton does not change the geometry of the COOH functional group to any appreciable extent. Firstly, the structural parameters of the COO^- group (σ_{kk}, S_k, ν_k^*) are assigned as equal to those of the COOH group. The Born cavity diameter of COO^- is obtained by applying the method proposed by Rashin and Honig [197] whereby $\sigma_{COO^-}^{Born} = 1.07\sigma_{COO^-}$, as discussed in Chapter 4. The form of like-interaction intermolecular potential is also assumed to resemble that of the COOH group, so the Mie potential exponents for COO^- are assigned to those previously optimised for COOH. Finally, the depth of the potential is calculated by applying Equation 3.96, which relates the ion–ion ε_{kk} parameter to the polarisability α_0 and ionisation potential I (electron affinity) of the COO^- functional group, experimental values for which are shown in Table 5.6. The SAFT-γ Mie model parameters for COO^- are collected in Table 5.5; the association sites assigned to this group to mediate cross-association (as will be discussed later on) are also included in this table for completeness, even though no self-association applies to the COO^- ion.

Table 5.5 SAFT-γ Mie model parameters for the carboxylate functional group.

Group, k	ν^*	S_k	σ_{kk}/Å	σ_{kk}^{Born}/Å	$\lambda_{r,k}$	$\lambda_{a,k}$	(ε_{kk}/k_B)/K	$n_{e,k}$
COO^-	1	0.55593	4.3331	4.6364	8.0000	6.0000	21.264	4

Table 5.6 Values for the polarisability α_0 and electron affinity I of the COO^- ion developed in this work, taken from Refs. [203] and [373] respectively.

Group, k	$\alpha_{0,k}$ / (10^{-24}cm^3)	I_k / eV
COO^-	4.2042	3.4700

With all model parameters for the carboxylate ion having been characterised either by referring to the parent carboxyl group or by applying appropriate combining rules, only the cross interaction parameters between COO^- and the relevant functional groups remain to be determined. For each cross interaction, the σ_{kl}, $\lambda_{\mathrm{r},kl}$, and $\lambda_{\mathrm{a},kl}$ model parameters are assigned to combining rule estimates using Equations 3.30 and 3.33. The unlike ion–ion dispersion energy for the COO^-–Na^+ pair is obtained through Equation 3.96, using the experimental values of α_0 and I shown in Tables 5.6 and 4.3. The ability of carboxylate ions to associate via the lone pair orbitals on the oxygen atoms must also be considered in mixtures containing water. In principle, the hydrated carboxylate ion may hydrogen bond with up to five water molecules. Some studies [374–376] have concluded through *ab initio* calculations that a hydrogen bonding scheme involving only three water molecules bound to the carboxylate ion is more favourable, since a bifurcated bonding scheme (in which a single water molecule associates with both oxygen atoms on the carboxylate group) is more stable; in this case, the maximum number of hydrogen bonds formed is four. The SAFT-γ Mie model for the COO^- group is assigned four 'e'-type association sites, capable of binding to the 'H'-type sites on the H_2O group. These COO^-–H_2O cross association model parameters ($\varepsilon^{\mathrm{HB}}_{ab,kl}$, $K^{\mathrm{HB}}_{ab,kl}$), together with the dispersion energy for the interaction between COO^- and each neutral group (ε_{kl}), are treated as adjustable parameters.

Group-contribution models for the carboxylate group are developed using the two SAFT-γ Mie approaches for molecular ions proposed in Chapter 3, employing a common optimisation procedure in both cases. The methodology involves a stepwise procedure using experimental data for the osmotic coefficient Φ of aqueous solutions of R–COONa salts with increasing alkyl chain lengths, obtained from Refs. [219, 368, 377]. The simplest molecular ion is chosen for identifying each unknown unlike group-interaction parameter, in a sequential

procedure. First, experimental data for aqueous sodium acetate at $m_{\text{salt}} \leq 1$ mol kg^{-1} are used to optimise the H_2O–COO^- and $^{\text{adj}}CH_3$–COO^- interactions. Then, data for aqueous sodium propanoate at $m_{\text{salt}} \leq 0.5$ mol kg^{-1} are used to optimise the CH_3–COO^- and $^{\text{adj}}CH_2$–COO^- interactions. Finally, data for aqueous sodium butanoate at $m_{\text{salt}} \leq 0.5$ mol kg^{-1} are used to obtain the CH_2–COO^- interaction. The range of concentrations included in the optimisation procedure takes into account the simplifying approximations regarding ion pairing and micelle formation in these solutions, therefore data at more dilute concentrations are used as the carboxylate ion's alkyl chain length increases.

5.2.2 Comparison of SAFT-γ Mie electrolyte formulations for alkyl carboxylate salts

The optimal model parameters obtained by applying the SAFT-γ Mie approach corresponding to spherically-approximated molecular ions (cf. Section 3.4.1) are shown in Table 5.7, and those obtained using the SAFT-γ Mie approach corresponding to free charged groups (cf. Section 3.4.2) are shown in Table 5.8. An important resemblance between the two sets of parameters is that the unlike cross-interaction parameters for the H_2O–COO^- pair (including ε_{kl}, $\varepsilon_{kl}^{\text{HB}}$, and K_{kl}^{HB}) are found to adopt very similar values in both modelling approaches. The H_2O–COO^- cross interaction parameters are therefore assigned the same values in both models, namely those optimised for the spherically-approximated ion. This resemblance potentially signifies that the two different approximations applied for the electrostatic free energy contribution primarily impact the charged group's interactions with other groups constituting the molecular ion; of course, more multicomponent mixtures need to examined to test this hypothesis. A further resemblance between the two SAFT-γ Mie modelling approaches is that, in both cases, the optimisation procedures conclude that the CH_3 interaction with COO^- is similar irrespective of whether the CH_3 group is adjacent to the COO^- group. A second-order group parameter representing the $^{\text{adj}}CH_3$–COO^- interaction is therefore omitted from both cases, as it does not impart an improvement to the performance of the

models. This is an unexpected result considering the improvement effected by the secondary $^{adj}CH_3$–COOH interaction for the neutral acid, as discussed in Section 5.1.0.1. A possible reason is that the Coulombic interactions dominate the behaviour of the acetate ion such that the effect of polarisation of the CH_3 group is overshadowed.

Table 5.7 SAFT-γ Mie group cross-interaction parameters corresponding to the approach where electrostatic interactions are accounted for by representing molecular ions as spherically-approximated charged species, following Section 3.4.1. The unlike segment diameter σ_{kl} and Mie potential exponents $\lambda_{y,kl}$ are obtained using the combining rules given by Equations 3.30 and 3.33.

Group		Site		$(\varepsilon^{HB}_{ab,kl}/k_B)$/K	$K^{HB}_{ab,kl}$ /Å^3	(ε_{kl}/k_B)/K
k	l	k,a	l,b			
COO^-	H_2O	e_1	H	1129.6	158.63	128.49
COO^-	CH_2	–	–	–	–	161.00
COO^-	$^{adj}CH_2$	–	–	–	–	287.13
COO^-	CH_3	–	–	–	–	559.99
COO^-	Na^+	–	–	–	–	9.9120

Table 5.8 SAFT-γ Mie group cross-interaction parameters corresponding to the approach where electrostatic interactions are accounted for by considering the charged functional group only, following Section 3.4.2. The unlike segment diameter σ_{kl} and Mie potential exponents $\lambda_{y,kl}$ are obtained using the combining rules given by Equations 3.30 and 3.33.

Group		Site		$(\varepsilon^{HB}_{ab,kl}/k_B)$/K	$K^{HB}_{ab,kl}$ /Å^3	(ε_{kl}/k_B)/K
k	l	k,a	l,b			
COO^-	H_2O	e_1	H	1129.6	158.63	128.49
COO^-	CH_2	–	–	–	–	202.08
COO^-	$^{adj}CH_2$	–	–	–	–	251.01
COO^-	CH_3	–	–	–	–	581.01
COO^-	Na^+	–	–	–	–	9.9120

The performance of the two SAFT-γ Mie modelling approaches for aqueous sodium carboxylate salts are evaluated by assessing the description of the solutions' thermodynamic properties which were not considered during optimisation: the mean ionic activity coefficient $\gamma_{\pm,m}$, liquid phase density ρ, and saturated vapour pressure p. The description of the osmotic coefficient beyond the concentration range included in the parameter estimation procedure is also assessed. Furthermore, the properties of sodium pentanoate and sodium hexanoate, which have been excluded from the optimisation procedure, are examined as a means of evaluating whether the two modelling approaches would be applicable to larger molecular ions.

5.2.2.1 Mean ionic activity coefficient and osmotic coefficient

Due to the combined effects of micellisation and ion pairing, the osmotic coefficients and MIACs of sodium carboxylate salts exhibit an increasingly atypical trend with composition as the anion chain length increases. In dilute solutions, the concentration dependence of these properties follow typical strong electrolyte behaviour, and the magnitude of Φ or $\gamma_{\pm,m}$

is reported to be higher as the anion chain length increases [219, 368, 377]. As the salt concentration rises, the experimental data show that Φ and $\gamma_{\pm,\mathrm{m}}$ reach a maximum and then decrease with further increase in salt concentration. This inversion of Φ and $\gamma_{\pm,\mathrm{m}}$ signifies that the adhesive forces between the particles are becoming stronger, and this is attributed to the formation of micelles. The critical micelle concentration is interpreted as the concentration at which Φ and $\gamma_{\pm,\mathrm{m}}$ reach a maximum. Since micelle formation is neglected in this work, the models are not expected to accurately reproduce the behaviour of highly concentrated solutions. Nevertheless, concentrations much higher than some solutions' critical micelle concentration are shown in the following plots in order to show the different predictions obtained from the two modelling approaches.

The concentration dependence of the osmotic coefficients at 298 K for aqueous solutions of each of the five sodium carboxylate salts (sodium ethanoate through to sodium hexanoate) are shown in Figure 5.8. The predicted MIACs at 298 K for these solutions are depicted in Figure 5.9. In these figures, results are shown for calculations performed with the SAFT-γ Mie approach for spherically-approximated ions (cf. Section 3.4.1) as well as with the approach for free charged groups (cf. Section 3.4.2). The two approaches describe the osmotic coefficient and MIAC similarly for the solutions consisting of shorter-length anions. Within the range of concentrations where the simplifying assumptions of the model are reasonable for each solution, i.e. below the critical micelle concentration of a given solution, the carboxylate salt solutions comprising long-chain anions appear to be better described by the SAFT-γ Mie approach for spherically approximated anions. In Figure 5.10 for sodium ethanoate solutions, the activity of water $a_{\mathrm{H_2O}}$ predicted as a function of temperature and concentration is consistently better predicted by the SAFT-γ Mie approach for free charged groups.

Differences between the two approaches are most distinct in the prediction of solution properties at higher concentrations for sodium butanoate, sodium pentanoate and sodium hexanoate. For the larger pentanoate and hexanoate anions, the approach in which electrostatic interactions are applied to the free charged groups is more effective in predicting

the reversal of the trend in osmotic coefficient and MIAC with respect to the anion chain length. This is an important feature despite the expected lack of quantitative agreement with the experimental data at concentrations beyond the critical micelle concentration: in the electrolyte approach corresponding to individual charged groups, the electrostatic interactions are not tied to a particular molecular geometry or configuration, and this appears to be advantageous when modelling fluid mixtures comprising organic ions exhibiting behaviours that cannot be explicitly included in the SAFT-γ Mie EOS. This aspect of the models' behaviour is considered here to be of greater significance for assessing their performance than the quantitative agreement attained with MIAC or Φ experimental data, especially considering that this type of data for these solutions originate from fairly old sources. This argument is supported by Figure 5.10 for sodium ethanoate solutions, where the activity of water a_{H_2O} predicted as a function of temperature and concentration is consistently better predicted – as compared to a recent set of experimental data – by the SAFT-γ Mie approach for free charged groups.

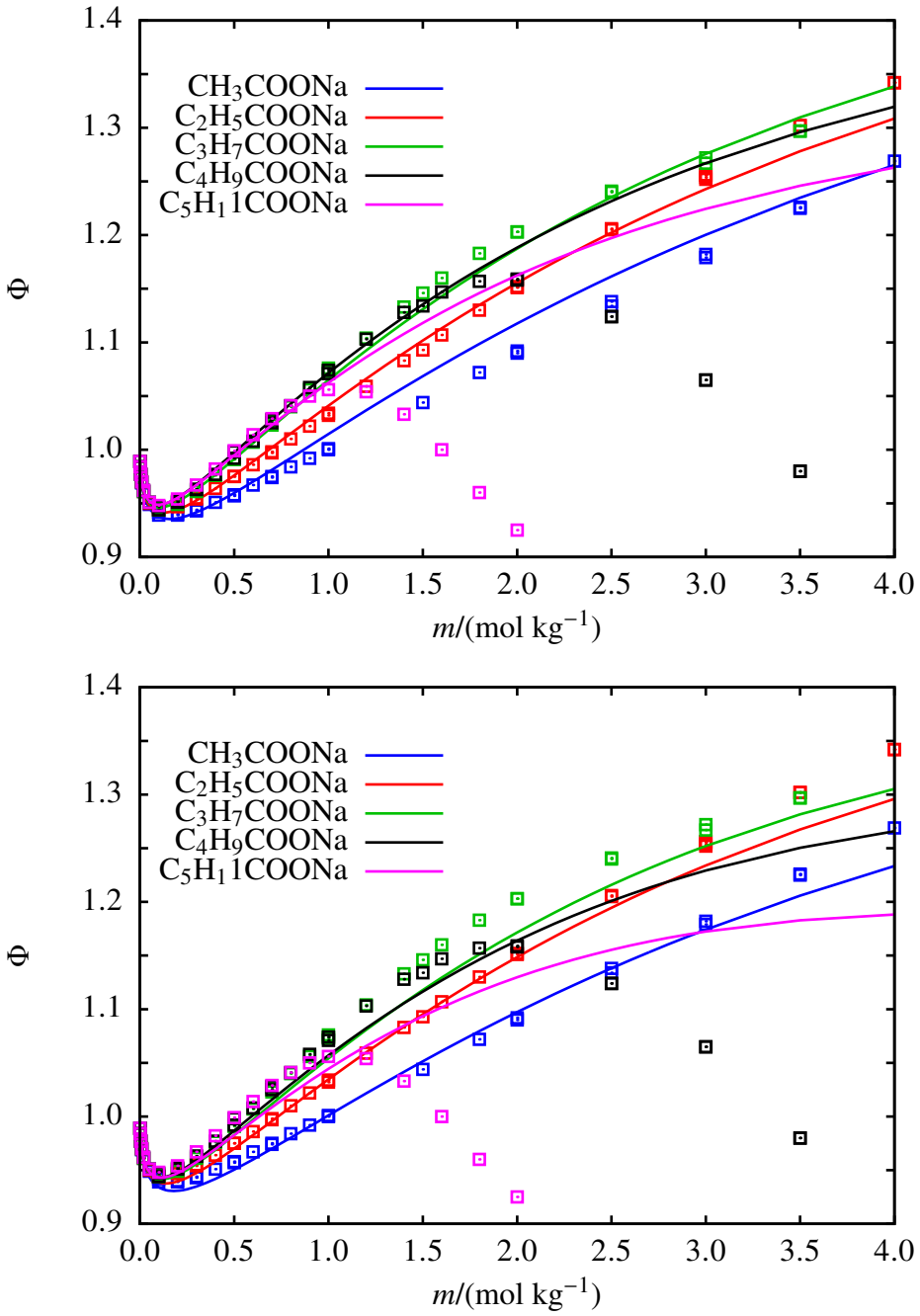

Figure 5.8 The concentration dependence of the osmotic coefficient Φ for aqueous sodium carboxylate salt solutions at 298 K. The continuous curves represent the predictions obtained with the SAFT-γ Mie EOS using the approach for spherically-approximated ions (top) and the approach for free charged groups (bottom). The symbols represent the experimental data [219, 368, 377].

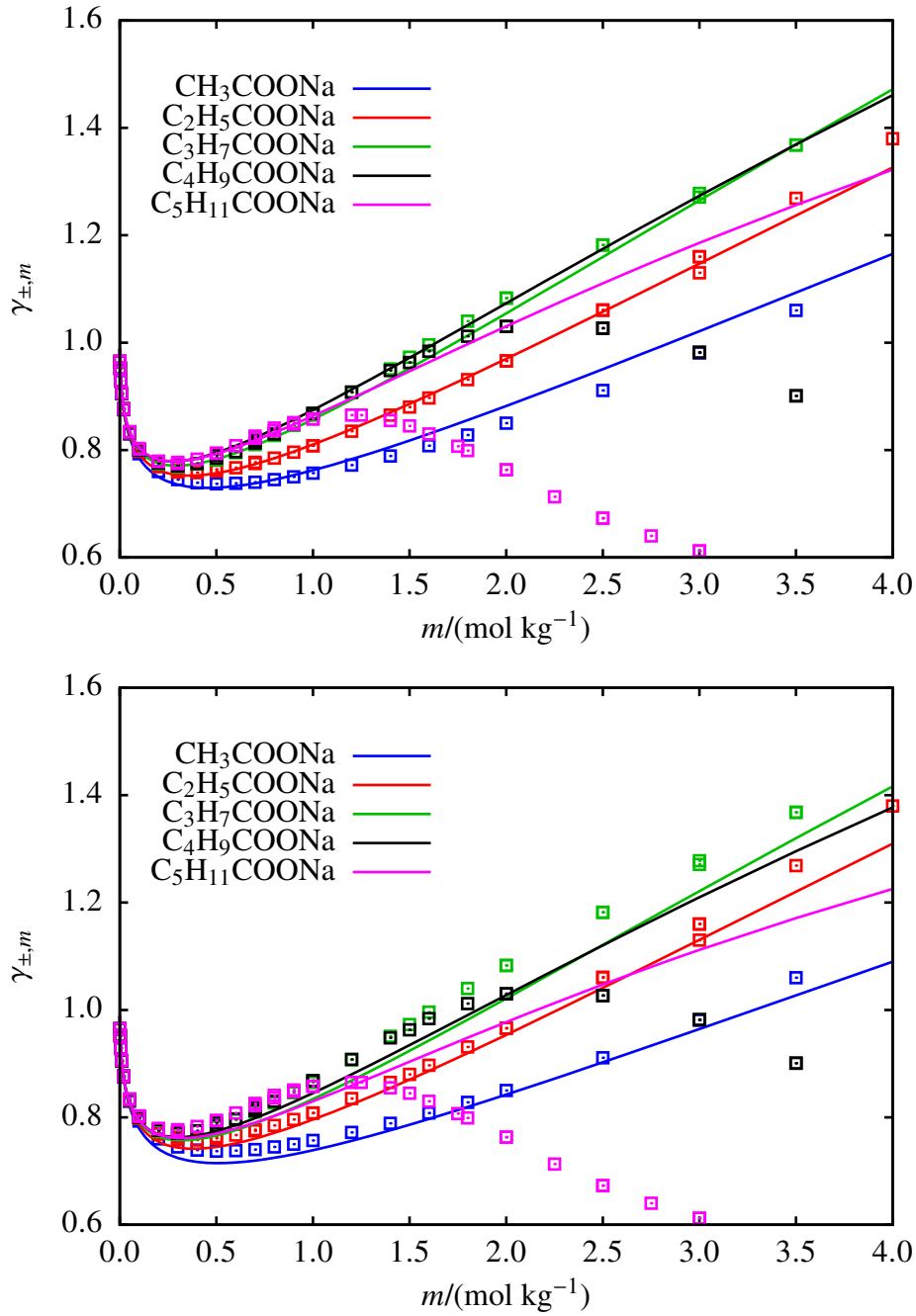

Figure 5.9 The concentration dependence of the MIAC $\gamma_{\pm,m}$ for aqueous sodium carboxylate salt solutions at 298 K. The continuous curves represent the predictions obtained with the SAFT-γ Mie EOS using the approach for spherically-approximated ions (top) and the approach for free charged groups (bottom). The symbols represent the experimental data [219, 368, 377].

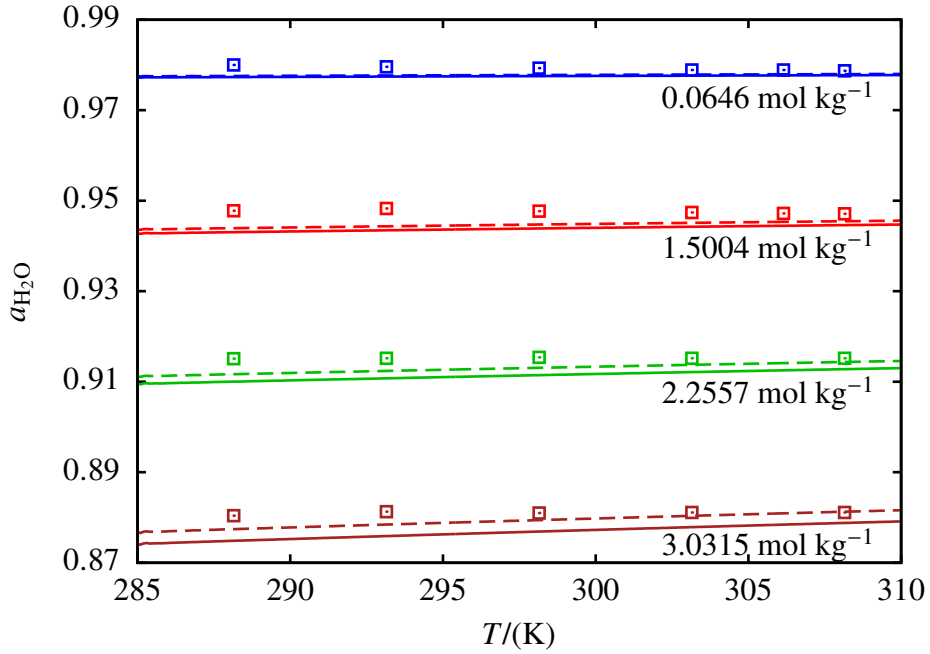

Figure 5.10 The temperature dependence of the activity of water a_{H_2O} for aqueous sodium ethanoate solutions at conditions of vapour–liquid equilibrium, at molalities in the range of 0.06464–3.0315 mol kg^{-1}. The continuous curves represent the predictions obtained with the SAFT-γ Mie EOS using the approach for spherically-approximated ions, and the dashed curves represent the predictions obtained with the SAFT-γ Mie EOS using the approach for free charged groups. The symbols represent the experimental data [378].

5.2.2.2 Solution densities and saturated vapour pressures

Evaluating the performance of the SAFT-γ Mie models with respect to the density and saturated vapour pressure of aqueous R–COONa solutions is difficult, as experimental data for these types properties are scarce for mixtures comprising the carboxylate anions larger than CH_3COO^-. The isobaric liquid density ρ of aqueous sodium ethanoate solutions at temperatures between 288–318 K is shown in Figure 5.11. The degree of agreement with experimental data achieved by each modelling approach is not consistent across temperature range considered, although this may be due to an apparent, yet unspecified, experimental error in the density measurements at the lowest considered temperature. If only the density data at higher temperatures is taken into account, then the SAFT-γ Mie approach for spherically

approximated molecules is seen to give a better description of the fluid phase. This is also observed in Figure 5.12 for the the density of aqueous solutions of sodium ethanoate and sodium butanoate at 298 K; however, in the same figure, the liquid phase density of sodium hexanoate is distinctly better described by the SAFT-γ Mie approach for individual charged groups. This is a reasonable outcome, as the approximation of an equivalent spherical ion becomes less structurally sound as the size of the ion increases.

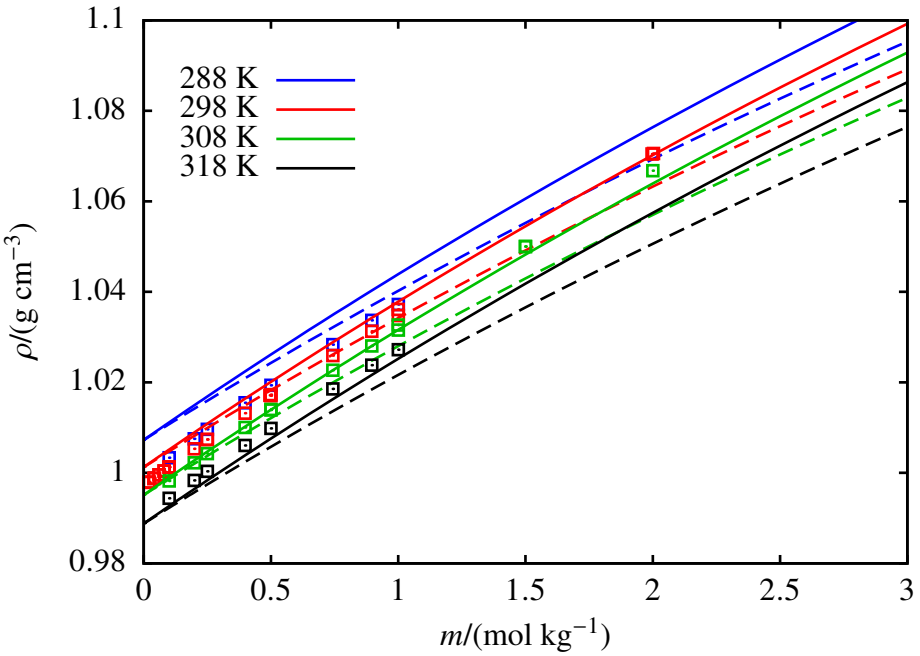

Figure 5.11 The concentration dependence of the of the liquid phase density ρ of aqueous solutions of sodium ethanoate at 1 bar, for temperatures in the range 288–318 K. The continuous curves represent the predictions obtained with the SAFT-γ Mie EOS using the approach for spherically-approximated ions, and the dashed curves represent the predictions obtained with the SAFT-γ Mie EOS using the approach for free charged groups. The symbols represent the experimental data [379–381].

In the less dense vapour phase, the differences in the structural approximations made in each SAFT-γ Mie modelling approach have a smaller impact on the predicted properties of the fluid. Very similar results are obtained by the two approaches for molecular ions for predictions of the solution's saturated vapour pressure p, as seen in Figure 5.13 for aqueous sodium ethanoate at 298 K and 308 K, and in Figure 5.14 for aqueous sodium ethanoate

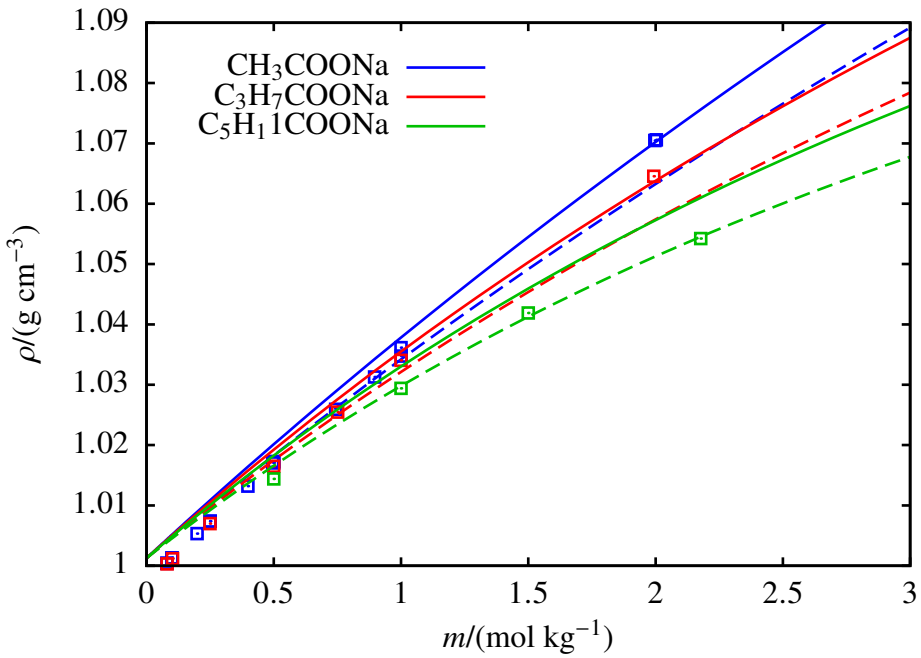

Figure 5.12 The concentration dependence of the of the liquid phase density ρ of aqueous solutions of sodium ethanoate, sodium butanoate, and sodium hexanoate at 298 K and 1 bar. The continuous curves represent the predictions obtained with the SAFT-γ Mie EOS using the approach for spherically-approximated ions, and the dashed curves represent the predictions obtained with the SAFT-γ Mie EOS using the approach for free charged groups. The symbols represent the experimental data [379, 380, 382].

and sodium pentanoate at 373 K. Even at higher concentrations of solutions comprising larger molecular ions, the two approaches provide a similar representation of the saturated vapour pressure. It must be noted that the data in Figure 5.14 obtained from Ref. [278] are very old, however they are included in this assessment as this is the only known source reporting on the vapour pressure of multiple solutions of sodium carboxylate salts; these measurements display a systematic yet unspecified measuring error, as seen from the fact that the value reported for the vapour pressure of water is slightly higher than its accepted value of 101.3 kPa. In combination with the SAFT-γ Mie model's ~1% underprediction of p for pure water, this leads to an apparently constant offset in the vapour pressure prediction for these solutions.

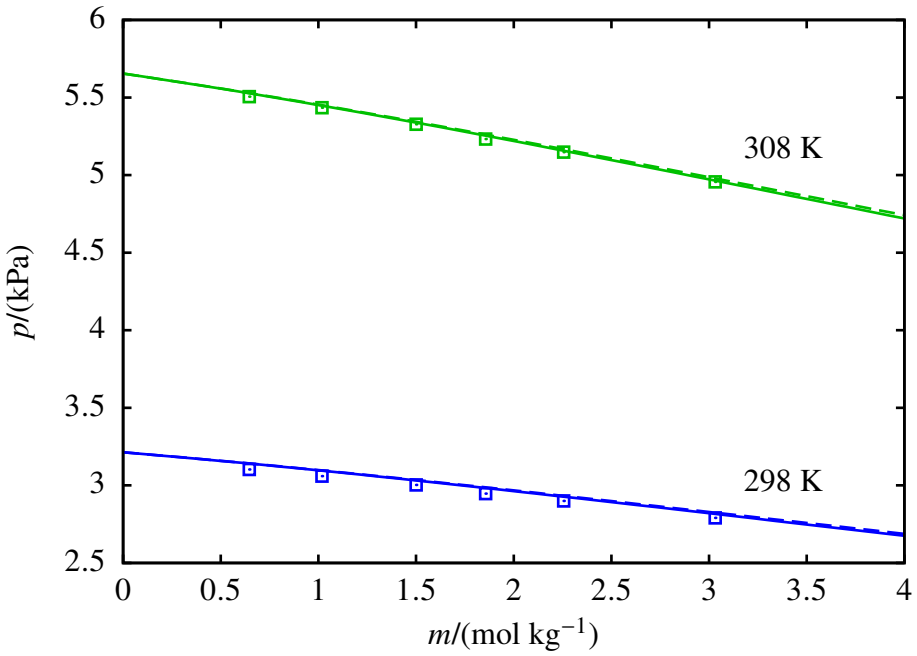

Figure 5.13 The concentration dependence of the of the saturated vapour pressure p of aqueous sodium ethanoate solution at 298 K and 308 K. The continuous curves representing the predictions obtained with the SAFT-γ Mie EOS using the approach for spherically-approximated ions are almost completely overlapped with the dashed curves representing the predictions obtained with the SAFT-γ Mie EOS using the approach for free charged groups. The symbols represent the experimental data [378].

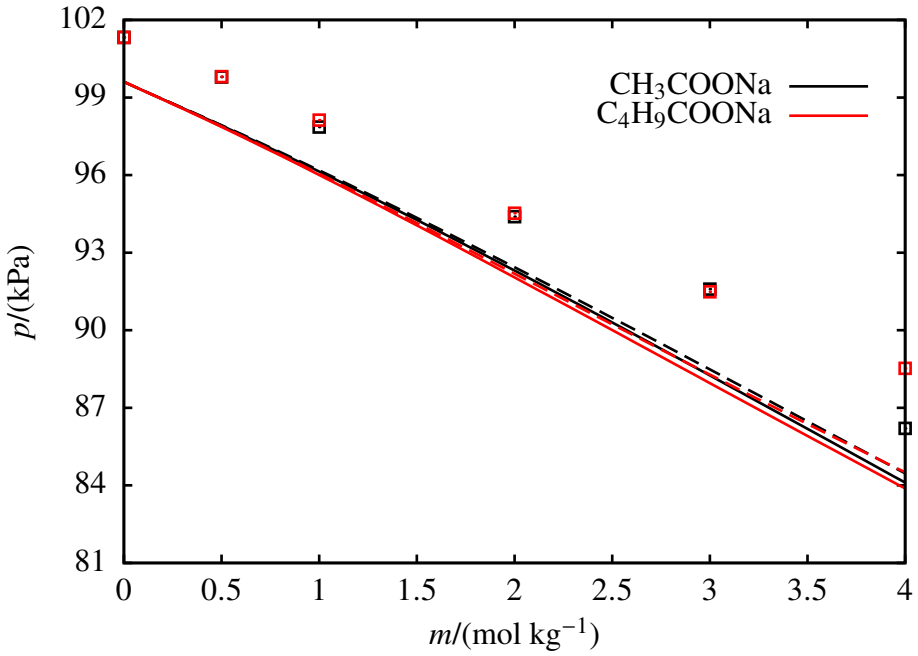

Figure 5.14 The concentration dependence of the of the saturated vapour pressure p of aqueous solutions of sodium ethanoate and sodium pentanoate at 373 K. The continuous curves represent the predictions obtained with the SAFT-γ Mie EOS using the approach for spherically-approximated ions, and the dashed curves represent the predictions obtained with the SAFT-γ Mie EOS using the approach for free charged groups. The symbols represent the experimental data [278].

5.3 Summary

In this chapter, the SAFT-γ Mie EOS was applied for the purpose of modelling sodium carboxylate salts. The two formulations for modelling molecular ions in a group-contribution framework, which were proposed in Chapter 3, were both used to develop models for COO^- functional group and its unlike interactions with coexisting groups in the mixture. The model for the COO^- group was determined without adjusting any self-interaction parameters to experimental data, by transferring the size and Mie potential parameters of the neutral group (COOH) to the deprotonated group (COO^-) and computing the dispersion energy using a combining rule. As a result, the same model for COO^- is applicable to both SAFT-γ Mie formulations and the difference in the models associated with each formulation lies in the unlike interactions of the carboxylate anion with other neutral groups comprising the molecular ion.

A modelling strategy for developing the SAFT-γ Mie model for the COO^- group's unlike interactions was determined by first carrying out a re-evaluation of the COOH group's interactions when modelling carboxylic acid molecules in pure and aqueous systems. Two phenomena were taken into account: firstly, the polarising effect of COOH on adjacent functional groups which is more pronounced in short-chain acids; and secondly, the effect of alkyl chain length on the hydrogen-bonding scheme between the carboxylic acid and water. This study led to the proposal of second-order cross-interaction parameters in order to achieve an accurate representation of the properties of pure short-chain carboxylic acids and their mixtures with water. The use of second-order parameters was therefore also adopted in the modelling strategy for the carboxylate group's unlike interactions, although it was found to be necessary for only one type of interaction as opposed to the three second-order interactions required for the carboxylic acid systems.

Two sets of models – one for each SAFT-γ Mie formulation – were obtained by optimisation to experimental data for aqueous solutions of sodium carboxylates with anion

alkyl chain lengths of C2–C4, and the properties of carboxylate salt solutions were evaluated for anion chain lengths up to C6. The range of concentrations to which the SAFT-γ Mie approach is applicable varies for each salt due to the formation of micelles occurring at lower concentration as the anion chain length increases. Nevertheless, both formulations are found to give comparable predictions for the appropriate concentration range of each sodium carboxylate salt. Even though quantitative agreement with experiment is not attained in concentrated solutions where micelles are present, the predictions obtained with the electrolyte formulation corresponding to individual charged groups depict a more realistic tendency of the solutions' behaviour with respect to anion chain length. This formulation is thus recommended as the more promising avenue for pursuing electrolyte thermodynamic modelling within the SAFT-γ Mie group-contribution framework.

Chapter 6

Weak electrolytes: inorganic acids and ion-paired salts

Thermodynamic modelling work on electrolytes has largely focused on solutions of completely ionised salts, as the composition of these mixtures is straightforwardly known from the stoichiometry of the salt. On the contrary, in order to determine the solution composition of weak electrolytes, the relevant chemical equilibria must be accounted for in the modelling procedure. In this chapter, the thermodynamic modelling of two types of aqueous electrolyte solutions is undertaken: solutions of incompletely dissociated weak acids, and solutions of weakly associated salts. Two common inorganic acids are selected, namely sulphuric acid and nitric acid, for which abundant information is available in the literature regarding their dissociation equilibria and bulk-phase solution properties. In the context of associated salts, the manifestation of ion pairing in solutions of alkali nitrate salts is examined.

6.1 Sulphuric acid

Sulphuric acid is a diprotic acid which is generally regarded as a 'strong' electrolyte owing to its complete first deprotonation step, although the second deprotonation step is incomplete. The ionic composition of aqueous H_2SO_4 depends on the equilibrium between the bisulphate (HSO_4^-) and sulphate (SO_4^{-2}) ions, and it is typically quantified through the degree of dissociation of the bisulphate ion, $\alpha_{HSO_4^-}$ (see Equation 6.9). The difficulty of ascertaining the true ionic composition of a sulphuric acid solution has led to diverging values reported in the literature for the thermodynamic equilibrium constant of the bisulphate dissociation. Properties linked to the ionic composition of the solution, for example the mean ionic activity coefficient, are therefore usually reported by adopting the assumption of stoichiometric solution composition.

Before attempting to model aqueous sulphuric acid, it is important to first understand the chemical equilibria relevant to this system and assess the available experimental data. Based on an analysis of these, a methodology for developing models for sulphuric acid is proposed. The resultant SAFT-γ Mie models for the sulphate and bisulphate ions are then applied to predict the bulk-phase thermodynamic properties of the aqueous acid.

6.1.1 Dissociation equilibrium

Sulphuric acid in aqueous solution undergoes two sequential dissociation steps, both of which entail a proton-transfer reaction with water:

$$H_2SO_4 + H_2O \overset{K_{a1}}{\rightleftharpoons} H_3O^+ + HSO_4^- , \tag{6.1}$$

$$HSO_4^- + H_2O \overset{K_{a2}}{\rightleftharpoons} H_3O^+ + SO_4^{-2} . \tag{6.2}$$

The acid dissociation constants K_{a1} and K_{a2} correspond to the first and second dissociation steps, respectively, and characterise the thermodynamic equilibrium for these reactions. According to the convention of approximating the activity of water as unity, these acid dissociation constants are defined on a molality scale as follows [383]:

$$K_{a1}(T) = \frac{a_{H_3O^+,m}(T,p,m)\, a_{HSO_4^-,m}(T,p,m)}{a_{H_2SO_4,m}(T,p,m)}, \tag{6.3}$$

$$K_{a2}(T) = \frac{a_{H_3O^+,m}(T,p,m)\, a_{SO_4^{-2},m}(T,p,m)}{a_{HSO_4^-,m}(T,p,m)}, \tag{6.4}$$

There is a consensus in the literature that the first dissociation step is complete, i.e. $K_{a1}(T) = \infty$, except at very high acid concentrations >14 mol L^{-1} [34, 384, 385], whereas the second dissociation step is comparatively weak. Within the composition range where the SAFT-γ Mie EOS is applicable ($\leq$10 mol kg^{-1}), the first dissociation step of sulphuric acid may be considered complete and therefore the reaction equilibrium for the first dissociation step does not need to be solved. The second dissociation step is solved by satisfying the acid dissociation constant K_{a2} is at the temperature of interest.

Significant experimental research effort has been put into determining the second acid dissociation constant of sulphuric acid. Dickson et al. [386] employed electrochemical cell measurements to determine K_{a2} and proposed an empirical equation applicable in the temperature range 283–523 K. Holmes and Mesmer [387] used Dickson's correlation together with new and previously published [383] isopiestic data to propose their own correlation for K_{a2}. A thorough examination of the thermodynamic data (osmotic coefficient, vapour pressure, e.m.f., enthalpy of dilution, heat capacity, and degree of dissociation) available at the time was performed by Clegg et al. [388], on the basis of which the value of 0.0105 mol kg^{-1} was recommended for K_{a2} at 298 K. Using this benchmark, Clegg et al. evaluated various correlations for K_{a2} based on their reproduction of critically assessed experimental data in the ranges of m = 0–6.1 mol kg^{-1} and T = 273–328 K using an extended Pitzer model, finally

recommending a truncated version of Dickson's equation, given as:

$$\log_{10} K_{a2} = 562.69486 - 102.5154 \ln(T) - 1.117033 \times 10^{-4}(T^2) + 0.2477538T - \frac{13273.75}{T} . \quad (6.5)$$

More recently, Sippola [389, 390] examined six dissociation constant equations, including those of Pitzer et al. [383], Matsushima and Okuwaki [391], Dickson et al. [386], Hovey and Hepler [392], Clegg et al. [388], and Knopf et al. [393]. The equations of Matsushima and Okuwaki [391], Dickson et al. [386], Hovey and Hepler [392], and Clegg et al. [388] were found to give the best values for K_{a2} overall, although the equation of Knopf was found more suitable for use at high temperatures. Sippola concludes that the choice of correlation ultimately depends on the temperature range of the intended application. For the purpose of this work, we choose to apply Clegg's correlation given by Equation 6.5. This equation has been developed so as to give an accurate K_{a2} value at 298 K, which is the temperature at which the most thermodynamic data is available for sulphuric acid.

6.1.1.1 Ion association

The precise reaction mechanisms for the dissociation of sulphuric acid in water are still disputed in the literature [394], with investigators proposing a range of intermediate proton transfer steps, hydrogen bonded ion-solvent complexes, and ion association equilibria [395–398]. In equation-of-state modelling approaches the intermediate reaction steps are not usually explicitly considered; however, it will be argued here that these intermediate reactions can give valuable insight into association interactions which can be incorporated in the present SAFT-γ Mie modelling approach.

Edward and Wang [395] measured the ultraviolet absorption of aqueous sulphuric acid solutions and also used the Raman spectral data of Young et al. [399] to propose the existence of sulphate-hydronium ion pairs $[H_3O^+ \cdot SO_4^{-2}]$ and ion triplets $[H_3O^+ \cdot SO_4^{-2} \cdot H_3O^+]$,

predominantly at high concentrations >7 mol L^{-1}. The authors argue this results from the abundant hydronium ions binding to water molecules through hydrogen bonds, thus limiting the amount of water available to hydrate the other ions and consequently promoting ion association for the unhydrated sulphate ions. A similar conclusion was reached by Irish and Chen [398], who examined Raman spectra of aqueous sulphuric acid and suggested that the second dissociation step is driven by a proton transfer equilibrium between the hydrated bisulphate ion $(H_2O)HSO_4^-$ and the sulphate–hydronium ion pair $[H_3O^+ \cdot SO_4^{-2}]$:

$$(H_2O)HSO_4^- \rightleftharpoons H_3O^+ \cdot SO_4^{-2} \,. \tag{6.6}$$

The bisulphate ion was argued to exist only in the hydrated form, while the sulphate–hydronium ion pair was suggested to persist in solution in favour of the free ions. In subsequent work, Chen and Irish [396] extended this argument by proposing the formation of the bisulphate–hydronium ion pair $[H_3O^+ \cdot HSO_4^-]$ through a further proton-transfer reaction equilibrium:

$$H_3O^+ \cdot HSO_4^- + SO_4^{-2} \rightleftharpoons HSO_4^- + H_3O^+ \cdot SO_4^{-2} \,. \tag{6.7}$$

Cox et al. [397] also analysed Raman spectra and put forward a dissociation sequence for sulphuric acid involving three equilibrium steps. In this scheme, the fist acid dissociation reaction given by Equation 6.1 is replaced by two equilibrium steps: first the formation of a hydrated bisulphate–hydronium ion pair,

$$H_2SO_4 + H_2O \rightleftharpoons (H_2O)HSO_4^- \cdot H_3O^+ \,, \tag{6.8}$$

followed by this ion pair's equilibrium with the free bisulphate and hydronium ions. The existence of the $[(H_2O)HSO_4^- \cdot H_3O^+]$ ion pair at high concentrations was first proposed by Irish and Chen [396, 398], as an alternative interpretation of the $[H_3O^+(H_2SO_4)]$ species suggested by Wyatt [400]. Cox et al. argued instead that the bisulphate–hydronium ion pair

is formed in the initial dissociation step and is present at all acid concentrations, including dilute solutions.

It should be noted that the presence of these various ion pair species has not been conclusively verified and the true composition of the aqueous sulphuric acid solution is still under debate [394]. The hydration state of the sulphate and bisulphate ions also remains unresolved. Both ions would be expected to form multiple hydrogen bonds with water and, in fact, studies have suggested that both HSO_4^- and SO_4^{-2} ions form complex hydrogen bonded clusters with water in solution. Yacovitch et al. [401] studied the hydration of the bisulphate ion using infrared spectroscopy, observing $HSO_4^-(H_2O)_n$ clusters involving up to 16 water molecules with inter-water bonding within these clusters starting at $n \geq 2$. In a study using photoelectron spectroscopy to study the hydration of the sulphate ion, Wang et al. [402] observed $SO_4^{-2}(H_2O)_n$ clusters involving up to 10 water molecules. A minimum of three water molecules were found necessary to stabilise the SO_4^{-2} ion, and inter-water bonding within the cluster was proposed to start at $n \geq 5$. Despite doubt over the longevity of the hydration clusters and inconclusive evidence of ion pairing, hydrogen bonding of HSO_4^- and SO_4^{-2} with water and with hydronium are examined in the SAFT-γ Mie modelling approach, the latter interaction intended to mimic the ion pairing phenomena.

6.1.2 Model development

Aqueous sulphuric acid is modelled as a mixture of the following components: H_2O, H_3O^+, HSO_4^- and SO_4^{-2}. The models for water and the hydronium ion are obtained from Chapter 4, while the SAFT-γ Mie models for the sulphate and bisulphate ions and their cross interactions are developed here. The model optimisation procedure considers bulk phase thermodynamic properties for aqueous sulphuric acid, limiting the use of experimental data only to those essential for representing the various aspects of the constituent species' thermodynamic behaviour. The solution of chemical equilibrium for the second acid dissociation step is performed by satisfying Equation 6.4, using the value for K_{a2} given by Equation 6.5.

The SAFT-γ Mie models are optimised such that the thermodynamic activities of the ions, and thereby their equilibrium compositions, are correctly reproduced with respect to the imposed K_{a2}. To this end, it is important to include speciation data of the acid in the optimisation procedure. Speciation data for sulphuric acid are typically reported as the degree of dissociation of the bisulphate ion, $\alpha_{HSO_4^-}$, which is given as follows:

$$\alpha_{HSO_4^-} = \frac{m_{SO_4^{-2}}}{m_{HSO_4^-} + m_{SO_4^{-2}}} = \frac{m_{SO_4^{-2}}}{m_{acid}} \,. \tag{6.9}$$

Compositions of all species can be related to $\alpha_{HSO_4^-}$ and the acid molality m_{acid} through the following material balances corresponding to the reactions given by Equations 6.1 and 6.2:

$$m_{HSO_4^-} = m_{acid}(1 - \alpha_{HSO_4^-}) \tag{6.10}$$

$$m_{SO_4^{-2}} = m_{acid}\alpha_{HSO_4^-} \tag{6.11}$$

$$m_{H_3O^+} = m_{acid}(1 + \alpha_{HSO_4^-}) \tag{6.12}$$

$$m_{H_2O} = m^0_{H_2O} - m_{acid}(1 + \alpha_{HSO_4^-}) \,, \tag{6.13}$$

where $m^0_{H_2O} = 1/MW_{H_2O}$ is the molal concentration of water were it not to react with the acid.

According to experimental data for $\alpha_{HSO_4^-}$ [396, 403, 404] (see Figure 6.1) an infinitely dilute solution of sulphuric acid contains a negligible fraction of bisulphate ions, with $\alpha_{HSO_4^-}$ approaching unity. The degree of dissociation quickly falls to a minimum of ~0.17, indicating that the majority of HSO_4^- ions do not dissociate, then rises to a maximum of ~0.37 before again decreasing steadily with increasing acid concentration. The optimisation dataset includes the minimum number of data points necessary to encompass these changes in ionic composition within the concentration range of interest, so data for molalities of up to 4.8 mol kg^{-1} are used.

Additional data included in the optimisation procedure for the HSO_4^- and SO_4^{-2} models must be consistent with the acid speciation data. For this reason, stoichiometrically defined properties are not well suited for use in this optimisation procedure, as they do not give a

direct link to the species' real activities or composition in solution. Instead of these properties, experimental data for the activity a_{H_2O} of the solvent are used, as these can be directly measured experimentally without knowledge of the either the stoichiometric or true solution composition. This choice aims to avoid inconsistencies in the data while providing the necessary information regarding the thermodynamic behaviour of the solvent. Experimental data for the liquid phase density is also included in order to facilitate the determination of cross-interaction parameters. The final optimisation dataset and the corresponding literature sources are given in Table 6.1. Model parameters for the HSO_4^- and SO_4^{-2} species are optimised simultaneously with their unlike interactions with coexisting species in the solution, namely H_2O and H_3O^+, by minimising an objective function of the form given by Equation 4.17.

The model parameters of the ionic groups are determined first following the methodology described in Chapter 4. A complete optimisation exercise for the remaining cross-interactions that need to be characterised in the aqueous sulphuric acid solution involves 16 parameters, including the dispersion energies, repulsive Mie exponents, association energies, and bonding volumes for each unlike pair of groups: HSO_4^-–H_3O^+, SO_4^{-2}–H_3O^+, HSO_4^-–H_2O, and SO_4^{-2}–H_2O. This leads to a complex parameter space, which would have to be navigated using limited experimental data. Instead, a step-wise procedure is adopted by which the influence of each of these unlike group interaction parameters on the behaviour of the solution mixture is examined, so that a complete understanding of the parameter interdependence is understood. This procedure is discussed below, following the presentation of the ionic models.

The intermolecular potential models of the HSO_4^- and SO_4^{-2} ions are developed by determining the structural and energetic parameters using information for well-studied properties of the ions. The ionic diameters σ_{kk} assigned to these ions must reflect the size and charge density of the species relative each other. The more negative charge and hence stronger repulsions in the SO_4^{-2} ion lead to a larger diameter compared to HSO_4^-, in which the gain of a proton leads to more tightly held electrons. The sizes of these ions, specifically

the thermochemical radius of the ions which corresponds to the radius of the ions in a crystal lattice, are reported in the literature. The thermochemical ionic sizes given by Krestov [405] are selected for both ions in this work; using a single internally consistent source for these parameters also satisfies the requirement of relative size mentioned above.

The Born diameter for the SO_4^{-2} model is obtained from the extensive study of Babu and Lim [406], in which the Born cavity size of ions was identified using molecular dynamics simulations. The bisulphate ion was not considered in their study, therefore the Born cavity diameter of HSO_4^- is determined by implementing the method proposed by Rashin and Honig [197], namely that a reasonable measure of the cavity size of anions can be obtained by applying a 7% increase to the ionic diameters of the ions. The diameter that Babu and Lim [406] recommend for the sulphate ion is 12% larger than the crystal ionic diameter assigned to this ion in this work. This is comparable to the 7% increase recommended by Rashin and Honig, hence the two sources are considered compatible.

The dispersion energy corresponding to the attractive interaction between any two ions is established by applying the ion–ion combining rule given by Equation 3.96. The polarisabilities of HSO_4^- and SO_4^{-2} are obtained from Pyper et al. [203] and Hou et al. [407], respectively, and the ionisation potentials of both ions are obtained from Wang et al. [408]; these values are collected in Table 6.4. The ion–ion combining rule also requires the exponents characterising the form of the Mie potential. Following the strategy described in Chapter 4, the Lennard-Jones potential is assigned to both HSO_4^- and SO_4^{-2} models, i.e. $\lambda_{a,k} = 6$, $\lambda_{r,k} = 12$. The HSO_4^-–H_3O^+ and SO_4^{-2}–H_3O^+ ε_{kl} parameters are characterised by the implementing the ion–ion combining rule (Equation 3.96), with the information for the H_3O^+ species given in Tables 6.4 and 6.2. Optimising the HSO_4^-–H_3O^+ pair interaction results in a relatively weak dispersion energy, so the comparably weak value obtained through the combining rule is taken as a reasonable estimate of the parameter. On the other hand, optimising the SO_4^{-2}–H_3O^+ pair interaction results in a very strong dispersion energy, thereby indicating potential ion pairing or hydrogen bonding. This finding for the interaction between the SO_4^{-2}–H_3O^+ pair aligns with the association schemes discussed previously in Section 6.1.1.1, specifically

the existence of the sulphate–hydronium ion pair [$H_3O^+ \cdot SO_4^{-2}$] proposed in multiple studies [396, 398, 399]. The weak dispersion energy obtained for the HSO_4^-–H_3O^+ pair further suggests that the proposed equilibria given by Equations 6.6 and 6.7 would be shifted heavily towards the sulphate–hydronium ion pair such that any bisulphate–hydronium association would be negligible, thus also diminishing the likelihood of the proposed equilibrium given by Equation 6.8. Given these considerations, the combining rule estimate for $\varepsilon_{SO_4^{-2}-H_3O^+}$ is maintained and association between the sulphate and hydronium ions is investigated instead.

Additional association interactions considered in the optimisation procedure for the aqueous sulphuric acid system include association between bisulphate and hydronium ions as well as association between water and the two ions. The HSO_4^- model was initially assigned four ‘e’-type sites and one ‘H’-type site following the work of Yacovitch et al. [401], and congruently the sulphate ion was assigned four ‘e’-type sites following the work of Wang et al. [402]. The dispersion energy ε_{H_2O-ion} between water and each of the ions is optimised alongside the association interactions. Both the dispersion and association energy parameters for each ion–water pair are found to tend towards very weak energies, suggesting that the ions are weakly hydrated. This finding is in accordance with the work of Simonin et al. [409], who proposed that the bisulphate ion is "unhydrated" in solution (i.e. lacking a coordinated solvation shell of water molecules), based on modelling solutions of associating acids with a MSA-NRTL model including ionic hydration and association. Association interactions between water and the ions are therefore omitted from the model. It would be physically unreasonable, however, to neglect the ion-water dispersion energies, therefore these are assigned to the moderate strength obtained from the geometric combining rule for unlike attractive energies calculated from Equation 3.32.

On optimising, it is found that association between the HSO_4^-–H_3O^+ pair is negligible, whereas the association between the SO_4^{-2}–H_3O^+ pair is found to exert an overwhelming influence over the thermodynamic behaviour of the solution mixture, specifically on the degree of dissociation of the bisulphate ion. This interaction appears to act as a driving force for the equilibrium governing the reaction shown in Equation 6.4, so it is unsurprising

that the magnitude of the energetic parameters for this pair's interaction is large irrespective of whether they are treated as dispersion or as association. In order to comply with the experimental evidence for the existence of the $[H_3O^+ \cdot SO_4^{-2}]$ ion pair entity, association is favoured over dispersion for representing the strong attraction between these species.

Ultimately, an optimal model for sulphuric acid is presented in which only two cross-interaction parameters are actually optimised by regression to experimental data, namely $\varepsilon^{HB}_{ab,kl}$ and $K^{HB}_{ab,kl}$ between 'H'-type sites on H_3O^+ and 'e'-type sites on SO_4^{-2}. The remaining parameters are found to be adequately assigned by making use of available data from the literature and implementing appropriate combining rules. The quality of the optimised SAFT-γ Mie model for aqueous sulphuric acid is quantified by the %AAD for each property with respect to the experimental data for that property using Equation 4.18; these are shown in Table 6.1.

Table 6.1 Experimental solution data and their sources included in the optimisation procedure for the SAFT-γ Mie models for the HSO_4^- and SO_4^{-2} ions. The ranges of temperature (T), maximum molality (m_{max}), and the number of data points per property (n_p) are summarised. Data include the degree of bisulphate dissociation $\alpha_{HSO_4^-}$, the liquid-phase density of the solution ρ at 1 atm, and the activity of water a_{H_2O}. The percentage average absolute deviation %AAD for each property is calculated with the SAFT-γ Mie EOS for each property.

	$\alpha_{HSO_4^-}$			ρ			a_{H_2O}		
	T (K)	m_{max} (mol kg^{-1})	n_p	T (K)	m_{max} (mol kg^{-1})	n_p	T (K)	m_{max} (mol kg^{-1})	n_p
Dataset	298	4.8	22	283–298	1.02	16	298	3.0	41
Sources		[395, 396, 403]			[392, 410–412]			[413–415]	
%AAD		13.14			0.33			0.33	

6.1.3 Description of thermodynamic properties

Aqueous sulphuric acid is modelled using the parameters presented in Tables 6.2 and 6.3, which collect the parameters for HSO_4^- and SO_4^{-2} and for their cross interactions with H_2O

and H_3O^+. The performance of the models is examined against a range of thermodynamic properties, including some which were not considered during model optimisation, namely the saturated vapour pressure and stoichiometric mean ionic activity coefficient, in addition to the bisulphate's degree of dissociation, the solution density, and the activity of water, which are also evaluated beyond the range included in the optimisation dataset.

6.1.3.1 Degree of dissociation and solution composition

The degree of dissociation of the bisulphate ion encompasses information for both the thermodynamic behaviour and speciation of the sulphuric acid solution, both of which must be described accurately by a successful modelling approach. Figure 6.1 illustrates the degree of dissociation of the bisulphate ion obtained with SAFT-γ Mie coupled with the reaction equilibrium condition defined by the thermodynamic acid dissociation constant given by Equation 6.4. The corresponding solution composition implied by the calculated degree of dissociation is shown in Figure 6.2. The ionic equilibrium composition of the solution is calculated in very good agreement with the experimental data, which leads one to expect similar agreement for a wider spectrum of thermodynamic properties.

6.1.3.2 Mean ionic activity coefficient and water activity

Further evaluation of the SAFT-γ Mie model performance is made by assessing the prediction of the stoichiometric MIAC $\gamma_{\pm}^{\text{stoich.}}$ of sulphuric acid, which allows one to examine the model performance with respect to the ionic components. According to Equation 2.23, $\gamma_{\pm}^{\text{stoich.}}$ is obtained as:

$$\gamma_{\pm,m}^{\text{stoich.}}(T,p,\mathbf{N}) = \left(\gamma_{H_3O^+,m}(T,p,\mathbf{N})\right)^2 \gamma_{SO_4^{-2},m}(T,p,\mathbf{N}) \left(\frac{m_{H_3O^+}^2 m_{SO_4^{-2}}}{4m_{\text{acid}}^2}\right). \tag{6.14}$$

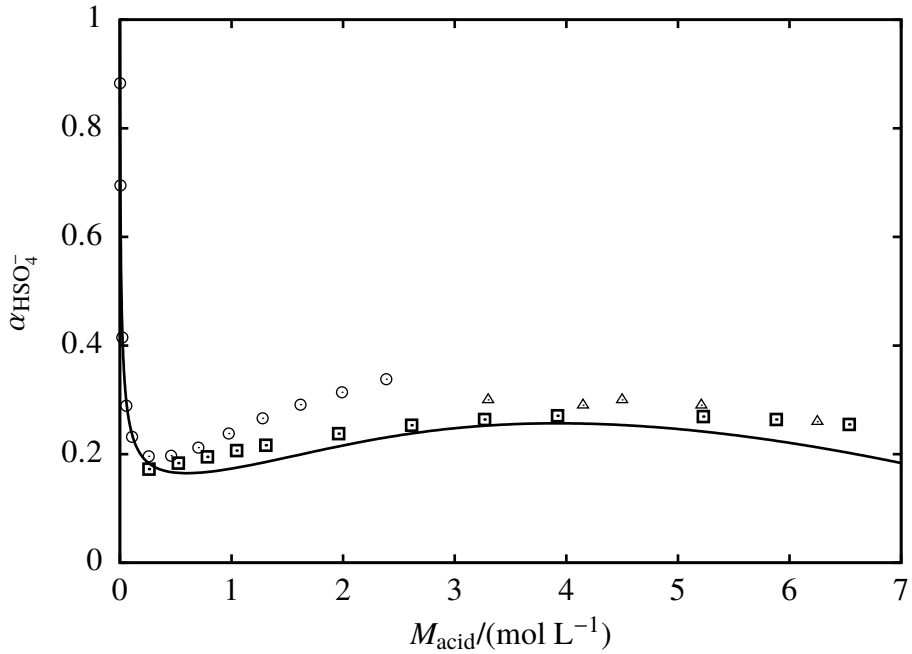

Figure 6.1 The degree of dissociation of the bisulphate ion ($\alpha_{HSO_4^-}$) in aqueous solution as a function of the sulphuric acid concentration at 298.15 K. HSO_4^- dissociates in water according to the reaction equilibrium shown in Equation 6.2, producing SO_4^{-2} and H_3O^+ ions. The continuous curve represents the SAFT-γ Mie prediction, and the symbols represent the experimental data (squares [396], circles [403], triangles [404]).

The SAFT-γ Mie predictions for the stoichiometric MIAC of sulphuric acid are shown in Figure 6.3 for temperatures in the range 298–448 K. Despite not considering this property in the model development, the SAFT-γ Mie predictions agree closely with the experimental data. The accurate prediction of this property at high temperatures not only demonstrates the predictive capability of the modelling approach, but also further validates the association scheme applied to the sulphuric acid solution. The model performance with respect to the solvent is examined by the description of the water activity a_{H_2O}. The calculation of this property with SAFT-γ Mie is shown at 298 K in Figure 6.4, which shows that the model gives a good description of the water activity even at high acid concentrations well beyond the limit considered in the parameter estimation procedure.

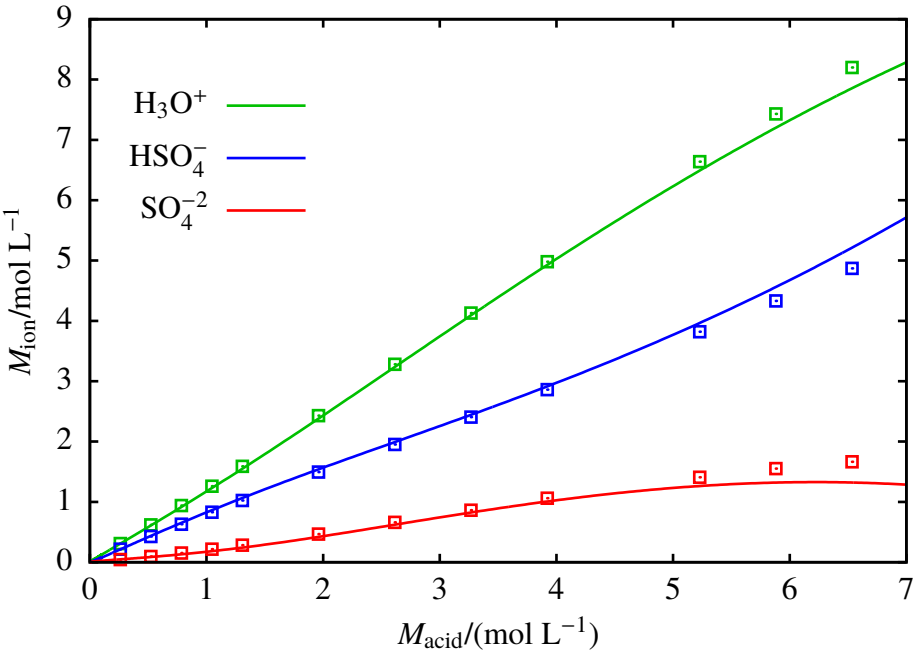

Figure 6.2 The composition of each type of ion in aqueous sulphuric acid solution as a function of the acid concentration at 298.15 K. Sulphuric acid dissociates in water according to the reaction equilibrium shown in Equations 6.1 and 6.2, producing HSO_4^-, SO_4^{-2}, and H_3O^+ ions. The continuous curves represent the SAFT-γ Mie predictions, and the symbols represent the experimental data [396].

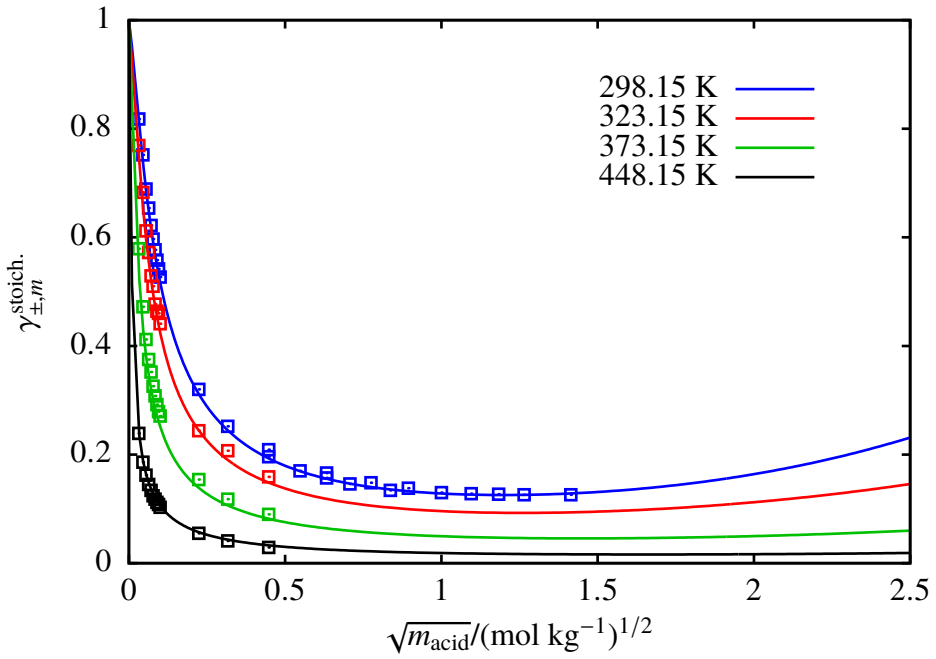

Figure 6.3 The concentration dependence of the stoichiometric MIAC $\gamma^{\text{stoich.}}_{\pm,m}$ for aqueous sulphuric acid solutions at temperatures between 298.15 and 448.15 K. The continuous curves represent the SAFT-γ Mie predictions, and the symbols represent the experimental data [416, 417].

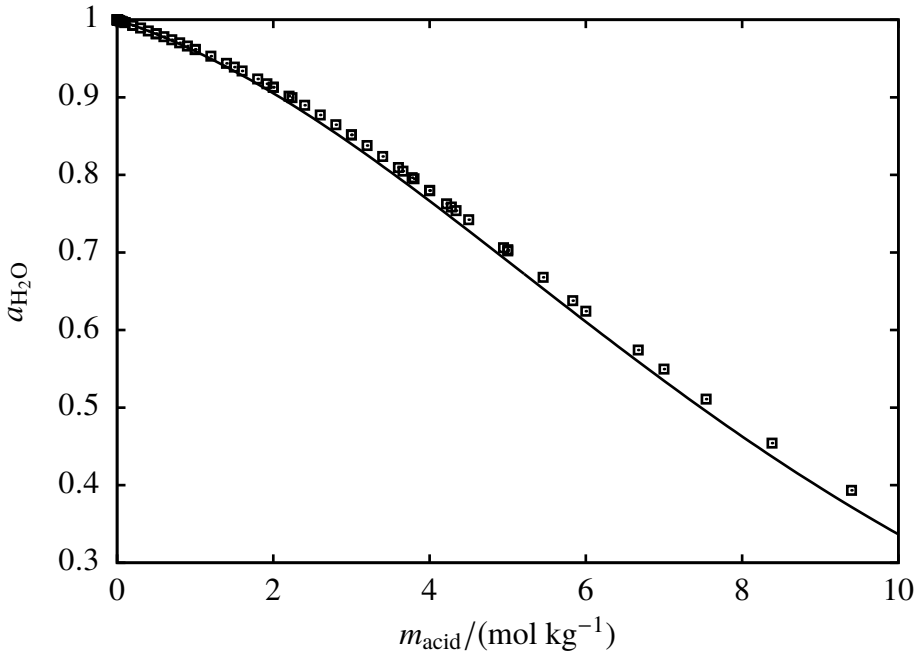

Figure 6.4 The concentration dependence of the activity of water a_{H_2O} in aqueous sulphuric acid solutions at 298.15 K. The continuous curve represents the SAFT-γ Mie predictions, and the symbols represent the experimental data [413–415].

6.1.3.3 Solution density and saturated vapour pressure

The liquid-phase density is a key property for quantifying the performance of the sulfuric acid model since most of the SAFT-γ Mie parameters exerting the greatest influence on the fluid density, namely the intermolecular attractive dispersion interactions, are all set by combining rules. Liquid-phase densities of aqueous sulphuric acid from 298–328 K at 1.01 bar are shown in Figure 6.5. Fair agreement is achieved between the SAFT-γ Mie prediction and the experimental data for the solution density beyond the concentration and temperature range considered in optimisation, indicating that suitable ionic diameters were assigned to the HSO_4^- and SO_4^{-2} ions, and that the choice to implement combining rules is appropriate for assigning the dispersion interactions in this system.

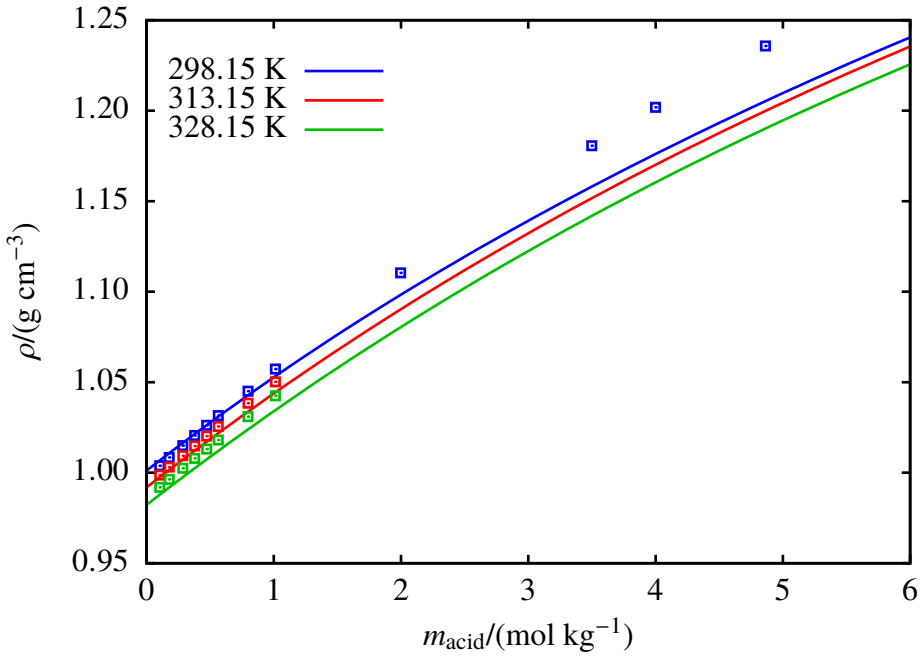

Figure 6.5 The concentration dependence of the liquid density of aqueous sulphuric acid solutions at 1.01 bar. The continuous curve represents the SAFT-γ Mie predictions, and the symbols represent the experimental data [392, 410].

The vapour pressure of the solution is also significantly impacted by the ion–solvent attractive dispersion interactions. The vapour pressure of aqueous sulphuric acid calculated

with SAFT-γ Mie for temperatures from 283–373 K are depicted in Figure 6.6. The vapour pressure is consistently well predicted, as compared to experimental data, across a wide temperature range. One can conclude, therefore, that setting the H_2O–HSO_4^- and H_2O–SO_4^{-2} dispersion interactions by combining rule gives a reasonable estimate of these parameters.

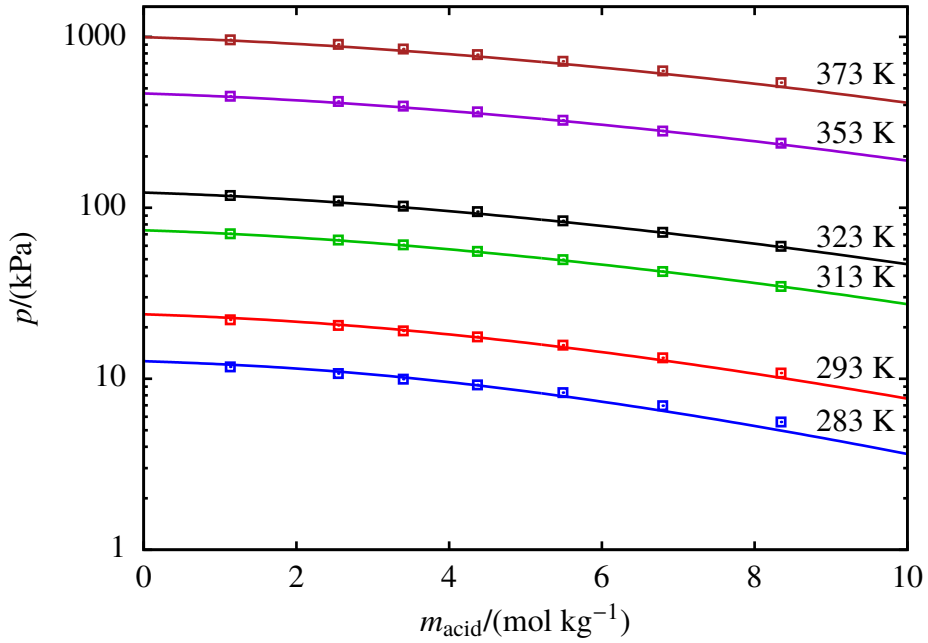

Figure 6.6 The concentration dependence of the saturated vapour pressure of aqueous sulphuric acid solutions at temperatures between 283 and 373 K. The continuous curves represent the SAFT-γ Mie predictions, and the symbols represent the experimental data [418, 419].

Table 6.2 SAFT-γ Mie model parameters for the species present in aqueous sulfuric acid and nitric acid solutions. The models for H_2O and H_3O^+ are taken from the work of Dufal et al. [177] and Chapter 4, respectively.

Species, k	ν_k^*	S_k	σ_{kk}/Å	$\sigma_{kk}^{\text{Born}}$/Å	$\lambda_{\text{r},kk}$	$\lambda_{\text{a},kk}$	$(\varepsilon_{kk}/k_\text{B})$/K	n_H	n_e	$(\varepsilon_{ab,kk}^{\text{HB}}/k_\text{B})$/K	$(\text{K}_{ab,kk}^{\text{HB}})$/Å^3
H_2O	1	1.0000	3.0063	–	17.020	6.0000	266.68	2	2	1985.4	101.69
H_3O^+	1	1.0000	3.0063	3.0063	17.020	6.0000	68.190	3	–	–	–
HSO_4^-	1	1.0000	4.1200	4.4084	12.000	6.0000	82.086	–	–	–	–
SO_4^{-2}	1	1.0000	4.6000	5.1600	12.000	6.0000	84.082	–	4	–	–
HNO_3	2	0.6726	3.6175	–	16.347	6.0000	495.33	1	3	1300.0	8.9978
NO_3^-	1	1.0000	3.5800	4.0000	12.000	6.0000	97.853	–	3	–	–

Table 6.3 SAFT-γ Mie cross-interaction parameters for species present in aqueous solutions of sulphuric acid and nitric acid. Structural cross-interaction parameters σ_{kl} and $\lambda_{y,kl}$ are omitted from this table as they are obtained by combining rules. The unlike ion dispersion energies are calculated using Equation 3.96. The procedures for arriving at the remaining parameters are detailed in the text.

Species		Site		$(\varepsilon^{\mathrm{HB}}_{ab,kl}/k_{\mathrm{B}})$/K	$\mathrm{K}^{\mathrm{HB}}_{ab,kl}$ /Å^3	$(\varepsilon_{kl}/k_{\mathrm{B}})$/K
k	l	k,a	l,b			
SO_4^{-2}	H_2O	–	–	–	–	114.65
SO_4^{-2}	H_3O^+	e	H	2236.0	43.700	52.983
HSO_4^-	SO_4^{-2}	–	–	–	–	83.246
HSO_4^-	H_2O	–	–	–	–	142.57
HSO_4^-	H_3O^+	–	–	–	–	53.932
NO_3^-	H_2O	e	H	1591.1	97.014	91.970
NO_3^-	H_3O^+	e	H	2494.1	6.1585	61.788
NO_3^-	HNO_3	–	–	–	–	220.15
HNO_3	H_2O	e	H	3611.6	1.4998	358.82
HNO_3	H_2O	H	e	1606.6	1.4998	358.82
HNO_3	H_3O^+	–	–	–	–	181.44

Table 6.4 Values for the polarisability and electron affinity of the ions developed in this work. Data for HSO_4^- and SO_4^{-2} are taken from Ref. [203, 407, 408], and data for NO_3^- ion are taken from Ref. [203, 420].

i	$\alpha_{0,i}$ / (10^{-24}cm^3)	I_i / eV
HSO_4^-	5.0890	4.7500
SO_4^{-2}	6.3270	5.1000
NO_3^-	4.4800	3.1450

6.2 Nitric acid

Nitric acid dissociates incompletely, yet appreciably, in aqueous solution, producing a solution mixture composed of solvated nitrate ions (NO_3^-) and hydronium ions (H_3O^+), as well as the molecular acid (HNO_3). It is generally regarded as a 'strong' acid due to its high degree of dissociation (α_{HNO_3}), with $\geq 95\%$ of the acid ionised at compositions ≤ 2 mol kg^{-1}. Within this range of solution compositions, nitric acid could be reasonably approximated as a strong electrolyte. However, in order to model nitric acid across as wide range of compositions it is useful to develop a general model that incorporates dissociation. Both approaches are pursued here as a means of demonstrating the relative benefit of explicit weak electrolyte modelling. A model for the molecular nitric acid species is also developed, as required for modelling the aqueous acid as a weak electrolyte.

6.2.1 Pure nitric acid model

Nitric acid is a challenging compound to work with in practice, with its unstable chemical behaviour making the pure acid difficult to maintain for experimental purposes. In the fluid phase, nitric acid undergoes spontaneous decomposition as well as self-ionic dissociation, meaning that a quantity of 'pure' acid would also contain nitrate, nitronium (NO_2^+), and hydronium ions, as well as water and nitrogen dioxide [421]. Nevertheless, experimental data for nitric acid are typically not accompanied by any such information regarding the degree to which HNO_3 decomposes or ionises, hence it is not possible to take this into account for the purpose model development. The assumption adopted here is that these reactions may be considered negligible such that experimental data may be taken to correspond to pure HNO_3.

6.2.1.1 Association scheme

A distinctive characteristic of the HNO_3 molecule is its strong affinity to hydrogen bonding. A spectroscopic study by Guillory and Bernstein [422] has suggested that nitric acid self-associates via intermolecular hydrogen bonding, forming doubly hydrogen bonded cyclic dimers – a structure that Odutola and Dyke [423] later confirmed. Nitric acid dimerisation is mediated in the SAFT-γ Mie model via association sites on the HNO_3 segment. In principle, the dimerisation can be achieved with one donor ('H'-type) site and one acceptor ('e'-type) site. However, since the HNO_3 group will also be used in aqueous mixtures, it is prudent to design the association scheme in such a way as to facilitate its association with water. McCurdy et al. [424] have concluded through spectroscopic observation and theoretical calculations that HNO_3 molecules form stable clusters with up to four water molecules, although they agree with previous work by Canagaratna et al. [425] that in any given cluster no more than two water molecules are directly bonded to the nitric acid molecule. Given the limited experimental evidence, the chosen association scheme includes one donor ('H'-type) site and three acceptor ('e'-type) sites on the HNO_3 segment, aiming to be able to simultaneously take into account the thermodynamic influence of both dimerisation and association with water.

6.2.1.2 Model development

The SAFT-γ Mie model for the HNO_3 molecule is developed by optimising the model parameters against the saturated vapour pressure and the saturated liquid density, making use of the whole temperature range for which data are available (see Table 6.5). Experimental data near the critical region are not available, possibly due to the aforementioned difficulties associated with nitric acid stability. Although predictions of the acid properties at the critical point have been reported by means of extrapolation from measurements at lower temperatures [426], these are excluded from the optimisation dataset.

The optimal model for nitric acid is presented in Table 6.2. All parameters are optimised, apart from the attractive Mie exponent which is set to $\lambda_a = 6.0$ and the number of association sites assigned as $n_H = 1$ and $n_e = 3$. The optimised parameters v^* and S_k prescribe a non-spherical geometry, a finding which is in accordance with the planar structure of the HNO_3 molecule [421]. Taking into account also the optimised segment diameter σ, the overall size of the HNO_3 group is $\sim 26\%$ larger than the size experimentally determined for the NO_3^- ion (see Section 6.2.2.3), as would be appropriate. In terms of the energetic parameters, the strong self-association energy at close range parallels the expected dimerisation behaviour.

The performance of the model is illustrated in Figures 6.7 and 6.8 in terms of the saturated vapour pressure and saturated density of pure nitric acid, respectively. The SAFT-γ Mie model predictions are in good agreement with the available experimental data. The model predictions for the critical point properties of the acid do not agree with the extrapolated values quoted in the literature; however, due to the scarcity of experimental data near the critical region, it is difficult to verify the acid's critical properties. The model nevertheless reproduces the acid's thermodynamic properties within the range of temperature and pressure conditions relevant to aqueous electrolyte solutions.

Table 6.5 Experimental data (and their sources) for pure nitric acid used in the optimisation procedure for the HNO_3 model. The ranges of temperature (T) and the number of data points per property (n_p) are summarised. The optimisation dataset includes phase equilibrium data for the vapour pressure (p) and saturated liquid density (ρ) of nitric acid.

		ρ				p	
T (K)	n_p	%AAD	Ref.	T (K)	n_p	%AAD	Ref.
253–323	33	0.38	[427–429]	273–355	27	1.74	[430–433]

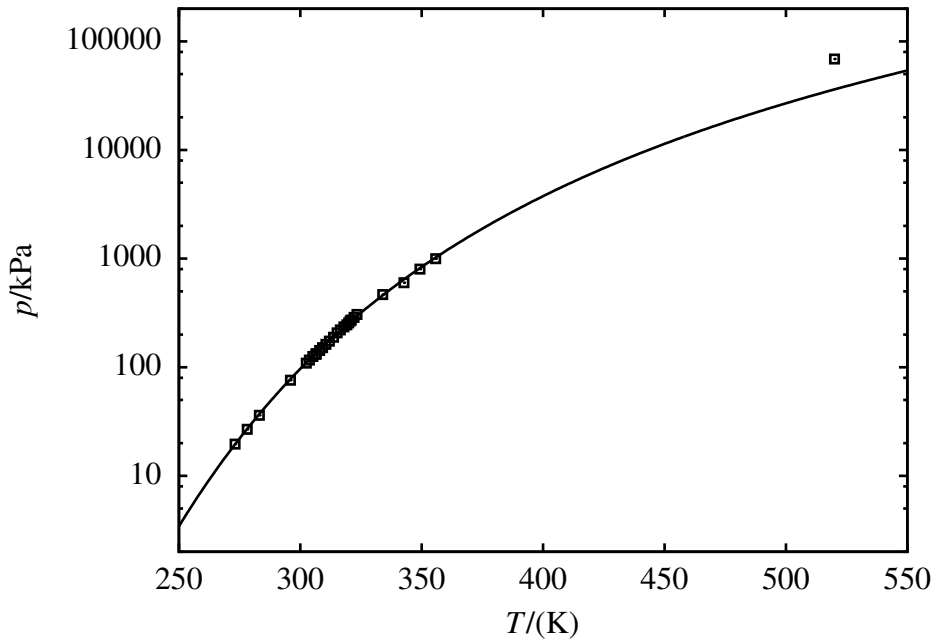

Figure 6.7 Saturated vapour pressure of pure nitric acid at temperatures between 250 and 550 K. The continuous curve represents the SAFT-γ Mie predictions, and the symbols represent the experimental data [426, 430–433]. Note that the critical point datum obtained from Ref. [426] is reported as an estimated value.

6.2.2 Aqueous nitric acid

Aqueous nitric acid is modelled here both as a strong electrolyte and as a weak electrolyte. In the weak acid implementation, the polarity of the HNO_3 molecule should contribute to the dielectric constant of the solvent medium assumed by the SAFT-γ Mie EOS. Considering the high degree of dissociation of nitric acid, however, the contribution of molecular nitric acid to the relative permittivity of the solvent medium is neglected as a means of simplifying the model.

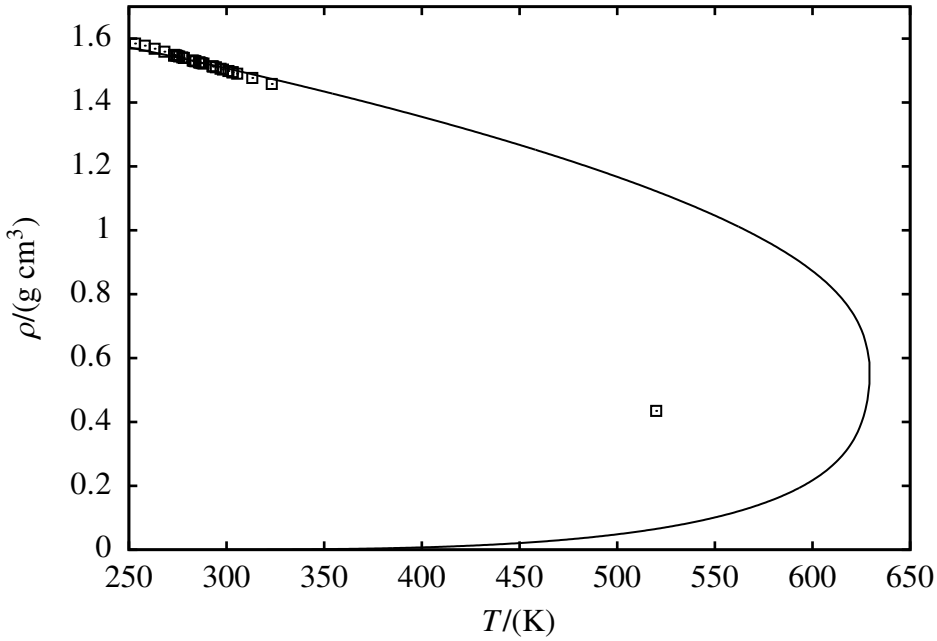

Figure 6.8 Saturated density of pure nitric acid at vapour-liquid phase coexistence. The continuous curve represents the SAFT-γ Mie predictions, and the symbols represent the experimental data [426–429]. Note that the critical point datum obtained from Ref. [426] is reported as an estimated value.

6.2.2.1 Dissociation equilibrium

In aqueous solution, nitric acid partially dissociates according to the following proton-transfer reaction with water [436]:

$$\mathrm{HNO_3 + H_2O} \overset{K_\mathrm{a}}{\rightleftharpoons} \mathrm{H_3O^+ + NO_3^-} \,. \tag{6.15}$$

The acid dissociation constant K_a characterising the thermodynamic equilibrium of this reaction is defined on a molality scale as:

$$K_\mathrm{a}(T) = \frac{a_{\mathrm{H_3O^+,m}}(T,p,m)\, a_{\mathrm{NO_3^-,m}}(T,p,m)}{a_{\mathrm{HNO_3,m}}(T,p,m)} \,. \tag{6.16}$$

Studies have determined the thermodynamic acid dissociation constant for nitric acid in water at specified temperatures, employing a range of experimental techniques. In an

Table 6.6 Experimental solution data used in the optimisation procedure for aqueous nitric acid models. An initial dataset is compiled for developing the model for the NO_3^- ion assuming nitric acid is a strong electrolyte completely dissociated in solution. A second dataset is used to optimise the cross interactions for the HNO_3 molecule in a solution mixture where the acid is treated as a partially dissociated weak electrolyte. The ranges of temperature (T), maximum molality ($m_{\max}$), and the number of data points per property (n_p) are summarised. The optimisation datasets include data for the osmotic coefficient ϕ, and the saturated vapour pressure p of the solution.

Dataset	ϕ					p				
	T (K)	$m_{\max}$ (mol kg^{-1})	n_p	%AAD	Ref.	T (K)	$m_{\max}$ (mol kg^{-1})	n_p	%AAD	Ref.
Strong acid	298	1.00	16	1.36	[219]	323	3.00	14	0.68	[434, 435]
Weak acid	298	6.00	29	1.32	[219]	-	-	-	-	-

early study, Hood and Reilly [437] determined the acid dissociation constant for aqueous nitric acid at three temperatures between 273–343 K by using proton magnetic resonance to obtain the dissociation quotient of the reaction and then combining this with activity coefficient measurements from previous studies to calculate K_a. Using flow calorimetry, Oscarson et al. [438] obtained K_a for three temperatures between 523–592 K, and later Chlistunoff et al. [439] measured the K_a at 653 K and 673 K using UV-vis spectroscopy. Taking an indirect approach, Marshall and Slusher [440] determined the thermodynamic dissociation constant of nitric acid by measuring the solubilty of calcium sulphate in aqueous nitric acid solutions. The measured solubility product for the salt and the known second acid dissociation constant of sulphuric acid were used to deduce the K_a of nitric acid by extrapolation. Marshall and Slusher [441] used the same approach to obtain the K_a of nitric acid from solubility measurements of magnesium sulphate in aqueous nitric acid, with comparable results. In each study, these authors proposed a correlation for calculating K_a as a function of temperature; the two correlations predict the nitric acid dissociation constant similarly. In the former publication [440], the authors included also data from other studies in the regression, obtaining a correlation which is applicable for temperatures between 273–623 K:

$$\log_{10} K_a = 5.424 - \frac{134.37}{T} - 0.01199T \, . \tag{6.17}$$

The above equation is chosen as the best means for calculating the nitric acid dissociation constant in the present work.

6.2.2.2 Association scheme

Nitrate ions have been shown to possess a strongly bound primary solvation shell, as interpreted by Irish and Davis [442] from Raman and infrared spectra. Payne [443] studied the adsorption of nitrate ions on mercury electrodes and proposed that hydrated nitrate ions engage in hydrogen bonding with water molecules in the primary solvation shell, each ion binding with three water molecules. This interpretation has been supported by *ab initio* theoretical calculations performed by Howell et al. [444], who showed that NO_3^- forms stable clusters with three water molecules, each of which doubly hydrogen bonds to the oxygen atoms on the NO_3^- ion. A study by Wang et al. [445] demonstrated using photoelectron spectroscopy that the first solvation shell of the nitrate ion consists of three water molecules, and also confirmed Howell's aforementioned hydrogen bonding scheme between NO_3^- and H_2O via density functional theory (DFT) calculations (see Figure 6.9). Subsequent DFT studies [446–448] concerning the nitrate–water solvation shell have suggested that the nitrate ion may directly hydrogen bond with up to six water molecules; however, these proposals are not accompanied by clear support from experiment.

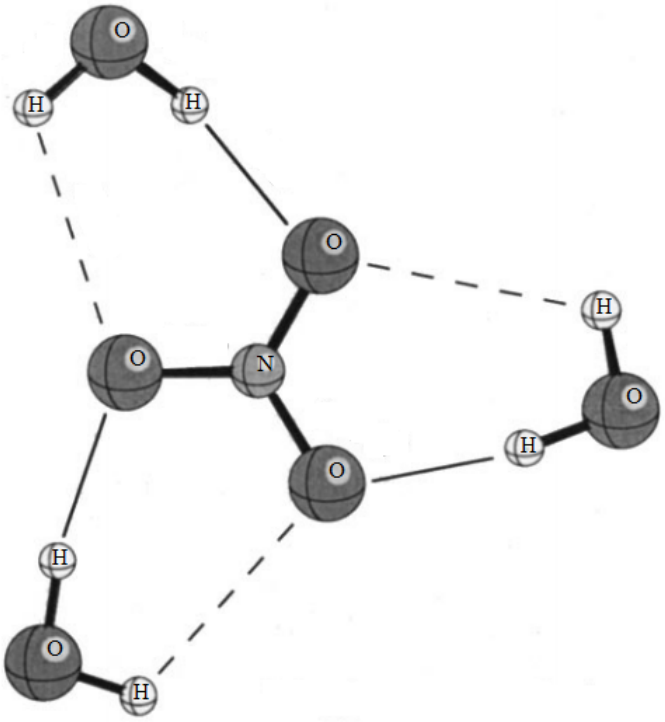

Figure 6.9 The hydrogen bonding scheme between the nitrate ion and three water molecules comprising the primary solvation shell, as proposed by Wang et al. [445]: each H_2O molecule doubly hydrogen bonds to NO_3^- through one strong hydrogen bond (represented by solid thin lines) and one weak hydrogen bond (represented by dashed thin lines). The image has been adapted from Ref. [445].

Spectroscopic and theoretical studies of hydrogen bonding between molecular nitric acid and water have suggested that HNO_3 associates with up to four H_2O molecules, with the acid ionising upon associating with the fourth water molecule. McCurdy et al. [424] identified $HNO_3(H_2O)_n$ clusters with n =1–3 using FTIR spectroscopy. Using first principles electronic structure calculations, the authors obtained the structures for clusters with n =1–4 and showed that for n =4 two stable hydrogen bonded clusters are feasible: $HNO_3(H_2O)_4$ as a global minimum and the solvated ion pair $NO_3^-(H_2O)_3H_3O^+$ as a local minimum. Shortly afterwards, Scott and Wright [449] studied the same $HNO_3(H_2O)_n$ clusters using *ab initio* and DFT molecular orbital calculations. Although this work proposed a different geometry for the nitrate–hydronium ion pair, the existence of both $HNO_3(H_2O)_4$ and $NO_3^-(H_2O)_3H_3O^+$

species was supported. The following reaction equilibrium is possible:

$$HNO_3(H_2O)_4 \rightleftharpoons NO_3^-(H_2O)_3H_3O^+ \,. \tag{6.18}$$

However, the $NO_3^-(H_2O)_3H_3O^+$ has not been experimentally observed and, since it is calculated to be less stable than the $HNO_3(H_2O)_4$ cluster, it is likely to be an intermediate product of the acid's dissociation. Indeed, Marinković et al. [450] have demonstrated that nitrate ions form contact ion pairs with hydronium ions, in a study using in-situ IR reflection spectroscopy to examine the electrolyte double layer on gold electrodes in nitric acid solutions. Whether the contact ion pairs observed in the double layer would also form in bulk solution remained undetermined.

The above studies are taken into consideration to inform the association interactions that must be accounted for in the SAFT-γ Mie model for aqueous nitric acid solutions. The NO_3^-–H_2O and HNO_3–H_2O hydrogen bonding interactions are straightforwardly assigned following the experimental evidence, while the formation of nitrate–hydronium ion pairs is investigated by allowing association between the two ions. Three 'e'-type sites are assigned to the NO_3^- group, allowing hydrogen bonding with 'H'-type sites of H_2O groups as shown in Figure 6.10. The 'e'-type sites the NO_3^- are also allowed to associate with the 'H'-type sites of H_3O^+ groups, i.e. the H_2O and H_3O^+ groups will compete for association with the NO_3^- group.

6.2.2.3 Model development

The SAFT-γ Mie groups required for modelling nitric acid solutions depend on the whether acid is considered to be strongly or weakly dissociated. The case of complete dissociation is considered first, eliminating the HNO_3 species such that only the NO_3^- parameters and its cross interactions with water and hydronium ions are necessary. For this assumption to be reasonable, the optimisation dataset (see Table 6.6) includes experimental osmotic coefficient

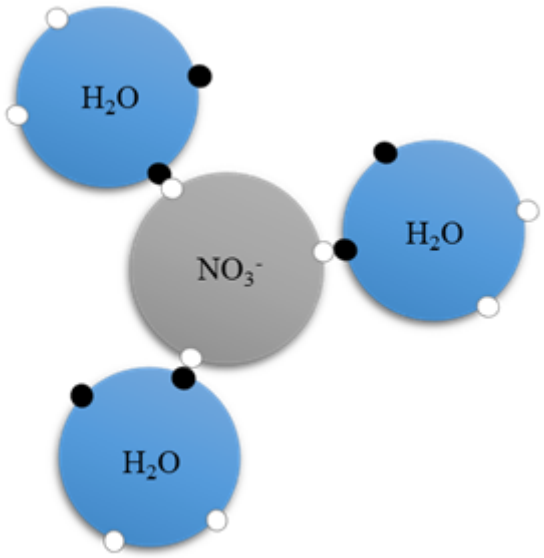

Figure 6.10 SAFT-γ Mie model interpretation of the hydrogen bonding scheme between NO_3^- and H_2O shown in Figure 6.9. The 'e'-type sites (shown as white circles) on NO_3^- interact with the 'H'-type sites (shown as black circles) on H_2O. Only three 'e'-type sites are assigned to the model for the nitrate ion, so that is possible to associate with a maximum of three water molecules.

data only up to 1 mol kg^{-1}, at which composition the acid is $\geq$ 97% dissociated [385, 437]. Vapour pressure and density measurements are scarce at such low concentrations, so data for these are included up to 3 mol kg^{-1}, at which the acid is still $\geq$ 90% dissociated.

The optimal set of model parameters for the NO_3^- ion and its cross interactions are shown in Tables 6.2 and 6.3. The diameter $\sigma_{NO_3^-}$ of NO_3^- is assigned according to the value corresponding to the ion's diameter in a crystal lattice, as reported by Marcus [451]. The corresponding Born diameter $\sigma_{NO_3^-}^{Born}$ is obtained from the molecular dynamics simulation study of Babu and Lim [406], in which the Born cavity diameter of NO_3^- was calculated to be 10.5% larger than the ionic diameter chosen here. This relative magnitude of the two sizes for the NO_3^- ion is aligned with the 7% increase recommended by Rashin and Honig [197], hence the value proposed by Babu and Lim is considered to be reasonable. A Lennard-Jones intermolecular potential ($\lambda_{a,NO_3^-} = 6$, $\lambda_{r,NO_3^-} = 12$) is found to be suitable for the NO_3^- group, and the group dispersion energy $\varepsilon_{NO_3^-}$ is obtained by applying the combining rule given by

Equation 3.96. The polarisability [203] and ionisation potential (negative electron affinity) [420] of NO_3^- are shown in Table 6.4.

The attractive dispersion energy ε_{kl} between the nitrate and hydronium ions is also calculated with Equation 3.96, using the parameters for H_3O^+ given in Chapter 4. Optimisation to experimental data is employed for ascertaining the nitrate–water dispersion energy as well as the association strength for the NO_3^-–H_2O and NO_3^-–H_3O^+ interactions, all of which are shown in Table 6.3. Comparing the relative strength of the association interaction optimised between the NO_3^- group and either H_2O or H_3O^+, one can discern a difference between the two physically different types of interactions. The strong association energy and small bonding volume between NO_3^- and H_3O^+ characterises a short-range attraction; this can be interpreted either as supporting the formation of contact ion pairs or, alternatively, the occurrence of the reaction shown in Equation 6.18, thereby driving the dissociation of nitric acid in solution. The association between NO_3^- and H_2O, on the other hand, is characterised by a weaker energy and larger bonding volume, of the order which is more characteristic of hydrogen bonding, hence substantiating the proposed hydration of the nitrate ion.

In principle, the parameters optimised for the nitrate ion assuming complete dissociation at low concentrations should be reasonably applicable in a model treating the acid as weakly dissociated. As a means of verifying this, the properties of weak nitric acid were computed using the nitrate ion parameters from the strong acid optimisation and applying combining rules to estimate the cross interaction parameters applicable to the HNO_3 group. With this approximated parameter set, a good prediction was achieved for the degree of dissociation of nitric acid, which is defined as:

$$\alpha_{HNO_3} = \frac{m_{NO_3^-}}{m_{HNO_3} + m_{NO_3^-}} = \frac{m_{NO_3^-}}{m_{acid}} \,. \tag{6.19}$$

Here $m_{acid} = m_{HNO_3} + m_{NO_3^-}$ corresponds to the molality of the solution. Having established that the correct speciation behaviour is predicted, the transferability of the NO_3^- model is further assessed by predicting the stoichiometric osmotic coefficient and stoichiometric

mean ionic activity coefficient of nitric acid assuming it is weakly ionised. Due to the 1:1 stoichiometry of HNO_3, the stoichiometric definitions of these properties for the weak acid are the same as the those corresponding to the strong acid:

$$\gamma_{\pm,m}^{\text{stoich.}} = \gamma_{\pm,m} = \left(\gamma_{NO_3^-,m}\gamma_{H_3O^+,m}\right)^{1/2}, \tag{6.20}$$

$$\phi^{\text{stoich.}} = \phi = -\frac{\ln a_{H_2O}}{2m_{\text{acid}}MW_{H_2O}}. \tag{6.21}$$

These two properties are also predicted reasonably well by the approximated parameter set at concentrations up to 6 mol kg^{-1}, indeed with improvement of the osmotic coefficient prediction compared to the strong acid case. However, the prediction of this property deteriorates at higher concentrations where the degree of dissociation of the acid falls below 80%. Given these observations, the nitrate ion model parameters are retained for the weak acid model, and only the cross interaction parameters of the HNO_3 group are taken forward for optimisation. The dataset used for this purpose includes only the osmotic coefficient of aqueous nitric acid, but considers data for higher acid concentrations where the HNO_3 species is more abundant (see Table 6.6).

The optimal cross-interaction parameters for the HNO_3 group are shown in Table 6.3. The association between nitric acid and water is mediated via the four association sites (one 'H'-type and three 'e'-type sites) already incorporated in the HNO_3 group, thus replicating the decrease of nitric acid dimer formation in solution due to the competition for association sites introduced by hydrogen bonding with water. The HNO_3–H_2O association is treated as asymmetric to reflect the proposition that a water molecule associating with the hydrogen site on the nitric acid molecule can lead to ionisation of the acid. Since the cross-interaction parameters calculated by combining rule are found to already provide a good description of the thermodynamic properties, only the asymmetric association interactions are included in the optimisation procedure. By assessing the sensitivity of the model predictions to

the magnitude of the remaining association parameters, it is found that the thermodynamic behaviour of the solution mixture is dominated by the $\varepsilon_{\mathrm{eH,\,HNO_3-H_3O^+}}$ parameter characterising the strength of association between the 'e'-type sites on HNO_3 and the 'H'-type sites on H_2O. The optimisation problem is therefore further simplified to include only this parameter, while all other cross interactions for the HNO_3 group are estimated by combining rules. The optimal model supports the reaction mechanism given by Equation 6.15, with H_2O found to bind strongly to the 'e'-type sites on the HNO_3 group and weakly to the 'H'-type site.

6.2.3 Thermodynamic properties of nitric acid solutions: comparison of the strong and weak acid models

Aqueous nitric acid is taken as an opportunity to assess the benefit in terms of predictive capability of modelling weak electrolytes explicitly by directly including reaction equilibria considerations in the modelling approach. The thermodynamic properties of the aqueous acid treated as both fully and partially ionised are evaluated by comparison to an experimental dataset including data for concentrations beyond the range considered during model development.

6.2.3.1 Degree of dissociation

A first step to comparing the relative performance of the strong and weak electrolyte approaches of modelling aqueous nitric acid is to verify that the degree of $\alpha_{\mathrm{HNO_3}}$ is predicted correctly. This is especially important since no information for $\alpha_{\mathrm{HNO_3}}$ is taken into account during the model development process. The prediction of $\alpha_{\mathrm{HNO_3}}$, which uses the NO_3^- model developed assuming complete dissociation and a single adjustable cross-interaction parameter for the weak electrolyte mixture, is shown in Figure 6.11. A good level of agreement with the experimental measurements is achieved, hence validating the efficacy of the weak electrolyte

approach in reproducing the mixture composition. Consequently, a fair comparison of the weak and strong acid approaches can be made.

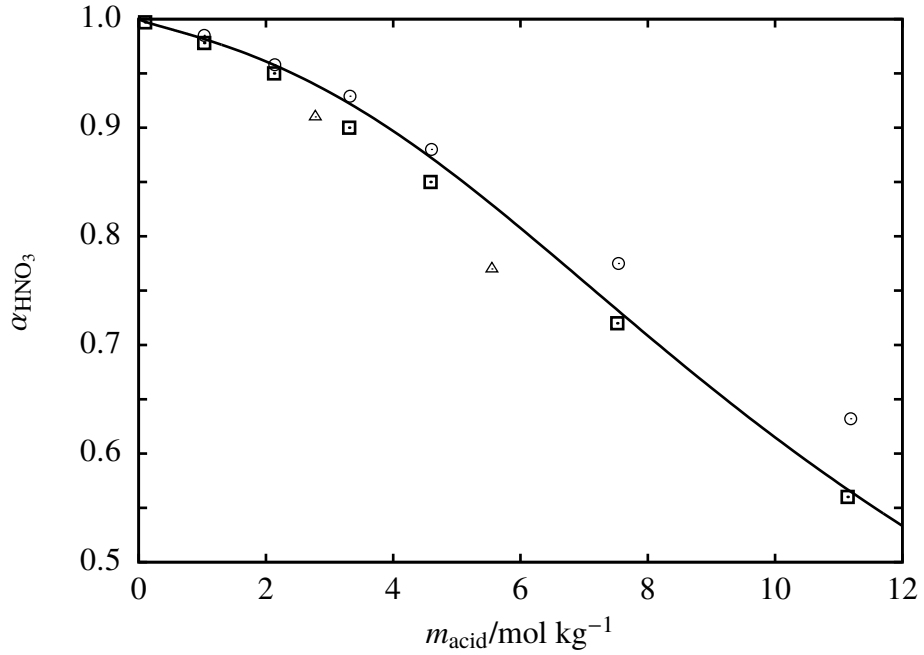

Figure 6.11 The degree of dissociation of nitric acid α_{HNO_3} in aqueous solution as a function of the acid concentration at 298.15 K and 1.01 bar. The degree of dissociation is defined by Equation 6.19. The continuous curve represents the SAFT-γ Mie prediction, and the symbols represent the experimental data (squares [385], circles [437], triangles [452]).

6.2.3.2 Osmotic coefficient and mean ionic activity coefficient

The osmotic coefficient for aqueous nitric acid as predicted by the two modelling approaches is shown in Figure 6.12. At low concentrations where the acid is extensively ionised the two approaches are comparable, although this is also in part due to the fact that the model parameters are optimised using information for this property at these concentrations. The predictive description of the osmotic coefficient at higher concentrations is more interesting: the weak electrolyte modelling approach offers a distinct improvement in the predictions attained, with the calculations closely following the trend of the experimental data even for

a very concentrated solution. The mean ionic activity coefficient of aqueous nitric acid is predicted similarly by the two approaches, as shown in Figure 6.13. This can be explained by the fact that the difference in the thermodynamic behaviour between the two modelling approaches is driven by the association interaction between HNO_3 and H_2O, which has a more direct effect on the chemical potential of the solvent rather than the electrolyte, and therefore will impact the osmotic coefficient to a greater extent than the MIAC.

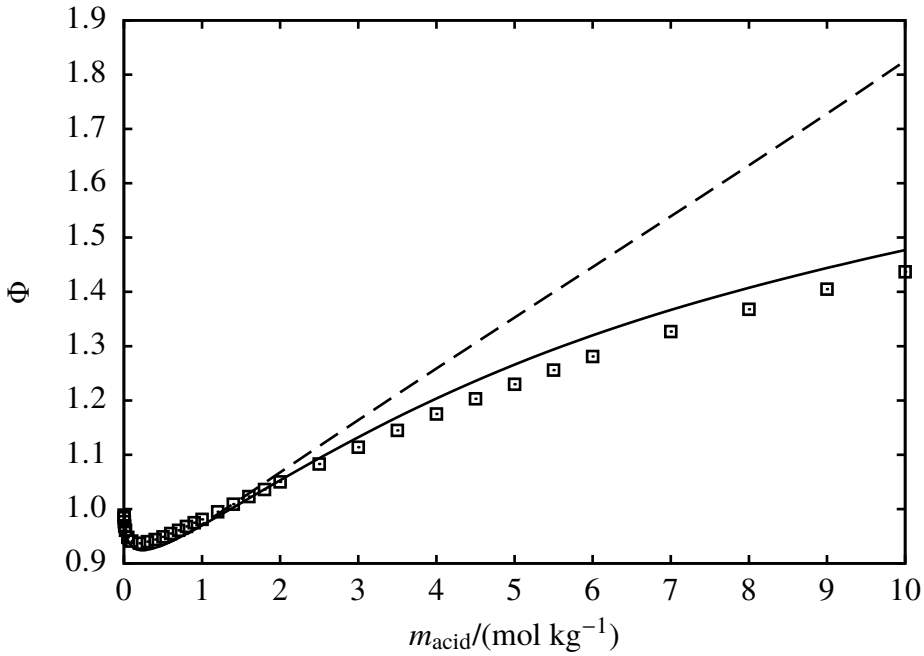

Figure 6.12 The concentration dependence of the osmotic coefficient Φ of aqueous nitric acid solutions at 298 K and 1.01 bar. The continuous curve represents the SAFT-γ Mie prediction for weak nitric acid, while the dashed curve represents the prediction for strong nitric acid. The symbols represent the experimental data [219].

6.2.3.3 Vapour pressure and liquid density

The description of the saturated vapour pressure of aqueous nitric acid is illustrated in Figure 6.14, from which the improved predictive capability gained by adopting a weak acid model is evident at higher concentrations. Including the HNO_3 species in the solution by ex-

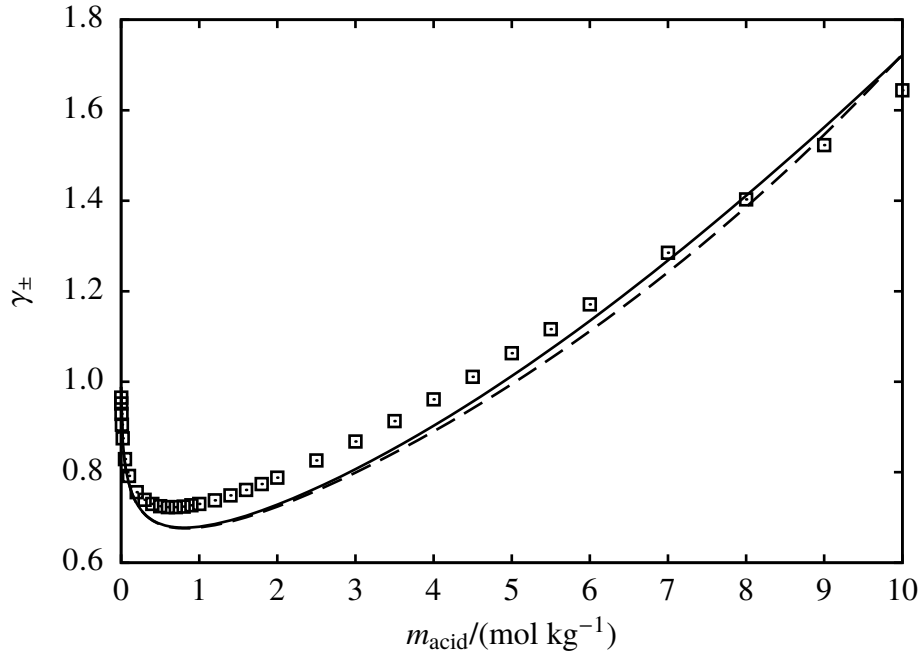

Figure 6.13 The concentration dependence of the mean ionic activity coefficient $\gamma_\pm$ of aqueous nitric acid solutions at 298 K and 1.01 bar. The continuous curve represents the SAFT-γ Mie prediction for weak nitric acid, while the dashed curve represents the prediction for strong nitric acid. The symbols represent the experimental data [219].

plicitly modelling the acid's partial ionisation allows all association interactions experienced by the solvent to be accounted for. The hydrogen bonding interactions between HNO_3 and H_2O partially inhibit the association between water molecules, thus disturbing the hydrogen bonded network of water in the liquid phase and making the solution more volatile. This leads to a corresponding increase in the predicted vapour pressure, as compared to what is obtained when assuming fully ionised nitric acid. In Figure 6.15, the liquid phase density of the solution predicted with the SAFT-γ Mie strong and weak acid approaches is shown up to high concentrations. The dependence of the solution density (which was not considered during model optimisation) with acid concentration is much better predicted when modelling the acid as partially ionised. This can again be explained with reference to the additional type of association interactions in the solution mixture which disrupt the network of inter-water hydrogen bonds thereby leading to a fluid phase with lower density.

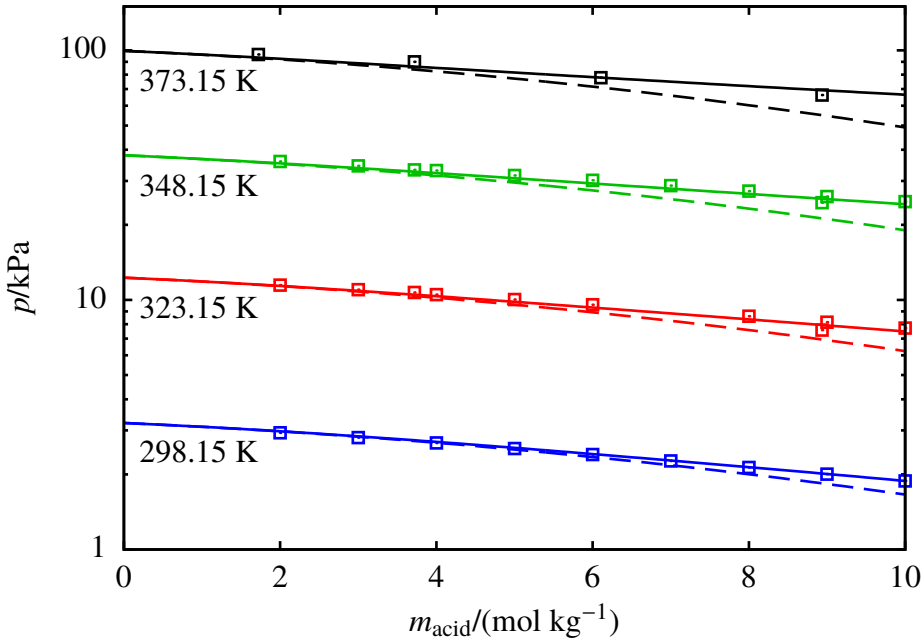

Figure 6.14 The concentration dependence of the saturated vapour pressure of aqueous nitric acid solutions at temperatures between 298 and 373 K. The continuous curves represents the SAFT-γ Mie predictions for weak nitric acid, while the dashed curves represent the predictions for strong nitric acid. The symbols represent the experimental data [434, 453].

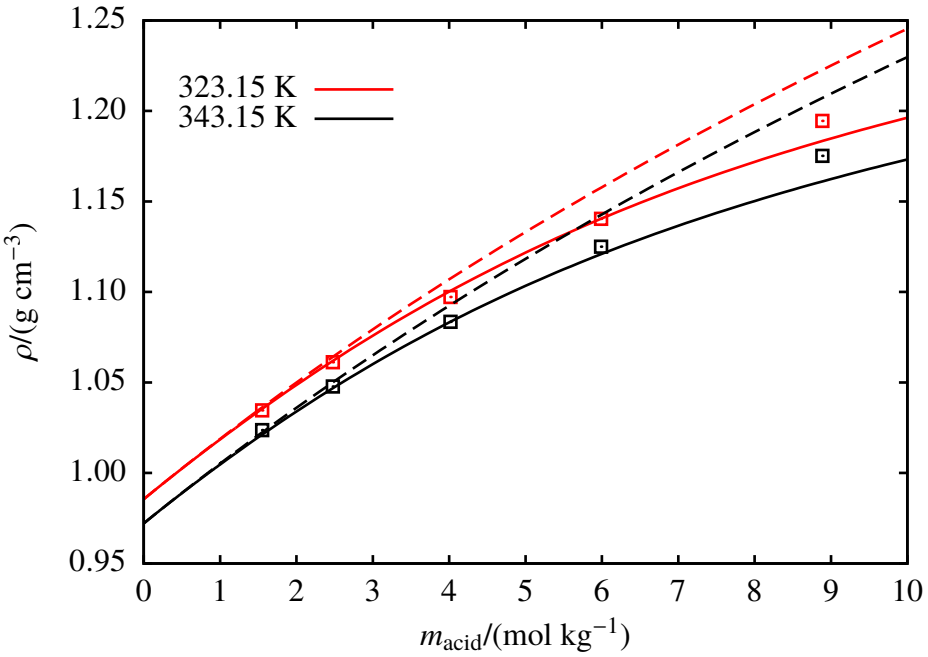

Figure 6.15 The concentration dependence of the liquid density of aqueous nitric acid solutions at 323.15 K and 343 K. The continuous curves represent the SAFT-γ Mie predictions for weak nitric acid, while the dashed curves represent the predictions for strong nitric acid. The symbols represent the experimental data [454].

6.3 A consideration of ion pairing in aqueous electrolyte solutions

Ion pairing equilibria are common in electrolyte solutions, especially in solutions containing oxoanions such as those discussed earlier in this chapter, yet consideration of ion pairing within the framework of SAFT equation-of-state modelling of electrolytes has been limited so far. An early study investigating ion pairing within the SAFT-VRE SW EOS was presented by Gil-Villegas et al. [56], in which ion pairing was mediated either through a single association site on each ion of the pair, or through an attractive square-well potential between the associating ions. The method was implemented only illustratively and did not solve for chemical reaction equilibrium. The study demonstrated the effect of ion pairing on the thermodynamic behaviour of an electrolyte solution by taking the example of vapour pressure over an aqueous NaCl solution: as the ions interact more strongly through ion pairing at higher salinity, the predicted vapour pressure was higher in models where ion pairing was included compared to models where it was omitted.

Using the ePC-SAFT equation of state, Held and Sadowski [137] treated ion pairs as distinct species with a net charge, by including the chemical reaction equilibrium associated with ion pairing. The associated ion pairing equilibrium constant (K_{IP}) was treated as an adjustable parameter (similarly to the approach employed in the preceding work of Tikanen and Fawcett [455]), optimised together with the ion pair's dispersive energy parameter against experimental data for the MIAC. The approach was effective in reproducing the behaviour of aqueous weak electrolyte solutions, including acetate, sulphate, and halide salts. However, the estimated K_{IP} values often deviated significantly from those determined experimentally, and the study did not consider whether the compositions of the solutions were reproduced well by the estimated K_{IP}.

In this work, ion pairing is examined with reference to aqueous solutions of nitrate salts. Having established a SAFT-γ Mie model for the NO_3^- ionic species, it used here together

with the ion models developed in Chapter 4 to model alkali metal nitrates: $NaNO_3$, $LiNO_3$, KNO_3, and $RbNO_3$. In these solutions, the NO_3^- ion and the alkali metal counter-ion have been shown to form ion pairs extensively even at moderate conditions of temperature and pressure [36, 442]. By studying these salt solutions using Raman spectroscopy, Frost and James [456–458] deduced that a sequence of ion association equilibria occurs similarly in all the above aqueous nitrate salt solutions. For a generic 1:1 nitrate salt MNO_3, ion association was proposed to occur as follows:

$$M^+(aq) + NO_3^-(aq) \overset{K_1}{\rightleftharpoons} \left[M^+ \cdot H_2O \cdot NO_3^-\right](aq) \overset{K_2}{\rightleftharpoons} \left[M^+ \cdot NO_3^-\right](aq) \,. \tag{6.22}$$

The equilibrium between free ions, solvent-shared ion pairs, and contact ion pairs is governed by the two thermodynamic equilibrium constants, K_1 and K_2, however these have not been quantified. In the absence of this information, ion pairing can be treated implicitly through strong attractive dispersion interactions, similarly to the approach examined by Gil-Villegas et al. [56]; this is pursued in Section 6.3.1. When quantitative experimental data on the degree of ion pairing is available, it is possible to model ion pairs explicitly as distinct species. The SAFT-γ Mie EOS presents the opportunity to model ion pairs in a group contribution manner using the already parameterised models for the individual ions. This will be discussed in Section 6.3.2 for the case of aqueous sodium nitrate.

6.3.1 Implicit treatment of ion pairing with ion-specific SAFT parameters

For electrolyte solutions modelled so far in Chapters 4 and 6, the approach to determining the strength of ion–ion dispersive interactions was to apply the combining rule given by Equation 3.96, usually resulting in the attractive energy ε_{kl} being fairly weak. This was found to be a reasonable approximation in solutions of strong electrolytes in which Coulombic interactions dominate the attraction between the free ions, and also in solutions of weak acids

where the ion pairing is treated by association. However, the strength of the ion–ion attraction approximated by Equation 3.96 proves to be too weak in solutions where a high degree of ion pairing is known to occur. For these solutions, the ε_{kl} parameter can be optimised so as to implicitly model ion pairing through strong ion–ion attraction. The Mie intermolecular potential characterising a given NO_3^-–M^+ interaction is determined by optimising ε_{kl} against data for the osmotic coefficient of the aqueous MNO_3 salt solution. The corresponding Mie potential exponents $\lambda_{a,kl}$ and $\lambda_{r,kl}$ are calculated using the combining rule given by Equation 3.33. Since the extent of ion pairing varies with salt concentration, it is found necessary to include experimental data across the whole range of concentrations of interest ($\leq$10 mol kg^{-1}) in the optimisation exercise. The cross interaction parameters between the nitrate ion and four cations (Li^+, Na^+, K^+, Rb^+) obtained in this way are shown in Table 6.7. In each case the ε_{kl} parameter signifies a very strong attractive interaction between NO_3^- and the cation, which emulates the formation of ion pairs in these nitrate salt solutions.

The performance of these optimised models in reproducing the thermodynamic properties of the aqueous salt solutions is illustrated by means of the MIAC and the osmotic coefficient in Figures 6.17 and Figure 6.16, respectively. The SAFT-γ Mie calculations for the osmotic coefficient have good quantitative agreement with the experimental data in both the low-salinity region where ion pairs are scarce as well as the high-salinity region where ion pairs are more abundant. Similarly, the SAFT-γ Mie predictions for the MIAC of the nitrate salts are in very good agreement with the experimental data across the range of concentrations considered here, despite not having considered this property in the model development. The behaviour of the whole concentration range is described well despite the change in solution composition with regard to ion pairs.

The fact that these electrolyte solutions can be modelled well even without regarding ion pairs as distinct species conforms to the interpretation of ion pairing as physically associated ions. Modelling ion pairing implicitly through strong dispersion interactions is shown to be adequate and effective for use in cases where quantitative data is not available for the ion pairing equilibrium constant.

Table 6.7 Optimised cross interaction parameters between the NO_3^- ion and four cations (Li^+, Na^+, K^+, Rb^+). Parameters labelled "Implicit IP" correspond to the modelling approach in which ion pair entities are neglected. Parameters labelled "Explicit IP" correspond to the modelling approach which explicitly includes ion pairs as distinct entities. In all cases, $\lambda_{a,kl}$ and $\lambda_{r,kl}$ are set using the combining rule given by Equation 3.33.

Group		(ε_{kl}/k_B)/K	
k	l	Implicit IP	Explicit IP
NO_3^-	Li^+	497.11	–
NO_3^-	Na^+	595.02	525.70
NO_3^-	K^+	632.80	–
NO_3^-	Rb^+	607.99	–

6.3.2 Explicit treatment of ion-pairing within a group-contribution approach

Modelling ion pairs explicitly with the SAFT-γ Mie equation of state requires a number of interrelated choices to be made concerning the geometry, net charge, and the nature of intermolecular interactions appropriate for the ion pair species. One can conceive a model for the ion pair entity either as distinct from the constituent ions, such that the model parameters need not bear resemblance to those of the free ions; or as being composed of the constituent ions in a group-contribution manner.

In the first case, a distinct ion pair species i would possess a net charge q_i equivalent to the sum of the charge on the individual ions. This means that the ion pair would experience attenuated Coulombic interactions compared to the free ions, or even no electrostatic interactions at all in cases where $q_i = 0$. All model parameters, including the structural parameters (σ_{ii}, ν_{ii}^*, S_{ii}), the form of the intermolecular potential (ε_{ii}, $\lambda_{a,ii}$, $\lambda_{r,ii}$), and the cross-interaction intermolecular potential parameters between the ion pair i and the solvent j would need to be determined.

In the case of modelling ion pairs using a group-contribution approach, the ion pair would be formed of charged groups k and l corresponding to previously parameterised models for

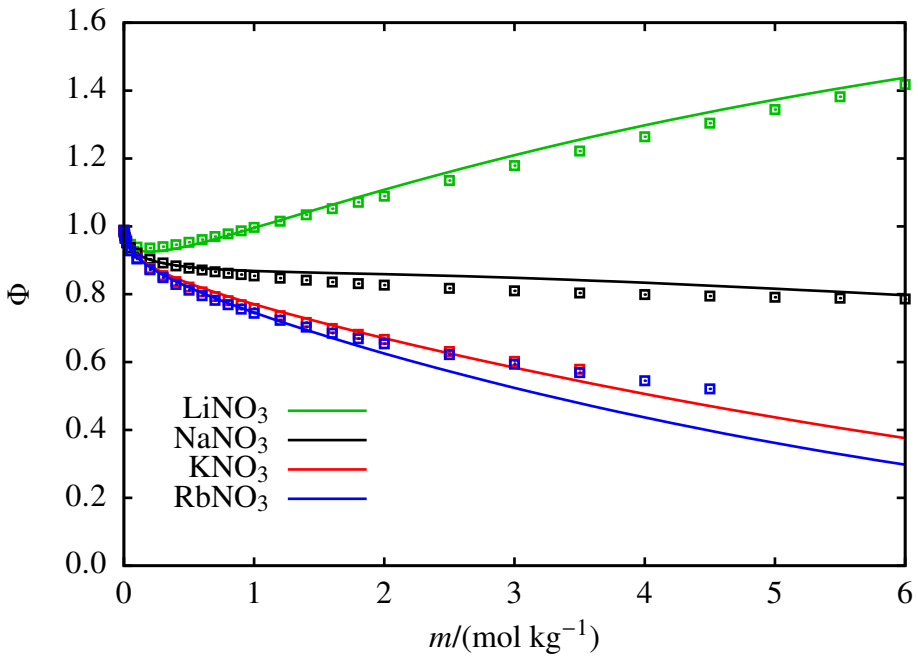

Figure 6.16 The concentration dependence of the osmotic coefficient of aqueous alkali metal nitrate salt solutions at 298.15 K and 1.01 bar, calculated using the model parameters corresponding to an implicit representation of ion pairing. The continuous curves represent the SAFT-γ Mie predictions and the symbols represent the experimental data [219].

the constituent ions. Each ionic group would retain its charge, such that the ion pair entity experiences electrostatic interactions regardless of the pair's net charge. Only intermolecular potential parameters describing the cross interaction between the ion pair's constituent ions k and l would need to be determined. A question arising here is whether a given pair of charged groups would interact similarly whether they represent free ionic species or form part of an ion pair species. If the interaction is considered to be the same then only one cross interaction needs to be optimised, but if the interactions are considered dissimilar then two types of cross interactions need to be determined.

Regardless of how the ion pair entity is modelled, an explicit treatment of ion pairing requires taking into consideration the equilibrium composition of ion pairs and free ions in the solution. The ability to model ion pairs explicitly therefore relies on the availability of experimental data of the equilibrium constant K_{IP}. Of the four nitrate salts considered in this work, such information is available for $NaNO_3$, which is consequently taken forward as a

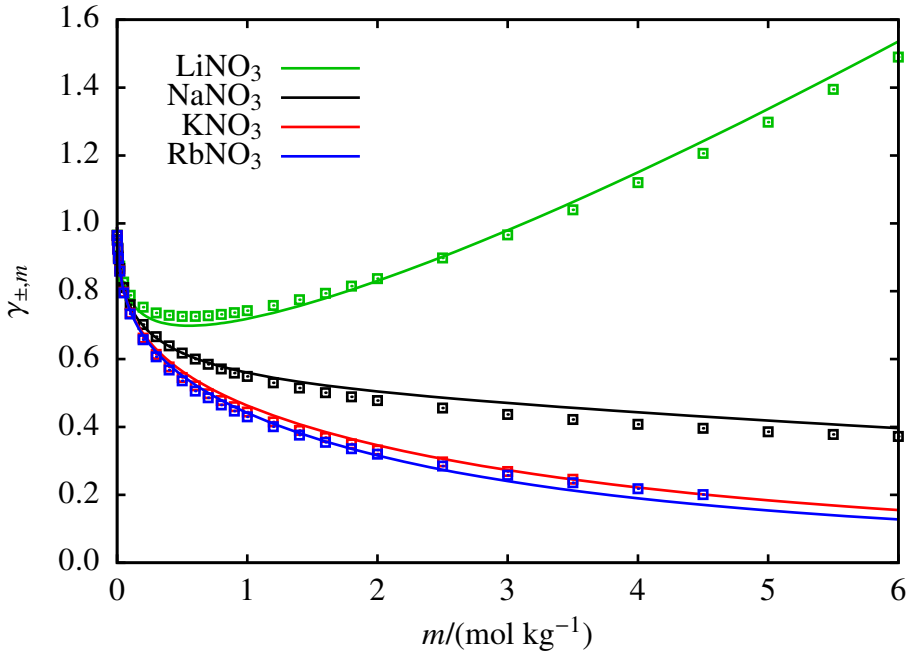

Figure 6.17 The concentration dependence of the mean ionic activity coefficient of aqueous alkali metal nitrate salt solutions at 298.15 K and 1.01 bar, calculated using the model parameters corresponding to an implicit representation of ion pairing. The continuous curves represent the SAFT-γ Mie predictions and the symbols represent the experimental data [219].

case study for explicit modelling of ion pairs. The group-contribution approach to modelling ion pairs is pursued in this work, as it is felt to align more closely with the physical system. This instance SAFT-γ Mie electrolyte formulation appropriate for this purpose is that where the electrostatic interactions correspond to the individual groups.

6.3.2.1 Case study: ion pairing in aqueous sodium nitrate

Ion pairing in aqueous $NaNO_3$ was studied by Riddell et al. [459] using Raman and infrared spectroscopy to determine the composition of the solution. The following ion pairing equilibrium was proposed:

$$Na^+(aq) + NO_3^-(aq) \overset{K_{IP}}{\rightleftharpoons} Na^+ \cdot NO_3^-(aq) \,. \tag{6.23}$$

The thermodynamic equilibrium constant, K_{IP}, is related to the equilibrium concentration quotient, Q_{C}, as follows:

$$K_{\mathrm{eq}} = \frac{a_{[\mathrm{Na^+ \cdot NO_3^-}]}}{a_{\mathrm{NO_3^-}} a_{\mathrm{Na^+}}} = \frac{\gamma_{[\mathrm{Na^+ \cdot NO_3^-}],m}}{\gamma_{\mathrm{NO_3^-},m} \gamma_{\mathrm{Na^+},m}} Q_{\mathrm{C}} \,, \tag{6.24}$$

Given that $m_{\mathrm{NO_3^-}} = m_{\mathrm{Na^+}}$ due to the 1:1 stoichiometry of the salt, the concentration quotient is given by

$$Q_{\mathrm{C}} = \frac{m_{[\mathrm{Na^+ \cdot NO_3^-}]}}{m^2_{\mathrm{NO_3^-}}} \,. \tag{6.25}$$

The fraction of freely dissociated nitrate ions, i.e. those not bound in an ion pair, is equivalent to the degree of dissociation of the ion pair, α_{IP}. In a sodium nitrate solution of molality m_{salt}, α_{IP} is expressed as

$$\alpha_{\mathrm{IP}} = \frac{m_{\mathrm{NO_3^-}}}{m_{\mathrm{NO_3^-}} + m_{\mathrm{IP}}} = \frac{m_{\mathrm{NO_3^-}}}{m_{\mathrm{salt}}} \,. \tag{6.26}$$

The compositions of each solute species in the solution can be related to α_{IP} and m through the following material balances:

$$m_{\mathrm{NO_3^-}} = m_{\mathrm{Na^+}} = \alpha_{\mathrm{IP}} m_{\mathrm{salt}} \,, \tag{6.27}$$

$$m_{\mathrm{IP}} = m_{\mathrm{salt}} (1 - \alpha_{\mathrm{IP}}) \,, \tag{6.28}$$

while the concentration quotient can also be rewritten as

$$Q_{\mathrm{C}} = \frac{1 - \alpha_{\mathrm{IP}}}{m_{\mathrm{salt}} \alpha^2_{\mathrm{IP}}} \,. \tag{6.29}$$

Riddell et al. [459] measured the solution concentrations of the bound ($m_{[\mathrm{Na^+ \cdot NO_3^-}]}$) and free ($m_{\mathrm{NO_3^-}}$) nitrate ions and calculated Q_{C} for concentrations between 1.23–9.38 mol kg^{-1} at 298.15 K. The equilibrium concentration quotient was found to be almost constant in this concentration range and also approximately equal to the thermodynamic equilibrium

constant, which was calculated as $K_{IP}(298\ K) = 0.06 \pm 0.006$ kg mol^{-1} by extrapolation to infinite dilution. As shown in Figure 6.18, the composition of the aqueous $NaNO_3$ solution is computed accurately across the whole range of applicable concentrations relevant to this work by setting $Q_C = 0.06$ kg mol^{-1}. Since it is possible to obtain the solution composition by satisfying a *practically* concentration-independent Q_C, the chemical equilibrium condition given by Equation 6.29 is not solved here. To be clear, the Q_C *is* dependent on concentration, but the change in Q_C for this particular system is small enough to be considered negligible and is hence assumed to be constant.

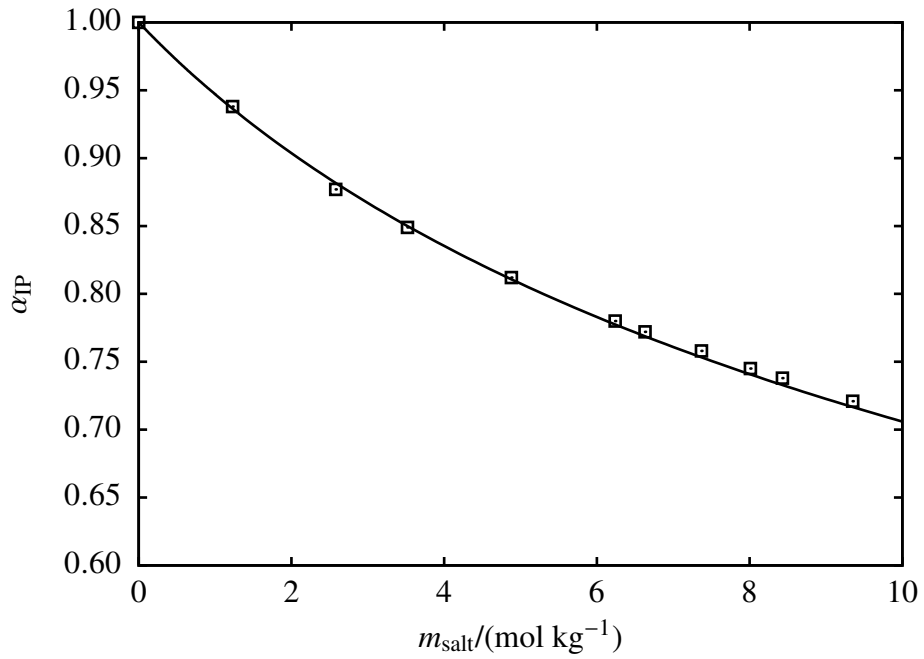

Figure 6.18 The fraction of freely dissociated nitrate ions in aqueous sodium nitrate solution, or, equivalently, the degree of dissociation of the $[Na^+ \cdot NO_3^-]$ ion pair, α_{IP}, at 298.15 K. The symbols represent the experimental data [459] and the continuous curve represents the concentration dependence of α_{IP} computed using Equations 6.28. Note that α_{IP} is not a prediction of the model, as the composition of the solution is obtained by setting the concentration quotient Q_C to a constant value.

The $[Na^+ \cdot NO_3^-]$ ion pair is modelled using the group contribution approach inherent in the SAFT-γ Mie equation of state: the Na^+ ion developed in Chapter 4 and the NO_3^- ion developed earlier in this chapter are used as charged groups comprising the $[Na^+ \cdot NO_3^-]$

species. The only unknown SAFT-γ Mie model parameters for the ion pair species are those describing the Mie cross interaction potential between the Na^+ and NO_3^- groups. The Mie potential exponents ($\lambda_{a,kl}$ and $\lambda_{r,kl}$) for the cross interaction are obtained using the combining rule given by Equation 3.33, while the depth of the potential (ε_{kl}) is estimated by optimisation using experimental data for the osmotic coefficient of the solution.

The optimisation procedure includes data for concentrations $\leq$10 mol kg^{-1} (where still less than 30% of nitrate ions are bound in ion pairs), so that sufficient concentration of ion pairs exist in solution to allow proper characterisation of their interactions. Two modelling approaches are investigated as part of the optimisation procedure: in the first approach, the bound ions experience different unlike interactions than free ions (i.e. second-order cross-interaction parameters are employed); while in the second approach, the unlike interactions are independent of the whether the ions are paired or free. The optimal model for the interaction between Na^+ and NO_3^- is found to be that following the second approach, where the $\varepsilon_{Na^+-NO_3^-}$ parameter corresponding to a free Na^+ ion interacting with a free NO_3^- ion is of equal magnitude as the $\varepsilon_{Na^+-NO_3^-}$ parameter corresponding to ions Na^+ and NO_3^- when they are bound in an ion pair. The unlike interaction between the Na^+ and NO_3^- groups obtained with this explicit ion pair modelling approach is shown in Table 6.7 and the description of the solution's thermodynamic properties is illustrated in Figures 6.19, 6.20, and 6.21.

6.3.3 Comparison of implicit and explicit modelling of ion-pairing phenomena

The magnitude of the $\varepsilon_{Na^+-NO_3^-}$ parameter when ion pairs are modelled explicitly is fairly similar to that obtained when the formation of ion pairs is excluded from the model. The similarity is reasonable considering that the strong ion–ion attraction necessary for mediating ion pairing is ultimately treated via dispersive interactions in both approaches. Nevertheless, as seen in Table 6.7, the existence of ion pair entities in the explicit modelling approach does

result in $\varepsilon_{Na^+-NO_3^-}$ being slightly weaker, as would be expected considering that a proportion of the ions are already defined as bound in ion pairs.

The performance of the two modelling approaches is compared with reference to the osmotic coefficient and MIAC, bearing in mind that the stoichiometric definition is applicable when ion pairs are explicitly modelled. For aqueous $NaNO_3$, the stoichiometric definitions of these properties are obtained by applying Equations 2.23 and 2.25, yielding:

$$\gamma_{\pm,m}^{\text{stoich.}} = \left(\gamma_{NO_3^-,m}\gamma_{Na^+,m}\right)\frac{m_{NO_3^-}}{m_{\text{salt}}} = \gamma_{\pm,m}\alpha_{\text{IP}}\,, \tag{6.30}$$

$$\phi^{\text{stoich.}} = \phi = -\frac{\ln a_{H_2O}}{2mMW_j}\,, \tag{6.31}$$

where the stoichiometric osmotic coefficient is equal to the real osmotic coefficient due to the salt's 1:1 stoichiometry.

The description of the osmotic coefficient of aqueous $NaNO_3$ given by the two modelling approaches is shown in Figure 6.19. Data for Φ were used for optimising both models, nevertheless the description of Φ given by the approach in which ion pairs are modelled explicitly is seen to follow the trend of the experimental data more closely, even though the two models perform similarly in the low-salinity region where the degree of ion pairing is low. The fact that the two models predict the MIAC of $NaNO_3$ equally well, as seen in Figure 6.17, suggests that the difference between the two modelling approaches lies in the manner in which the solvent interacts with the charged solute species. In Figure 6.21 the prediction of the aqueous $NaNO_3$ solution density as a function of salt concentration is shown at 298 K and 343 K. At high concentrations, where the degree of ion pairing is high, a notable improvement in the prediction of the density is achieved by modelling ion pairs explicitly. The presence of ion pairs as distinct species means that at a specified salt

concentration the ions bound in an ion pair occupy less space compared to the case where ion are free in solution, hence the solution will have higher density.

Based on this case study, it appears that the approach of modelling ion pairs explicitly provides a better physical representation of associated electrolyte solutions. Of course, more salts must be examined before a conclusion can be reached. Ion pairing mediated through Wertheim association is also worth investigating, this method having been shown earlier in this chapter to be successful for representing ion pairs in weak acid solutions. Further indication that this could be a suitable modelling approach for ion pairs arises from the work of Chremos et al. [460], in which the SAFT-γ SW EOS was used to describe chemical reactions via a physical association model. By introducing strong intermolecular association among reacting molecules, the reaction products were modelled without introducing these as distinct species in the mixture. Without having pursued further work on ion pairing, one can only suggest that explicit ion pairing is effective in the manner it is performed here, yet it warrants further study following indications from both the present and prior work.

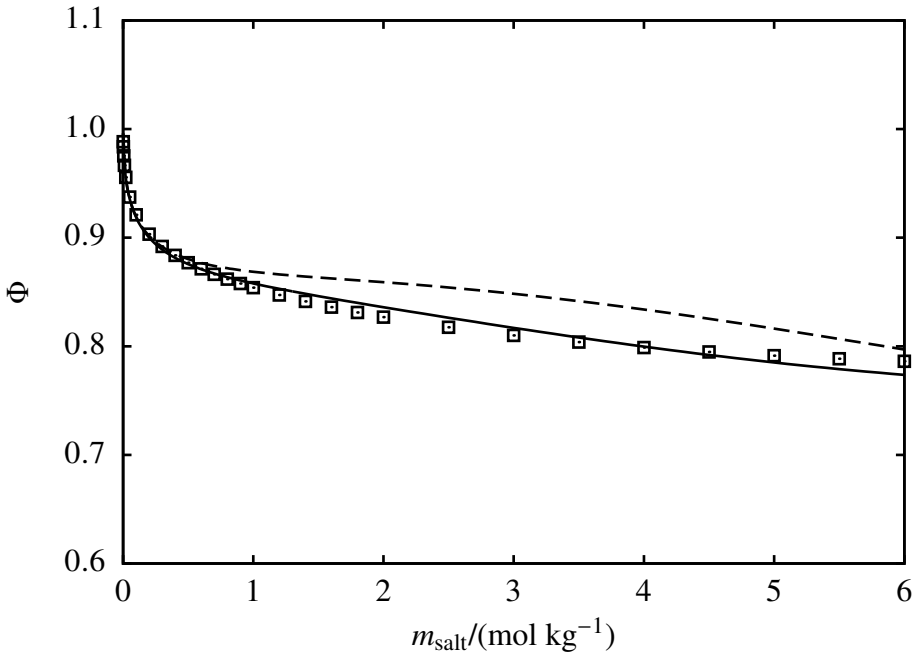

Figure 6.19 The concentration dependence of the osmotic coefficient of aqueous sodium nitrate salt 298.15 K and 1.01 bar, obtained by models in which the formation of ion-pairs is treated implicitly (dashed curve) and in which the ion-pairing equilibrium is explicitly modelled (continuous curve). The symbols represent the experimental data [219].

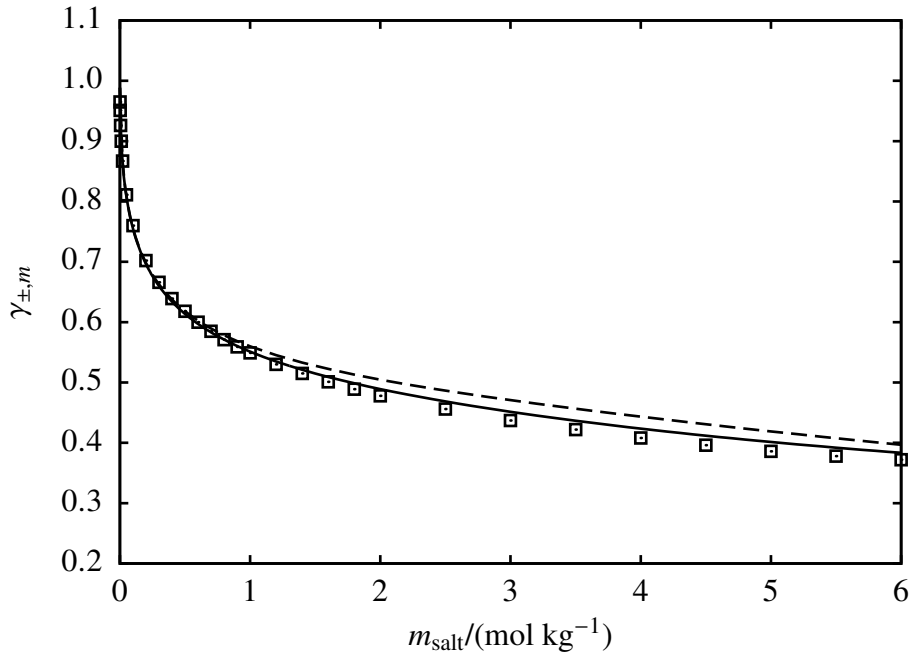

Figure 6.20 The concentration dependence of the mean ionic activity coefficient of aqueous sodium nitrate salt 298.15 K and 1.01 bar, obtained by models in which the formation of ion-pairs is treated implicitly (dashed curve) and in which the ion-pairing equilibrium is explicitly modelled (continuous curve). The symbols represent the experimental data [219].

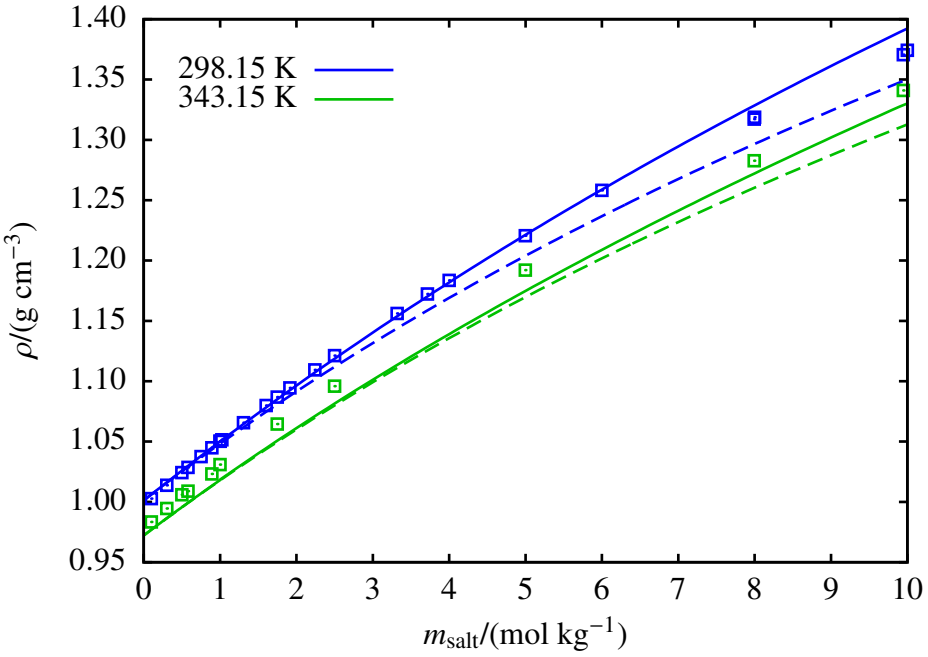

Figure 6.21 The concentration dependence of the liquid density of aqueous sodium nitrate salt at 298.15 K and 343.15 K, at 1.01 bar, obtained by models in which the formation of ion-pairs is treated implicitly (dashed curves) and in which the ion-pairing equilibrium is explicitly modelled (continuous curves). The symbols represent the experimental data [216, 461, 462].

6.4 Summary

The SAFT-γ Mie EOS has been applied in this chapter in the context of modelling solutions of weak electrolytes. This has included two incompletely dissociated acids, H_2SO_4(aq) and HNO_3(aq), and ion pairing in alkali nitrate salts.

Aqueous sulphuric acid has been described by explicitly solving the chemical reaction equilibrium governing the second dissociation step, i.e. the deprotonation of the bisulphate ion, using the thermodynamic equilibrium constant obtained from the literature. The molecular acid is not present in aqueous sulphuric acid solutions at the conditions of interest in this work, therefore the model development procedure involved the HSO_4^- and SO_4^{-2} ions only. The association parameters characterising the interaction between the sulphate ion and hydronium ion were found to be the only ones requiring adjustment to experimental data. The fact that a highly accurate description of the thermodynamic properties of aqueous sulphuric acid has been achieved with only two adjustable cross-interaction parameters for only one of the two newly proposed ionic species acts as a testament to the predictive capability of the SAFT-γ Mie approach and the reliability of the parameterisation procedure employed in this work.

Modelling of aqueous nitric acid was performed in two ways: firstly, by treating the acid as a completely dissociated in solution; and secondly, by considering its partial dissociation by using the thermodynamic acid dissociation constant from the literature. In order to model aqueous nitric acid as a weak electrolyte, the molecular acid was first modelled by developing a SAFT-γ Mie model for the HNO_3 species using experimental information for the pure acid. A comparison of the two modelling approaches for nitric acid has shown that – provided the same experimental information is used to develop the models – a much more accurate prediction of the weak acid's thermodynamic properties can be achieved by explicitly modelling the incomplete dissociation.

Ion-pairing phenomena in solutions of alkali nitrate salts have been considered in this chapter both implicitly, through strong unlike dispersion interactions, and explicitly, by introducing in the solution mixture a distinct contact ion pair component formed of two charged groups representing the paired ions. The former approach is convenient as it does not require knowledge of the ion pairing equilibrium constant. However, a comparison of the implicit and explicit ion pairing approaches for solutions of sodium nitrate has suggested that the latter should be favoured when K_{IP} data are available.

Chapter 7

Conclusions and outlook

The SAFT-γ Mie equation of state has found widespread application in recent years as a thermodynamic modelling tool for fluid systems. Owing to the heteronuclear group-contribution nature of the formalism, it has been applied successfully across numerous chemical families [9, 10, 175, 176]. In this thesis, the SAFT-γ Mie EOS has been extended with additional capabilities that permit it to be used for modelling fluid mixtures containing electrolytes, thereby further broadening its scope of application in the chemical industry and beyond.

Thermodynamic modelling approaches for the properties of electrolytes are abundant in the scientific literature, as has been discussed in Chapter 2. In recent years, the increasing popularity of statistical-mechanical equation-of-state approaches that take into account the structure of molecules has provided a platform for the consideration of non-spherical ionic species. New avenues have thus been opened for pursuing thermodynamic modelling of systems such as those containing ionisable pharmaceutical compounds [28] or ionic liquids [139, 140]. A contribution is presented in the current work towards this pursuit, by delivering a fit-for-purpose thermodynamic modelling tool within the framework of the SAFT-γ Mie approach.

The extension of SAFT-γ Mie to mixtures with charged components has been performed through the addition of two contributions to the Helmhotz free-energy expression of the EOS. A free-energy contribution term representing electrostatic charge–charge interactions in the system was included using the primitive model of the mean spherical approximation (MSA-PM) integral-equation theory. This theory describes how hard spheres with embedded point charges interact via the Coulombic potential in the presence of a uniform dielectric medium. The second addition made to the SAFT-γ Mie EOS is the Born theory of solvation, which accounts for the contribution to the free energy of transferring charged particles into spherical cavities in the dielectric medium at infinite dilution. The Born free-energy term therefore incorporates an important aspect of ion solvation effects. Although both the MSA and Born theories treat the solvent implicitly, the remaining terms of the SAFT-γ Mie free-energy expression treat the solvent explicitly. This type of semi-explicit approach has been adopted successfully in the past within the SAFT-VR family of models (to which SAFT-γ Mie belongs), and it is also found to be effective within the SAFT-γ Mie framework in this work.

An important part of this work has been the reformulation of the MSA-PM theory and the Born theory so as to make them compatible with the group-contribution formalism of SAFT-γ Mie. This has necessitated a redefinition of what constitutes the spherical charged species to which the Coulomb potential applies. Two possible formulations have been proposed in Chapter 3: one involves the conversion of a non-spherical ionic species into an equivalent-volume sphere for the purposes of the MSA and Born calculations; the second formulation considers that the MSA and Born terms apply to the specific charged functional groups comprising the ionic components. Each option presents a different set of advantages and limitations, which were discussed in Chapter 3. In Chapter 5, the two electrolyte formulations were applied to develop two sets of SAFT-γ Mie models for the COO^- functional group and its interactions with other groups, by considering alkyl carboxylate anions. Both electrolyte formulations – with their corresponding group models – were found to perform in a similar manner within the range of solution compositions to which the assumptions of the theory hold.

This should not come as a surprise, considering that the assumptions made when proposing each formulation are ultimately absorbed in the adjustable parameters of the model as part of the optimisation procedure. A selection of the most appropriate formulation to adopt in future applications of the SAFT-γ Mie EOS should therefore be made by weighing the relative advantages of each option. From this perspective, the formulation in which electrostatic interactions are applicable to individual charged groups is considered preferable as it aligns more closely with the group-contribution methodology. A more stringent assessment of the adequacy of the theoretical approximations is needed nonetheless, and this can be performed by direct comparison with molecular simulation data. This future avenue of work is already being pursued in the Molecular Systems Engineering group at Imperial College.

A large proportion of the work performed for this thesis has been devoted to the development of models for ionic species. In Chapter 4, models were developed for twelve atomic ions (group I & II metal cations, and halide anions) and two polyatomic ions (hydroxide and hydronium), by considering aqueous solutions of strong electrolytes. This is a necessary first step, as it establishes a set of models for commonly encountered ions. Since it was decided *a priori* that these ions would be treated as spherical monomers, the SAFT-γ Mie EOS simplifies to the SAFT-VRE Mie formalism [122] and is thus referred to as such throughout Chapter 4. By carrying out the parameter optimisation using only carefully selected experimental data – with a particular emphasis on the osmotic coefficient – at solution concentrations where the assumption of complete dissociation is reasonable, a robust set of models has been obtained. These models have been applied to aqueous single-salt solutions and good descriptions of a wide range of thermodynamic properties have been achieved.

Having established this fundamental set of models, more challenging ionic species were pursued. The caboxylate functional group was developed with reference to aqueous sodium carboxylate salts, as discussed above. In Chapter 6, models for the sulphate, bisulphate, and nitrate ions were presented; these were developed within the context of weak electrolytes. Aqueous solutions of sulphuric acid and nitric acid were modelled by explicitly taking into consideration the acid dissociation equilibria, by satisfying the condition of chemical equilib-

rium set by the corresponding thermodynamic equilibrium constant. A significant challenge in modelling these weak acids is the ambiguity regarding the association interactions – including both hydrogen bonding and ion pairing – relevant to these mixtures, especially in the case of sulphuric acid. A review of the proposed ion-pairing equilibria in aqueous sulphuric acid and nitric acid was undertaken in order to inform the development of model parameters for the ionic species. Ultimately, ion pairing in these solutions was mediated by including unlike ion–ion association interactions.

Ion pairing was further examined in Chapter 6 by considering the formation of ion pairs in alkali nitrate salt solutions. In these systems, ion pairing was implicitly accounted for via strong dispersion interactions between the anion and cation. This is a simplistic yet effective approach for cases where quantitative data regarding the ion-pairing equilibria are not available. Explicit consideration of ion-pairing equilibria was possible for solutions of sodium nitrate, as the ion-pairing equilibrium constant for this salt is reported in the literature. In this case, the ion-pair species was composed in a group-contribution manner using the anion and cation as constituent groups, using the SAFT-γ Mie electrolyte formulation for individual charged groups (and hence validating the choice of carrying forward this formulation). A third option for modelling ion pairs is to assign association sites specifically for the formation of these species, similarly to the approach adopted for ion pairing in sulphuric and nitric acid solutions. This option has not been pursued for the alkali nitrate salts in this thesis, but it is considered worthy of consideration in future work.

The primary objective of this thesis was to extend the scope of the SAFT-γ Mie equation of state to fluid mixtures containing electrolytes, with the purpose of contributing towards the development of a comprehensive thermodynamic modelling platform for fluid mixtures. The intricacies associated with the application of group-contribution methods to electrolyte systems have been addressed, and an appropriate formulation has been proposed by suitably adapting established theories for electrostatic interactions. With this framework in place, models for a range of common ionic species have been developed, and the properties of both strong and weak electrolytes were described to a high level of accuracy. Using these

models as a foundation, as well as the insight gained for treating weak electrolytes and ion pairing, the SAFT-γ Mie EOS can be applied in future work to model ever more complex ionic molecules and multicomponent electrolytes solutions.

Bibliography

[1] S. Gupta and J. D. Olson. Industrial needs in physical properties. *Industrial & Engineering Chemistry Research*, 42(25):6359–6374, 2003.

[2] W. G. Chapman, K. E. Gubbins, G. Jackson, and M. Radosz. SAFT: Equation-of-state solution model for associating fluids. *Fluid Phase Equilibria*, 52:31–38, 1989.

[3] W. G. Chapman, K. E. Gubbins, G. Jackson, and M. Radosz. New reference equation of state for associating liquids. *Industrial & Engineering Chemistry Research*, 29(8): 1709–1721, 1990.

[4] I. G. Economou. Statistical Associating Fluid Theory: A successful model for the calculation of thermodynamic and phase equilibrium properties of complex fluid mixtures. *Industrial & Engineering Chemistry Research*, 41(5):953–962, 2002.

[5] C. McCabe and A. Galindo. In A. R. H. Goodwin, J. V. Sengers, and C. J. Peters, editors, *Applied Thermodynamics of Fluids*. Royal Society of Chemistry, Cambridge, 2010.

[6] A. Lymperiadis, C. S. Adjiman, A. Galindo, and G. Jackson. A group contribution method for associating chain molecules based on the statistical associating fluid theory (SAFT-γ). *The Journal of Chemical Physics*, 127(23):234903, 2007.

[7] A. Lymperiadis, C. S. Adjiman, G. Jackson, and A. Galindo. A generalisation of the SAFT-γ group contribution method for groups comprising multiple spherical segments. *Fluid Phase Equilibria*, 274(1):85–104, 2008.

[8] V. Papaioannou, T. Lafitte, C. Avendaño, C. S. Adjiman, G. Jackson, E. A. Müller, and A. Galindo. Group contribution methodology based on the statistical associating fluid theory for heteronuclear molecules formed from Mie segments. *The Journal of Chemical Physics*, 140(5):054107, 2014.

[9] S. Dufal, V. Papaioannou, M. Sadeqzadeh, T. Pogiatzis, A. Chremos, C. S. Adjiman, G. Jackson, and A. Galindo. Prediction of thermodynamic properties and phase behavior of fluids and mixtures with the SAFT-γ Mie group-contribution equation of state. *Journal of Chemical & Engineering Data*, 59:3272–3288, 2014.

[10] P. Hutacharoen, S. Dufal, V. Papaioannou, R. M. Shanker, C. S. Adjiman, G. Jackson, and A. Galindo. Predicting the solvation of organic compounds in aqueous environments: from alkanes and alcohols to pharmaceuticals. *Industrial & Engineering Chemistry Research*, 2017.

[11] A. Anderko, P. Wang, and M. Rafal. Electrolyte solutions: from thermodynamic and transport property models to the simulation of industrial processes. *Fluid Phase Equilibria*, 194:123–142, 2002.

[12] Characteristic Features of Surfactants. In M. J. Rosen and J. T. Kunjappu, editors, *Surfactants and Interfacial Phenomena*. John Wiley & Sons, Inc., New Jersey, 4th edition, 2012.

[13] K. T. Savjani, A. K. Gajjar, and J. K. Savjani. Drug solubility: importance and enhancement techniques. *ISRN Pharmaceutics*, 2012:195727, 2012.

[14] H. D. Williams, N. L. Trevaskis, S. A. Charman, R. M. Shanker, and W. N. Charman. Strategies to address low drug solubility in discovery and development. *Pharmacological Reviews*, 65(1):315–499, 2013.

[15] A. Davis and S. E. Ward, editors. *The Handbook of Medicinal Chemistry: Principles and Practice*. RSC Publishing, Cambridge, UK, 2015.

[16] J. Huuskonen. Estimation of aqueous solubility for a diverse set of organic compounds based on molecular topology. *Journal of Chemical Information and Computer Sciences*, 40(3):773–777, 2000.

[17] G. Klopman and H. Zhu. Estimation of the aqueous solubility of organic molecules by the group contribution approach. *Journal of Chemical Information and Computer Sciences*, 41(2):439–445, 2001.

[18] I. V. Tetko, V. Y. Tanchuk, T. N. Kasheva, and A. E. P Villa. Estimation of aqueous solubility of chemical compounds using E-state indices. *Journal of Chemical Information and Computer Sciences*, 41(6):1488–93, 2001.

[19] J. Huuskonen, D. J. Livingstone, and D. T. Manallack. Prediction of drug solubility from molecular structure using a drug-like training set. *SAR and QSAR in Environmental Research*, 19(3-4):191–212, 2008.

[20] J. Taskinen and J. Yliruusi. Prediction of physicochemical properties based on neural network modelling. *Advanced Drug Delivery Reviews*, 55(9):1163–1183, 2003.

[21] J. Gross and G. Sadowski. Application of perturbation theory to a hard-chain reference fluid: an equation of state for square-well chains. *Fluid Phase Equilibria*, 168(2): 183–199, 2000.

[22] J. Gross and G. Sadowski. Perturbed-Chain SAFT: An equation of state based on a perturbation theory for chain molecules. *Industrial & Engineering Chemistry Research*, 40(4):1244–1260, 2001.

[23] F. Ruether and G. Sadowski. Modeling the solubility of pharmaceuticals in pure solvents and solvent mixtures for drug process design. *Journal of Pharmaceutical Sciences*, 98(11):4205–4215, 2009.

[24] T. Spyriouni, X. Krokidis, and I. G. Economou. Thermodynamics of pharmaceuticals: Prediction of solubility in pure and mixed solvents with PC-SAFT. *Fluid Phase Equilibria*, 302(1-2):331–337, 2011.

[25] J.-B. Grosse Daldrup, C. Held, F. Ruether, G. Schembecker, and G. Sadowski. Measurement and modeling solubility of aqueous multisolute amino-acid solutions. *Industrial & Engineering Chemistry Research*, 49(3):1395–1401, 2010.

[26] D. Fuchs, J. Fischer, F. Tumakaka, and G. Sadowski. Solubility of amino acids: Influence of the pH value and the addition of alcoholic cosolvents on aqueous solubility. *Industrial & Engineering Chemistry Research*, 45(19):6578–6584, 2006.

[27] J.-B. Grosse Daldrup, C. Held, G. Sadowski, and G. Schembecker. Modeling pH and solubilities in aqueous multisolute amino acid solutions. *Industrial & Engineering Chemistry Research*, 50(6):3503–3509, 2011.

[28] J. Cassens, A. Prudic, F. Ruether, and G. Sadowski. Solubility of pharmaceuticals and their salts as a function of pH. *Industrial & Engineering Chemistry Research*, 52(7): 2721–2731, 2013.

[29] H. Ohtaki and T. Radnai. Structure and dynamics of hydrated ions. *Chemical Reviews*, 93(3):1157–1204, 1993.

[30] M. Soniat, G. Pool, L. Franklin, and S. W. Rick. Ion association in aqueous solution. *Fluid Phase Equilibria*, 407:31–38, 2016.

[31] Z. Liu, W. Wang, and Y. Li. An equation of state for electrolyte solutions by a combination of low-density expansion of non-primitive mean spherical approximation and statistical associating fluid theory. *Fluid Phase Equilibria*, 227(2):147–156, 2005.

[32] C. Held, L. F. Cameretti, and G. Sadowski. Modeling aqueous electrolyte solutions. Part 1. Fully dissociated electrolytes. *Fluid Phase Equilibria*, 270(1-2):87–96, 2008.

[33] J. M. Smith, H. Van Ness, and M. M. Abbott. *Introduction to Chemical Engineering Thermodynamics*. McGraw-Hill, Singapore, International 7th edition, 2005.

[34] R. A. Robinson and R. H. Stokes. *Electrolyte Solutions*. Butterworths, London, 2nd edition, 1968.

[35] N. J. Bjerrum. *Untersuchungen über Ionenassoziation*. Kongelige Danske Videnskabernes Selskab, 1926.

[36] Y. Marcus. *Ion Solvation*. Wiley Interscience, Great Britain, 1st edition, 1985.

[37] Chiral anion-mediated asymmetric ion pairing chemistry, author=Lacour, J. and Moraleda, D., journal=Chemical Communications, number=46, pages=7073–7089, year=2009, publisher=Royal Society of Chemistry.

[38] M. L. Michelsen and J. M. Mollerup. *Thermodynamic Models: Fundamentals & Computational Aspects*. Tie-Line Publications, Holte, Denmark, 2nd edition, 2007.

[39] J. M. Prausnitz, R. N. Lichtenthaler, and E. Gomes de Azevedo. *Molecular Thermodynamics of Fluid-Phase Equilibria*. Prentice Hall, New Jersey, USA, 3rd edition, 1999.

[40] S. I. Sandler. *Models for Thermodynamic and Phase Equilibria Calculations*. Dekker, New York, USA, 1994.

[41] G. M. Kontogeorgis and G. K. Folas. *Thermodynamic Models for Industrial Applications: From Classical and Advanced Mixing Rules to Association Theories*. Wiley, New York, 2nd edition, 2010.

[42] S. I. Sandler. *Chemical, Biochemical, and Engineering Thermodynamics*. John Wiley and Sons, New Jersey, USA, 4th edition, 2006.

[43] P. Atkins and J. de Paula. *Atkins' Physical Chemistry*. Oxford University Press, Oxford, UK, 9th edition, 2010.

[44] J. O. Bockris and A. K. N. Reddy. *Modern Electrochemistry 1. Ionics*. Plenum Press, New York, USA, 2nd edition, 1998.

[45] P. Debye and E. Hückel. Zur Theorie der Elektrolyte. I. Gefrierpunktserniedrigung und verwandte Erscheinungen. *Physikalische Zeitschrift*, 24(9):185–206, 1923.

[46] E. Waisman and J. L. Lebowitz. Exact solution of an integral equation for the structure of a primitive model of electrolytes. *The Journal of Chemical Physics*, 52(8):4307, 1970.

[47] L. Blum. Mean spherical model for asymmetric electrolytes: I. Method of solution. *Molecular Physics*, 30(5):1529–1535, 1975.

[48] L. Blum and J. S. Hoye. Mean spherical model for asymmetric electrolytes. 2. Thermodynamic properties and the pair correlation function. *The Journal of Physical Chemistry*, 81(13):1311–1316, 1977.

[49] L. Blum and D. Q. Wei. Analytical solution of the mean spherical approximation for an arbitrary mixture of ions in a dipolar solvent. *The Journal of Chemical Physics*, 87 (1):555–565, 1987.

[50] D. Wei and L. R. Blum. The mean spherical approximation for an arbitrary mixture of ions in a dipolar solvent: Approximate solution, pair correlation functions, and thermodynamics. *The Journal of Chemical Physics*, 87(5):2999–3007, 1987.

[51] J. A. Myers, S. I. Sandler, and R. H. Wood. An equation of state for electrolyte solutions covering wide ranges of temperature, pressure, and composition. *Industrial & Engineering Chemistry Research*, 41(13):3282–3297, 2002.

[52] P. Paricaud, A. Galindo, and G. Jackson. Recent advances in the use of the SAFT approach in describing electrolytes, interfaces, liquid crystals and polymers. *Fluid Phase Equilibria*, 194-197:87–96, 2002.

[53] R.-S. Wu and L. L. Lee. Vapor-liquid equilibria of mixed-solvent electrolyte solutions: ion-size effects based on the MSA theory. *Fluid Phase Equilibria*, 78:1–24, 1992.

[54] B. Maribo-Mogensen, G M. Kontogeorgis, and K. Thomsen. Comparison of the Debye–Huckel and the Mean Spherical Approximation theories for electrolyte solutions. *Industrial & Engineering Chemistry Research*, 51(14):5353–5363, 2012.

[55] A. Galindo, A. Gil-Villegas, G. Jackson, and A. N. Burgess. SAFT-VRE: Phase behavior of electrolyte solutions with the Statistical Associating Fluid Theory for potentials of variable range. *The Journal of Physical Chemistry B*, 103(46):10272–10281, 1999. ISSN 1520-6106.

[56] A. Gil-Villegas, A. Galindo, and G. Jackson. A statistical associating fluid theory for electrolyte solutions (SAFT-VRE). *Molecular Physics*, 99(6):531–546, 2001.

[57] M. Born. Volumen und Hydratationswärme der Ionen. *Zeitschrift für Physik*, 1(1): 45–48, 1920.

[58] A. H. Harvey and J. M. Prausnitz. Thermodynamics of high-pressure aqueous systems containing gases and salts. *AIChE Journal*, 35(4):635–644, 1989.

[59] J. Wu and J. M. Prausnitz. Phase equilibria for systems containing hydrocarbons, water, and salt: An extended Peng-Robinson equation of state. *Industrial & Engineering Chemistry Research*, 37(5):1634–1643, 1998.

[60] R. Inchekel, J.-C. de Hemptinne, and W. Fürst. The simultaneous representation of dielectric constant, volume and activity coefficients using an electrolyte equation of state. *Fluid Phase Equilibria*, 271(1-2):19–27, 2008.

[61] J. M. A. Schreckenberg, S. Dufal, A. J. Haslam, C. S. Adjiman, G. Jackson, and A. Galindo. Modelling of the thermodynamic and solvation properties of electrolyte solutions with the Statistical Associating Fluid Theory for potentials of variable range. *Molecular Physics*, 112(17):2339–2364, 2014.

[62] A. Schlaikjer, K. Thomsen, and G. M. Kontogeorgis. Simultaneous description of activity coefficients and solubility with eCPA. *Industrial & Engineering Chemistry Research*, 56(4):1074–1089, 2017.

[63] S. P. Tan, H. Adidharma, and M. Radosz. Recent advances and applications of Statistical Associating Fluid Theory. *Industrial & Engineering Chemistry Research*, 47(21):8063–8082, 2008.

[64] C.-C. Chen and P. M. Mathias. Applied thermodynamics for process modeling. *AIChE Journal*, 48(2):194–200, 2002.

[65] K. S. Pitzer. Thermodynamics of electrolytes. I. Theoretical basis and general equations. *The Journal of Physical Chemistry*, 77(2):268–277, 1973.

[66] K. S. Pitzer. Thermodynamics of electrolytes. V. Effects of higher-order electrostatic terms. *Journal of Solution Chemistry*, 4(3):249–265, 1975.

[67] K. S. Pitzer and G. Mayorga. Thermodynamics of electrolytes. II. Activity and osmotic coefficients for strong electrolytes with one or both ions univalent. *The Journal of Physical Chemistry*, 77(19):2300–2308, 1973.

[68] K. S. Pitzer and J. J. Kim. Thermodynamics of electrolytes. IV. Activity and osmotic coefficients for mixed electrolytes. *Journal of the American Chemical Society*, 98(18): 5701–5707, 1974.

[69] K. S. Pitzer and L. F. Silvester. Thermodynamics of electrolytes. VI. Weak electrolytes including H_3PO_4. *Journal of Solution Chemistry*, 5(4):269–278, 1976.

[70] T. J. Edwards, G. Maurer, J. Newman, and J. M. Prausnitz. Vapor-liquid equilibria in multicomponent aqueous solutions of volatile weak electrolytes. *AIChE Journal*, 24 (6):966–976, 1978.

[71] T. J. Edwards, J. Newman, and J. M. Prausnitz. Thermodynamics of aqueous solutions containing volatile weak electrolytes. *AIChE Journal*, 21(2):248–259, 1975.

[72] D. Beutier and H. Renon. Representation of NH_3-H_2S-H_2O, NH_3-CO_2-H_2O, and NH_3-SO_2-H_2O vapor-liquid equilibria. *Industrial & Engineering Chemistry Process Design and Development*, 17(3):220–230, 1978.

[73] H. T. Kim and W. J. Frederick Jr. Evaluation of Pitzer ion interaction parameters of aqueous electrolytes at 25°C. 1. Single salt parameters. *Journal of Chemical and Engineering Data*, 33(2):177–184, 1988.

[74] H. T. Kim and W. J. Frederick Jr. Evaluation of Pitzer ion interaction parameters of aqueous mixed electrolyte solutions at 25°CC. 2. Ternary mixing parameters. *Journal of Chemical and Engineering Data*, 33(3):278–283, 1988.

[75] H. Renon and J. M. Prausnitz. Local compositions in thermodynamic excess functions for liquid mixtures. *AIChE Journal*, 14(1):135–144, 1968.

[76] D. S. Abrams and J. M. Prausnitz. Statistical thermodynamics of liquid mixtures: A new expression for the excess gibbs energy of partly or completely miscible systems. *AIChE Journal*, 21(1):116–128, 1975.

[77] E. A. Guggenheim. Statistical thermodynamics of mixtures with non-zero energies of mixing. *Proceedings of the Royal Society A: Mathematical, Physical and Engineering Sciences*, 183(993):213–227, 1944.

[78] E. A. Guggenheim. Statistical thermodynamics of co-operative systems (a generalization of the quasi-chemical method). *Transactions of the Faraday Society*, 44: 1007–1012, 1948.

[79] A. Frendenslund, R. L. Jones, and J. M. Prausnitz. Group-contribution estimation of activity coefficients in nonideal liquid mixtures. *AIChE Journal*, 21(6):1086–1099, 1975.

[80] C.-C. Chen, H. Britt, and J. F. Boston. Local composition model for excess Gibbs energy of electrolyte systems. Part I: Single solvent, sinlge completely dissociated electrolyte systems. *AIChE Journal*, 28(4):588–596, 1982.

[81] B. Mock, L. B. Evans, and C.-C. Chen. Thermodynamic representation of phase equilibria of mixed-solvent electrolyte systems. *AIChE Journal*, 32(10):1655–1664, 1986.

[82] C.-C. Chen and L. B Evans. A local composition model for the excess Gibbs energy of aqueous electrolyte systems. *AIChE Journal*, 32(3):444–454, 1986.

[83] C.-C. Chen and Y. Song. Generalized electrolyte-NRTL model for mixed-solvent electrolyte systems. *AIChE Journal*, 50(8):1928–1941, 2004.

[84] D. M. Austgen, G. T. Rochelle, and C. C. Chen. Model of vapor-liquid equilibria for aqueous acid gas-alkanolamine systems using the electrolyte-NRTL equation. *Industrial & Engineering Chemistry Research*, 28(7):1060–1073, 1989.

[85] M. L. Posey and G. T. Rochelle. A thermodynamic model of methyldiethanolamine-CO_2-H_2S-water. *Industrial & Engineering Chemistry Research*, 36(9):3944–3953, 1997.

[86] C. Christensen, B. Sander, A. Frendenslund, and P. Rasmussen. Towards the extension of UNIFAC to mixtures with electrolytes. *Fluid Phase Equilibria*, 13:297–309, 1983.

[87] B. Sander, A. Fedenslund, and P. Rasmussen. Calculation of vapour-liquid equilibria in mixed solvent/salt systems using an extended UNIQUAC equation. *Chemical Engineering Science*, 41(5):1171–1183, 1986.

[88] H. Nicolaisen, P. Rasmussen, and J. M. Sorensen. Correlation and prediction of mineral solubilities in the reciprocal salt system (Na^+, K^+)(Cl^-, SO_4^{2-})-H_2O at 0-100(°c. *Chemical Engineering Science*, (18):3149–3158.

[89] K. Thomsen, P. Rasmussen, and R. Gani. Correlation and prediction of thermal properties and phase behaviour for a class of aqueous electrolyte systems. *Chemical Engineering Science*, 51(14):3675–3683, 1996.

[90] K. Thomsen and P. Rasmussen. Modeling of vapor-liquid-solid equilibrium in gas-aqueous electrolyte systems. *Chemical Engineering Science*, 54(12):1787–1802, 1999.

[91] G. Soave. Equilibrium constants from a modified Redlich-Kwong equation of state. *Chemical Engineering Science*, 27(6):1197–1203, 1972.

[92] K. Thomsen. Modeling electrolyte solutions with the extended universal quasichemical (UNIQUAC) model. *Pure and Applied Chemistry*, 77(3):531–542, 2005.

[93] L. Kaewsichan, O.a Al-Bofersen, V. F. Yesavage, and M. S. Selim. Predictions of the solubility of acid gases in monoethanolamine (MEA) and methyldiethanolamine (MDEA) solutions using the electrolyte-UNIQUAC model. *Fluid Phase Equilibria*, 183-184:159–171, 2001.

[94] I. Kikic and M. Fermeglia. UNIFAC prediction of vapor-liquid equilibria in mixed solvent-salt systems. *Chemical Engineering Science*, 46(11):2775–2780, 1991.

[95] C. Achard, C. G. Dussap, and J. B. Gros. Representation of vapour-liquid equilibria in water-alcohol-electrolyte mixtures with a modified UNIFAC group-contribution method. *Fluid Phase Equilibria*, 98:71–89, 1994.

[96] W. Yan, M. Topphoff, C. Rose, and J. Gmehling. Prediction of vapor-liquid equilibria in mixed-solvent electrolyte systems using the group contribution concept. *Fluid Phase Equilibria*, 162(1-2):97–113, 1999.

[97] W. Furst and H. Renon. Representation of excess properties of electrolyte solutions using a new equation of state. *AIChE Journal*, 39(2):335–343, 1993.

[98] J. Schwartzentruber, H. Renon, and S. Watanasiri. Development of a new cubic equation of state for phase equilibrium calculations. *Fluid Phase Equilibria*, 52: 127–134, 1989.

[99] J. Y. Zuo, D. Zhang, and W. Fürst. Predicting LLE in mixed-solvent electrolyte systems by an electrolyte EOS. *AIChE Journal*, 46(11):2318–2329, 2000.

[100] J. Y. Zuo, D. Zhang, and W. Fürst. Extension of the electrolyte EOS of Fürst and Renon to mixed solvent electrolyte systems. *Fluid Phase Equilibria*, 175(1):285–310, 2000.

[101] D.-Y. Peng and D. B. Robinson. A new two-constant equation of state. *Industrial & Engineering Chemistry Fundamentals*, 15(1):59–64, 1976.

[102] G. M. Kontogeorgis, E. C. Voutsas, I. V. Yakoumis, and D. P. Tassios. An equation of state for associating fluids. *Industrial & Engineering Chemistry Research*, 35: 4310–4318, 1996.

[103] Y. Lin, K. Thomsen, and J.-C. de Hemptinne. Multicomponent equations of state for electrolytes. *AIChE Journal*, 53(4):989–1005, 2007.

[104] X. Courtial, N. Ferrando, J.-C. De Hemptinne, and P. Mougin. Electrolyte CPA equation of state for very high temperature and pressure reservoir and basin applications. *Geochimica et Cosmochimica Acta*, 142:1–14, 2014.

[105] B. Maribo-Mogensen, K. Thomsen, and G. M. Kontogeorgis. An electrolyte CPA equation of state for mixed solvent electrolytes. *AIChE Journal*, 61(9):2933–2950, 2015.

[106] B. Maribo-Mogensen, G. M. Kontogeorgis, and K. Thomsen. Modeling of dielectric properties of aqueous salt solutions with an equation of state. *The Journal of Physical Chemistry B*, 117(36):10523–33, 2013.

[107] B. Maribo-Mogensen, G. M. Kontogeorgis, and K. Thomsen. Modeling of dielectric properties of complex fluids with an equation of state. *The Journal of Physical Chemistry B*, 117(12):3389–97, 2013.

[108] P. Vimalchand and M. D. Donohue. Thermodynamics of quadrupolar molecules: the perturbed-anisotropic-chain theory. *Industrial & Engineering Chemistry Fundamentals*, 24(2):246–257, 1985.

[109] G. Jin and M. D. Donohue. An equation of state for electrolyte solutions. 1. Aqueous systems containing strong electrolytes. *Industrial & Engineering Chemistry Research*, 27(6):1073–1084, 1988.

[110] G. Jin and M. D Donohue. An equation of state for electrolyte solutions. 2. Single volatile weak electrolytes in water. *Industrial & Engineering Chemistry Research*, 27 (9):1737–1743, 1988.

[111] G. Jin and M. D. Donohue. An equation of state for electrolyte solutions. 3. aqueous solutions containing multiple salts. *Industrial & Engineering Chemistry Research*, 30 (1):240–248, 1991.

[112] G. D. Ikonomou and M. D. Donohue. Thermodynamics of hydrogen-bonded molecules: The associated perturbed anisotropic chain theory. *AIChE Journal*, 32(10): 1716–1725, 1986.

[113] I. G. Economou and M. D. Donohue. Equation of state with multiple associating sites for water and water-hydrocarbon mixtures. *Industrial & Engineering Chemistry Research*, 31(10):2388–2394, 1992.

[114] I. G. Economou, C. J. Peters, and J. de Swaan Arons. Water-salt phase equilibria at elevated temperatures and pressures: model development and mixture predictions. *The Journal of Physical Chemistry*, 99(16):6182–6193, 1995.

[115] X. Ji, S. P. Tan, H. Adidharma, and M. Radosz. Statistical associating fluid theory coupled with restrictive primitive model extended to bivalent ions. SAFT2: 2.Brine/seawater properties predicted. *The Journal of Physical Chemistry B*, 110 (33):16700–16706, 2006.

[116] B.-S. Lee and K.-C. Kim. Modeling of aqueous electrolyte solutions based on perturbed-chain statistical associating fluid theory incorporated with primitive mean spherical approximation. *Korean Journal of Chemical Engineering*, 26(6):1733–1747, 2009.

[117] J. Rozmus, J.-C. de Hemptinne, A. Galindo, S. Dufal, and P. Mougin. Modeling of strong electrolytes with ePPC-SAFT up to high temperatures. *Industrial & Engineering Chemistry Research*, 52(29):9979–9994, 2013.

[118] H. Jiang, A. Z. Panagiotopoulos, and I. G. Economou. Modeling of CO_2 solubility in single and mixed electrolyte solutions using statistical associating fluid theory. *Geochimica et Cosmochimica Acta*, 176:185–197, 2016.

[119] A. Gil-Villegas, A. Galindo, P. J. Whitehead, S. J. Mills, G. Jackson, and A. N. Burgess. Statistical associating fluid theory for chain molecules with attractive potentials of variable range. *The Journal of Chemical Physics*, 106(10):4168, 1997.

[120] A. Galindo, L. A Davies, A. Gil-Villegas, and G. Jackson. The thermodynamics of mixtures and the corresponding mixing rules in the SAFT-VR approach for potentials of variable range. *Molecular Physics*, 93(2):241–252, 1998.

[121] B. H. Patel, P. Paricaud, A. Galindo, and G. C. Maitland. Prediction of the salting-out effect of strong electrolytes on water + alkane solutions. *Industrial & Engineering Chemistry Research*, 42(16):3809–3823, 2003.

[122] S. Dufal. *Development and application of advanced thermodynamic molecular description for complex reservoir fluids containing carbon dioxide and brines*. PhD thesis, Imperial College London, 2013.

[123] B. Behzadi, B. H. Patel, A. Galindo, and C. Ghotbi. Modeling electrolyte solutions with the SAFT-VR equation using Yukawa potentials and the mean-spherical approximation. *Fluid Phase Equilibria*, 236(1-2):241–255, 2005.

[124] B. Behzadi, C. Ghotbi, and A. Galindo. Application of the simplex simulated annealing technique to nonlinear parameter optimization for the SAFT-VR equation of state. *Chemical Engineering Science*, 60(23):6607–6621, 2005.

[125] S. P. Tan, H. Adidharma, and M. Radosz. Statistical Associating Fluid Theory Coupled with Restricted Primitive Model To Represent Aqueous Strong Electrolytes. *Industrial & Engineering Chemistry Research*, 44(12):4442–4452, 2005.

[126] S. P. Tan, X. Ji, H. Adidharma, and M. Radosz. Statistical associating fluid theory coupled with restrictive primitive model extended to bivalent ions. SAFT2: 1.Single salt + water solutions. *The Journal of Physical Chemistry B*, 110(33):16694–16699, 2006.

[127] H. Adidharma and M. Radosz. Prototype of an engineering equation of state for heterosegmented polymers. *Industrial & Engineering Chemistry Research*, 37(11): 4453–4462, 1998.

[128] X. Ji, S. P. Tan, H. Adidharma, and M. Radosz. Statistical Associating Fluid Theory coupled with restricted primitive model to represent aqueous strong electrolytes: Multiple-salt solutions. *Industrial & Engineering Chemistry Research*, 44(19):7584–7590, 2005.

[129] X. Ji and H. Adidharma. Ion-based SAFT2 to represent aqueous single- and multiple-salt solutions. *Industrial & Engineering Chemistry Research*, 45(22):7719–7728, 2006.

[130] X. Ji and H. Adidharma. Ion-based statistical associating fluid theory (SAFT2) to represent aqueous single-salt solutions at temperatures and pressures up to 473.15 K and 1000 bar. *Industrial & Engineering Chemistry Research*, 46(13):4667–4677, 2007.

[131] X. Ji and H. Adidharma. Ion-based SAFT2 to represent aqueous multiple-salt solutions at ambient and elevated temperatures and pressures. *Chemical Engineering Science*, 63(1):131–140, 2008.

[132] H. Jiang and H. Adidharma. Study of thermodynamic properties of symmetric and asymmetric electrolyte systems in mixture with neutral components: Monte Carlo simulation results and integral equation predictions. *Molecular Simulation*, 41(9): 727–734, 2015.

[133] L. F. Cameretti, G. Sadowski, and J. M. Mollerup. Modeling of aqueous electrolyte solutions with perturbed-chain statistical associated fluid theory. *Industrial & Engineering Chemistry Research*, 44(9):3355–3362, 2005.

[134] C. Held, T. Reschke, S. Mohammad, A. Luza, and G. Sadowski. ePC-SAFT revised. *Chemical Engineering Research and Design*, 92(12):2884–2897, 2014.

[135] C. Held, A. Prinz, V. Wallmeyer, and G. Sadowski. Measuring and modeling alcohol/salt systems. *Chemical Engineering Science*, 68(1):328–339, 2012.

[136] D. Nguyen-Huynh, J.-C. de Hemptinne, R. Lugo, J.-P. Passarello, and P. Tobaly. Modeling liquid–liquid and liquid–vapor equilibria of binary systems containing water with an alkane, an aromatic hydrocarbon, an alcohol or a gas (methane, ethane, CO_2 or H_2S), using group contribution polar perturbed-chain statistical associating fluid theory. *Industrial & Engineering Chemistry Research*, 50(12):7467–7483, 2011.

[137] C. Held and G. Sadowski. Modeling aqueous electrolyte solutions. Part 2. Weak electrolytes. *Fluid Phase Equilibria*, 279(2):141–148, 2009.

[138] T. Reschke, S. Naeem, and G. Sadowski. Osmotic coefficients of aqueous weak electrolyte solutions: influence of dissociation on data reduction and modeling. *The Journal of Physical Chemistry B*, 116(25):7479–7491, 2012.

[139] R. Shahriari, M. Reza Dehghani, and B. Behzadi. Thermodynamic modeling of aqueous ionic liquid solutions using PC-SAFT equation of state. *Industrial & Engineering Chemistry Research*, 51(30):10274–10282, 2012.

[140] H. Jiang and H. Adidharma. Thermodynamic modeling of aqueous ionic liquid solutions and prediction of methane hydrate dissociation conditions in the presence of ionic liquid. *Chemical Engineering Science*, 102:24–31, 2013.

[141] H. Zhao, M. C. dos Ramos, and C. McCabe. Development of an equation of state for electrolyte solutions by combining the statistical associating fluid theory and the mean spherical approximation for the nonprimitive model. *The Journal of Chemical Physics*, 126(24):244503, 2007.

[142] H. Zhao and C. McCabe. Phase behavior of dipolar fluids from a modified statistical associating fluid theory for potentials of variable range. *The Journal of Chemical Physics*, 125(10):104504, 2006.

[143] G. Das, S. Hlushak, M. C. dos Ramos, and C. McCabe. Predicting the thermodynamic properties and dielectric behavior of electrolyte solutions using the SAFT-VR+DE equation of state. *AIChE Journal*, 61(9):3053–3072, 2015.

[144] S. Herzog, J. Gross, and W. Arlt. Equation of state for aqueous electrolyte systems based on the semirestricted non-primitive mean spherical approximation. *Fluid Phase Equilibria*, 297(1):23–33, 2010.

[145] M. S. Wertheim. Fluids with highly directional attractive forces. I. Statistical thermodynamics. *Journal of Statistical Physics*, 35(1-2):19–34, 1984.

[146] M. S. Wertheim. Fluids with highly directional attractive forces. II. Thermodynamic perturbation theory and integral equations. *Journal of Statistical Physics*, 35(1-2): 35–47, 1984.

[147] M. S. Wertheim. Fluids with highly directional attractive forces. III. Multiple attraction sites. *Journal of Statistical Physics*, 42(3-4):459–476, 1986.

[148] M. S. Wertheim. Fluids with highly directional attractive forces. IV. Equilibrium polymerization. *Journal of Statistical Physics*, 42(3-4):477–492, 1986.

[149] M. S. Wertheim. Fluids of dimerizing hard spheres, and fluid mixtures of hard spheres and dispheres. *The Journal of Chemical Physics*, 85(5):2929–2936, 1986.

[150] M. S. Wertheim. Thermodynamic perturbation theory of polymerization. *The Journal of Chemical Physics*, 87(12):7323, 1987.

[151] G. Jackson, W. G. Chapman, and K. E Gubbins. Phase equilibria of associating fluids: Spherical molecules with multiple bonding sites. *Molecular Physics*, 1(65):1–31, 1988.

[152] W. G. Chapman, G. Jackson, and K. E. Gubbins. Phase equilibria of associating fluids. *Molecular Physics*, 65(5):1057–1079, 1988.

[153] W. Sutherland. LII. The viscosity of gases and molecular force. *The London, Edinburgh, and Dublin Philosophical Magazine and Journal of Science*, 36(223):507–531, 1893.

[154] H. Yukawa. On the interaction of elementary particles. I. *Proceedings of the Physico-Mathematical Society of Japan. 3rd Series*, 17:48–57, 1935.

[155] J. E. Lennard-Jones. Cohesion. *Proceedings of the Physical Society*, 43(5):461, 1931.

[156] G. Mie. Zur kinetischen Theorie der einatomigen Körper. *Annalen der Physik (Berlin, Germany)*, 316(8):657–697, 1903.

[157] S. H. Huang and M. Radosz. Equation of state for small, large, polydisperse, and associating molecules. *Industrial & Engineering Chemistry Research*, 29(11):2284–2294, 1990.

[158] F. J. Blas and L. F. Vega. Thermodynamic behaviour of homonuclear and heteronuclear Lennard-Jones chains with association sites from simulation and theory. *Molecular Physics*, 92(1):135–150, 1997.

[159] T. Lafitte, D. Bessieres, M. M. Piñeiro, and J.-L. Daridon. Simultaneous estimation of phase behavior and second-derivative properties using the Statistical Associating Fluid Theory with variable range approach. *The Journal of Chemical Physics*, 124(2): 024509, 2006.

[160] S. Dufal, T. Lafitte, A. Galindo, G. Jackson, and A. J. Haslam. Developing intermolecular-potential models for use with the SAFT-VR Mie equation of state. *AIChE Journal*, 61(9):2891–2912, 2015.

[161] S. Tamouza, J.-P Passarello, P. Tobaly, and J.-C. de Hemptinne. Group contribution method with SAFT EOS applied to vapor liquid equilibria of various hydrocarbon series. *Fluid Phase Equilibria*, 222:67–76, 2004.

[162] S. Tamouza, J.-P. Passarello, P. Tobaly, and J.-C. de Hemptinne. Application to binary mixtures of a group contribution SAFT EOS (GC-SAFT). *Fluid phase equilibria*, 228: 409–419, 2005.

[163] J. Vijande, M. M. Pineiro, D. Bessieres, H. Saint-Guirons, and J. L. Legido. Description of PVT behaviour of hydrofluoroethers using the PC-SAFT EOS. *Physical Chemistry Chemical Physics*, 6(4):766–770, 2004.

[164] A. Tihic, G. M. Kontogeorgis, N. von Solms, M. L. Michelsen, and L. Constantinou. A predictive group-contribution simplified PC-SAFT equation of state: Application to polymer systems. *Industrial & Engineering Chemistry Research*, 47(15):5092–5101, 2007.

[165] M. Banaszak, C. K. Chen, and M. Radosz. Copolymer saft equation of state. thermodynamic perturbation theory extended to heterobonded chains. *Macromolecules*, 29 (20):6481–6486, 1996.

[166] J. Gross, O. Spuhl, F. Tumakaka, and G. Sadowski. Modeling copolymer systems using the perturbed-chain saft equation of state. *Industrial & Engineering Chemistry Research*, 42(6):1266–1274, 2003.

[167] A. Dominik and W. G. Chapman. Thermodynamic model for branched polyolefins using the pc-saft equation of state. *Macromolecules*, 38(26):10836–10843, 2005.

[168] C. McCabe, A. Gil-Villegas, G. Jackson, and F. Del Rio. The thermodynamics of heteronuclear molecules formed from bonded square-well (BSW) segments using the SAFT-VR approach. *Molecular Physics*, 97(4):551–558, 1999.

[169] Y. Peng, K. D. Goff, M. C. dos Ramos, and C. McCabe. Developing a predictive group-contribution-based SAFT-VR equation of state. *Fluid Phase Equilibria*, 277(2): 131–144, 2009.

[170] V. Papaioannou, C. S. Adjiman, G. Jackson, and A. Galindo. Simultaneous prediction of vapour-liquid and liquid-liquid equilibria (VLE and LLE) of aqueous mixtures with the SAFT-γ group contribution approach. *Fluid Phase Equilibria*, 306(1):82–96, 2011.

[171] C. Avendaño, T. Lafitte, A. Galindo, C. S. Adjiman, G. Jackson, and E. A. Müller. SAFT-γ force field for the simulation of molecular fluids. 1. A single-site coarse grained model of carbon dioxide. *The Journal of Physical Chemistry B*, 115(38): 11154–69, 2011.

[172] T.s Lafitte, C. Avendaño, V. Papaioannou, A. Galindo, C. S. Adjiman, G. Jackson, and E. A. Müller. SAFT- γ force field for the simulation of molecular fluids: 3. Coarse-grained models of benzene and hetero-group models of n-decylbenzene. *Molecular Physics*, 110(11-12):1189–1203, 2012.

[173] C. Avendaño, T. Lafitte, C. S. Adjiman, A. Galindo, E. A. Müller, and G. Jackson. SAFT-γ force field for the simulation of molecular fluids: 2. Coarse-grained models of greenhouse gases, refrigerants, and long alkanes. *The Journal of Physical Chemistry B*, 117(9):2717–33, 2013.

[174] T. Lafitte, A. Apostolakou, C. Avendaño, A. Galindo, C. S. Adjiman, E. A. Müller, and G. Jackson. Accurate statistical associating fluid theory for chain molecules formed from Mie segments. *The Journal of Chemical Physics*, 139(15):154504, 2013.

[175] M. Sadeqzadeh, V.s Papaioannou, S. Dufal, C. S. Adjiman, G. Jackson, and A. Galindo. The development of unlike induced association-site models to study the phase behaviour of aqueous mixtures comprising acetone, alkanes and alkyl carboxylic acids with the SAFT-γ Mie group contribution methodology. *Fluid Phase Equilibria*, 407: 39–57, 2016.

[176] V. Papaioannou, F. Calado, T. Lafitte, S. Dufal, M. Sadeqzadeh, G. Jackson, C. S. Adjiman, and A. Galindo. Application of the SAFT-γ Mie group contribution equation of state to fluids of relevance to the oil and gas industry. *Fluid Phase Equilibria*, 416: 104–119, 2016.

[177] S. Dufal, T. Lafitte, A. J. Haslam, A. Galindo, G. N. I. Clark, C. Vega, and G. Jackson. The A in SAFT: Developing the contribution of association to the Helmholtz free energy within a Wertheim TPT1 treatment of generic Mie fluids. *Molecular Physics*, 113(9–10):948–984, 2015.

[178] L. L. Lee. *Molecular Thermodynamics of Nonideal Fluids*. Butterworth, Boston, 1988.

[179] J. A. A. Barker and D. Henderson. Perturbation theory and equation of state for fluids: The square-well potential. *The Journal of Chemical Physics*, 47(8):2856–2861, 1967.

[180] J. A. A. Barker and D. Henderson. Perturbation theory and equation of state for fluids. II. A successful theory of liquids. *The Journal of Chemical Physics*, 47(11): 2856–2861, 1967.

[181] J. A. Barker and D. Henderson. What is "liquid"? Understanding the states of matter. *Review of Modern Physics*, 48(4):587–671, 1976.

[182] T. Boublík. Hard-sphere equation of state. *The Journal of Chemical Physics*, 53(1): 471, 1970.

[183] G. A. Mansoori. Equilibrium thermodynamic properties of the mixture of hard spheres. *The Journal of Chemical Physics*, 54(4):1523, 1971.

[184] L. S. Ornstein and F. Zernike. Fortuitous density changes and opalescence at the critical point of an element. *Proceedings of the Royal Academy of Sciences of Amsterdam*, 23: 582, 1914.

[185] J. L. Lebowitz. Exact solution of generalized Percus-Yevick equation for a mixture of hard spheres. *Physical Review*, 133(4A), 1964.

[186] G. H. Hudson and J.C. McCoubrey. Intermolecular forces between unlike molecules. A more complete form of the combining rules. *Transactions of the Faraday Society*, 56:761–766, 1960.

[187] A. J. Haslam, A. Galindo, and G. Jackson. Prediction of binary intermolecular potential parameters for use in modelling fluid mixtures. *Fluid Phase Equilibria*, 266(1-2): 105–128, 2008.

[188] D. K. Eriksen. *Molecular-based approaches to modelling carbonate-reservoir fluids: Electrolyte phase equilibria, and the description of the fluid-fluid interface*. PhD thesis, Imperial College London, 2017.

[189] F. London. The general theory of molecular forces. *Transactions of the Faraday Society*, 33(8):8b, 1937.

[190] L. Pauling. Atomic radii and interatomic distances in metals. *Journal of the American Chemical Society*, 69(3):542–553, 1947.

[191] R. D. Shannon. Revised effective ionic radii and systematic studies of interatomic distances in halides and chaleogenides. *Acta Crystallographica, Section A: Crystal Physics, Diffraction, Theoretical and General Crystallography*, 32(5):751–767, 1976.

[192] C. Grossmann and G. Maurer. On the calculation of phase equilibria in aqueous two-phase systems containing ionic solutes. *Fluid Phase Equilibria*, 106(1-2):17–25, 1995.

[193] D. W. Marquardt. An algorithm for least-squares estimation of nonlinear parameters. *Journal of the Society for Industrial and Applied Mathematics*, 11(2):431–441, 1963.

[194] K. Levenberg. A method for the solution of certain non-linear problems in least squares. *Quarterly of Applied Mathematics*, 2:164–168, 1944.

[195] K. P. Jensen and W. L. Jorgensen. Halide, ammonium, and alkali metal ion parameters for modeling aqueous solutions. *Journal of Chemical Theory and Computation*, 2(6): 1499–1509, 2006.

[196] I. Gladich, P. Shepson, I. Szleifer, and M. Carignano. Halide and sodium ion parameters for modeling aqueous solutions in TIP5P-Ew water. *Chemical Physics Letters*, 489(1):113–117, 2010.

[197] A. A. Rashin and B. Honig. Reevaluation of the Born model of ion hydration. *The Journal of Physical Chemistry*, 89(26):5588–5593, 1985.

[198] H. C. Helgeson and D. H. Kirkham. Theoretical prediction of the thermodynamic properties of aqueous electrolytes at high pressures and temperatures. III. Equation of state for aqueous species at infinite dilution. *American Journal of Science*, 276(2): 97–240, 1976.

[199] Y. Marcus. Thermodynamics of solvation of ions. Part 5.—Gibbs free energy of hydration at 298.15 K. *Journal of the Chemical Society, Faraday Transactions*, 87 (18):2995–2999, 1991.

[200] W. R Fawcett. Thermodynamic parameters for the solvation of monatomic ions in water. *The Journal of Physical Chemistry B*, 103(50):11181–11185, 1999.

[201] D. M. Camaioni and C. A. Schwerdtfeger. Comment on "accurate experimental values for the free energies of hydration of H^+, OH^-, and H_3O^+". *The Journal of Physical Chemistry A*, 109(47):10795–10797, 2005.

[202] D. R. Lide, editor. *CRC Handbook of Chemistry and Physics*. CRC Press, London, UK, 86th edition, 2005. ISBN 0849304865.

[203] N. C. Pyper, C. G. Pike, and P. P. Edwards. The polarizabilities of species present in ionic solutions. *Molecular Physics*, 76(2):353–372, 1992.

[204] L. M. Branscomb. Photodetachment cross section, electron affinity, and structure of the negative hydroxyl ion. *Physical Review*, 148(1):11, 1966.

[205] S. Klein, E. Kochanski, and A. Strich. Electric properties of the oxonium ion in its ground and two lowest excited states. *Chemical Physics Letters*, 260(1):34–42, 1996.

[206] M. I. Al-Joboury and D. W. Turner. Molecular photoelectron spectroscopy. Part VI. Water, methanol, methane, and ethane. *Journal of the Chemical Society B: Physical Organic*, pages 373–376, 1967.

[207] R. Heyrovská. Volumes of ions, ion pairs, and electrostriction of alkali halides in aqueous solutions at 25° C. *Marine Chemistry*, 70(1):49–59, 2000.

[208] M. Eigen. Proton Transfer, acid-base catalysis, and enzymatic hydrolysis. Part I: Elementary processes. *Angewandte Chemie International Edition in English*, 3(1): 1–19, 1964.

[209] O. Markovith and N. Agmon. Structure and energetics of the hydronium hydration shells. *The Journal of Physical Chemistry A*, 111(12):2253–2256, 2007.

[210] W. H. Robertson, E. G. Diken, E. A. Price, J.-W. Shin, and M. A. Johnson. Spectroscopic determination of the OH^- solvation shell in the $OH^-\cdot(H_2O)_n$ clusters. *Science*, 299(5611):1367–1372, 2003.

[211] A. Apelblat. The vapour pressures of saturated aqueous LiCl, NaBr, $NaNO_3$, NH_4NO_3), and NH_4Cl at temperatures from 283 K to 313 K. *The Journal of Chemical Thermodynamics*, 25(1):63–71, 1993.

[212] K. R. Patil, A. D. Tripathi, G. Pathak, and S. S. Katti. Thermodynamic properties of aqueous electrolyte solutions. 2. Vapor pressure of aqueous solutions of NaBr, NaI, KCl, KBr, KI, RbCl, CsCl, CsBr, CsI, $MgCl_2$, $CaCl_2$, $CaBr_2$, CaI_2, $SrCl_2$, $SrBr_2$, SrI_2, $BaCl_2$, and $BaBr_2$. *Journal of Chemical & Engineering Data*, 36(2):225–230, 1991.

[213] K. R. Patil, F. Olivé, and A. Coronas. Experimental measurements of vapor pressures of electrolyte solutions by differential static method. *Journal of Chemical Engineering of Japan*, 27(5):680–681, 1994.

[214] V. K. Filippov, M. A. Yakimov, V. M. Makarevskii, and L. G. Lukina. Activity of Water in the CdCl–KCl–H_2O, CdBr–KBr–H_2O, and CdI–KI–H_2O Ternary Systems at 25°C. *Russian Journal of Inorganic Chemistry*, 16:1653–1655, 1971.

[215] I. M. Abdulagatov and N. D. Azizov. Densities, apparent and partial molar volumes of aqueous KBr solutions at high temperatures and high pressures. *Fluid Phase Equilibria*, 246(1):96–110, 2006.

[216] J. Kiepe, A. Karine de Araújo Rodrigues, S. Horstmann, and J. Gmehling. Experimental determination and correlation of liquid density data of electrolyte mixtures containing water or methanol. *Industrial & Engineering Chemistry Research*, 42(9): 2022–2029, 2003.

[217] N. Rohman, N. N. Dass, and S. Mahiuddin. Isentropic compressibility, effective pressure, classical sound absorption and shear relaxation time of aqueous lithium bromide, sodium bromide and potassium bromide solutions. *Journal of Molecular Liquids*, 100(3):265–290, 2002.

[218] M. Taha and M.-J. Lee. Interaction of biological buffers with electrolytes: Densities of aqueous solutions of two substituted aminosulfonic acids and ionic salts from T=(298.15 to 328.15) K. *The Journal of Chemical Thermodynamics*, 41(5):705–715, 2009.

[219] W. J. Hamer and Y.-C. Wu. Osmotic coefficients and mean activity coefficients of uni-univalent electrolytes in water at 25°C. *The Journal of Physical Chemistry Reference Data*, 1(4):1047–1100, 1972.

[220] A. Apelblat. Vapour pressures of $H_2{}^{16}O$ and $H_2{}^{18}O$, and saturated aqueous solutions of KCl fromT= 298K toT= 318K by the isoteniscopic method. *The Journal of Chemical Thermodynamics*, 30(10):1191–1198, 1998.

[221] S. Behme, G. Sadowski, and W. Arlt. Improved instrument for measuring vapor-pressure above concentrated polymer-solutions and use of the measured data in thermodynamic simulation of an extruder. *Chemie Ingenieur Technik*, 67(6):757–760, 1995.

[222] T. M. Herrington and R. J. Jackson. Osmotic coefficients of aqueous potassium chloride solutions at 50 and 70°C. *Journal of the Chemical Society, Faraday Transactions 1*, 69:1635–1647, 1973.

[223] J. I. Partanen and A. K. Covington. Re-evaluation of the thermodynamic activity quantities in aqueous sodium and potassium chloride solutions at 25°C. *Journal of Chemical & Engineering Data*, 54(2):208–219, 2008.

[224] E. Amado and L. H. Blanco. Osmotic and activity coefficients of aqueous solutions of KCl at temperatures of 283.15, 288.15, 293.15 and 298.15 K: a new isopiestic apparatus. *Fluid Phase Equilibria*, 226:261–265, 2004.

[225] S. Manohar, J. Ananthaswamy, and G. Atkinson. Activity coefficients of KCl and ionic interactions in the system KCl–Me_4NCl–H_2O at 25, 35 and 45°C. *Journal of the Chemical Society, Faraday Transactions*, 88(7):991–995, 1992.

[226] R. T. Pabalan and K. S. Pitzer. Apparent molar heat capacity and other thermodynamic properties of aqueous potassium chloride solutions to high temperatures and pressures. *Journal of Chemical & Engineering Data*, 33(3):354–362, 1988.

[227] A. Lannung. Measurement of the vapor pressure of aqueous solutions of the alkali halogenides. *Zeitschrift für Physikalische Chemie, Abteilung A: Chemische Thermodynamik, Kinetik, Elektrochemie, Eigenschaftslehre*, 170:134–144, 1934.

[228] J. E. Desnoyers, M. Arel, G. Perron, and C. Jolicoeur. Apparent molal volumes of alkali halides in water at 25°C. Influence of structural hydration interactions on the concentration dependence. *The Journal of Physical Chemistry*, 73(10):3346–3351, 1969.

[229] F. J. Millero, G. K. Ward, and P. V. Chetirkin. Relative sound velocities of sea salts at 25°C. *Journal of the Acoustical Society of America*, 61(6):1492–1498, 1977.

[230] T. G. Pedersen, C. Dethlefsen, and A. Hvidt. Volumetric properties of aqueous solutions of alkali halides. *Carlsberg Research Communications*, 49(3):445–455, 1984.

[231] A. Apelblat and E. Manzurola. Volumetric and thermal properties of some aqueous electrolyte solutions: Part 5. kbr and ki 0.1, 0.5, and 1.0 mol kg^1 solutions at temperatures from t= 278.15 to 338.15 k. *Journal of Molecular Liquids*, 118(1):77–88, 2005.

[232] L. A. Dunn. Apparent molar volumes of electrolytes. Part 2. Some 1–1 electrolytes in aqueous solution at 25°C. *Transactions of the Faraday Society*, 64:1898–1903, 1968.

[233] D. J. P. Out and J. M. Los. Viscosity of aqueous solutions of univalent electrolytes from 5 to 95°C. *Journal of Solution Chemistry*, 9(1):19–35, 1980.

[234] D. A. Boryta, A. J. Maas, and C. B. Grant. Vapor pressure-temperature-concentration relation for system LiBr and water (40-70% LiBr). *Journal of Chemical & Engineering Data*, 20(3):316–319, 1975.

[235] K. R. Patil, A. D. Tripathi, G. Pathak, and S. S. Katti. Thermodynamic properties of aqueous electrolyte solutions. 1. Vapor pressure of aqueous solutions of lithium chloride, lithium bromide, and lithium iodide. *Journal of Chemical & Engineering Data*, 35(2):166–168, 1990.

[236] M. Renz. *Determination of the thermophysical properties of aqueous and methyl alcoholic solutions of salts*. Thesis, Universität Essen, 1981.

[237] E. Sada, T. Morisue, and K. Miyahara. Salt effects on vapor-liquid equilibrium of isopropanol-water system. *Journal of Chemical Engineering of Japan*, 8(3):196–201, 1975.

[238] M. M. Palaiologou, I. E. Molinou, and N. G. Tsierkezos. Viscosity studies on lithium bromide in water+ dimethyl sulfoxide mixtures at 278.15 K and 293.15 K. *Journal of Chemical & Engineering Data*, 47(5):1285–1289, 2002.

[239] H. F. Holmes and R. E. Mesmer. An isopiestic study of aqueous solutions of the alkali metal bromides at elevated temperatures. *The Journal of Chemical Thermodynamics*, 30(6):723–741, 1998.

[240] A. N. Campbell and O. N. Bhatnagar. Osmotic and activity coefficients of lithium chloride in water from 50 to 150°C. *Canadian Journal of Chemistry*, 57(19):2542–2545, 1979.

[241] S. K. Chaudhari and K. R. Patil. Thermodynamic properties of aqueous solutions of lithium chloride. *Physics and Chemistry of Liquids*, 40(3):317–325, 2002.

[242] W. Kangro and A. Groeneveld. Concentrated aqueous solutions, I. *Zeitschrift für Physikalische Chemie*, 32(1_2):110–126, 1962.

[243] A. Apelblat and E. Manzurola. Volumetric properties of aqueous solutions of LiCl at temperatures from 278.15 K to 338.15 K and molalities (0.1, 0.5, and 1.0) mol kg^1. *The Journal of Chemical Thermodynamics*, 33(9):1133–1155, 2001.

[244] E. Vercher, S. Solsona, M. I. Vázquez, and A. Martınez-Andreu. Apparent molar volumes of lithium chloride in 1-propanol + water in the temperature range from 288.15 to 318.15 K. *Fluid Phase Equilibria*, 209(1):95–111, 2003.

[245] H. F. Gibbard Jr and G. Scatchard. Liquid-vapor equilibrium of aqueous lithium chloride, from 25 to 100°C and from 1.0 to 18.5 molal, and related properties. *Journal of Chemical & Engineering Data*, 18(3):293–298, 1973.

[246] I. M. Abdulagatov and N. D. Azizov. Densities and apparent molar volumes of aqueous LiI solutions at temperatures from (296 to 600) K and at pressures up to 30 MPa. *Journal of Chemical Thermodynamics*, 36(10):829–843, 2004.

[247] J. Safarov. (p,ρ,T) and (p_s,ρ_s,T_s) properties, and apparent molar volumes V_ϕ of LiI (aq) at T= 298.15 to 398.15 K and at pressures up to p= 60 MPa. *Journal of Molecular Liquids*, 123(2):139–145, 2006.

[248] Da. Salavera, X. Esteve, K. R. Patil, A. M. Mainar, and A. Coronas. Solubility, heat capacity, and density of lithium bromide + lithium iodide + lithium nitrate + lithium chloride aqueous solutions at several compositions and temperatures. *Journal of Chemical & Engineering Data*, 49(3):613–619, 2004.

[249] Y. A. Sanmamed, D. González-Salgado, J. Troncoso, C. A. Cerdeirina, and L. Romani. Viscosity-induced errors in the density determination of room temperature ionic liquids using vibrating tube densitometry. *Fluid Phase Equilibria*, 252(1):96–102, 2007.

[250] J. A. Rard and D. G. Archer. Isopiestic investigation of the osmotic and activity coefficients of aqueous NaBr and the solubility of $NaBr{\cdot}2H_2O$(cr) at 298.15 K: Thermodynamic properties of the NaBr + H2O system over wide ranges of temperature and pressure. *Journal of Chemical & Engineering Data*, 40(1):170–185, 1995.

[251] A. Mersrnann. Phase equilibria and phase diagrams of electrolytes. Chemistry Data Series, Vol. XI, Part 1. *Chemie Ingenieur Technik*, 64(6):585–585, 1992.

[252] K. Nasirzadeh, D. Zimin, R. Neueder, and W. Kunz. Vapor-pressure measurements of liquid solutions at different temperatures: apparatus for use over an extended temperature range and some new data. *Journal of Chemical & Engineering Data*, 49 (3):607–612, 2004.

[253] L. H. Blanco and A. P. Rozo. Osmotic and activity coefficients of trimethyloctylammonium bromide and decyltrimethylammonium bromide in aqueous solutions as a function of temperature. *Journal of Solution Chemistry*, 39(12):1819–1827, 2010.

[254] H. F. Gibbard Jr, G. Scatchard, R. A. Rousseau, and J. L. Creek. Liquid-vapor equilibrium of aqueous sodium chloride, from 298 to 373 K and from 1 to 6 mol kg−1, and related properties. *Journal of Chemical & Engineering Data*, 19(3):281–288, 1974.

[255] A. G. Guseinov, M. V. Imanova, R. T. Akhundov, A. D. Tairov, and A. I. Iskenderov. Experimental investigation of the thermal properties of aqueous NaF solutions. *Izvestiya Vysshikh Uchebnykh Zavedenii, Neft i Gaz*, 9–10:45–47, 1991.

[256] F. J. Millero and J. H. Knox. Apparent molal volumes of aqueous NaF, Na_2SO_4, KCl, K_2SO_4, MgCl, and $MgSO_4$ solutions at 0 and 50°C. *Journal of Chemical & Engineering Data*, 18(4):407–411, 1973.

[257] H. Yamamoto, T. Terano, M. Yanagisawa, and J. Tokunaga. Salt effect of $CaCl_2$, NH_4I and NaI on vapor-liquid equilibrium of ethanol + water system at 298.15 K. *Canadian Journal of Chemical Engineering*, 73(5):779–783, 1995.

[258] M. Palma and J.-P. Morel. Viscosity of ternary mixtures. II. Water-*tert*-butyl alcohol-alkali halides. *Journal of Solution Chemistry*, 8(11):767–777, 1979.

[259] K.-L. Zho, Y. Zhao, L.-X. Yang, Q. Liu, and J.-J. Wang. Volumetric properties for the electrolyte (NaCl, NaBr and NaI) monosaccharide (D-mannose and D-ribose)-water systems at 298.15 K. *Journal of the Chinese Chemical Society (Peking)*, 53(4): 961–970, 2006.

[260] A. Stagis and K. P. Mishchenko. Some thermodynamic characteristics of aqueous solutions of salts at the full-hydration limit in the temperature range from -10 to +50°C. *Journal of General Chemistry of the USSR*, 40(10):2127–2129, 1970.

[261] G. P. Baxter and C. C. Wallace. Changes in volume upon solution in water of the halogen salts of the alkali metals. II. *Journal of the American Chemical Society*, 38 (1):70–105, 1916.

[262] M. K. Karapetyants, V. A. Vasilev, B. V. Mikhailin, and V. N. Strakhov. Heat-capacity and density of aqueous-solutions of sodium and rubidium bromides at 25°C. *Zhurnal Fizicheskoi Khimii*, 53(1):207–209, 1979.

[263] A. G. Ostroff, B. S. Snowden Jr, and D. E. Woessner. Viscosities of protonated and deuterated water solutions of alkali metal chlorides. *The Journal of Physical Chemistry*, 73(8):2784–2785, 1969.

[264] M. Singh and M. Pandey. Excess viscosities (η^E) of glycine with halide salts of alkali metals of IA group in aqueous solutions at 310.15 K for structural interactions. *Journal of the Indian Chemical Society*, 82(12):1091–1102, 2005.

[265] F. C. Quiroz. *Molecular thermodynamics of strong electrolytes at high temperatures*. PhD thesis, RWTH Aachen, 1986.

[266] R. Haase, H. Naas, and H. Thumm. Experimental investigation on the thermodynamic behavior of concentrated halogen hydrogen acids. *Zeitschrift für Physik Chem.*, 37: 210–229, 1963.

[267] M. P. Susarev and R. V. Prokofeva. Liquid-vapour equilibrium in the system water-hydrogen chloride-ferric chloride at 25°C. *Zhurnal Fizicheskoi Khimii*, 37(11):2408–2412, 1963.

[268] T. M. Herrington, A. D. Pethybridge, and M. G. Roffey. Densities of hydrochloric, hydrobromic, hydriodic, and perchloric acids from 25 to 75°C at 1 atm. *Journal of Chemical & Engineering Data*, 30(3):264–267, 1985.

[269] P. Rizzo, J. G. Albright, and D. G. Miller. Measurements of interdiffusion coefficients and densities for the system HCl+H_2O at 25°C. *Journal of Chemical & Engineering Data*, 42(3):623–630, 1997.

[270] G. Wüster, G. Wozny, and Z. Giazitzoglou. Thermodynamic description of the electrolytic mixed system HBr-H_2O at moderate pressures by use of gas phase p, v, T and total pressure measurements. *Fluid Phase Equilibria*, 6(1):93–111, 1981.

[271] N. Elm, J. Zipprian, and K. Schaber. Vapour-liquid equilibria of binary and ternary aqueous systems with HCl, HBr and $CaCl_2$ at highly diluted vapour phases. *Fluid Phase Equilibria*, 189(1):163–178, 2001.

[272] J. B. Macaskill and R. G. Bates. Osmotic coefficients and activity coefficients of aqueous hydrobromic acid solutions at 25°C. *Journal of Solution Chemistry*, 12(9): 607–619, 1983.

[273] L. S. Lilich and M. D. Anikeeva. Vapor pressure in the systems CaX_2 - HX - H_2O. *Zhurnal Neorganicheskoi Khimii*, 4(11):2630–2634, 1959.

[274] T. M. Herrington, A. D. Pethybridge, and M. G. Roffey. Densities of aqueous lithium, sodium and potassium hydroxides from 25 to 75°C at 1 atm. *Journal of Chemical & Engineering Data*, 31(1):31–34, 1986.

[275] G. Vázquez, E. Alvarez, R. Varela, A. Cancela, and J. M. Navaza. Density and viscosity of aqueous solutions of sodium dithionite, sodium hydroxide, sodium dithionite + sucrose, and sodium dithionite + sodium hydroxide + sucrose from 25°C to 40°C. *Journal of Chemical & Engineering Data*, 41(2):244–248, 1996.

[276] V. P. Mashovets, B. S. Krumgalz, I. A. Dibrov, and R. P. Matveeva. Vapor pressure of KOH solutions up to 400°C and activity of water in LiOH, NaOH and KOH solutions over a wide range of concentrations. *Russian Journal of Applied Chemistry*, 38:2294, 1965.

[277] H. R. Corti, R. F. Prini, and F. Svarc. Densities and partial molar volumes of aqueous solutions of lithium, sodium, and potassium hydroxides up to 250°C. *Journal of Solution Chemistry*, 19(8):793–809, 1990.

[278] G. Tammann. The vapor tensions of solutions. *Zeitschrift für Physik Chem. (Leipzig)*, 2:42–47, 1888.

[279] H. C. Jones and H. P. Bassett. The approximate composition of the hydrates formed by certain electrolytes in aqueous solutions at different concentrations. *Journal of the American Chemical Society*, 33:534–586, 1905.

[280] R. N. Goldberg and R. L. Nuttall. Evaluated activity and osmotic coefficients for aqueous solutions: the alkaline earth metal halides. *Journal of Physical and Chemical Reference Data*, 7(1):263–310, 1978.

[281] E. Rodil and J. H. Vera. The activity of ions: analysis of the theory and data for aqueous solutions of $MgBr_2$, $CaBr_2$ and $BaBr_2$ at 298.2 K. *Fluid Phase Equilibria*, 205(1):115–132, 2003.

[282] Z. Adamcova and J. Farkova. Vapor pressure of water over aqueous solutions of $MgCl_2$ at the temperatures of 25–80°C and concentrations of 0.82–5.08 mol/kg and calculation of thermodynamic quantities. *Papers of the Prague Institute of Chemical Technology, N: Physical Chemistry*, 7:69–83, 1986.

[283] L. S. Lee, I. C. Ho, C. H. Lin, and C. L. Lin. Measurements, correlations, and estimations of the vapor pressures of $CaCl_2$, $MgCl_2$, and $BaCl_2$ aqueous solutions between 298.15 K and 328.15 K. *Journal of the Chinese Institute of Chemical Engineers*, 36(3):271–280, 2005.

[284] T. Sako, T. Hakuta, and H. Yoshitome. Vapor pressures of binary (H_2O-HCl,-$MgCl_2$, and -$CaCl_2$) and ternary (H_2O-$MgCl_2$-$CaCl_2$) aqueous solutions. *Journal of Chemical & Engineering Data*, 30(2):224–228, 1985.

[285] A. L. Surdo, E. M. Alzola, and F. J. Millero. The (p,V,T) properties of concentrated aqueous electrolytes I. Densities and apparent molar volumes of NaCl, Na_2SO_4, $MgCl_2$, and $MgSO_2$ solutions from 0.1 mol kg^{-1} to saturation and from 273.15 to 323.15 K. *The Journal of Chemical Thermodynamics*, 14(7):649–662, 1982.

[286] P. P. S. Saluja, D. J. Jobe, J. C. LeBlanc, and R. J. Lemire. Apparent molar heat capacities and volumes of mixed electrolytes:[NaCl (aq)+ $CaCl_2$ (aq)], [NaCl (aq)+ $MgCl_2$ (aq)], and [$CaCl_2$ (aq)+ $MgCl_2$ (aq)]. *Journal of Chemical & Engineering Data*, 40(2):398–406, 1995.

[287] J. A. Rard and D. G. Miller. Isopiestic determination of the osmotic and activity coefficients of aqueous magnesium chloride solutions at 25°C. *Journal of Chemical & Engineering Data*, 26(1):38–43, 1981.

[288] M. A. Bagherinia, M. Giahi, M. Pournaghdy, and G. R. Vaghar. Thermodynamic investigation of the ternary mixed aqueous electrolyte ($MgCl_2$+ $MgSO_4$) system by potentiometric method at T= 298.15 K. *The Journal of Chemical Thermodynamics*, 44(1):169–176, 2012.

[289] R. A. Robinson and R. H. Stokes. A thermodynamic study of bivalent metal halides in aqueous solution. Part I. The activity coefficients of magnesium halides at 25°C. *Transactions of the Faraday Society*, 6:733–734, 1940.

[290] R. H. Stokes. A thermodynamic study of bivalent metal halides in aqueous solution. Part XVII—Revision of data for all 2:1 and 1:2 electrolytes at 25°C, and discussion of results. *Transactions of the Faraday Society*, 44:259–307, 1948.

[291] W. Grzybkowski and G. Atkinson. Thermodynamics of concentrated electrolyte mixtures. Part 8. Apparent molal volumes, adiabatic compressibilities, and hydration numbers of aqueous zinc bromide, calcium bromide, and sodium bromide at 25°C. *Journal of Chemical & Engineering Data*, 31(3):309–312, 1986.

[292] M. S. Gruszkiewicz and J. M. Simonson. Vapor pressures and isopiestic molalities of concentrated $CaCl_2$ (aq), $CaBr_2$ (aq), and NaCl (aq) to T= 523 K. *The Journal of Chemical Thermodynamics*, 37(9):906–930, 2005.

[293] M. F. Bechtold and R. F. Newton. The vapor pressures of salt solutions. *Journal of the American Chemical Society*, 62(6):1390–1393, 1940.

[294] M. Filiz and J. Gülen. Investigation of the aqueous salt solutions of some first and second group metals at various pressures. *Fluid Phase Equilibria*, 267(1):18–22, 2008.

[295] A. Lannung. Measurements of the vapor pressure of the system calcium chloride – water. *Zeitschrift für Anorganische und Allgemeine Chemie*, 228:1–18, 1936.

[296] B. Li, Y. Luo, and Z. Zhu. Vapor-liquid equilibria for salt-containing systems by equation of state — Measurement and correlation of vapor pressures for salt solutions with single solvent. *Journal of the Chinese Institute of Chemical Engineers*, 1(2): 102–110, 1986.

[297] L. S. Lilich and M. D. Anikeeva. Study of the thermodynamical functions of the solutions $CaCl_2 – H_2O$, NaCl – H_2O and $CaCl_2$ – NaCl – H_2O. *Vestnik Leningradskogo Universiteta, Seriya 4: Fizika, Khimiya*, 4:85–93, 1967.

[298] L. S. Lilich and M. D. Anikeeva. Vapor pressure in systems: $MeCl_2$ – HCl – H_2O 2. The System $CaCl_2$ – HCl – H2O. *Vestnik Leningradskogo Universiteta, Seriya 4: Fizika, Khimiya*, 22:97–103, 1956.

[299] A. I. Mun. Vapor pressure of the systems NaCl - $CaCl_2$ - H_2O and KCl - $CaCl_2$ - H_2O. *Journal of General Chemistry of the USSR*, 26(4):1161–1165, 1956.

[300] E. Plake. Boiling point elevation of aqueous solutions of strong electrolytes. *Zeitschrift für Physikalische Chemie, Abteilung A: Chemische Thermodynamik, Kinetik, Elektrochemie, Eigenschaftslehre*, 172:113–128, 1935.

[301] N. V. Sidgwick and E. K. Ewbank. CCCII.—The measurement of the vapour pressures of aqueous salt solutions by the depression of the freezing point of nitrobenzene. *Journal of the Chemical Society, Transactions*, 125:2268–2273, 1924.

[302] R. H. Stokes and R. A. Robinson. Standard solutions for humidity control at 25°C. *Industrial and Engineering Chemistry*, 41(9):2013–2013, 1949.

[303] T. Isono. Density, viscosity, and electrolytic conductivity of concentrated aqueous electrolyte solutions at several temperatures. Alkaline-earth chlorides, lanthanum chloride, sodium chloride, sodium nitrate, sodium bromide, potassium nitrate, potassium bromide, and cadmium nitrate. *Journal of Chemical & Engineering Data*, 29(1): 45–52, 1984.

[304] J. A. Rard and S. L. Clegg. Critical evaluation of the thermodynamic properties of aqueous calcium chloride. 1. Osmotic and activity coefficients of 0–10.77 mol kg^{-1} aqueous calcium chloride solutions at 298.15 K and correlation with extended Pitzer ion-interaction models. *Journal of Chemical & Engineering Data*, 42(5):819–849, 1997.

[305] R. F. Platford. Osmotic coefficients of aqueous solutions of seven compounds at 0°C. *Journal of Chemical & Engineering Data*, 18(2):215–217, 1973.

[306] H. G. McLeod and A. R. Gordon. The thermodynamics of aqueous solutions of calcium chloride at temperatures from 15-35°C from EMF measurements on cells with transference. *Journal of the American Chemical Society*, 68(1):58–60, 1946.

[307] T. M. Davis, L. M. Duckett, C. E. Garvey, J. M. Hollifield, and C. S. Patterson. Osmotic coefficients of aqueous lithium chloride and calcium chloride from their isopiestic ratio to sodium chloride at 50°C. *Journal of Chemical & Engineering Data*, 31(1):54–55, 1986.

[308] C. W. Childs and R. F. Platford. Excess free energies of mixing at temperatures below 25°C . Isopiestic measurements on the systems H_2O-NaCl-Na_2SO_4 and H_2O-NaCl-$MgSO_4$. *Australian Journal of Chemistry*, 24(12):2487–2491, 1971.

[309] S. J. Baabor, M. A. Gilchrist, and E. J. Delgado. Isopiestic study of (calcium chloride+water) and (calcium chloride+magnesium chloride+water) at T=313.15 K. *The Journal of Chemical Thermodynamics*, 33(4):405–411, 2001.

[310] J. Ma, X. Zhang, K. Zhuo, H. Liu, and J. Wang. Activity coefficients of $CaCl_2$ in (serine or proline + water) mixtures at T=298.15 K. *The Journal of Chemical Thermodynamics*, 42(5):689–694, 2010.

[311] A. C. Schneider, C. Pasel, M. Luckas, K. G. Schmidt, and J. D. Herbell. Determination of ion activity coefficients in aqueous solutions with the aid of ion-selective electrodes. *Chemie Ingenieur Technik*, 75(3):244–249, 2003.

[312] K. Zhuo, H. Liu, H. Zhang, Y. Liu, and J. Wang. Activity coefficients of $CaCl_2$ in (maltose+water) and (lactose+water) mixtures at 298.15 K. *The Journal of Chemical Thermodynamics*, 40(5):889–896, 2008.

[313] R. A. Robinson. A thermodynamic study of bivalent metal halides in aqueous solution. Part IX. The activity coefficients of some alkaline earth metal bromides and iodides. *Transactions of the Faraday Society*, 38:445–446, 1942.

[314] J. A. Rard and D. G. Miller. Isopiestic determination of the osmotic and activity coefficients of aqueous CsCl, $SrCl_2$, and mixtures of NaCl and CsCl at 25°C. *Journal of Chemical & Engineering Data*, 27(2):169–173, 1982.

[315] J. B. Macaskill, D. R. White Jr, R. A. Robinson, and R. G. Bates. Isopiestic measurements on aqueous mixtures of sodium chloride and strontium chloride. *Journal of Solution Chemistry*, 7(5):339–347, 1978.

[316] S. L. Clegg, J. A. Rard, and D. G. Miller. Isopiestic determination of the osmotic and activity coefficients of NaCl + $SrCl_2$ + H_2O at 298.15 K and representation with an extended ion-interaction model. *Journal of Chemical & Engineering Data*, 50(4): 1162–1170, 2005.

[317] R. N. Roy, L. N. Roy, W. B. Davis, D. W. Larkin, D. Willard, D. A. Johnson, and F. J. Millero. The thermodynamic behavior of hydrogen bromide in aqueous solutions of barium bromide. *The Journal of Chemical Thermodynamics*, 25(1):155–172, 1993.

[318] C. S. Patterson, L. O. Gilpatrick, and B. A. Soldano. 545. The osmotic behaviour of representative aqueous salt solutions at 100°. *Journal of the Chemical Society*, pages 2730–2734, 1960.

[319] K. S. Pitzer, J. C. Peiper, and R. H. Busey. Thermodynamic properties of aqueous sodium chloride solutions. *Journal of Physical and Chemical Reference Data*, 13(1): 1–102, 1984.

[320] H. S. Harned and L. F. Nims. The thermodynamic properties of aqueous sodium chloride solutions from 0 to 40 °. *Journal of the American Chemical Society*, 54(2): 423–432, 1932.

[321] H. S. Harned and M. A. Cook. The thermodynamics of aqueous sodium chloride solutions from 0 to 40 °from electromotive force measurements. *Journal of the American Chemical Society*, 61(2):495–497, 1939.

[322] G. J. Janz and A. R. Gordon. The thermodynamics of aqueous solutions of sodium chloride at temperatures from 15-45°C from e.m.f. measurements on cells with transference. *Journal of the American Chemical Society*, 65(2):218–221, 1943.

[323] J. Kiepe and M. Topphoff. Unpublished. Accessed on DETHERM Thermophysical Database., 1999.

[324] X. Ji, X. Lu, S. Li, L. Zhang, Y. Wang, and J. Shi. Determination of the activity coefficients of NaCl in the system NaCl–NH_4Cl–H_2O. *Journal of Solution Chemistry*, 30(5):463–473, 2001.

[325] F. Sirbu, O. Iulian, A. C. Ion, and I. Ion. Activity coefficients of electrolytes in the NaCl + Na_2SO_4 + H_2O ternary system from potential difference measurements at (298.15, 303.15, and 308.15) K. *Journal of Chemical & Engineering Data*, 56(12): 4935–4943, 2011.

[326] J. Yao, W.-D.g Yan, Y.-J. Xu, and S.-J. Han. Activity coefficients for NaCl in MeOH + H_2O by electromotive force measurements at 308.15 K and 318.15 K. *Journal of Chemical & Engineering Data*, 44(3):497–500, 1999.

[327] Donald D Wagman, William H Evans, Vivian B Parker, R. H. Schumm, and I. Halow. The NBS tables of chemical thermodynamic properties. Selected values for inorganic and C1 and C2 organic substances in SI units. *The Journal of Physical Chemistry Reference Data*, 11 Supplement 2, 1982.

[328] V. K. Filippov, L. P. Vivcharik, and E. A. Gubanikhin. Thermodynamic Study of the cadmium iodide-lithium iodide-water system at 25 °C. *Russian Journal of Inorganic Chemistry*, 20(6):941–943, 1975.

[329] Y. Yao, B. Sun, P. S. Song, Z. Zhang, R. L. Wang, and J. Q. Chen. Thermodynamics of lithium-containing aqueous electrolyte solutions. Isopiestic determination of osmotic and activity coefficients in lithium chloride-magnesium chloride-water system at 25°C. *Acta Chimica Sinica (Chinese Edition)*, 50:839–848, 1992.

[330] J. N. Pearce and A. F. Nelson. The vapor pressures of aqueous solutions of lithium nitrate and the activity coefficients of some alkali salts in solutions of high concentration at 25°C. *Journal of the American Chemical Society*, 54(9):3544–3555, 1932.

[331] F. Hernández-Luis, R. Rodríguez-Raposo, and D. Grandoso. Activity coefficients of NaBr in aqueous mixtures with high relative permittivity cosolvent: formamide + water at 298.15 K. *Journal of Chemical & Engineering Data*, 56(10):3940–3948, 2011.

[332] J. A. Rard. Isopiestic determination of the osmotic and activity coefficients of aqueous $MnCl_2$, $MnSO_4$, and RbCl at 25°C. *Journal of Chemical & Engineering Data*, 29(4): 443–450, 1984.

[333] E. Sanz and C. Vega. Solubility of kf and nacl in water by molecular simulation. *The Journal of Chemical Physics*, 126(1):014507, 2007.

[334] F. Moucka, M. Lisal, J. Skvor, J. Jirsak, I. Nezbeda, and W. R. Smith. Molecular simulation of aqueous electrolyte solubility. 2. osmotic ensemble monte carlo methodology for free energy and solubility calculations and application to nacl. *The Journal of Physical Chemistry B*, 115(24):7849–7861, 2011.

[335] F. Moucka, M. Lisal, and W. R. Smith. Molecular simulation of aqueous electrolyte solubility. 3. alkali-halide salts and their mixtures in water and in hydrochloric acid. *The Journal of Physical Chemistry B*, 116(18):5468–5478, 2012.

[336] C. Balarew, C. Christov, V. Valyashko, and S. Petrenko. Thermodynamics of formation of carnallite type double salts. *Journal of Solution Chemistry*, 22(2):173–181, 1993.

[337] Y. G. Vlasov and B. L. Seleznev. Thermodynamics of rubidium iodide and rubidium bromide water system at 25°C. *Russian Journal of Physical Chemistry*, 45(6):772, 1971.

[338] D. K. Eriksen, G. Lazarou, A. Galindo, G. Jackson, C. S. Adjiman, and A. J. Haslam. Development of intermolecular potential models for electrolyte solutions using an electrolyte SAFT-VR Mie equation of state. *Molecular Physics*, 114(18):2724–2749, 2016.

[339] P. Hutacharoen. *Prediction of partition coefficients and solubilities of active pharmaceutical ingredients with the SAFT-γ Mie group-contribution approach*. PhD thesis, Imperial College London, 2017.

[340] J. A. Riddick, W. B. Bunger, and T. K. Sakano. *Organic Solvents*. Wiley, New York, 4th edition, 1986.

[341] A. Trummal, L. Lipping, I. Kaljurand, I. A. Koppel, and I. Leito. Acidity of strong acids in water and dimethyl sulfoxide. *The Journal of Physical Chemistry A*, 120(20): 3663–3669, 2016.

[342] Y. Alexeev, T. L. Windus, C.-G. Zhan, and D. A. Dixon. Accurate heats of formation and acidities for h_3po_4, h_2so_4, and h_2co_3 from *ab initio* electronic structure calculations. *International Journal of Quantum Chemistry*, 102(5):775–784, 2005.

[343] D. Ambrose, J. H. Ellender, C. H. S. Sprake, and R. Townsend. Thermodynamic properties of organic oxygen compounds xlv. the vapour pressure of acetic acid. *The Journal of Chemical Thermodynamics*, 9(8):735–741, 1977.

[344] A. Apelblat, A. Tamir, and M. Wagner. Association in carboxylic acid–aliphatic alcohol mixtures. *Zeitschrift für Physikalische Chemie*, 134(1):1–8, 1983.

[345] E. Lladosa, J. B. Montón, M. C. Burguet, and R. Muñoz. Phase equilibrium for the esterification reaction of acetic acid+ butan-1-ol at 101.3 kpa. *Journal of Chemical & Engineering Data*, 53(1):108–115, 2007.

[346] J. L. Hales, H. A. Gundry, and J. H. Ellender. Liquid densities from 288 to 490 k of four organic oxygen compounds. *The Journal of Chemical Thermodynamics*, 15(3): 211–215, 1983.

[347] F. Comelli, R. Francesconi, and C. Castellari. Liquid-phase enthalpy of mixing for binary mixtures with associated components. the mixture of 1,3-dioxolane-acetic acid. *Journal of Chemical & Engineering Data*, 34(3):284–286, 1989.

[348] T. Sun, D. Ly, and A. S. Teja. Densities of acetic acid+water mixtures at high temperatures and concentrations. *Industrial & engineering chemistry research*, 34(4): 1327–1331, 1995.

[349] S. D. Christian. Liquid–vapor equilibrium in the system acetic acid–propionic acid at 20°. *The Journal of Physical Chemistry*, 61(10):1441–1442, 1957.

[350] A. Apelblat and F. Kohler. Excess gibbs energy of methanol + propionic acid and of methanol + butyric acid. *The Journal of Chemical Thermodynamics*, 8(8):749–756, 1976.

[351] D. Ambrose, J. H. Ellender, H. A. Gundry, D. A. Lee, and R. Townsend. Thermodynamic properties of organic oxygen compounds li. the vapour pressures of some esters and fatty acids. *The Journal of Chemical Thermodynamics*, 13(8):795–802, 1981.

[352] F. Leyva, A. Orjuela, I. Gil, J. Vargas, and G. Rodríguez. Vapor–liquid equilibrium of isoamyl alcohol + isoamyl propionate and propionic acid + isoamyl propionate systems at 50.00, 101.33 and 150.00 kpa. *Fluid Phase Equilibria*, 356:56–62, 2013.

[353] J. M. Costello and S. T. Bowden. The temperature variation of orthobaric density difference in liquid-vapour systems. IV. Fatty acids. *Recueil des Travaux Chimiques des Pays-Bas*, 77(9):803–810, 1958.

[354] A. Estrada-Baltazar, A. De León-Rodríguez, K. R. Hall, M. Ramos-Estrada, and G. A. Iglesias-Silva. Experimental densities and excess volumes for binary mixtures containing propionic acid, acetone, and water from 283.15 to 323.15 K at atmospheric pressure. *Journal of Chemical & Engineering Data*, 48(6):1425–1431, 2003.

[355] M. Behroozi and H. Zarei. Volumetric properties of highly nonideal binary mixtures containing ethanoic acid and propanoic acid with butan-2-ol, methyl-2-propanol, and 2-methyl-2-butanol at different temperatures. *Journal of Chemical & Engineering Data*, 57(4):1089–1094, 2012.

[356] I. Bahadur, N. Deenadayalu, P. Naidoo, and D. Ramjugernath. Density, speed of sound, and refractive index measurements for the binary systems (butanoic acid + propanoic acid, or 2-methyl-propanoic acid) at T=(293.15 to 313.15) K. *The Journal of Chemical Thermodynamics*, 57:203–211, 2013.

[357] S. Singh, I. Bahadur, G. G. Redhi, E. E. Ebenso, and D. Ramjugernath. Density and speed of sound of 1-ethyl-3-methylimidazolium ethyl sulphate with acetic or propionic acid at different temperatures. *Journal of Molecular Liquids*, 199:518–523, 2014.

[358] E. E. Schrier, M. Pottle, and H. A. Scheraga. The influence of hydrogen and hydrophobic bonds on the stability of the carboxylic acid dimers in aqueous solution. *Journal of the American Chemical Society*, 86(17):3444–3449, 1964.

[359] J. Chen, C. L. Brooks, and H. A. Scheraga. Revisiting the carboxylic acid dimers in aqueous solution: Interplay of hydrogen bonding, hydrophobic interactions, and entropy. *The Journal of Physical Chemistry B*, 112(2):242–249, 2008.

[360] N. Calvar, A. Dominguez, and J. Tojo. Vapor–liquid equilibria for the quaternary reactive system ethyl acetate+ ethanol + water + acetic acid and some of the constituent binary systems at 101.3 kPa. *Fluid Phase Equilibria*, 235(2):215–222, 2005.

[361] K. Granados, J. Gracia-Fadrique, A. Amigo, and R. Bravo. Refractive index, surface tension, and density of aqueous mixtures of carboxylic acids at 298.15 K. *Journal of Chemical & Engineering Data*, 51(4):1356–1360, 2006.

[362] S. Amer Amezaga. Vapor-liquid equilibrium at 760 mm of binary systems formed by propionic acid with water and n-amyl, isoamyl, secamyl, tert-amyl, and n-hexyl alcohols. *Anales de Quimica (1968-1979)*, 71:127, 1975.

[363] D. W. Archer and C. B. Monk. Ion-association constants of some acetates by pH (glass electrode) measurements. *Journal of the Chemical Society*, pages 3117–3122, 1964.

[364] P. G. Daniele, A. De Robertis, C. De Stefano, S. Sammartano, and C. Rigano. On the possibility of determining the thermodynamic parameters for the formation of weak complexes using a simple model for the dependence on ionic strength of activity coefficients: Na^+, K^+, and Ca^{2+} complexes of low molecular weight ligands in aqueous solution. *Journal of the Chemical Society, Dalton Transactions*, (11):2353–2361, 1985.

[365] J. L. Oscarson, S. E. Gillespie, J. J. Christensen, R. M. Izatt, and P. R. Brown. Thermodynamic quantities for the interaction of H+ and Na+ with C2H3O2- and Cl- in aqueous solution from 275 to 320°C. *Journal of Solution Chemistry*, 17(9):865–885, 1988.

[366] J. S. Uejio, C. P. Schwartz, A. M. Duffin, W. S. Drisdell, R. C. Cohen, and R. J. Saykally. Characterization of selective binding of alkali cations with carboxylate by x-ray absorption spectroscopy of liquid microjets. *Proceedings of the National Academy of Sciences*, 105(19):6809–6812, 2008.

[367] E. F. Aziz, N. Ottosson, S. Eisebitt, W. Eberhardt, B. Jagoda-Cwiklik, R. Vácha, P. Jungwirth, and B. Winter. Cation-specific interactions with carboxylate in amino acid and acetate aqueous solutions: X-ray absorption and ab initio calculations. *The Journal of Physical Chemistry B*, 112(40):12567–12570, 2008.

[368] E. R. B. Smith and R. A. Robinson. The vapour pressures and osmotic coefficients of solutions of the sodium salts of a series of fatty acids at 25°. *Transactions of the Faraday Society*, 38:70–78, 1942.

[369] G. Douhéret and A. Viallard. Activity coefficients and micellar equilibria. I. The mass action law model applied to aqueous solutions of sodium carboxylates at 298.15 K. *Fluid Phase Equilibria*, 8(3):233–250, 1982.

[370] P. Ekwall and P. Stenius. The properties and structures of aqueous sodium caprylate solutions. VII. Activities of caprylate anions, and counter ion binding to the miccelles. *Acta Chem. Scand*, 21(7), 1967.

[371] F. Eriksson, J. C. Eriksson, and P. Stenius. Thermodynamics of micelle formation: model calculations for alkyl carboxylates. *Colloids and Surfaces*, 3(4):339–356, 1981.

[372] P. Stenius and C.-H. Zilliacus. Association equilibria and micelle formation of fatty acid sodium salts. *Acta Chemica Scandinavica*, 25(6):2232–2250, 1971.

[373] Z. Lu and R. E. Continetti. Dynamics of the acetyloxyl radical studied by dissociative photodetachment of the acetate anion. *The Journal of Physical Chemistry A*, 108(45): 9962–9969, 2004.

[374] W. L. Jorgensen and J. Gao. Monte Carlo simulations of the hydration of ammonium and carboxylate ions. *The Journal of Physical Chemistry*, 90(10):2174–2182, 1986.

[375] I. Lukovitz, A. Karpfen, H. Lischka, and P. Schuster. Ab initio LCMO studies on the hydration of formate ion. *Chemical Physics Letters*, 63(1):151–154, 1979.

[376] A. Pullman and B. Pullman. New paths in the molecular orbital approach to solvation of biological molecules. *Quarterly Reviews of Biophysics*, 7(4):505–566, 1974.

[377] O. D. Bonner. Osmotic and activity coefficients of the sodium salts of formic, acetic and propionic acids. *Journal of Solution Chemistry*, 17(10):999–1002, 1988.

[378] R. Beyer and M. Steiger. Vapour pressure measurements and thermodynamic properties of aqueous solutions of sodium acetate. *The Journal of Chemical Thermodynamics*, 34(7):1057–1071, 2002.

[379] T. S. Banipal, K. Singh, P. K. Banipal, A. K. Sood, P. Singh, G. Singh, and P. Patyar. Volumetric and viscometric studies of some metal acetates in aqueous solutions at T=(288.15 to 318.15) K. *Journal of Chemical & Engineering Data*, 53(12):2758–2765, 2008.

[380] S. Bochmann, P. M. May, and G. Hefter. Molar volumes and heat capacities of aqueous solutions of short-chain aliphatic sodium carboxylates at 25°C. *Journal of Chemical & Engineering Data*, 56(12):5081–5087, 2011.

[381] J. Wang, Z. Yan, K. Zhuo, and J. Lu. Partial molar volumes of some α-amino acids in aqueous sodium acetate solutions at 308.15 K. *Biophysical chemistry*, 80(3):179–188, 1999.

[382] Z.-N. Yan, Q.-T. Cheng, J.-J. Wang, and D.-Z. Liu. The volumetric properties of some α-amino acids in aqueous sodium butyrate solutions at 308.15 K. *Acta Physico–Chimica Sinica*, 15(07):662–667, 1999.

[383] K. S. Pitzer, Ra. N. Roy, and L. F. Silvester. Thermodynamics of electrolytes. 7. sulfuric acid. *Journal of the American Chemical Society*, 99(15):4930–4936, 1977.

[384] T. F. Young. Recent developments in the study of interactions between molecules and ions, and of equilibrium in solutions. *Record of Chemical Progress*, 12:81–95, 1951.

[385] H. S. Harned and B. B. Owen. *The Physical Chemistry of Electrolytic Solutions*. Reinhold, New York, 3rd edition, 1958.

[386] A. G. Dickson, D. J. Wesolowski, D. A. Palmer, and R. E. Mesmer. Dissociation constant of bisulfate ion in aqueous sodium chloride solutions to 250°C. *Journal of Physical Chemistry*, 94(20):7978–7985, 1990.

[387] H. F. Holmes and R. E. Mesmer. Isopiestic studies of H_2SO_4 (aq) at elevated temperatures: Thermodynamic properties. *The Journal of Chemical Thermodynamics*, 24(3): 317–328, 1992.

[388] S. L. Clegg, J. A. Rard, and K. S. Pitzer. Thermodynamic properties of 0–6 mol kg–1 aqueous sulfuric acid from 273.15 to 328.15 K. *Journal of the Chemical Society, Faraday Transactions*, 90(13):1875–1894, 1994.

[389] H. Sippola. Critical evaluation of the 2nd dissociation constants for aqueous sulfuric acid. *Thermochimica Acta*, 532:65–77, 2012.

[390] H. Sippola. Critical evaluation of the second dissociation constants for aqueous sulfuric acid over a wide temperature range. *Journal of Chemical & Engineering Data*, 58(11):3009–3032, 2013.

[391] Y. Matsushima and A. Okuwaki. The second dissociation constant of sulfuric acid at elevated temperatures from potentiometric measurements. *Bulletin of the Chemical Society of Japan*, 61(9):3344–3346, 1988.

[392] J. K. Hovey and L. G. Hepler. Thermodynamics of sulphuric acid: apparent and partial molar heat capacities and volumes of aqueous HSO_4^- from 10–55°C and calculation of the second dissociation constant to 350°C. *Journal of the Chemical Society, Faraday Transactions*, 86(16):2831–2839, 1990.

[393] D. A. Knopf, B. P. Luo, U. K. Krieger, and T. Koop. Thermodynamic dissociation constant of the bisulfate ion from Raman and ion interaction modeling studies of aqueous sulfuric acid at low temperatures. *The Journal of Physical Chemistry A*, 107 (21):4322–4332, 2003.

[394] D. Fraenkel. Electrolytic nature of aqueous sulfuric acid. 1. activity. *The Journal of Physical Chemistry B*, 116(38):11662–11677, 2012.

[395] J. T. Edward and I. C. Wang. Ultraviolet study of the ionization of bisulfate ion. *Canadian Journal of Chemistry*, 43(10):2867–2871, 1965.

[396] H. Chen and D. E. Irish. A Raman spectral study of bisulfate-sulfate systems. II. Constitution, equilibriums, and ultrafast proton transfer in sulfuric acid. *The Journal of Physical Chemistry*, 75(17):2672–2681, 1971.

[397] R. A. Cox, Ü. L. Haldna, K. L. Idler, and K. Yates. Resolution of Raman spectra of aqueous sulfuric acid mixtures using principal factor analysis. *Canadian Journal of Chemistry*, 59(17):2591–2598, 1981.

[398] D. E. Irish and H. Chen. Equilibria and proton transfer in the bisulfate–sulfate system. *The Journal of Physical Chemistry*, 74(21):3796–3801, 1970.

[399] T F Young, L F Maranville, and H M Smith. In W. J. Hamer, editor, *The Structure of Electrolyte Solutions*. John Wiley, New York, 1959.

[400] P. A. H. Wyatt. The constitution of 80–100% aqueous sulphuric acid: a case of overlapping equilibria. *Transactions of the Faraday Society*, 56:490–497, 1960.

[401] T. I. Yacovitch, T. Wende, L. Jiang, N. Heine, G. Meijer, D. .M Neumark, and K. R. Asmis. Infrared Spectroscopy of hydrated bisulfate anion clusters: $HSO_4^-(H2O)_{1-16}$. *The Journal of Physical Chemistry Letters*, 2(17):2135–2140, 2011.

[402] X.-B. Wang, J. B. Nicholas, and L.-S. Wang. Electronic instability of isolated SO_4^{2-} and its solvation stabilization. *The Journal of Chemical Physics*, 113(24):10837–10840, 2000.

[403] R. E. Lindstrom and H. E. Wirth. Estimation of the bisulfate ion dissociation in solutions of sulfuric acid and sodium bisulfate. *The Journal of Physical Chemistry*, 73 (1):218–223, 1969.

[404] G. C. Hood and C. A. Reilly. Ionization of strong electrolytes. V. Proton magnetic resonance in sulfuric acid. *The Journal of Chemical Physics*, 27(5):1126–1128, 1957.

[405] G. A. Krestov. *Thermodynamics of Solvation*. Ellis Horwood, England, 1st edition, 1991.

[406] C. S. Babu and C. Lim. Theory of ionic hydration: Insights from molecular dynamics simulations and experiment. *The Journal of Physical Chemistry B*, 103(37):7958–7968, 1999.

[407] M. Hou, R. Lu, and A. Yu. Polarizability series of aqueous polyatomic anions revealed by femtosecond Kerr effect spectroscopy. *RSC Advances*, 4(44):23078–23083, 2014.

[408] X.-B. Wang, J. B. Nicholas, and L.-S. Wang. Photoelectron spectroscopy and theoretical calculations of $SO4^-$and $HSO4^-$: Confirmation of high electron affinities of SO4 and HSO4. *The Journal of Physical Chemistry A*, 104(3):504–508, 2000.

[409] J.-P. Simonin, S. Krebs, and W. Kunz. Inclusion of ionic hydration and association in the MSA-NRTL model for a description of the thermodynamic properties of aqueous ionic solutions: Application to solutions of associating acids. *Industrial & Engineering Chemistry Research*, 45(12):4345–4354, 2006.

[410] A.-P. Hyvärinen, H. Lihavainen, K. Hautio, T. Raatikainen, Y. Viisanen, and A. Laaksonen. Surface tensions and densities of sulfuric acid + dimethylamine + water solutions. *Journal of Chemical & Engineering Data*, 49(4):917–922, 2004.

[411] C. E. L. Myhre, C. J. Nielsen, and O. W. Saastad. Density and surface tension of aqueous H_2SO_4 at low temperature. *Journal of Chemical & Engineering Data*, 43(4): 617–622, 1998.

[412] E. Königsberger, L.-C. Königsberger, I. Szilágyi, and P. M. May. Measurement and prediction of physicochemical properties of liquors relevant to the sulfate process for titania production. 1. Densities in the $TiOSO_4$ + $FeSO_4$ + H_2SO_4 + H_2O system. *Journal of Chemical & Engineering Data*, 54(2):520–525, 2008.

[413] J. A. Rard, A. Habenschuss, and F. H. Spedding. A review of the osmotic coefficients of aqueous sulfuric acid at 25°C. *Journal of Chemical and Engineering Data*, 21(3): 374–379, 1976.

[414] S. Shankman and A. R. Gordon. The vapor pressure of aqueous solutions of sulfuric acid. *Journal of the American Chemical Society*, 61(9):2370–2373, 1939.

[415] B. R Staples. Activity and osmotic coefficients of aqueous sulfuric acid at 298.15 K. *Journal of Physical and Chemical Reference Data*, 10(3):779–798, 1981.

[416] M. R. Schoenberg, S.-C. Yen, and T. W. Chapman. Thermodynamics of aqueous sulfuric acid up to 175°C. *Journal of Solution Chemistry*, 44(7):1339–1357, 2015.

[417] H.i Majima and Y. Awakura. Water and solute activities of the solution systems of H_2So_4-$CuSo_4$-H_2O and HCl-$CuCl_2$-H_2O. *Metallurgical Transactions B*, 19:347–354, 1988.

[418] C. H. Greenewalt. Partial pressure of water out of aqueous solutions of sulfuric acid. *Industrial & Engineering Chemistry*, 17(5):522–523, 1925.

[419] A. Bosen and H. Engels. Description of the phase equilibrium of sulfuric acid with the NRTL equation and a solvation model in a wide concentration and temperature range. *Fluid Phase Equilibria*, 43(2-3):213–230, 1988.

[420] J. Berkowitz, W. A. Chupka, and D. Gutman. Electron affinities of O2, O3, NO, NO2, NO3 by endothermic charge transfer. *The Journal of Chemical Physics*, 55(6): 2733–2745, 1971.

[421] N. N. Greenwood and A. Earnshaw. *Chemistry of the Elements*. Elsevier, 2nd edition, 1997.

[422] W. A. Guillory and M. L. Bernstein. Infrared spectrum of matrix-isolated nitric acid. *The Journal of Chemical Physics*, 62(3):1058–1060, 1975.

[423] J. A. Odutola and T. R. Dyke. Polarity of hydrogen-bonded complexes: Nitric acid and carboxylic acid dimers. *The Journal of Chemical Physics*, 68(12):5663–5665, 1978.

[424] P. R. McCurdy, W. P. Hess, and S. S. Xantheas. Nitric acid – water complexes: Theoretical calculations and comparison to experiment. *The Journal of Physical Chemistry A*, 106(33):7628–7635, 2002.

[425] M. Canagaratna, J. A. Phillips, M. E. Ott, and K. R. Leopold. The nitric acid–Water Complex: Microwave spectrum, structure, and tunneling. *The Journal of Physical Chemistry A*, 102(9):1489–1497, 1998.

[426] Design Institute for Physical Properties, Sponsored by AIChE. *DIPPR Project 801 - Full Version*. Design Institute for Physical Property Research/AIChE, 2005; 2008; 2009; 2010; 2011; 2012; 2015; 2016. URL http://app.knovel.com/hotlink/toc/id:kpDIPPRPF7/dippr-project-801-full/dippr-project-801-full.

[427] G. L. Antipenko, E. S. Beletskaya, and A. G. Krylova. Density-temperature dependence of pure nitric acid. *Zhurnal Prikladnoi Khimii*, 31(6):859–863, 1958.

[428] S. A. Stern and W. B. Kay. The orthobaric density of pure nitric acid. *Journal of the American Chemical Society*, 76(21):5353–5354, 1954.

[429] B. Fine. Density of solutions of ammonium nitrate and tetramethylammonium nitrate in nitric acid. *Journal of Chemical & Engineering Data*, 7(1):91–94, 1962.

[430] G. L. Wilson and F. D. Miles. The partial pressures of nitric acid-water mixtures from 0°–20°C. *Transactions of the Faraday Society*, 35:356–363, 1940.

[431] J. Prošek. Gleichgewicht zwischen der flüssigen und der gasförmigen Phase in Salpetersäure enthaltenden Systemen. *Collection of Czechoslovak Chemical Communications*, 32:2397–2404, 1967.

[432] F. Rivenq. Boiling point diagrams of water-HNO3 mixtures under reduced pressure. *Bulletin de la Societe Chimique de France*, pages 822–826, 1959.

[433] T. Marnac and M. Enjalbert. Equilibres liquide-vapeur. III. Systeme eau–acide nitrique. *Chimie & Industrie, Genie Chimique*, 98(6):1047–1051, 1967.

[434] R. Haas, K. H. Dücker, and H. A. Küppers. Activity coefficients and dissociation constants of aqueous nitric acid and perchloric acid solutions. *Berichte der Bunsengesellschaft für Physikalische Chemie*, 69(2):97–109, 1965.

[435] R. J. Lemire, C. P. Brown, and A. B. Campbell. Vapor pressures of nitric acid and water in the systems nitric acid-water and nitric acid-thorium (iv) nitrate-water at 50°c. *Journal of Chemical and Engineering Data*, 30(4):421–424, 1985.

[436] D. E. Irish and O. Puzic. Raman spectral study of the constitution and equilibria of nitric acid and d-nitric acid. *Journal of Solution Chemistry*, 10(6):377–393, 1981.

[437] G. C. Hood and C. A. Reilly. Ionization of strong electrolytes. VIII. Temperature coefficient of dissociation of strong acids by proton magnetic resonance. *The Journal of Chemical Physics*, 32(1):127–130, 1960.

[438] J. L. Oscarson, S. E. Gillespie, R. M. Izatt, X. Chen, and C. Pando. Thermodynamic quantities for the ionization of nitric acid in aqueous solution from 250 to 319°C. *Journal of Solution Chemistry*, 21(8):789–801, 1992.

[439] J. Chlistunoff, K. J. Ziegler, L. Lasdon, and K. P. Johnston. Nitric/nitrous acid equilibria in supercritical water. *The Journal of Physical Chemistry A*, 103(11): 1678–1688, 1999.

[440] W. L. Marshall and R. Slusher. The ionization constant of nitric acid at high temperatures from solubilities of calcium sulfate in HNO_3 H_2O, 100–350°C; activity coefficients and thermodynamic functions. *Journal of Inorganic and Nuclear Chemistry*, 37(5):1191–1202, 1975.

[441] W. L. Marshall and R. Slusher. Experimental and calculated solubilities of magnesium sulfate monohydrate in aqueous nitric acid and related solubilities, 200–350°C; ionization constants of nitric acid at 300–370°C. *Journal of Inorganic and Nuclear Chemistry*, 37(10):2165–2170, 1975.

[442] D. E. Irish and A. R. Davis. Interactions in aqueous alkali metal nitrate solutions. *Canadian Journal of Chemistry*, 46(6):943–951, 1968.

[443] R. Payne. Structure of the electrical double layer at a mercury electrode in the presence of adsorbed nitrate ions. *The Journal of Physical Chemistry*, 69(12):4113–4123, 1965.

[444] J. M. Howell, A. M. Sapse, E. Singman, and G. Snyder. Ab initio SCF calculations of NO_2-$(H_2O)_n$ and $NO_3^-(H_2O)_n$ clusters. *The Journal of Physical Chemistry*, 86(13): 2345–2349, 1982.

[445] X.-B. Wang, X. Yang, L.-S. Wang, and J. B. Nicholas. Photodetachment and theoretical study of free and water-solvated nitrate anions, $NO_3^-(H_2O)_n$ (n=0–6). *The Journal of Chemical Physics*, 116(2):561–570, 2002.

[446] A. K. Pathak, T. Mukherjee, and D. K. Maity. Microhydration of NO_3^-: A theoretical study on structure, stability and IR spectra. *The Journal of Physical Chemistry A*, 112 (15):3399–3408, 2008.

[447] D. J. Goebbert, E. Garand, T. Wende, R. Bergmann, G. Meijer, K. R. Asmis, and D. M. Neumark. Infrared spectroscopy of the microhydrated nitrate ions $NO_3^-(H2O)_{1-6}$. *The Journal of Physical Chemistry A*, 113(26):7584–7592, 2009.

[448] Y.-R. Liu, H. Wen, T. Huang, X.-X. Lin, Y. B. Gai, C. J. Hu, W.-J. Zhang, and W. Huang. Structural exploration of water, nitrate/water, and oxalate/water clusters with basin-hopping method using a compressed sampling technique. *The Journal of Physical Chemistry A*, 118(2):508–516, 2014.

[449] J. R. Scott and J. B. Wright. Computational investigation of the solvation of nitric acid: Formation of the NO_3^- and H_3O^+ ion pair. *The Journal of Physical Chemistry A*, 108(47):10578–10585, 2004.

[450] N. S. Marinković, J. J. Calvente, A. Kloss, Z. Kováčová, and W. R. Fawcett. SNIFTIRS studies of the electrochemical double layer: Part II. Au (111) electrode in solutions with specifically adsorbed nitrate ions. *Journal of Electroanalytical Chemistry*, 467 (1):325–334, 1999.

[451] Y.k Marcus. Ionic radii in aqueous solutions. *Chemical Reviews*, 88(8):1475–1498, 1988.

[452] N. Minogue, E. Riordan, and J. R. Sodeau. Raman spectroscopy as a probe of low-temperature ionic speciation in nitric and sulfuric acid stratospheric mimic systems. *The Journal of Physical Chemistry A*, 107(22):4436–4444, 2003.

[453] E. Sepp and G. Rayalo. The vapour pressure of volatile components in the system succinic acid–nitric acid–water. *Proceedings of the Academy of Sciences of the Estonian SSR, Chemistry*, 27(2):117–119, 1978.

[454] V. Granzhan and S. Laktionova. The densities, viscosities, and surface tensions of aqueous nitric acid solutions. *Russian Journal of Physical Chemistry*, 49:1448, 1975.

[455] A. C. Tikanen and W. R. Fawcett. Application of the mean spherical approximation and ion association to describe the activity coefficients of aqueous 1: 1 electrolytes. *Journal of Electroanalytical Chemistry*, 439(1):107–113, 1997.

[456] R. L. Frost and D. W. James. Ion–ion–solvent interactions in solution. Part 3.–Aqueous solutions of sodium nitrate. *Journal of the Chemical Society, Faraday Transactions 1: Physical Chemistry in Condensed Phases*, 78(11):3223–3234, 1982.

[457] R. L. Frost and D. W. James. Ion–ion–solvent interactions in solution. Part 4.–Raman spectra of aqueous solutions of some nitrates with monovalent cations. *Journal of the Chemical Society, Faraday Transactions 1: Physical Chemistry in Condensed Phases*, 78(11):3235–3247, 1982.

[458] R. L. Frost and D. W. James. Ion–ion–solvent interactions in solution. Part 5.–Influence of added halide, change in temperature and solvent deuteration on ion association in aqueous solutions of nitrate salts. *Journal of the Chemical Society, Faraday Transactions 1: Physical Chemistry in Condensed Phases*, 78(11):3249–3261, 1982.

[459] J. D. Riddell, D. J. Lockwood, and D. E. Irish. Ion pair formation in $NaNO_3/D_2O$ solutions: Raman and infrared spectra, partial molal volumes, conductance, and viscosity. *Canadian Journal of Chemistry*, 50(18):2951–2962, 1972.

[460] A. Chremos, E. Forte, V. Papaioannou, A. Galindo, G. Jackson, and C. S. Adjiman. Modelling the phase and chemical equilibria of aqueous solutions of alkanolamines and carbon dioxide using the SAFT-γ SW group contribution approach. *Fluid Phase Equilibria*, 407:280–297, 2016.

[461] I. M. Abdulagatov and N. D. Azizov. Densities, apparent molar volumes and viscosities of concentrated aqueous $NaNO_3$ solutions at temperatures from 298 to 607 K and at pressures up to 30 MPa. *Journal of Solution Chemistry*, 34(6):645–685, 2005.

[462] A. B. Zdanovskii. Partial heats of dilution for aqueous solutions of salts. *Russian Journal of Physical Chemistry*, 68(4):556–561, 1994.